

**NASA
Reference
Publication
1080**

November 1981

NASA-RP-1080-VOL-3
19820008276

ATS-6 Final Engineering Performance Report

Volume III - Telecommunications and Power

LIBRARY COPY

APR 12 1982

LANGLEY RESEARCH CENTER
LIBRARY, NASA
HAMPTON, VIRGINIA

APR 12 1982
LANGLEY RESEARCH CENTER
LIBRARY, NASA
HAMPTON, VIRGINIA

NASA

**NASA
Reference
Publication
1080**

1981

ATS-6 Final Engineering Performance Report

Volume III - Telecommunications and Power

Robert O. Wales, *Editor*
Goddard Space Flight Center
Greenbelt, Maryland

NASA

National Aeronautics
and Space Administration

Scientific and Technical
Information Branch

An Engineering Evaluation
in
Six Volumes

- Volume I: Program and System Summaries; Mechanical and Thermal Details
 - Part A: Program Summary
 - Part B: Mechanical Subsystems
 - Part C: Thermal Control and Contamination Monitor
- Volume II: Orbit and Attitude Controls
 - Part A: Attitude Control
 - Part B: Pointing Experiments
 - Part C: Spacecraft Propulsion
 - Part D: Propulsion Experiment
- Volume III: Telecommunications and Power
 - Part A: Communications Subsystem
 - Part B: Electrical Power Subsystem
 - Part C: Telemetry and Command Subsystem
 - Part D: Data Relay Experiments
- Volume IV: Television Experiments
 - Part A: The Department of Health, Education and Welfare Sponsored Experiments
 - Part B: Satellite Instructional Television Experiment (India)
 - Part C: Independent Television Experiments
- Volume V: Propagation Experiments
 - Part A: Experiments at 1550 MHz to 1650 MHz
 - Part B: Experiments at 4 GHz to 6 GHz
 - Part C: Experiments Above 10 GHz
- Volume VI: Scientific Experiments

This document makes use of international metric units according to the *Système International d'Unités* (SI). In certain cases, utility requires the retention of other systems of units in addition to the SI units. The conventional units stated in parentheses following the computed SI equivalents are the basis of the measurements and calculations reported.

For sale by the National Technical Information Service
Springfield, Virginia 22161
Price

VOLUME III
CONTENTS

	<i>Page</i>
FOREWORD.....	xix
INTRODUCTION.....	xxv

PART A
COMMUNICATIONS SUBSYSTEM

CHAPTER 1 – INTRODUCTION.....	3
FUNCTIONAL REQUIREMENTS.....	3
Communication and Technological Experiments.....	3
Scientific Experiments.....	3
Special Investigations.....	4
CHAPTER 2 – FUNCTIONAL DESCRIPTION.....	7
INTRODUCTION.....	7
PRIME-FOCUS FEED AND EARTH COVERAGE HORNS.....	11
C-Band Prime-Focus Feed and Earth-Coverage Horns.....	11
S-Band Prime-Focus Feed.....	15
L-Band Prime-Focus Feed.....	17
VHF Prime-Focus Feed.....	17
UHF Prime-Focus Feed.....	18
COMMUNICATIONS TRANSPONDER.....	20
Receivers.....	20
C-Band Receiver.....	20
S-Band Receiver.....	22
L-Band Receiver.....	22
VHF Receiver.....	22

VOLUME III
CONTENTS (continued)

	<i>Page</i>
Downconverters	22
I.F. Input Switching Matrix.....	23
I.F. Amplifiers.....	23
Frequency Translation Mode.....	25
Remodulation Mode	25
Beacon	25
Discriminator	26
Monopulse.....	26
I.F. Output Switching Matrix	26
Upconverters.....	26
Transmitters	26
C-Band Transmitter.....	29
S-Band Transmitter.....	29
L-Band Transmitter.....	29
UHF Transmitter.....	29
Synthesizer	30
Monopulse Unit.....	30
Wideband Data Unit	32
Power Supply and Distribution.....	32
Transponder Command Decoder.....	32
RFI Experiment Transponder.....	34
DESIGN VALIDATION	35
CHAPTER 3 – IN-ORBIT PERFORMANCE	37
 INITIAL 30-DAY CHECKOUT (SPECIFICATION/COMPLIANCE)	37
Experiments and Modes of Operation.....	38
Tracking and Data Relay Experiment	38
Television Relay Using Small Terminals Experiment.....	38
Position Location and Aircraft Communication Experiment.....	38
Monopulse Tracking	39
Millimeter Wave Experiment.....	43
COMSAT Propagation Experiment	43

VOLUME III
CONTENTS (continued)

	<i>Page</i>
Radio Frequency Interference Measurements Experiment	44
Very High Resolution Radiometer	44
VHF High Gain RF Link	44
Range and Range Rate	44
Health, Education, Telecommunications Experiment	44
TV Camera Reflector Monitor	45
Radio Beacon Experiment	45
Transponder Signal Characteristics	45
Antenna Patterns	45
OVERALL MISSION PERFORMANCE	46
IN-ORBIT ANOMALIES	46
C-Band Power "Dips"	46
HET-2 Driver Relay	47
S-Band Transmitter Failure	47
L-Band Transmitter Output Noise	48
Spacecraft I.F. AGC Calibration	48
CONCLUSIONS AND RECOMMENDATIONS	48

PART B
ELECTRICAL POWER SUBSYSTEM

CHAPTER 4 – INTRODUCTION	53
POWER SUBSYSTEM REQUIREMENTS	53
Mission Normal Power	53
Eclipse/Occult Power	53
Bus Voltage Distribution	55
Protective Features	55
Load Control (Experiment and Communication System)	55
CHAPTER 5 – DESIGN DESCRIPTION	57
OVERALL DESCRIPTION	57

VOLUME III
CONTENTS (continued)

	<i>Page</i>
SOLAR ARRAY.....	59
BATTERIES.....	63
POWER REGULATION UNIT.....	66
Controller.....	66
Shunt Driver.....	66
Boost Regulator.....	66
Battery Chargers.....	68
Malfunction Protection.....	68
POWER CONTROL UNIT.....	70
SHUNT DISSIPATORS.....	70
LOAD INTERFACE CIRCUITS.....	71
ARRAY HARNESS.....	72
SPECIAL POWER SUBSYSTEM PROTECTIVE FEATURES.....	74
Nonessential Bus Undervoltage/Overload Protection.....	74
Power Amplifier Overload Protection/Experiment Bus Overload.....	74
POWER DISSIPATION CONTROL.....	74
PERFORMANCE CHARACTERISTICS.....	76
Dynamic Regulation.....	76
Output Impedance.....	78
Overload Protection.....	79
Load Interface Circuits.....	80
ELECTRICAL POWER SUBSYSTEM TEST REQUIREMENTS.....	81
SPECIAL TESTS AND OPERATIONS.....	84

VOLUME III
CONTENTS (continued)

	<i>Page</i>
Solar Array Panel Environmental and Performance Tests	84
Solar Cell Cleaning Operations	87
Squib Interface Unit/Titan Timing Test	88
Shunt Regulator Dynamic Response Test With Simulated Umbilical Cable.....	88
Solar Array Bus Electromagnetic Interference Filtering	88
Battery Cell Characterization Tests	88
END-OF-MISSION TESTS	89
CHAPTER 6 – IN-ORBIT PERFORMANCE AND OPERATIONS.....	91
SOLAR ARRAY.....	91
ELECTRONICS	93
Power Control Unit and Load Interface Circuits.....	93
Power Regulation Unit	94
Shunt Dissipators	94
BATTERY PERFORMANCE	95
CHAPTER 7 – IN-ORBIT ANOMALIES AND CONCLUSIONS	101
BATTERY END-OF-CHARGE TERMINAL VOLTAGE	101
SOLAR ARRAY REDUCED OUTPUT.....	101
OTHER MINOR ANOMALIES.....	102
CONCLUSIONS AND RECOMMENDATIONS.....	103
Electrical Power Subsystem Design	103
Battery Temperature Control	103
Noneclipse Cycling of Synchronous Orbit Batteries	103
Conclusions.....	104

PART C
TELEMETRY AND COMMAND SUBSYSTEM

CHAPTER 8 – INTRODUCTION.....	107
-------------------------------	-----

VOLUME III
CONTENTS (continued)

	<i>Page</i>
FUNCTIONAL REQUIREMENTS	107
DESIGN DESCRIPTION.....	107
Command Function	108
Telemetry Function	113
Overall Subsystem Operation	116
Component Description/Function.....	119
DESIGN VALIDATION	122
Development.....	123
Command Interface Circuits	123
Command Detector Circuits	123
Vhf Antenna Coverage	123
Subsystem Level	125
Spacecraft Level	125
CHAPTER 9 – IN-ORBIT PERFORMANCE AND OPERATIONS.....	127
INITIAL THIRTY-DAY CHECKOUT.....	127
OVERALL MISSION PERFORMANCE.....	129
FINAL ENGINEERING TESTS	131
IN-ORBIT ANOMALIES.....	132
DACU-1 Anomaly.....	132
Description	132
Assessment	138
DACU-2 Anomaly.....	139
Description	139
Data Review	140

VOLUME III
CONTENTS (continued)

	<i>Page</i>
Assessment	140
Affect of Anomalies	142
IN-ORBIT OPERATIONS.....	144
CHAPTER 10 – TELEMETRY AND COMMAND GROUND SUPPORT	147
INTRODUCTION.....	147
SOFTWARE CAPABILITIES	147
HARDWARE AND SOFTWARE	152
INTEGRATION AND TEST SUPPORT TO OPERATIONS.....	152
PERSONNEL	152
OPERATIONS PLANS AND PROCEDURES.....	152
REAL-TIME RECOVERIES	153
CHECKOUT OF REMOTE SITES	153
Rosman Ground Station	154
Mojave Ground Station	154
Hybrid Terminal, Madrid, Spain	154
SUMMARY AND CONCLUSIONS.....	155
Control Center Operations	155
Operations and Maintenance	155
Experimenter Role in ATSOCC.....	156
Scheduling.....	156
Anomaly Investigation	156
CHAPTER 11 – CONCLUSIONS AND RECOMMENDATIONS	159
DESIGN CONSIDERATIONS.....	159

VOLUME III
CONTENTS (continued)

	<i>Page</i>
PERFORMANCE CONSIDERATIONS.....	160
OPERATIONS CONSIDERATIONS.....	160
GENERAL CONSIDERATIONS.....	160
 PART D DATA RELAY EXPERIMENTS 	
CHAPTER 12 – TRACKING AND DATA RELAY EXPERIMENT.....	165
EXPERIMENT OBJECTIVES.....	165
Scientific.....	165
Technological	165
EXPERIMENT DESCRIPTION.....	165
Tracking Experiment.....	165
Nimbus-6.....	166
GEOS-3.....	167
Data Relay/Command Relay.....	167
Nimbus-6/ATS-6 Command Relay	167
Simulated Digital Data	169
Tracking and Orbit Determinations.....	170
Multipath	173
SYSTEM CONFIGURATION.....	175
Ground Station Equipment.....	175
Operations Control Centers.....	177
Spacecraft Parameters.....	178

VOLUME III
CONTENTS (continued)

	<i>Page</i>
ATS-6 Parameters	178
Nimbus-6 Parameters	178
GEOS-3 Parameters	180
EXPERIMENT RESULTS	181
Data Reduction	181
Range and Range Rate	181
Digital Evaluation Module	182
Experimental Results	185
Range and Range Rate	185
Digital Evaluation Module	187
Multipath Results	192
Spacecraft Telemetry	202
Data Relay/Command Relay Results	202
Tracking	202
SUMMARY AND CONCLUSIONS	204
CHAPTER 13 – APOLLO-SOYUZ TEST PROGRAM	207
INTRODUCTION	207
Mission Signal Sources for ASTP	209
ASTP Television Configuration	211
U.S.S.R. Configuration	211
U.S. Configuration	215
TECHNICAL AND OPERATIONAL EVALUATIONS	222
Moscow to Houston Video Transmission	222
Moscow to Houston Television Audio	226
Apollo Field Sequential Video Relayed Through ATS-6	227
Buitrago to Houston Video Transmission	228
Johnson Space Center Audio Processing and Transmission	229
Johnson Space Center System Timing	230
Johnson Space Center Processing and Distribution	230

VOLUME III
CONTENTS (continued)

	<i>Page</i>
APPENDIX A – SAMPLE LINK CALCULATION	235
APPENDIX B – IN-ORBIT MEASUREMENT OF G/T OF A HARD-LIMITING TRANSPONDER WITH AUTOMATIC GAIN CONTROL	237
APPENDIX C – I.F. AUTOMATIC GAIN CONTROL CALIBRATION	243
APPENDIX D – L-BAND TRANSMITTER NOISE	247
APPENDIX E – E.I.R.P. AND G/T SUMMARY	251
APPENDIX F – 9.14-METER ANTENNA PATTERN MEASUREMENTS	259
APPENDIX G – ACRONYMS AND ABBREVIATIONS	283
BIBLIOGRAPHY	297

List of Illustrations

<i>Figure</i>	<i>Page</i>
Frontispiece—Apollo-Soyuz Test Program	xxvi
2-1 Simplified Communication Subsystem Block Diagram	8
2-2 Prime-Focus Feed Components and Earth-Coverage Horns	12
2-3 Physical Arrangement of Composite Feed Element (Feed Plate viewed from reflector side)	13
2-4 Prime-Focus Feed (Center Element)	13
2-5 C-Band Antenna Unit RF Schematic	14
2-6 S-Band Feed RF Schematic	16
2-7 L-Band RF Schematic (Shown Selected to Fan Beam)	18
2-8 VHF RF System Simplified Block Diagram	19

VOLUME III
CONTENTS (continued)

<i>Figure</i>		<i>Page</i>
2-9	Transponder Functional Block Diagram	21
2-10	I.F. Amplifier Block Diagram	24
2-11	Communications Subsystem Upconverters	27
2-12	Communications Subsystem Transmitters.....	28
2-13	Communications Subsystem Synthesizer.....	31
2-14	Communications Subsystem Wideband Data Unit.....	33
3-1	C-Band Monopulse Error Curves	40
3-2	S-Band Monopulse Error Curves	41
3-3	VHF Monopulse Error Curves.....	42
4-1	Spacecraft Mode Power Requirements	54
4-2	Peak Power Available at End-of-Life (Specification).....	54
5-1	Power Subsystem Functional Block Diagram	58
5-2	Basic Block Diagram Shunt-Boost Subsystem	59
5-3	Array/Shunt-Boost Power Interface Characteristic	60
5-4	Power Subsystem Regulation Control Modes	61
5-5	Solar Array Capabilities.....	62
5-6	Solar Array Temperature versus Equinox Orbit Position.....	63
5-7	Solar Cell Stack.....	64
5-8	Main Charger Characteristics.....	65
5-9	Controller Block Diagram	67

VOLUME III
CONTENTS (continued)

<i>Figure</i>		<i>Page</i>
5-10	Basic Schematic of Shunt Dissipator	71
5-11	LIC Regulation Characteristics	73
5-12	Shunt Dissipation	75
5-13	Dynamic Regulation (Shunt Mode) 500-Watt Solar Array.	77
5-14	Dynamic Regulation (Shunt/Boost Mode) with 400-Watt Solar Array	78
5-15	Dynamic Regulation (Boost Mode) with 0-Watt Solar Array.	79
5-16	Output Impedance	80
5-17	PCU/PRU Timing Scheme for Bus Protection	81
5-18	Bus Response to Nonessential Bus Overload	82
5-19	Bus Response to Essential Bus Overload	82
5-20	LIC Input-Ripple Voltage Attenuation versus Frequency (300-Watt Unit)	83
5-21	Load Interface Circuit Output Impedance (300-Watt Unit).	83
5-22	Panel Electrical Performance versus Thermal Vacuum Cycles	85
5-23	Spacecraft Setup for Solar Array Flash Illumination.	86
5-24	String I-V Curve	87
6-1	ATS-6 Available Power	92
6-2	Regulated Bus Data	94
6-3	Preflight Deadbands	95
6-4	Battery Discharge Profile for SITE Operations	97
6-5	Battery Discharge Curves for Eclipse Seasons 1 Through 8	98

VOLUME III
CONTENTS (continued)

<i>Figure</i>		<i>Page</i>
6-6	Battery Discharge Characteristics	99
6-7	Discharge Characteristics.	100
7-1	Battery Charge Characteristics.	102
8-1	ATS-6 Telemetry and Command Subsystem Block Diagram	109
8-2	Telemetry and Command Subsystem Functional Block Diagram	110
8-3	Command Subsystem Functional Block Diagram CDD Expanded.	112
8-4	Command Word Formats	113
8-5	Telemetry Subsystem Functional Block Diagram	114
8-6	Data Acquisition and Control Unit	118
8-7	Command Receiver/Decoders Interconnections	122
8-8	Spacecraft Test Configuration.	124
9-1	Telemetry RF and Baseband Configuration.	130
9-2	Command Configuration.	131
9-3	DACU-2 Typical Telemetry Anomaly Frequency	143
9-4	Remote Command Test Configuration	144
9-5	Special Data Link Configuration	145
12-1	Nimbus-6 T&DRE Command System Block Diagram	168
12-2	Relaying DEM Data from Nimbus-6 to ATS/Madrid Configuration.	171
12-3	Basic Tracking Geometry	172
12-4	General S-Band Satellite-to-Satellite Multipath Experiment	174

VOLUME III
CONTENTS (continued)

<i>Figure</i>		<i>Page</i>
12-5	Ground Station Equipment Block Diagram	176
12-6	ATS-6 Block Diagram of Configuration for T&DRE	179
12-7	Bit-Error Rate Detector Output of Synchronizer	184
12-8	Typical GEOS-3 per Pass Orbit Residuals	187
12-9	Bit-Error Rate vs. Bit-Energy to Noise-Power-Density Ratio for Revolution 4576	189
12-10	Bit-Error Rate vs. Bit-Energy to Noise-Power Density Ratio for Revolution 4764	190
12-11	Bit-Error Rate vs. Bit-Energy to Noise-Power-Density Ratio for Revolution 4765	191
12-12	Predicted and Measured Carrier-to-Noise Power Density Ratios as a Function of Time for Nimbus-6 Revolution 4951	193
12-13	Predicted and Measured Carrier-to-Noise Power Density Ratios as a Function of Time for Nimbus-6 Revolution 4763	194
12-14	Predicted and Measured Carrier-to-Noise Power Density Ratios as a Function of Time for Nimbus-6 Revolution 4764	195
12-15	Nimbus-6 Orbit and Corresponding Specular Point Trace for Nimbus-6 Revolution 2795	198
12-16	Normalized Carrier-to-Specular Multipath Ratio Measured During Nimbus-6 Revolution 2795	199
12-17	Specular Point Ground Track for Nimbus-6 Revolution 2795	200
12-18	Typical Power Spectral Density Plot	201
12-19	A Comparison of Recorded and Relayed THIR Data	203
12-20	ATSOCC Tracking Display Showing Variations Between Monopulse and Program Track	205

**VOLUME III
CONTENTS (continued)**

<i>Figure</i>		<i>Page</i>
13-1	ATS-6 Coverage of ASTP	208
13-2	Relay Services	210
13-3	U.S.S.R. Television Configuration	213
13-4	ASTP Video Moscow to Houston	216
13-5	JSC System Distribution	223

LIST OF TABLES

<i>Table</i>		<i>Page</i>
1-1	Prime-Focus Feed and Earth Coverage Horn Pattern Usage	5
1-2	Typical Communication Subsystem Functions	6
2-1	Communications Subsystem Characteristics	9
3-1	Communication Subsystem Performance Comparison (30-Day In-Orbit Checkout)	37
3-2	Monopulse Error Signal Characteristics	43
5-1	PRU Malfunction Protection	69
5-2	Dynamic Regulation Requirements (30.5 V Bus)	76
6-1	Electrical Power Subsystem: In-Orbit Performance	93
6-2	Shunt Dissipator Power Sharing	96
6-3	Battery Discharge Cycles for First 2½ Years of Operation	96
8-1	ATS-6 Command Characteristics	111
8-2	ATS-6 Telemetry Parameters	115

VOLUME III
CONTENTS (continued)

<i>Table</i>		<i>Page</i>
8-3	Percent of Sphere Having Gains of -10 dBi or Better	125
9-1	Telemetry and Command Subsystem Performance Comparison	127
9-2	Uplink Command Receiver Signal Levels.	128
9-3	Downlink Performance	128
9-4	Telemetry Transmitter Frequency Performance	129
9-5	Telemetry Downlink Performance.	129
9-6	DACU-1 Operation—November 30, 1974	134
9-7	DACU-1 Operation—December 27, 1974	136
9-8	DACU-1 Error Status—December 19, 1975.	137
9-9	DACU-2 Anomaly Chronology	139
9-10	DACU-2 Anomaly Trends in Review Data.	141
12-1	Tracked Satellite Characteristics	180
12-2	Nimbus-6 to ATS-6 to Hybrid Return Link Power Budget	183
12-3	Nimbus-6 T&DRE Tracking Data Quality	185
12-4	GEOS-3 Residual Summary.	188
12-5	Minutes of Multipath Data Recorded	196
12-6	Minutes of Multipath Data Analyzed Relative to Grazing Angle (ϕ)	197

FOREWORD

ATS-6 has been referred to as Arthur C. Clarke's "Star," because Mr. Clarke originated the idea for synchronous communications satellites in an article that he wrote in 1945. In 1975, Mr. Clarke was actively engaged in monitoring the Indian Satellite Instructional Television Experiment on ATS-6 and giving feedback to the Indian Space Research Organization. We, therefore, felt that it would be appropriate for him to contribute the foreword for this report.

An excerpt from his response to our request and selected paragraphs from his contribution, "School-master Satellite," follow.



ශ්‍රී ලංකා මොරටුව විශ්වවිද්‍යාලයේ

කුලපති කායාර්ථයෙන්

FROM THE DESK OF THE CHANCELLOR
UNIVERSITY OF MORATUWA, SRI LANKA

ආචාර්ය ඩී. ක්ලාර්ක්

බී.ආයි.සී., ඇල්.ආර්.ඒ.ආයි., ඇල්.බී.ආයි.ආයි.
ලන්ඩනයේ කිංග්ස් විද්‍යාලයේ අධ්‍යයන පාඨවිභාගී

Arthur C. Clarke

B.Sc., F.R.A.S., F.B.I.S.
Fellow of King's College, London.

දුරකථන අංකය: 94255
කැබල්ල: අන්ඩර්සී
කොළඹ 7

Tel: 94255
Cable: Undersea
Colombo

"ලෙස්ලිගේ නිවස"
25, බාර්න්ස් ප්ලේස්,
කොළඹ 7.

"Leslie's House"
25, Barnes Place,
Colombo 7.

24th September 1980

The extracts that follow are from an essay that was written in 1971, almost five years before the SITE program became fully operational, and originally appeared in the *Daily Telegraph Colour Magazine* for 17 December 1971. It was later read into the *Congressional Record* (27 January 1972) by Representative William Anderson, first commander of the nuclear submarine *Nautilus*, and now forms Chapter 12 of *The View From Serendip* (Random House, 1977; Ballantine, 1978).

To me, it brings back vivid recollections of my meetings with Dr. Sarabhai, the chief instigator of the program. I would like to dedicate it to his memory – and to that of another good friend, also closely associated with the project – Dr. Wernher von Braun.

Chancellor
University of Moratuwa
Sri Lanka

Arthur C. Clarke
Vikram Sarabhai Professor, Physical Research
Laboratory, Ahmedabad
India

SCHOOLMASTER SATELLITE

“For thousands of years, men have sought their future in the starry sky. Now this old superstition has at last come true, for our destinies do indeed depend upon celestial bodies—those that we have created ourselves . . .

“In 1974 there will be a new Star of India; though it will not be visible to the naked eye, its influence will be greater than that of any zodiacal signs. It will be the satellite ATS-F (Applications Technology Satellite F), the latest in a very successful series launched by America’s National Aeronautics and Space Administration. For one year, under an agreement signed on September 18, 1969, ATS-F will be loaned to the Indian Government by the United States, and will be “parked” 22,000 miles above the Equator, immediately to the south of the sub-continent. At this altitude it will complete one orbit every 24 hours and will therefore remain poised over the same spot on the turning Earth; in effect, therefore, India will have a TV tower 22,000 miles high, from which programmes can be received with almost equal strength over the entire country . . .

“ATS-F, now being built by the Fairchild-Hiller Corporation, represents the next step in the evolution of communications satellites. Its signals will be powerful enough to be picked up, not merely by multi-million dollar Earth stations, but by simple receivers, costing two or three hundred dollars, which all but the poorest communities can afford. This level of cost would open up the entire developing world to every type of electronic communication—not only TV; the emerging societies of Africa, Asia and South America could thus by-pass much of today’s ground-based technology, and leap straight in to the space age. Many of them have already done something similar in the field of transportation, going from ox-cart to aeroplane with only a passing nod to roads and railways.

“It can be difficult for those from nations which have taken a century and a half to slog from semaphore to satellite to appreciate that a few hundred pounds in orbit can now replace the continent-wide networks of microwave towers, coaxial cables and ground transmitters that have been constructed during the last generation. And it is perhaps even more difficult, to those who think of television exclusively in terms of old Hollywood movies, giveaway contests and soap commercials to see any sense in spreading these boons to places which do not yet enjoy them. Almost any other use of the money, it might be argued, would be more beneficial . . .

“Those who actually live in the East, and know its problems, are in the best position to appreciate what cheap and high-quality communications could do to improve standards of living and reduce social inequalities. Illiteracy, ignorance and superstition are not merely the results of poverty—they are part of its cause, forming a self-perpetuating system which has lasted for centuries, and which cannot be changed without fundamental advances in education. India is now beginning a Satellite Instructional Television Experiment (SITE) as a bold attempt to harness the technology of space for this task; if it succeeds, the implications for all developing nations will be enormous.

“Near Ahmedabad is the big 50-foot diameter parabolic dish of the Experimental Satellite Communication Ground Station through which the programmes will be beamed up to the hovering satellite. Also in this area is AMUL, the largest dairy co-operative in the world, to which more than a quarter of a million farmers belong. After we had finished filming at the big dish, our camera team drove out to the AMUL headquarters, and we accompanied the Chief Veterinary Officer on his rounds.

SCHOOLMASTER SATELLITE

“At our first stop, we ran into a moving little drama that we could never have contrived deliberately, and which summed up half the problems of India in a single episode. A buffalo calf was dying, watched over by a tearful old lady who now saw most of her worldly wealth about to disappear. If she had called the vet a few days before—there was a telephone in the village for this very purpose—he could easily have saved the calf. But she had tried charms and magic first; they are not always ineffective, but antibiotics are rather more reliable . . .

“I will not quickly forget the haggard, tear-streaked face of that old lady in Gujerat; yet her example could be multiplied a million times. The loss of real wealth throughout India because of ignorance or superstition must be staggering. If it saved only a few calves per year, or increased productivity only a few per cent, the TV set in the village square would quickly pay for itself. The very capable men who run AMUL realise this; they are so impressed by the possibilities of TV education that they plan to build their own station to broadcast to their quarter of a million farmers. They have the money, and they cannot wait for the satellite—though it will reach an audience two thousand times larger, for over 500 million people will lie within range of ATS-F . . .

“And those who are unimpressed by mere dollars should also consider the human aspect—as demonstrated by the great East Pakistan cyclone of 1971. That was tracked by the weather satellites—but the warning network that might have saved several hundred thousand lives did not exist. Such tragedies will be impossible in a world of efficient space communications.

“Yet it is the quality, not the quantity, of life that really matters. Men need information, news, mental stimulus, entertainment. For the first time in 5,000 years, a technology now exists which can halt and perhaps even reverse the flow from the country to the city. The social implications of this are profound; already, the Canadian Government has discovered that it has to launch a satellite so that it can develop the Arctic. Men accustomed to the amenities of civilisation simply will not live in places where they cannot phone their families, or watch their favourite TV show. The communications satellite can put an end to cultural deprivation caused by geography. It is strange to think that, in the long run, the cure for Calcutta (not to mention London, New York, Tokyo), may lie 22,000 miles out in space . . .

“The SITE project will run for 1 year, and will broadcast to about 5,000 TV sets in carefully selected areas. This figure may not seem impressive when one considers the size of India, but it requires only one receiver to a village to start a social, economic and educational revolution. If the experiment is as great a success as Dr. Sarabhai and his colleagues hope (and deserves), then the next step would be for India to have a full-time communications satellite of her own. This is, in any case, essential for the country’s internal radio, telegraph, telephone and telex services . . .

“Kipling, who wrote a story about “wireless” and a poem to the deep-sea cables, would have been delighted by the electronic dawn that is about to break upon the sub-continent. Gandhi, on the other hand, would probably have been less enthusiastic; for much of the India that he knew will not survive the changes that are now coming.

SCHOOLMASTER SATELLITE

“One of the most magical moments of Satyajit Ray’s exquisite Pather Panchali is when the little boy Apu hears for the first time the Aeolean music of the telegraph wires on the windy plain. Soon those singing wires will have gone forever; but a new generation of Apus will be watching, wide-eyed, when the science of a later age draws down pictures from the sky—and opens up for all the children of India a window on the world.”

A. C. Clarke

ACKNOWLEDGMENTS

Many scientists, engineers, and technicians, too numerous to mention by name, have contributed to these volumes. Engineers at Fairchild Space and Electronics Company and Westinghouse Defense and Electronic Systems Center composed the chapters from material supplied by subsystems designers of the various systems and experiments, and have worked closely with the editors to complete this report. They have the editor's gratitude.

In particular, thanks go to Mr. Ralph Hall at Fairchild Space and Electronics Company and Mr. James Meenen of Westinghouse Defense and Electronic Systems Center for their patient cooperation, thorough review, and constructive comments and suggestions.

INTRODUCTION

ATS-6 was the final satellite in a series of six of the Applications Technology Satellite Program of the National Aeronautics and Space Administration. It was designed and built by Fairchild Space and Electronics Company, Germantown, Maryland, under NASA Contract NAS5-21100 from NASA Goddard Space Flight Center.

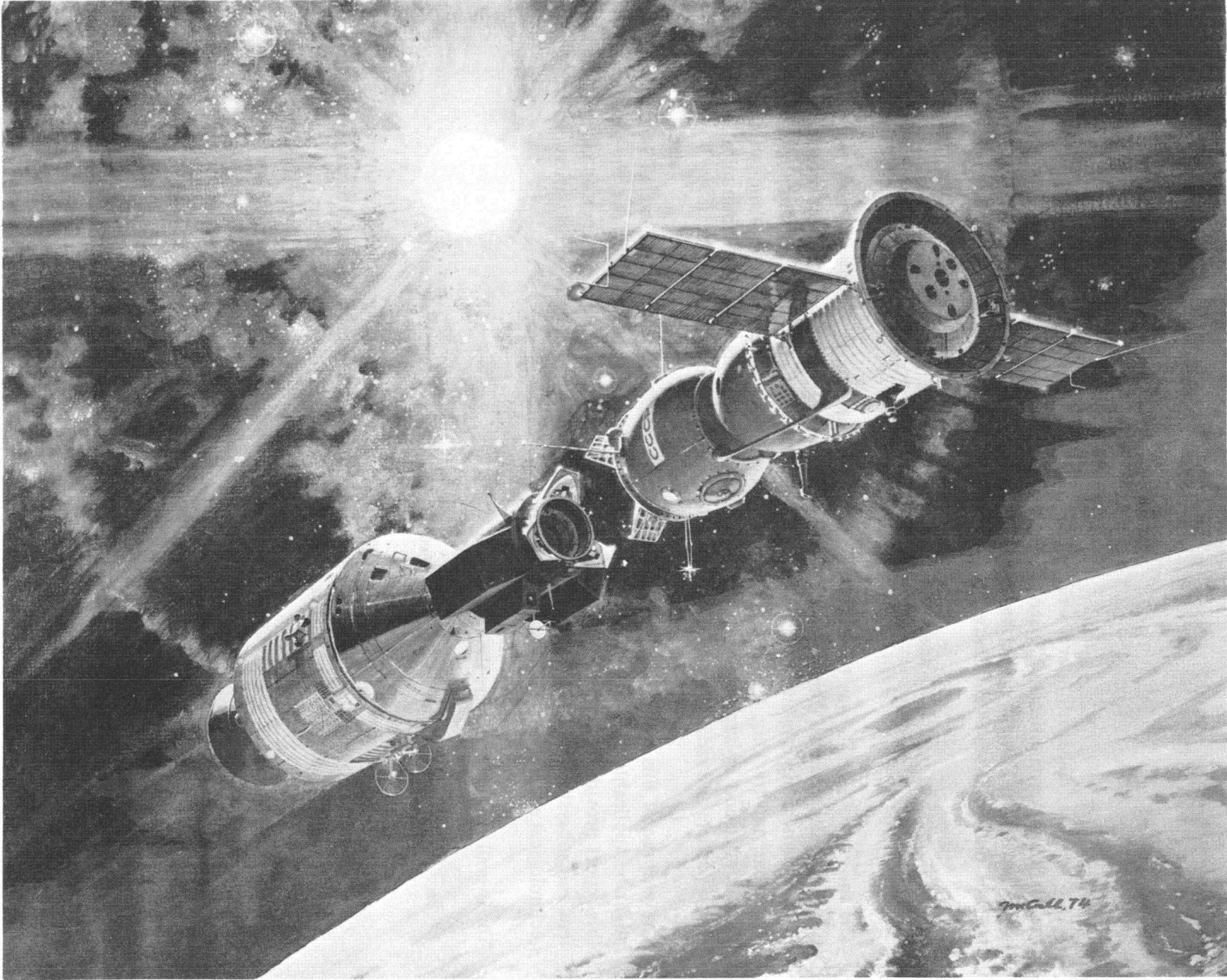
At the time of its launch, it was the largest and most powerful communications satellite to go into orbit.

The mission of ATS-6 was to demonstrate and evaluate the application of new technologies for future satellite systems. This it accomplished by demonstrating the first direct-broadcast television from geosynchronous orbit; by demonstrating many new communications technologies; by relaying data from, and tracking, low-orbiting satellites; by relaying communications and positions of ships and aircraft; and by supporting a variety of other experiments involving communications, meteorology, particle and radiation measurements, and spacecraft technology.

The purpose of this report is to document the lessons learned from the 5-year ATS-6 mission that might be applicable to spacecraft programs of the future. To satisfy this purpose, the six volumes of this report provide an engineering evaluation of the design, operation, and performance of the system and subsystems of ATS-6 and the effect of their design parameters on the various scientific and technological experiments conducted.

The overall evaluation covers the following:

- A summary of the ATS-6 mission objectives, operations, and results
- A summary description of the spacecraft system and subsystem requirements, the designs evolved to meet these requirements, and special analyses and ground testing performed to validate these designs and to confirm the flight integrity of the spacecraft
- A comparative evaluation of the 5-year performance and operations in orbit relative to those specified and demonstrated during ground tests prior to launch
- A summary of anomalies that occurred in the hardware, probable causes, and recommendations for future spacecraft systems
- A summary evaluation of the various technological and scientific experiments conducted
- A summary of conclusions and recommendations at the spacecraft system and subsystems levels that address considerations that might be relevant to future spacecraft programs or similar experiments.



Apollo-Soyuz Test Program

Part A
Communications Subsystem

CHAPTER 1 INTRODUCTION

FUNCTIONAL REQUIREMENTS

The functional requirements for the ATS-6 communications subsystem were dictated by the need to support a variety of communication, technological and scientific experiments as well as special investigations including spacecraft orbit determination. The areas of support were as follows:

Communication and Technological Experiments

1. Health, Education, Telecommunications (HET)
2. Satellite Instructional Television Experiment (SITE)
3. Television Relay Using Small Terminals (TRUST)
4. Position Location and Aircraft Communications Experiment (PLACE)
5. Tracking and Data Relay Experiment (TDRE)
6. Radio Frequency Interference Measurements Experiment (RFIME)
7. Millimeter Wave (MMW) Propagation Experiment
8. Very High Resolution Radiometer (VHRR)
9. Spacecraft Attitude Precision Pointing and Slewing Adaptive Control (SAPPSAC)
10. Comsat Propagation Experiment (Comsat)

Scientific Experiments

1. Radio Beacon Experiment (RBE)
2. Environmental Measurements Experiments (EME)
3. U.S./U.S.S.R. Magnetic Correlation Experiment (Mage)

Special Investigations

1. Television Camera Reflector Monitor
2. Interferometer High Data Rate Acquisition System
3. Range and Range Rate

In addition to the foregoing, the communications subsystem served as backup for the telemetry and command subsystem and provided the means for monopulse tracking.

The communications transponder was a major component in the communications subsystem and permitted simultaneous operation in up to three radio frequency (rf) bands on separate channels. Each channel was selectable to be 12 MHz or 40 MHz wide with the latter satisfying the television bandwidth requirements. Additionally, as in the Radio Frequency Interference (RFI) Experiment, the whole 500-MHz allocation in C-band was made available by use of the rfi transponder.

The communications subsystem satisfied most requirements by means of frequency translation through the transponder; however, some experiments required an interface at baseband. For the radiometer and interferometer modes, this was accomplished through the wideband data unit.

All up and down frequency conversion was accomplished in a single step process; the appropriate local oscillator signal was derived from the spacecraft master oscillator. In the coherent mode, the master oscillator was phase locked to the C-band signal carrier transmitted from the ground to the spacecraft. In the noncoherent mode, the master oscillator was allowed to free run.

The communications subsystem required the ability to broadcast television signals to small ground terminals, as in the TRUST experiment. This was only possible with the very large effective isotropic radiated power (e.i.r.p.) afforded by the large 9.14-m diameter parabolic reflector and the versatility of a multiband transponder. For wide-angle Earth coverage communications, Earth coverage horns (ECH) were needed for both reception and transmission at C-band.

Typical functions of each prime-focus feed (PFF) antenna mode may be seen by referring to Table 1-1. As shown in this table, most experiments involved the C-band Earth coverage horns. The PFF permitted operation with spot beams and, in the case of the Tracking and Data Relay Experiment, the S-band array permitted selection of one of 21 possible spot beams. Table 1-2 summarizes a number of the key functional modes involving the transponder. The composite shows the range of functional requirements imposed upon the communications subsystem by the ATS-6 experiments.

The communication subsystem was designed and built by the Ford Aerospace and Communications Corporation under the direction of the prime contractor, Fairchild Space and Electronics Company of Fairchild Industries, Inc.

Table 1-1
Prime-Focus Feed and Earth Coverage
Horn Pattern Usage

Mode	Typical Experiment Application	Nominal Frequency (MHz)
PFF C-Band Receive	Monopulse, HET RFIME	6150, 6350 5925-6425
PFF C-Band Transmit	HET, TRUST	3750, 3950
ECH C-Band Receive	TDRE, SITE PLACE, MMW HET Command Backup	6350, 6150, 5950
ECH C-Band Transmit	TDRE, PLACE, HET MMW, TRUST Radiometer RFIME	3750, 3950, 4150 3700-4200
PFF S-Band Receive (Scan) (On Axis)	TDRE TDRE, Monopulse	2250 2250
PFF S-Band Transmit (Scan) (On Axis) (HET Elements)	TDRE TDRE HET	2075 2075 2569, 2670
PFF L-Band Receive (Pencil) (Fan)	PLACE PLACE	1650 1650
PFF L-Band Transmit (Pencil) (Fan)	PLACE PLACE	1550 1550
PFF UHF Transmit	SITE, TRUST	860
PFF VHF Receive	Monopulse Command	150 148, 154
PFF VHF Transmit	Telemetry	136, 137

Table 1-2
Typical Communication Subsystem Functions

Function	Parameter or Setting	Typical Application
Channel Bandwidth	40 MHz	HET
	12 MHz	PLACE
	500 MHz	RFIME
Narrow Band	1.5 MHz	PLACE
C-Band Transmitter Power	20 watts nominal	Single Carrier
	40 watts nominal	Weak link (dual TWTA)
UHF Transmitter Power	80 watts	SITE, TRUST
	40 watts	(Commandable settings)
	20 watts	
	10 watts	
I. F. Mode	Remodulation	PLACE (multiple access)
	Frequency translation	HET
	Linear	Special
Reference Oscillator	Coherent operation	Interferometer
I. F. Beacon	ON	Ground Tracking
Wideband Data Unit	ON	Radiometer, interferometer, telemetry, TV camera monitor
I. F. Discriminator	IN	Command data

CHAPTER 2

FUNCTIONAL DESCRIPTION

INTRODUCTION

A simplified block diagram of the communication subsystem is shown in Figure 2-1. It was capable of receiving on the C, S, L, or very high frequency (vhf) bands while simultaneously transmitting on the C, S, L, and/or ultrahigh frequency (uhf) bands. Table 2-1 lists the nominal performance parameters. The communications package was functionally divided into five major areas: antennas, receivers, intermediate frequency (i.f.) amplifiers, frequency synthesizer, and transmitters. Each major area contained self-sufficient circuitry along with redundancy for each frequency band and could be commanded to provide frequency translation from any receive band to any transmit band.

The antennas were in two major categories: the Earth coverage horns and the prime-focus feeds using the 9.14-meter diameter parabolic reflector. The two Earth-coverage horns (one 4 GHz and one 6 GHz) were used only with the C-band transmitters and receivers. The wide field-of-view of the Earth coverage horns allowed continuous wide-band data communication with the spacecraft during experiments requiring a change of spacecraft attitude. This lack of restricted pointing requirements made the Earth-coverage horn the normal antenna for most transmission of experiment data. The spacecraft primary telemetry and command was provided at vhf.

The high gain antenna system consisted of the 9.14-meter diameter deployable parabolic reflector and a series of prime-focus feeds that had a variety of feed options for each band.

The receiver included preamplifiers, monopulse modulators, mixers, filters, and the required interconnecting circuits. The C- and S-bands had redundant preamplifiers. The vhf receiver included only a preamplifier with no mixer, since the i.f. pass band was adequate to pass the operating frequency without conversion.

The i.f. amplifier section consisted of three similar amplifiers, selected by i.f. input and output switch matrices. Each amplifier operated at 150 MHz with a selectable bandwidth of 40 or 12 MHz.

The synthesizer used a single frequency (100 MHz) master oscillator from which all local oscillator frequencies were synthesized. It could operate in the coherent mode, in which the voltage controlled crystal oscillator (VCXO) and all the frequencies derived from it, were phase locked to the received carrier, or in the noncoherent mode in which case the VCXO was allowed to free run (the input to the VCXO was clamped to a reference voltage).

The transmitter portion of the system consisted of the upconverters, the rf drivers and power amplifiers for C-band, S-band, L-band, and uhf. Each band had a transmitter chain with commandable redundant circuitry and output switching to allow operation with the selected feed.

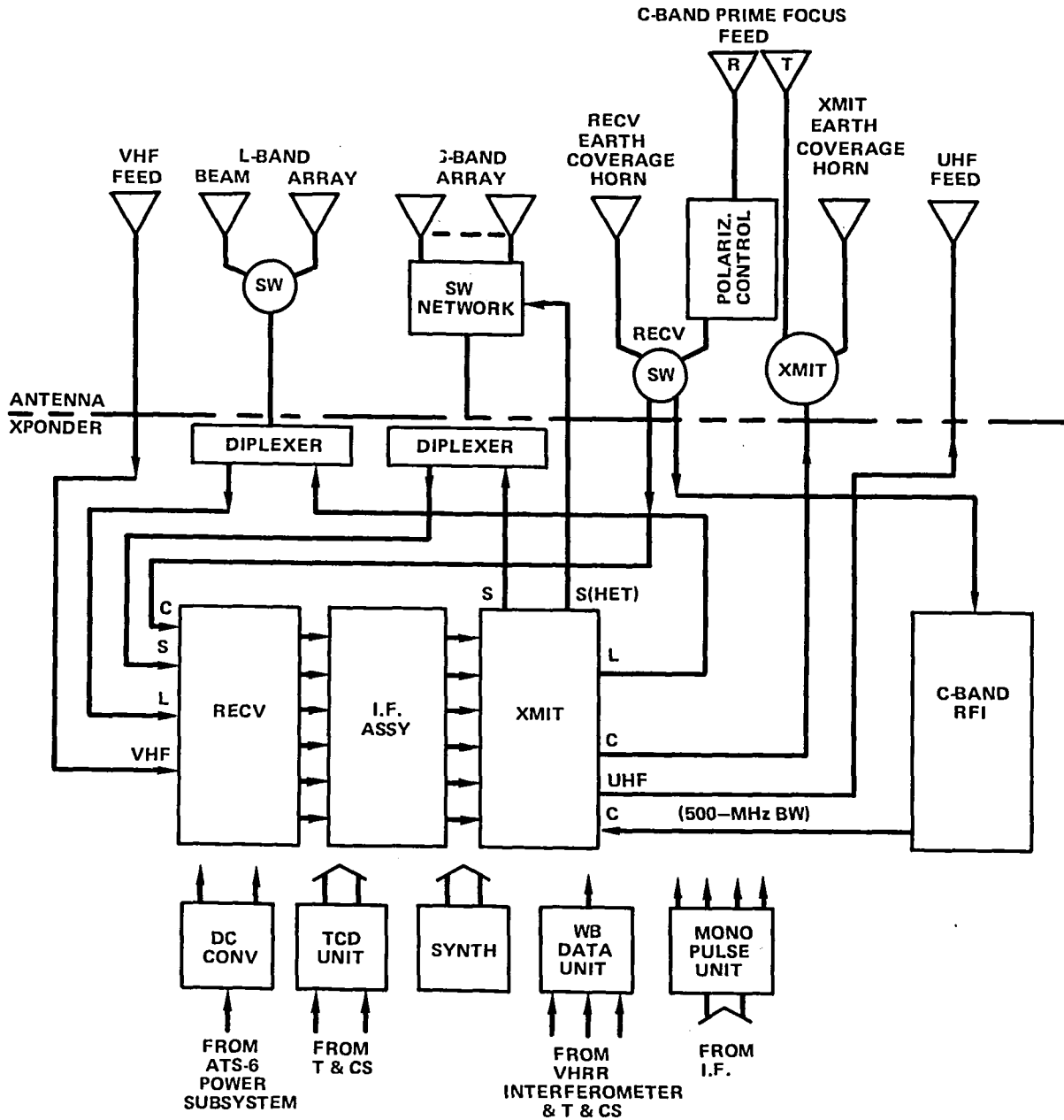


Figure 2-1. Simplified Communication Subsystem Block Diagram

Table 2-1
Communication Subsystem Characteristics

Mode	User	Nominal Freq. (MHz)	Bandwidth (MHz)	Polarization	Antenna FOV (°)	Peak Antenna gain (dB)	RECEIVER		TRANSMITTER		
							Min. G/T Over FOV (dB/K)	G/T Peak (dB/K)	XMTR Output Pwr. (watts)	Min. E.I.R.P. Over FOV (dB/W)	E.I.R.P. Peak (dB/W)
<u>RECEIVE</u> 9.14-m Parabolic Antenna C-band	HET	6350	40	Linear	0.4	49.0	10.5	13.5	-	-	-
	MMW	6150	12								
	Monopulse RFIME	6150	500	Horiz., Vert., RCP	0.4	48.5	N/A	N/A	N/A	N/A	N/A
S-band • Scan • On axis	T&DRE	2250	40	RCP	9	40.5	-	-	-	-	-
	T&DRE	2250	12	RCP	-	40.5	-	9.5	-	-	-
	Monopulse		40								
L-band • Pencil beam • Fan beam	PLACE	1650	12	RCP	1.5	38.5	2.5	5.5	-	-	-
	PLACE	1650	40, 12	RCP	1 x 7.5	31.5	-5.0	-2	-	-	-
VHF	Monopulse	150	6	RCP	15	17	-20	-18	-	-	-
	Command	148.26, 154.2	0.03	RCP	15	17	-20	-18	-	-	-
<u>Horn Antenna</u> C-band	T&DRE, SITE, PLACE, MMW ATSR	6350 6150 5950	40 12	Linear	20	16.5	-20	-17	-	-	-

FUNCTIONAL DESCRIPTION

Table 2-1
Communication Subsystem Characteristics (continued)

Mode	User	Nominal Freq. (MHz)	Bandwidth (MHz)	Polarization	Antenna FOV (°)	Peak Antenna gain (dB)	RECEIVER		TRANSMITTER		
							Min. G/T Over FOV (dB/K)	G/T Peak (dB/K)	XMTR Output Pwr. (watts)	Min. E.I.R.P. Over FOV (dB/W)	E.I.R.P. Peak (dB/W)
<u>TRANSMIT</u>											
<u>9.14-m Parabolic Antenna</u>											
C-band	HET	3750	40	Linear	0.6	46.0	-	-	21	51.5 (1)	54.5 (1)
	MMW	3950								47.2 (2)	50.1 (2)
S-band	HET	2569.2	40	LCP	0.9 (3)	43.2	-	-	12	44.5 (3)	53
		2670.0	40						12		
• On axis • Scan	T&DRE	2075	12	RCP	-	39.5	-	-	20.0		50.5
	T&DRE	2075	12	RCP	9	39.0	-	-	20	48.0	-
L-band • Pencil beam • Fan beam	PLACE	1550	40, 12	RCP	1.5	38.5	-	-	40	49	51
	PLACE	1550	40, 12	RCP	1 X 7.5	31.5	-	-	40	42	45
UHF	SITE TRUST	860	40	RCP	3	33.0	-	-	80, 40, 20 10 (4)	48	51
VHF	TLM, EME	136.23 137.11	2	RCP	15	17	-	-	2.0	17	20
<u>Horn Antenna</u>											
C-band	T&DRE, PLACE, BEACON	3950	40	Linear	10	16.6	-	-	21.0	25.0 (1)	28.0 (1)
	MMW	3750								20.7 (2)	23.7 (2)
	VHRR	4150									
	HET, TRUST	3950	500	Linear	10	16.7	-	-	20.0		

(1) Single carrier operation; (2) Dual carrier operation; (3) Either of two offset beams; (4) Redundant transmitter rated 1.6 dB higher.

PRIME-FOCUS FEED AND EARTH COVERAGE HORNS

The prime-focus feed (PFF) comprised a number of feed elements covering the vhf, uhf, L-, S-, and C-frequency bands. It also included monopulse comparators, a polarization control system, power dividers, switches, hybrids, and filters. The assembly of these elements into the communication module, and the placement of the Earth coverage horns on the Earth-viewing face of the experiment module is illustrated in Figure 2-2. The arrangement of the feed elements on the feed plate is shown in Figure 2-3, with an enlargement of the center portion shown in Figure 2-4.

The central position was occupied by both a C-band monopulse feed and an S-band annulus that surrounded it. The C-band feed provided a pencil beam coincident with the spacecraft mechanical axis and had the highest antenna gain. The S-band annulus also formed an axial beam. The L-band, HET, and S-band scan feeds were offset from the spacecraft mechanical axis and formed beams whose boresights were offset from the spacecraft Z-axis. The uhf and vhf feeds were symmetrically disposed about the spacecraft mechanical axis and formed beams with boresights coincident with the spacecraft Z-axis.

C-Band Prime-Focus Feed and Earth-Coverage Horns

An rf schematic for the C-band PFF circuitry and switching arrangement with the Earth-coverage horns is shown in Figure 2-5. The C-band prime-focus feed contained two transmit ports, four receive ports, and a conical receive feed horn. The two transmit ports were fed by a power divider and provided linear polarization with the E-plane parallel to the spacecraft north-south axis. The four receive ports located on the east and west sides of the C-band array were fed to a comparator to provide pitch and roll error signals for C-band monopulse operation. The center horn of the feed provided the sum channel for monopulse operation, the receive channel for the C-band communication subsystem, and the input to the rfi transponder. The center horn channel contained a polarization control switch that provided either of two orthogonal linear polarizations or right or left circular polarization. The nonlatching polarization control switch had a fail-safe or normal position that put it in the east-west linear polarization.

RF ferrite switches allowed the C-band transmitters and receivers to be switched independently to either the prime-focus feed or the Earth-coverage horn. When using the prime-focus feed receive path, the center (circular) receive port was used to feed the C-band signal to the C-band transponder. When transmitting at C-band using the prime-focus feed, the signal was routed by one of the alternate paths through the redundant transmit switch to a power divider that split the signal and radiated it through the two transmit ports of the prime-focus feed. Since each of the switches was operated independently, it was possible to receive through the prime-focus feed and transmit through the Earth-coverage horn or vice versa.

When the antenna receive select switch was in the Earth-coverage horn position for the C-band transponder, the rfi transponder was connected to the center port of the prime-focus feed through the polarization switch.

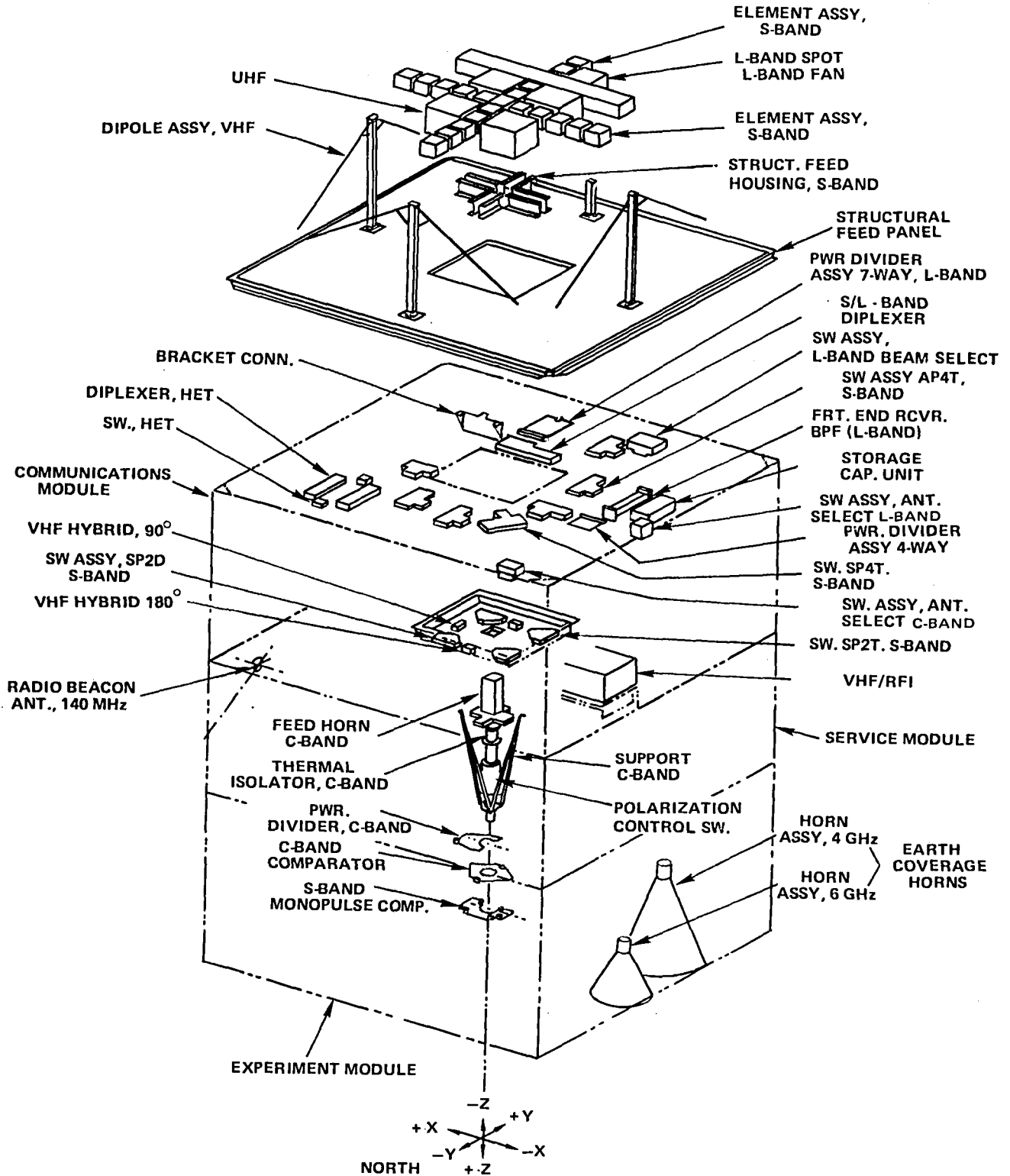


Figure 2-2. Prime-Focus Feed Components and Earth-Coverage Horns

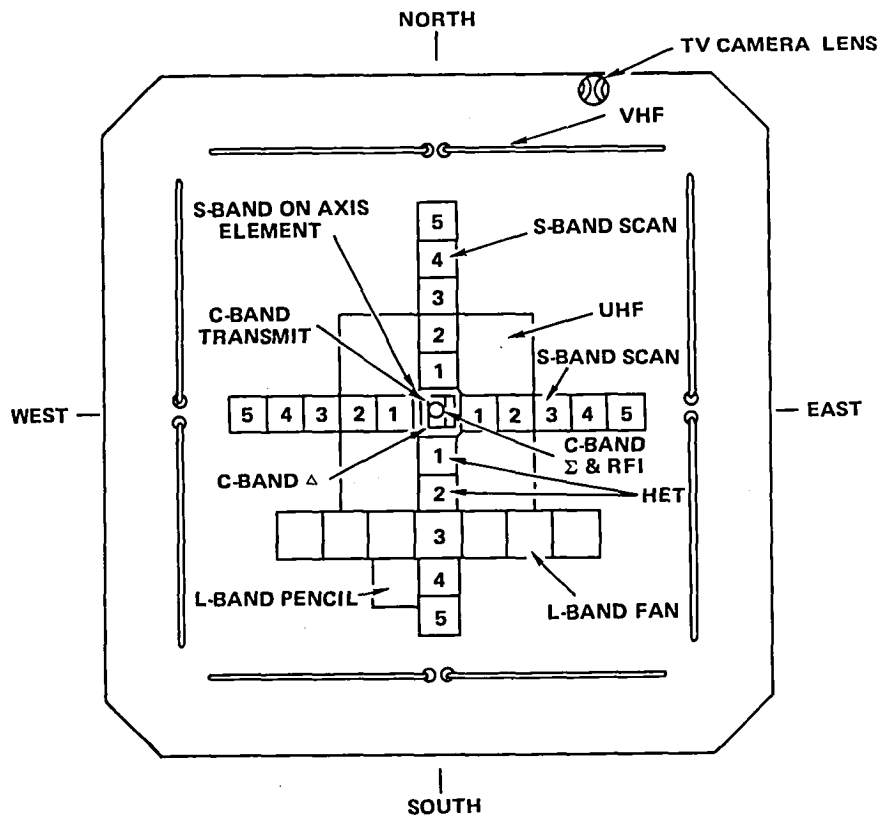


Figure 2-3. Physical Arrangement of Composite Feed Element
(Feed Plate viewed from reflector side)

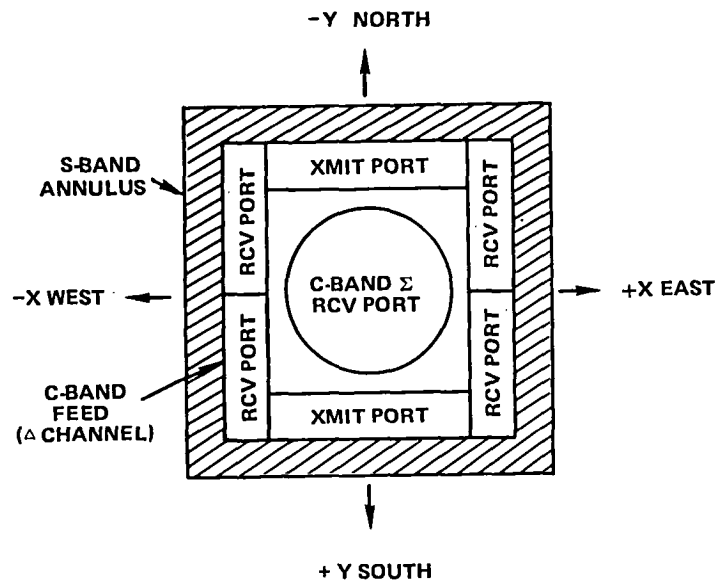


Figure 2-4. Prime-Focus Feed (Center Element)

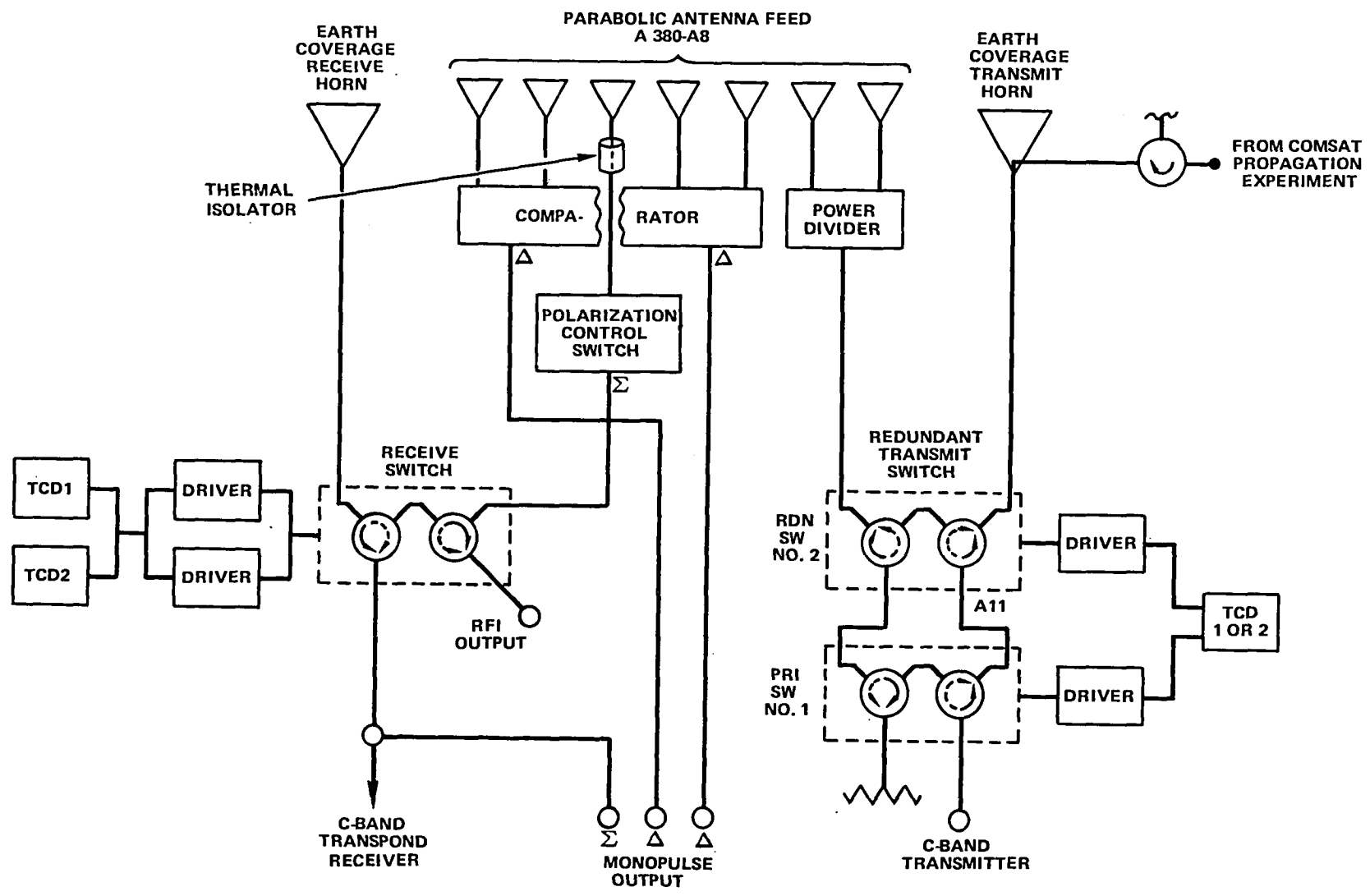


Figure 2-5. C-Band Antenna Unit RF Schematic

In the monopulse mode of operation, the four receive ports of the C-band prime-focus feed were used to generate delta roll and delta pitch information for the monopulse processor, while the center horn of the prime-focus feed served as the reference or sum channel. With the receiver select switch in this position, the sum channel was also fed to the communications subsystem receiver while the Earth-coverage horn was fed to the rfi transponder. In the monopulse mode of operation, the polarization switch was placed in the normal linear east-west plane.

The transmit Earth-coverage horn included a separate feed (mounted 90 degrees from the normal feed) for use by the Comsat Propagation Experiment. The Comsat C-band downlink polarization was orthogonal to the communications subsystem.

S-Band Prime-Focus Feed

The S-band feeds were configured in an X-pattern, the arms of which were coincident with the X-axis (east-west) and Y-axis (north-south) of the spacecraft. As shown in Figure 2-3, there were five elements on each of the four sides of the annulus element. The annulus and the elements on the north, east, and west sides of the annulus, and the two outermost elements on the south side of the annulus (S4 and S5) were used for S-band functions only. The remaining south side elements were shared between the S-band and HET (S1 and S2), and the L-band feed (S3). The annulus, a ring-type port, was located on the periphery of the C-band horn centered about the spacecraft Z-axis. The annulus and the elements N1, S1, E1, and W1 formed the S-band monopulse feed.

The 21 elements of the S-band feed were all right-hand circularly polarized at the S-band transmit and receive frequencies of 2075 MHz and 2253 MHz, respectively. Elements S1 and S2, when transmitting at either of the two HET band frequencies (2569.2 MHz or 2670 MHz), were left-hand circularly polarized.

As shown in Figure 2-6, the selection of an element in the east-west or north-south array required the signal to go through from two to four switches, depending upon the element selected. It should also be noted that the selection of a particular element allowed both receive and transmit signals through the selected element; however, it was not possible to receive on one element and transmit on another, except for the S-band HET configuration where any S-band feed could be used to receive the uplink signal.

The S-band switches were pin diode switches that were nonlatching. These switches operated by applying a bias to the unwanted path that reflected an open circuit signal to its input. Thus, in the case of an SP4T switch, three of the diodes were biased to select the desired path. The bias voltage source came from the transponder power supply at 5 volts direct current (Vdc) that was dropped to 1.2 Vdc in the transponder command decoder (TCD). Latching relays in the TCD retained the S-band configuration last commanded, and logic circuitry provided the continuous bias voltage necessary to retain the selected path. Even when the TCD or transponder power supply was turned off, the S-band relays would retain the selected state.

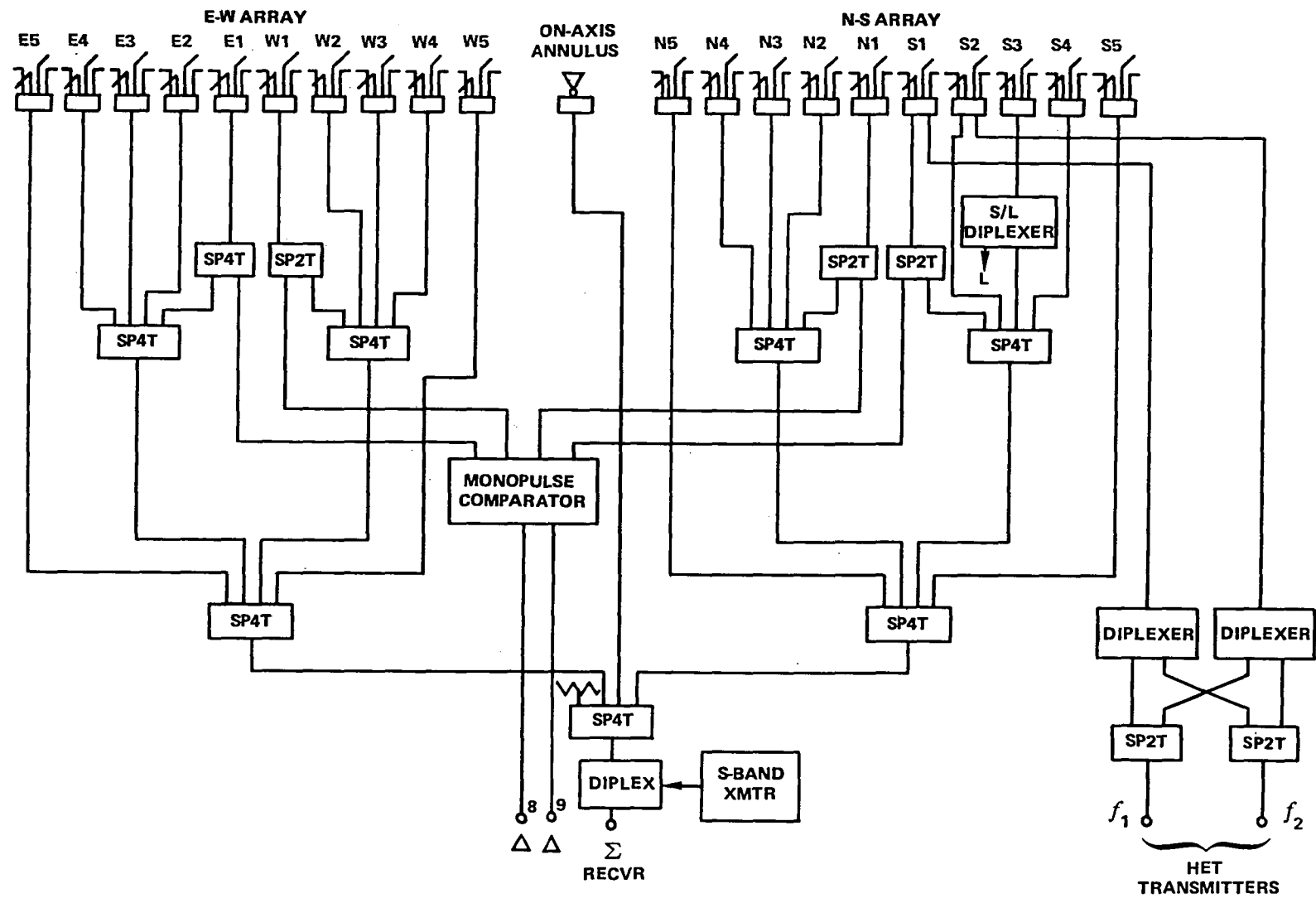


Figure 2-6. S-Band Feed RF Schematic

The S-band array was used in two modes of operation: the communications mode and the monopulse mode.

In the communications mode, any one of the 21 S-band elements (including the on-axis annulus) could be selected to provide a one- or two-way (transmit and receive) communications link. The feed element designations (north, south, east, or west) were opposite from the direction of the secondary beam that was pointed to the Earth. For example, the south elements projected the rf beam north of the spacecraft subsatellite point and the east elements projected it in a westerly pointing beam. Command designators refer to the secondary beam pointing.

In the monopulse tracking mode, the first feed (E-1, S-1, W-1, and N-1) of each arm in the S-band array was used to provide pitch and roll errors and the annulus provided the sum beam. Figure 2-6 shows how the S-band switch matrix is used to interconnect the E1, S1, W1, and N1 elements into the monopulse comparator. Here, the error signals were derived and fed to the S-band transponder for further processing, together with the sum signal. The error signals were fed to the attitude control subsystem (ACS).

The S-band feed could also transmit two simultaneous rf signals for the HET experiment. These two signals shared the same elements as the regular S-band S1 and S2 but had left-hand circular polarization (opposite sense from the regular S-band). Figure 2-6 shows that the two HET transmitters could be individually switched to either one of the elements, or both could be routed together to either element.

L-Band Prime-Focus Feed

The L-band prime-focus feed was composed of an array of seven feeds offset approximately 3 degrees in the -Y direction from the X-axis to yield a fan-shaped footprint and a separate feed to yield a single pencil beam (offset 1 degree in the +X direction, and 4 degrees in the -Y direction). The fan-shaped pattern was designed to support the PLACE experiment with coverage of the North Atlantic air traffic corridor. All feeds received and transmitted right-hand circular polarization by means of a set of cross dipoles at the back of each cavity. Duplex operation was obtained by the antenna select switch and bandpass filter/diplexer allowing simultaneous transmission on 1550 MHz and reception on 1650 MHz using either fan or pencil beam feeds.

The center element of the fan beam was shared with the S-3 element of the S-band feed. Figure 2-7 shows the S/L diplexer that was used with the S-3 element to allow transmission and reception of both S- and L-band frequencies. The single element L-band feed (pencil beam) could be selected instead of the fan beam by using the beam-select switch shown in the figure.

VHF Prime-Focus Feed

The vhf prime-focus feed consisted of a four-element dipole array. As shown in Figure 2-3, the four elements of the vhf prime-focus feed array were equally spaced around the outer edges of the prime focus feed assembly. The vhf prime-focus feed operated at transmit frequencies of 136/137 MHz (telemetry) and receive frequencies of 150 MHz (monopulse) and 148/154 MHz (command).

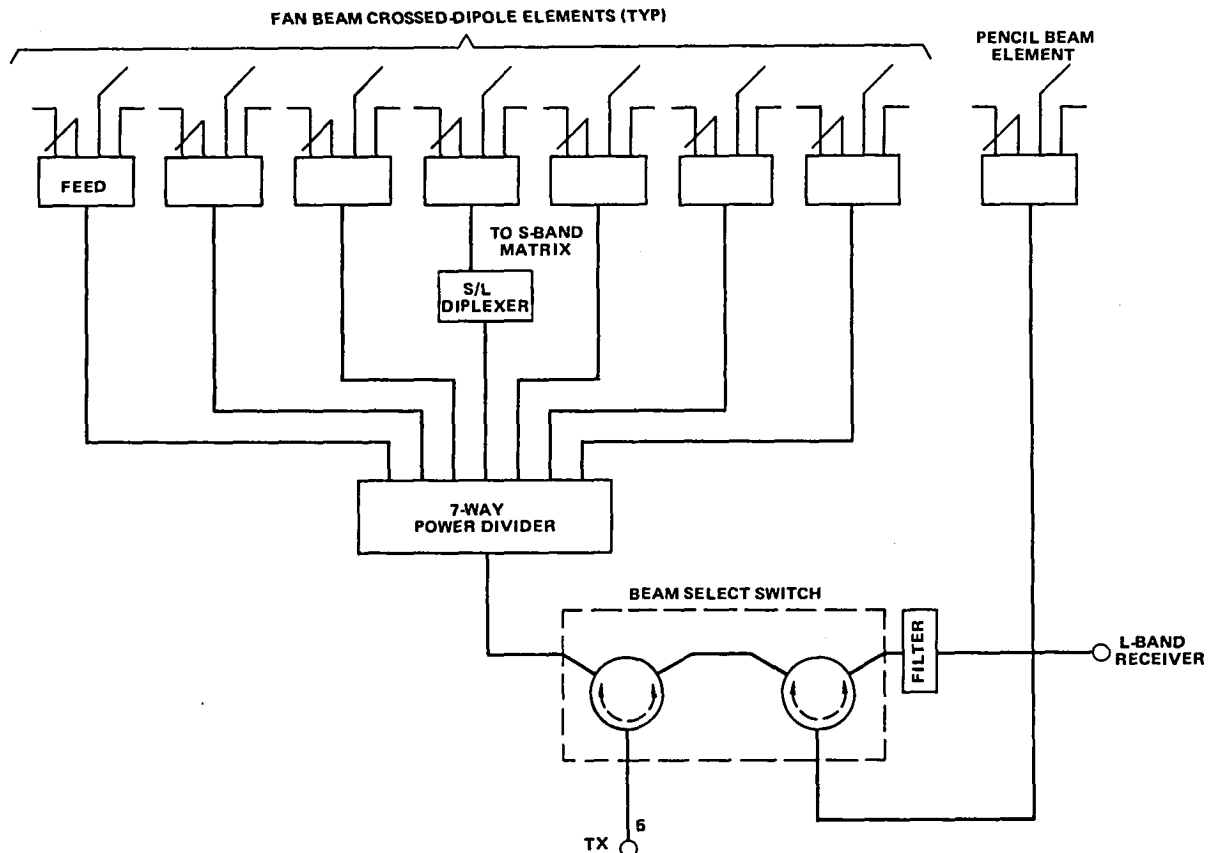


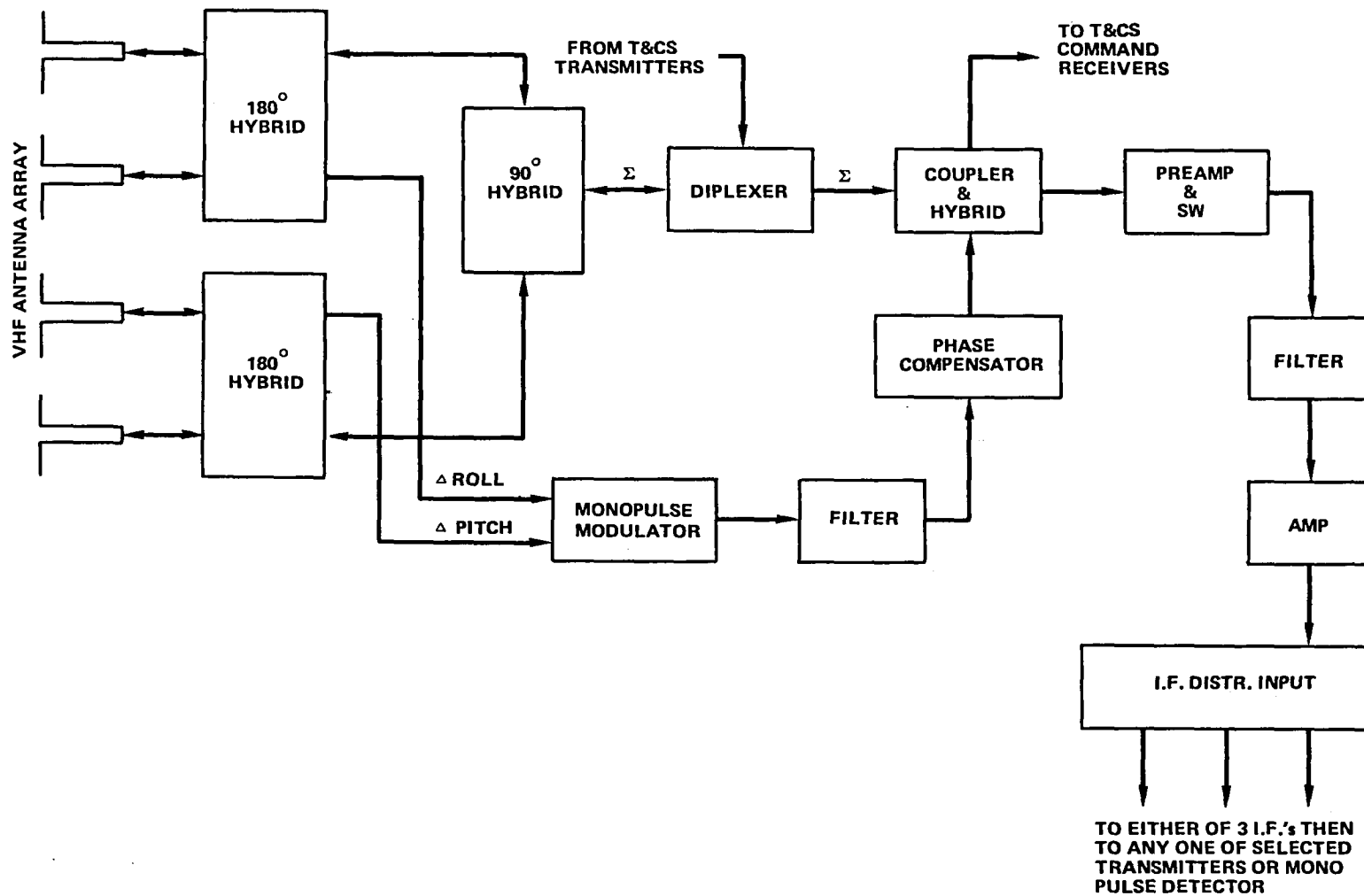
Figure 2-7. L-Band RF Schematic (Shown Selected to Fan Beam)

When used in the communications mode, the vhf prime-focus feed provided an alternative path for the vhf links used by the telemetry and command subsystem. The vhf dipole array was summed as shown in Figure 2-8 and the sum signal fed to a vhf diplexer in the communications module where the telemetry and command signals were separated into two signal lines. One line (136/137 MHz) was tied directly to the T&CS transmitters while the other line (148/150/154 MHz) was fed to a coupler and hybrid. One output of the hybrid was fed directly to the T&CS command receivers and the other output was fed first to a preamplifier and filter (8-MHz bandpass) and then to the i.f. distribution network of the communication subsystem.

The four vhf antenna elements were fed into a monopulse comparator (two 180-degree hybrids) where the roll and pitch error signals were developed (Figure 2-8). These error signals were processed with the sum signal in the communications subsystem and, when selected by ground command, could be used by the ACS for pitch and roll attitude control.

UHF Prime-Focus Feed

The uhf prime-focus feed consisted of a four-element, cavity-backed crossed-dipole array. Each of the four elements were driven from a four-way power splitter. The elements were equally spaced around the center feed of the prime-focus feed (Figure 2-3), resulting in an on-axis beam. The uhf



FUNCTIONAL DESCRIPTION

Figure 2-8. VHF RF System Simplified Block Diagram

array produced a right-hand circularly polarized beam and operated at a transmit frequency of 860 MHz.

COMMUNICATIONS TRANSPONDER

The signal interface diagram in Figure 2-1 identifies the major components of the transponder. Receivers at the C-, S-, and L-bands were downconverted to a common i.f. frequency of 150 MHz. Up to three different receive channels could then be fed to the three i.f. amplifiers for further processing. If the signal was to be retransmitted, it was fed to the appropriate upconverter to be transmitted by the C, and/or S, L, HET or uhf transmitters. Information originating within the spacecraft (such as the VHRR experiment data) was fed to the wideband data unit where it was routed to the selected upconverter and transmitter. Command signals, usually transmitted on a vhf carrier, were fed to a selectable discriminator circuit located in each of the i.f., amplifiers. Monopulse data, received at C, S, or vhf, were fed to a monopulse processor and then to the ACS and/or telemetered by the T&CS. A redundant frequency synthesizer provided local oscillator frequencies for downconverters and upconverters except for the HET and C-band rfi experiments that had their own local oscillators. (The uhf local oscillator was also a separate oscillator that was physically located within the synthesizer package.) Figure 2-9 provides a functional block diagram including nominal input and output signal levels.

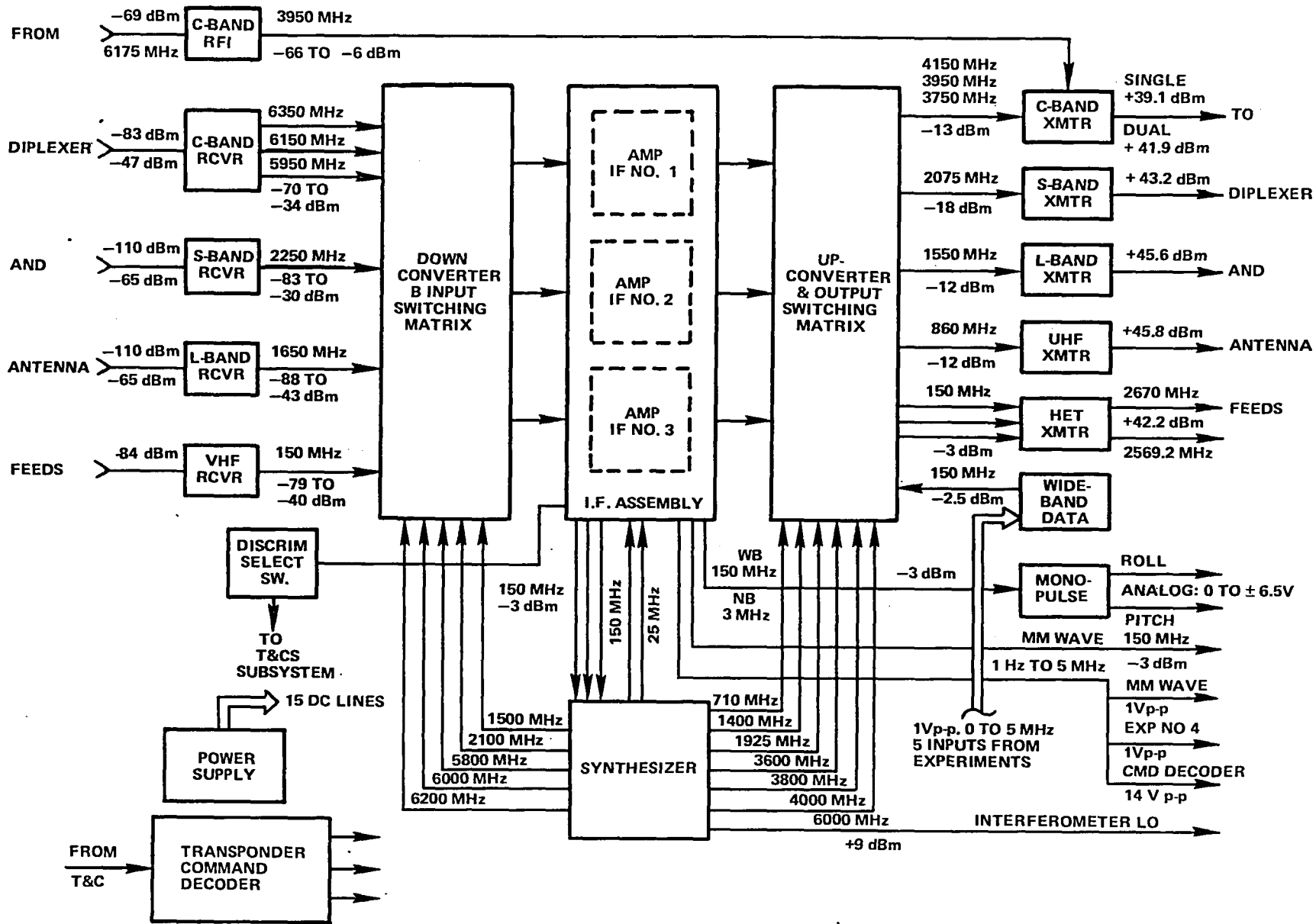
Receivers

The receiver assembly included preamplifiers, monopulse modulators, mixers, appropriate filters, and interconnecting circuitry. Preamplifiers were provided at C-, S-, L-band and vhf to achieve maximum transponder signal-to-noise ratio. The C-band preamplifiers were tunnel diode types with a noise figure of 5.5 dB and a gain of 17 dB. The S-band and L-band preamplifiers used transistors with noise figures of 3.7 dB and 4.4 dB, and gains of 30 dB and 25 dB, respectively. Redundancy was accomplished by providing selectable backup amplifiers for the C- and S-bands and output switching systems to allow operation of each receiver with any of three similar i.f. sections. The L-band and vhf receivers had no backup preamp, because of their projected limited use.

C-Band Receiver

When the C-band receiver was switched to the prime-focus feed, the rfi transponder was automatically switched to the Earth coverage horn and vice versa. Separate commands selected and turned on either the prime or backup preamplifiers. Another separate command turned off power to both preamplifiers but left the input and output select switches as last configured. If one of the preamplifiers was already on and the second one was commanded on, the second command would automatically turn off the power to the first preamplifier.

The C-band preamplifiers were broad-band devices and passed the entire 500-MHz composite C-band spectrum. The output of the preamplifier went to a triplexer that was used to separate the three C-band channels (5950, 6150, and 6350 MHz) and also to provide image suppression. Interdigital filters were used for this application.



FUNCTIONAL DESCRIPTION

Figure 2-9. Transponder Functional Block Diagram

The C-band monopulse receiver was turned on or off by separate commands. The monopulse receiver had no backup unit.

S-Band Receiver

Switching between the two S-band preamplifiers was accomplished in the same manner as the C-band (i.e., the preamplifiers were interlocked so that only one could be on at a time). Like the C-band preamplifiers, a single command set both the input and output select switches and applied power to the commanded channel. Separate commands were again used to turn the S-band monopulse receiver on or off. Unlike the C-band monopulse receiving antenna system, which was permanently connected to the four receive ports of the C-band prime-focus feed, the S-band monopulse error antenna elements (N_1 , S_1 , E_1 , and W_1) had to be selected into the monopulse comparator by a command from the ground. A single command would connect all four elements to the monopulse comparator, and would connect the annulus feed to the sum receive channel. They would remain connected until any of the other S-band antenna select commands were sent.

L-Band Receiver

The L-band receiver did not have a redundant preamplifier; therefore, only one command was required to turn on the preamplifier. Another command was used to select the antenna beam to be used (fan or pencil). The antenna selected connected both transmitter and receiver to the same antenna and a ferrite circulator switch and bandpass filter performed the diplexing function.

VHF Receiver

No antenna selection commands were necessary for the vhf receiver, since both the sum and error channels were permanently connected to the vhf prime-focus feed antenna. Since the vhf preamplifier was nonredundant, a single command was used to apply power to the preamplifier, the monopulse modulator, and to switch the sum channel into the i.f. input switching network. Because the vhf rf frequency was within the passband of the i.f., amplifiers, no down conversion was necessary.

Downconverters

The outputs of the C-, S-, and L-band receivers were fed to mixers where the appropriate frequency from the synthesizer was used to downconvert to the 150-MHz i.f. frequency. Following the downconversion, the signals were fed through a dual-stage transistor isolation amplifier prior to the switching matrix. The C-band was different because the receiver had a triplexer that separated the received frequency into three paths. Each of the signals was mixed with the appropriate local oscillator frequency to downconvert to 150 MHz and fed to the i.f. switch matrix through an isolation amplifier. This resulted in the 6350 MHz, 6150 MHz, and 5950 MHz receive frequencies all being converted to the 150-MHz i.f. frequency. Ferrite isolators, used at the mixer inputs from the receivers and the synthesizer, provided impedance matching to optimize the mixing efficiency. The vhf receive frequency was already in the i.f. passband; therefore, no frequency conversion was necessary. Power to each dual amplifier pair was applied when the appropriate command was sent to select the input of any of the three i.f. amplifiers. Regardless of which i.f. amplifier had been

selected, a single command removed power from the isolating amplifier and disconnected the switch to the i.f. amplifier input.

I.F. Input Switching Matrix

The i.f. input switching matrix allowed any of the downconverter outputs to be switched into any of the three i.f. channels. Two single-pole, double-throw relays were used in series to obtain isolation of approximately 60 dB. Any one of the commands to connect a given downconverter to any of the i.f. amplifiers initiated the dual function of selecting the appropriate switches and applying power to the downconverter dual amplifier. A separate command, associated with each downconverter, opened all switches in that downconverter path, and removed power from the dual amplifier. No interlocks were employed to prevent one or more downconverters from being connected to more than one i.f. amplifier, since no damage would be incurred; however, an impedance mismatch would result.

I.F. Amplifiers

The three i.f. amplifiers could be used independently or as standby redundant units. The primary features of each i.f. amplifier were as follows:

- Frequency translation (FT) mode (40- or 12-MHz bandwidth)

- Remodulation mode (1.5- or 5-MHz modulation bandwidth)

- Discriminator

- Monopulse driver

- Beacon (offset 30 MHz above the 150-MHz i.f.)

The i.f. amplifier unit contained a voltage controlled amplifier (VCA) to provide a constant output level (Figure 2-10). The VCA was controlled to provide up to 60 dB dynamic range. The bandwidth commands selected either a bandpass filter of 40 MHz centered at 150 MHz or a filter with a bandpass of 12 MHz centered at 156 MHz. The automatic gain control (AGC) mode-select switches and the output mode-select switches were ganged together so that when the "I.F. MODE SELECT PHASE MOD" command was sent, the AGC loop was controlled from the output of the product detector and the phase modulator output was fed to the i.f. output switch matrix. When the command "I.F. MODE SELECT NORMAL (FT)" was sent, the AGC loop was controlled from the output of the splitter amplifier (at the 150-MHz i.f. frequency) and the output of the limiter was switched to the i.f. output switch matrix.

Following bandwidth selection, the i.f. signal was amplified and split into six paths in a splitter/amplifier module. One path went to the synthesizer via the synthesizer driver module where it served as a reference for the phase-lock loop in the coherent mode of operation. Another path was to an AGC module and into the normal frequency translation mode detector. One of the paths went to a test point that, in i.f. amplifier No. 3, was used to provide an output to the C-band No. 2 upconverter for the linear-mode operation (the limiter normally used in the frequency translation

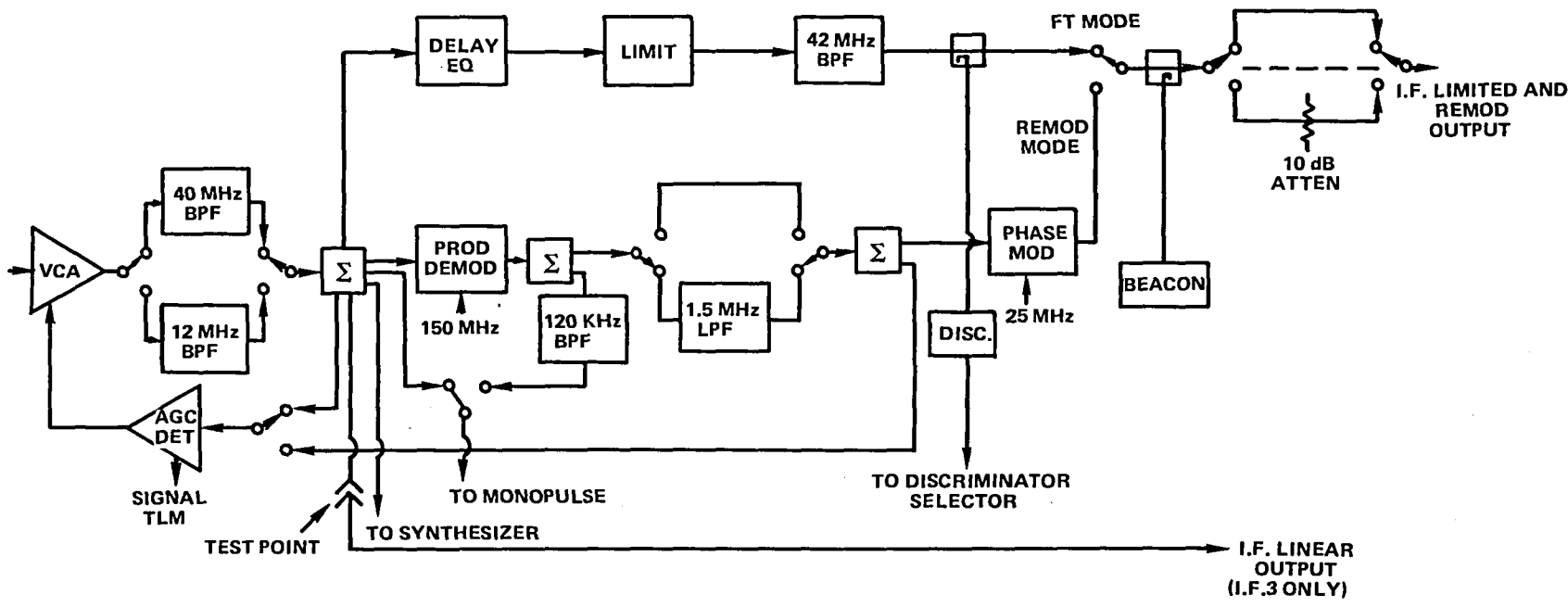


Figure 2-10. I.F. Amplifier Block Diagram

mode was bypassed). A fourth path was fed to a monopulse driver module where, after amplification, the i.f. could be selected for processing by the monopulse unit. The other two outputs were fed to the two main signal paths; to the equalizer for the frequency translation mode; and to the product detector for the remodulation mode.

Frequency Translation Mode

One output from the splitter/amplifier module was fed to the equalizer module where linear and parabolic group delay equalizing was accomplished. The signal then was fed through the limiter module where "hard limiting" was performed, so that the traveling wave tube amplifiers would operate near peak power. Limiting also reduced the amplitude modulation (AM) to phase modulation (PM) conversion to near zero. After the limiter module, the signal was fed to the filter/combiner module where it first passed through a 40-MHz filter and then to the mode select switch. Prior to this switch, a directional coupler was used to provide a signal to a discriminator module. Because of the location of this coupler, it was possible to obtain a baseband signal from the discriminator even though the i.f. remodulation mode had been selected.

Remodulation Mode

The remodulation mode was designed primarily to accommodate the multiple-carrier operation required by the PLACE experiment. The advantage of this mode was that by mixing down to baseband (without detection), the separate carriers were then used to phase modulate the downlink rf carrier. This "demodulation" followed by remodulation of the downlink reduced the intermodulation products relative to what would occur in the straight frequency translation mode (during a multiple-carrier operation). A product detector module received one of the signals from a splitter amplifier module and mixed it with a 150-MHz reference signal from the frequency synthesizer. The output signals from the mixer were between 1.5 kHz and 5 MHz. A command "I.F. LOWPASS SELECT 5.0 MHz" allowed the output to go directly to a power divider (after amplification) for distribution to the AGC detector and to the phase modulator. Another command "I.F. LOWPASS SELECT 1.5 MHz" switched in a 1.5-MHz lowpass filter. In front of the filter switch location, a signal was tapped off to a monopulse driver module. The main signal path went to a phase modulator module. The phase modulator consisted of a 25-MHz modulator followed by X2 and X3 multipliers. Following multiplication and filtering, the 150-MHz signal was fed to the filter/combiner module where it could be selected in lieu of the normal FT mode.

Beacon

A beacon oscillator was provided within the i.f. amplifier to provide an unmodulated carrier for ground station tracking purposes. The beacon oscillator could be selected on or off independently from the i.f. power ON command; however, it would not be powered unless the i.f. had been turned on. The beacon output of the i.f. was 180 MHz, approximately 19 dB down from the main i.f. output (except when the linear mode was being used) and would provide a beacon 30 MHz above the carrier frequency of whichever transmitter was being fed by the i.f. The beacon oscillator measured long term stability was on the order of 7×10^{-6} .

Discriminator

Each i.f. amplifier contained a broadband discriminator to obtain baseband data from the rf uplink. The discriminator was only used by the T&C command decoder and could be used regardless of which i.f. mode had been selected, since it was fed directly from the splitter module.

The outputs of all three i.f. amplifiers were fed to the discriminator select switch where the appropriate i.f. amplifier was selected.

Monopulse

A monopulse driver module received inputs from the splitter amplifier module (normal FT mode) and the product detector module (remodulation mode). Data derived from the monopulse modulator were fed to the monopulse unit for generation of pitch and roll error signals. In the remodulation mode, an additional AGC stage provided a narrow-band constant level output. The main purpose of this unit was to select the monopulse mode (narrow-band or wide-band) and provide an equal level to the monopulse unit.

I.F. Output Switching Matrix

The i.f. output switching matrix assembly switched the outputs from each of the three i.f. amplifiers to any one or more than one of the various upconverters and the Millimeter Wave Experiment. The i.f. output switch assembly also accepted inputs from the wideband data unit and the i.f. 3 linear output.

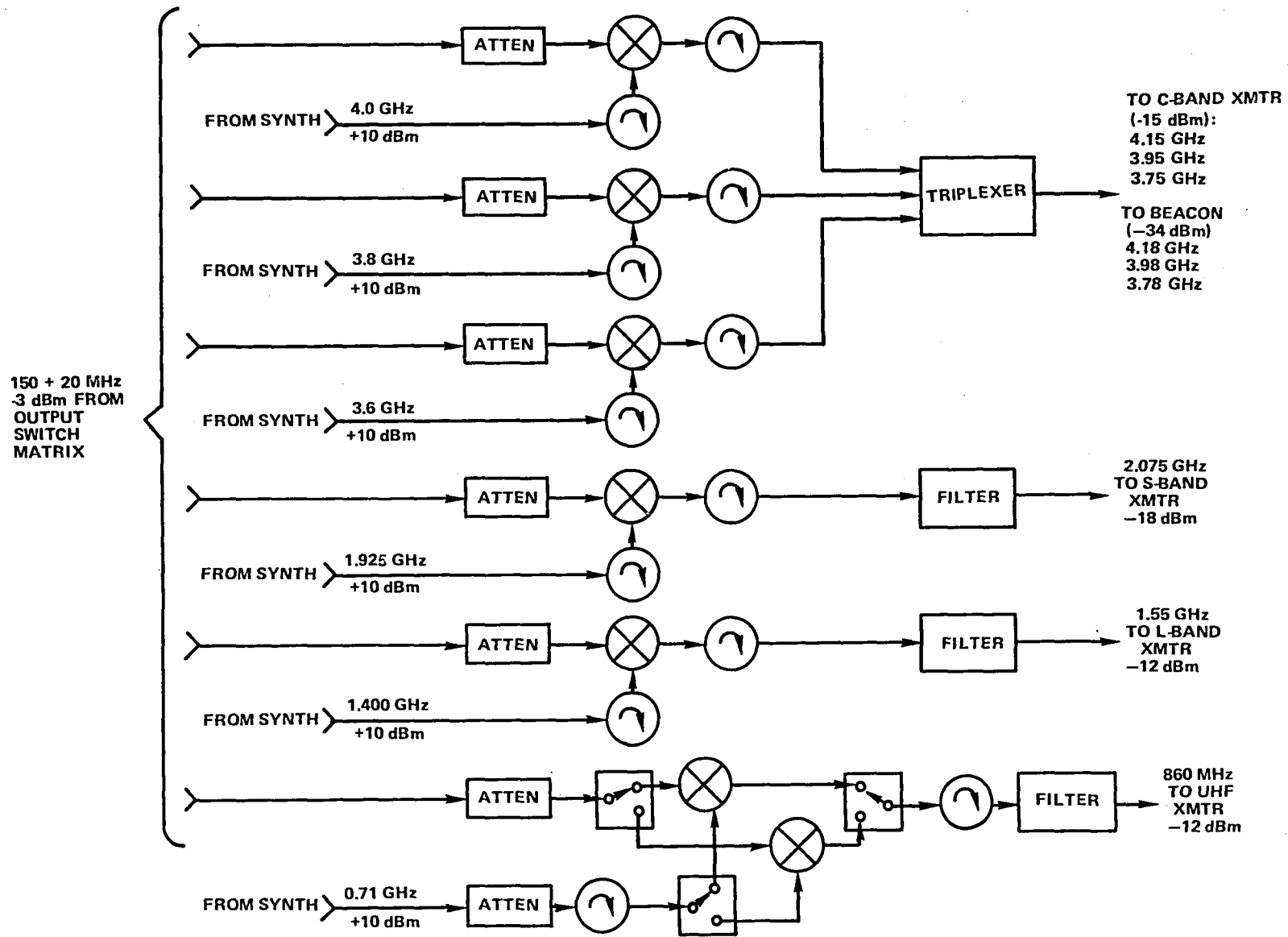
Upconverters

The main upconverter assembly (Figure 2-11) provided appropriate mixing of the 150-MHz i.f. signal with an output from the synthesizer to produce the desired rf carrier frequency. For operation at C-band, S-band (2075 MHz), and L-band, the synthesizer input was derived from the same common master oscillator and could be operated in coherent or noncoherent modes depending upon how the synthesizer had been configured. The uhf signal input for mixing with the i.f. was derived from a separate local oscillator located within the synthesizer. Ferrite circulators were used at the mixer outputs and local oscillator inputs to provide impedance matching.

The HET experiment had independent local oscillators and upconverters for generating two rf carriers at 2569.2 MHz and 2670 MHz (not shown in Figure 2-11). Each transmitter was operated independently and either could be switched to the S-1 or the S-2 HET feed or both could be fed simultaneously to either feed through the cross-switching matrix and diplexer arrangement. However, one transmitter could not feed both elements at the same time.

Transmitters

All transmitters were solid state with the exception of the C-band power amplifier (Figure 2-12). The C-band consisted of two 10-watt traveling wave tube amplifiers that could be used singly



FUNCTIONAL DESCRIPTION

Figure 2-11. Communications Subsystem Upconverters

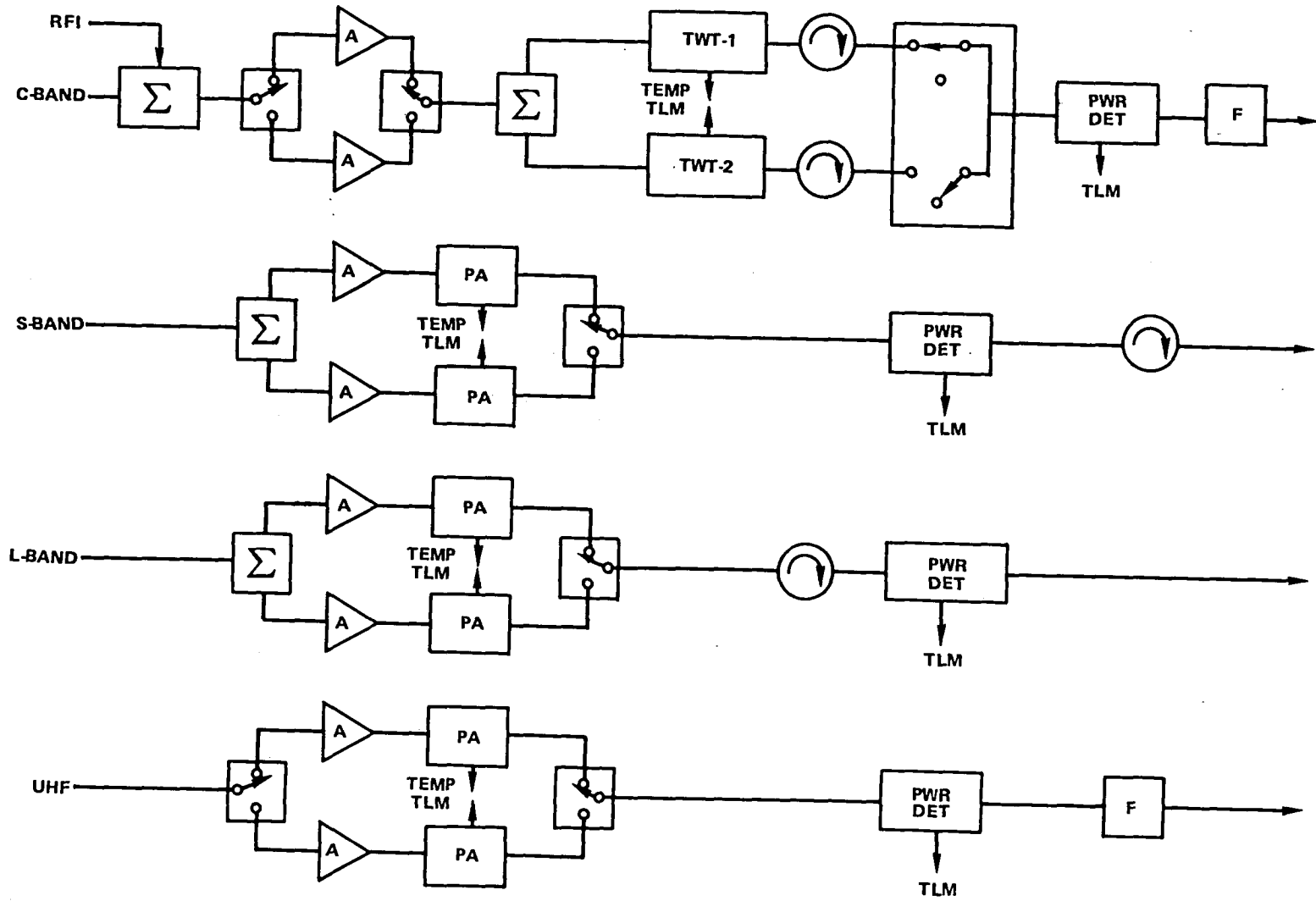


Figure 2-12. Communications Subsystem Transmitters

(normal mode), or in parallel to obtain a higher power output. All transmitters had redundant drivers and power amplifiers, except for the HET experiment where only one driver and power amplifier were available at each frequency. With the exception of uhf, all transmitters had output isolators to protect against operation in an improper configuration. The output of the uhf transmitters was hardwired to the antenna array, thus an isolator was not necessary. All other transmitter outputs could be switched to different antennas depending upon the mode of operation.

C-Band Transmitter

The input to the C-band transmitter was fed from the output of a triplexer, or from the RFI Experiment by means of a 10-dB coupler. Turn-on of the C-band transmitter was interlocked to prevent turn on and off of the traveling wave tube power amplifiers and drivers in an improper sequence. Turn on of the TWTA was accomplished prior to the drivers being turned on, and turn off of the TWT high-voltage was accomplished after driver power had been removed. Turn on sequences for each operating mode were accomplished by the use of "command groups" in the ATSOCC operational data base.

The C-band TWTA was designed to operate with one, two, or three of the C-band carriers present; however, normally only one of the three carriers would be on (3750, 3950, or 4150 MHz). When operating with the RFI Experiment, the TWTA provided a 500-MHz bandwidth rf link. The C-band transmitter configuration allowed cross-strapping of drivers with TWTA's.

S-Band Transmitter

The S-band solid state transmitters used four MSC 3905 transistor amplifier stages in parallel to obtain the required power output. Hybrids were used to assure proper power division and impedance matching and to prevent a complete failure of the transmitter if one of the transistors failed. Interlocks similar to the C-band transmitter assured proper sequence of turn on and off. Unlike C-band, each driver was tied directly to its power amplifier, and therefore cross-strapping was not possible.

L-Band Transmitter

The L-band solid state transmitters used eight MSC 3005 transistor amplifier stages tied in parallel with hybrids. Interlocking of commands was also provided and, like the S-band transmitter, drivers and PA's could not be cross-strapped between redundant units.

UHF Transmitter

The uhf transmitter was similar in configuration to the L-band transmitter; however, MSC 2010 transistors were employed because of the different operating frequency. The unique feature of the uhf transmitter was that it allowed power backoff of 2.5 dB, 6 dB, or 8 dB. Power backoff was accomplished by turning off stages of the power amplifier in pairs.

Synthesizer

The frequency synthesizer (Figure 2-13) used a 100-MHz crystal oscillator to generate the frequencies required throughout the transponder and the local oscillator signal for the interferometer subsystem. Chains of varactor multipliers and dividers were used with filtering at each stage to keep spurious outputs below interference levels. The synthesizer also contained a separate local oscillator for the uhf upconverter.

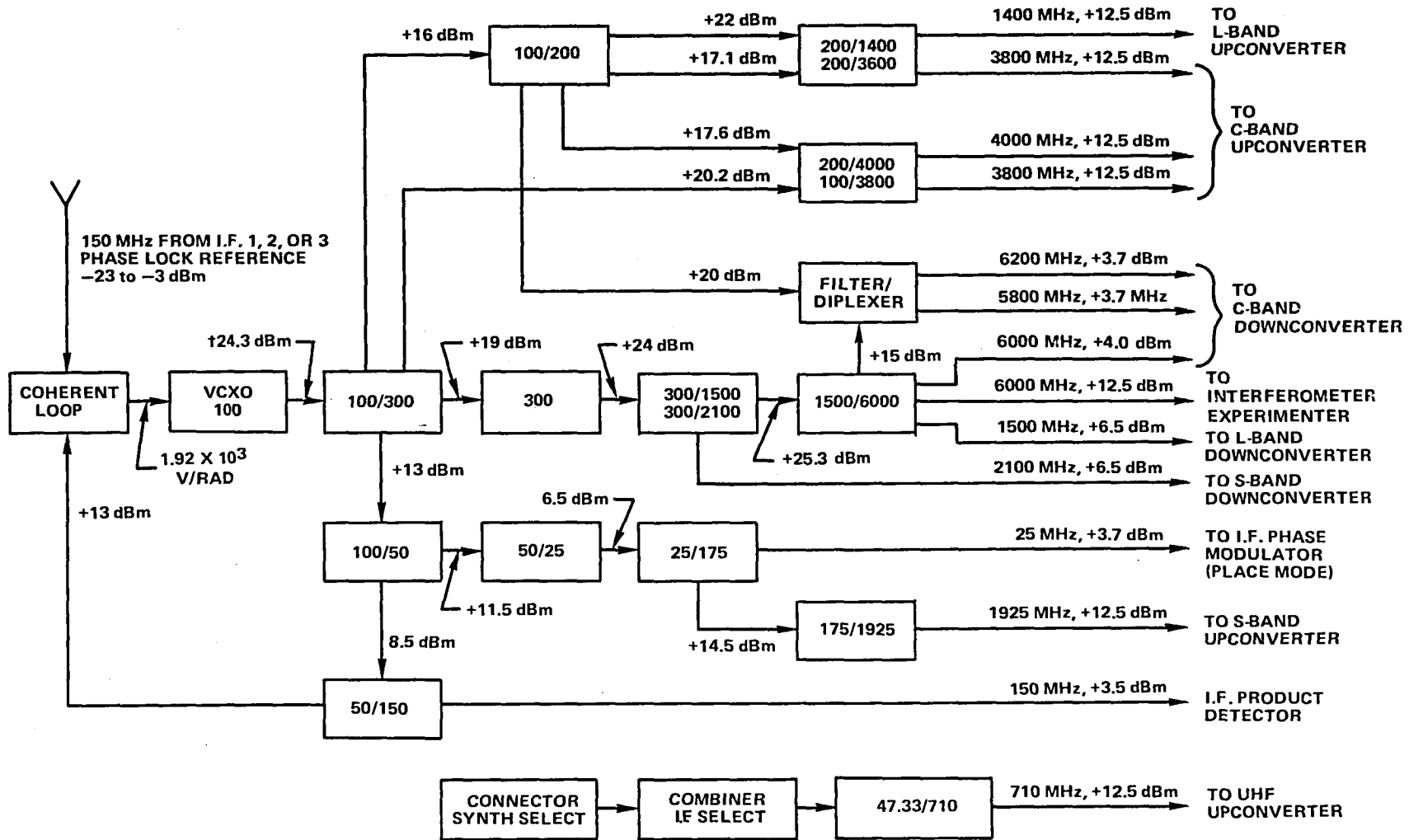
The synthesizer was operated in either the coherent or noncoherent mode. In the noncoherent mode, the phase-lock loop module was turned off and the VCXO module selected a reference voltage input clamp to provide maximum stability. When the coherent mode was selected, the phase-lock loop module compared the phase of the VCXO output (multiplied by 3/2) to the phase of the 150-MHz signal derived from an uplink C-band carrier. When the phase of the two signals was equal, the loop was locked and lock was indicated by telemetry. The outputs of the redundant synthesizers were combined through hybrids (only one synthesizer could be powered at one time).

Monopulse Unit

The monopulse comparator operated with the L, S, or vhf receivers to produce rf difference signals in the pitch and roll axes. The monopulse modulator located in each receiver provided a time division multiplexed output of +delta pitch, -delta pitch (180 degrees phase reversal) +delta roll, and -delta roll. The time multiplexed signal was coherent with the sum channel and was used to amplitude modulate the sum channel. The amplitude modulation was removed by the monopulse detector and the time division multiplexed error signals synchronously detected to yield error voltages used by the spacecraft attitude control system. The techniques of adding the monopulse delta channels allowed the sum channel downconverter and amplifier system to process the delta channels also.

The monopulse system operated in two modes: wideband and narrowband. In the wideband mode, the monopulse detector received 40-MHz or 12-MHz bandwidth signals depending on the state of the i.f. bandpass filter. In the narrowband mode, the monopulse detector received a 120-kHz bandwidth signal centered at 3 MHz (derived by mixing the receiver i.f. signal with a 150-MHz local oscillator signal). When the wideband i.f. filter was selected (130 to 170 MHz), the monopulse detector received both noise sidebands (corresponding to i.f. frequencies of 147 and 153 MHz). When the narrowband i.f. filter was selected (150 to 162 MHz), only noise centered at an i.f. frequency of 153 MHz was received.

When the monopulse system was operating, pointing errors would produce control signal voltages (called "error" voltages). When the spacecraft was pointed to the positive pitch or roll side of the monopulse source, the error voltage produced was negative. The control system used the sign of the error voltage to determine the direction in which to apply torque to keep the monopulse error voltage below a selected value, ± 0.35 volt. When the error voltage magnitude exceeded 0.35 volt and was positive (+), indicating a negative pointing, the spacecraft attitude control system applied a positive torque to the spacecraft, and when the error voltage sign was negative (-), a negative torque was applied. The attitude of the spacecraft was therefore controlled in pitch and roll to within



FUNCTIONAL DESCRIPTION

Figure 2-13. Communications Subsystem Synthesizer

± 0.35 volt which was converted to degrees by knowing the shape of the error voltage versus angle off boresight ("S") curve.

Wideband Data Unit

Figure 2-14 shows a block diagram of the wideband data unit. This subsystem accepted wideband signals (data) from four sources: VHRR; IHSDL (interferometer high speed data link); TV camera; and spacecraft telemetry. The sources were filtered as shown in Figure 2-14, then selected and amplified by the video amplifier module to either 5 volts peak to peak in the case of the TV camera signal, or 0.56 volt peak to peak in the other cases. The wideband signal selected was either the TV camera or a combination of the other sources and was applied simultaneously to free running 200-MHz and 237.5-MHz VCO's. This signal frequency modulated these oscillators out of phase and resulted, after mixing, in doubling the frequency deviation seen at either one of the voltage-controlled oscillators. The mixer output of 37.5 MHz was multiplied by 4 to yield a 150-MHz signal to be converted up on the C-band transmitter upconverter.

Power Supply and Distribution

The power control unit (PCU) of the power subsystem provided two percent regulated power (300 watts) for the transmitter power amplifiers and the C-band polarization switch. These regulators could be cross-strapped at the PCU, so that any power amplifier could be powered from either bus. In addition, the power regulation unit of the power subsystem provided the 30.5-volt nonessential bus to power the two-transponder dc/dc converters, transponder command decoder (TCD) No. 1, and the radio beacon experiment. TCD No. 2 was tied to the essential bus.

The 28-volt regulators in the PCU provided overcurrent protection for the rf power amplifiers and were commandable on or off from the ground station.

The transponder power supply (dc/dc converter) provided both overvoltage and undervoltage protection on both the input and output of the converter. On the input side, the overvoltage protection was 38 volts, ± 2 volts and the undervoltage was 24 volts, ± 2 volts. Once the voltage reached either condition, a 0.5-second timer was activated that shut off the converter unless proper voltage was restored. The converter also provided overcurrent protection by causing the output voltage to drop when undervoltage was reached (same time delay). Output over and under voltage protection was a function of the operating voltage. The converter provided the various voltage outputs to power all electronics of the communications subsystem except the power amplifiers, TCD's, and polarization switch.

Transponder Command Decoder

The transponder command decoder (TCD) accepted 9-bit commands for controlling all functions of the communications subsystem. A normal discrete command turned on power to the selected

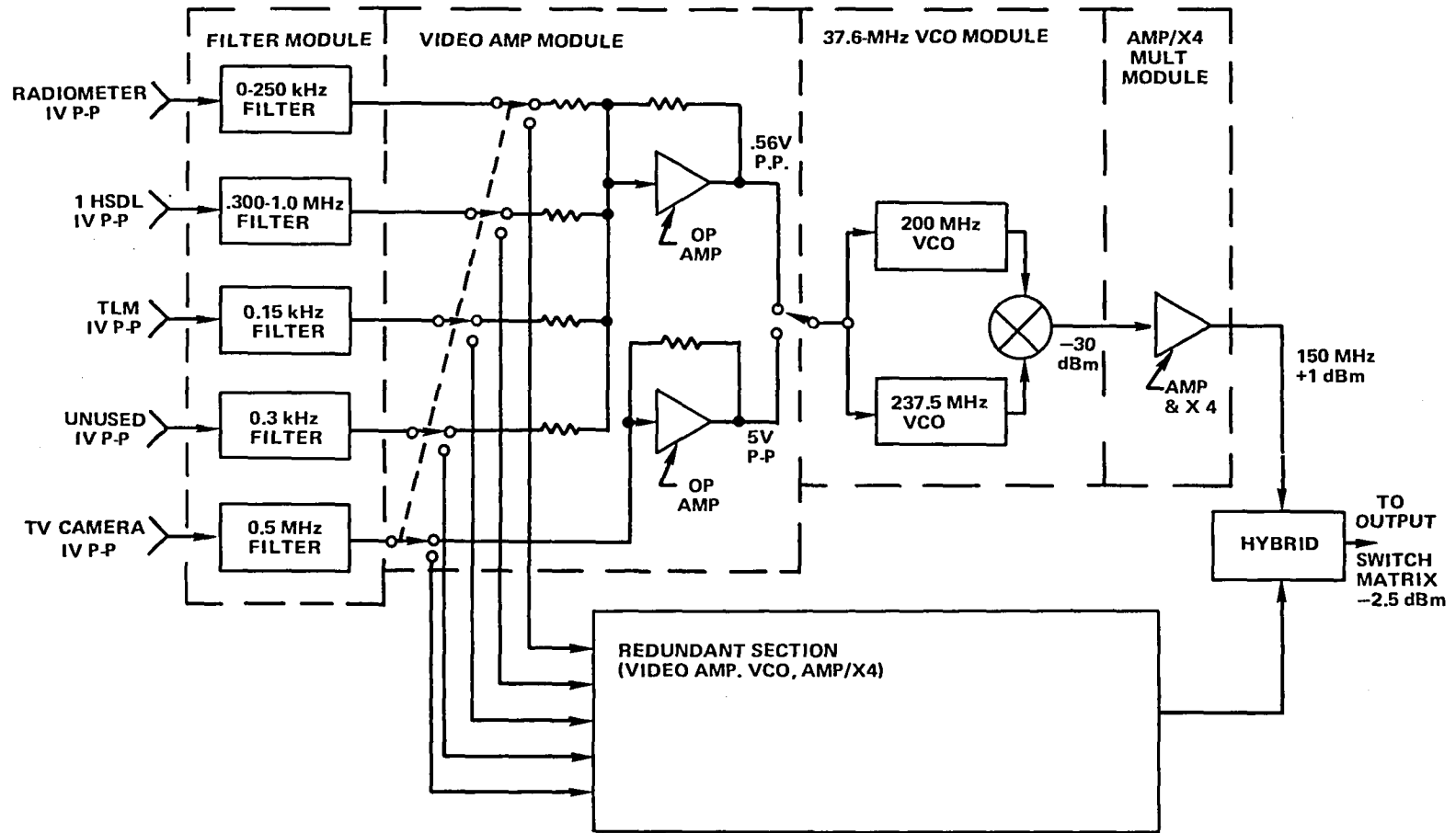


Figure 2-14. Communications Subsystem Wideband Data Unit

TCD and it could also be commanded off. The TCD provided command control for the communications subsystem, and performed the following functions:

- All telemetry was monitored through the TCD. Without a TCD on, there was no telemetry available to indicate the status of the communications subsystem.
- Interlocking of commands was provided so that commands could not be sent out of sequence.
- The TCD provided the relay drive for the 6-hour clock turn-off of the HET and uhf transmitters. Without a TCD on, the 6-hour clock pulse (+5 volts) would be received but not acted upon.
- A set of latched relays remembered the last position of the S-band antenna array, with or without power on; however, this state could not be changed unless the TCD was on and a proper command sent.

RFI Experiment Transponder

The C-band RFI Experiment used a separate local oscillator for generation of the translation carrier and provided a bandwidth of 500 MHz. The characteristics of this unit follow:

Input

Frequency Band: 5925 to 6425 MHz

Level Range: Noise to -69 dBm

Output

Frequency Band: 3700 to 4200 MHz

Maximum Level: -1 dBm

Transfer Characteristics

Noise Figure	7.0 dB maximum
Maximum Translation Variation	1 part 10 ⁶ per month
Translation Sense	Noninverting
Amplitude Ripple, In Band	2.0 dB peak-to-peak maximum
Linear Gain Modes*	70/66/60/56/48 dB, ±0.5 dB
Gain Variation	0.2 dB per day

Two-Signal C/I

Each Input at -75.5 dBm 47 dB minimum

Gain = 52 dB

*Assumes C-band transmitter linear gain of 44 dB from rfi transponder output to antenna feed connector.

Regulated DC Power Requirements

Maximum Drain (+12 Vdc)

12 W

The RFI Experiment transponder used a 445-MHz voltage controlled oscillator that was multiplied five times and fed to a mixer input (2225 MHz). Spacecraft signals (5.9 to 6.4 GHz) were received and mixed to provide a 3.7- to 4.2-GHz spacecraft downlink. The transponder used the communications transponder C-band transmitter for transmission by the Earth coverage horn. The transmitter input switches allowed both the communications transponder and the RFI Experiment transponder to drive the C-band transmitter; however, this was not a normal mode of operation.

DESIGN VALIDATION

The tests on the communications subsystem encompassed functional and environmental tests on modules, components, and the whole subsystem at both acceptance and qualification test levels.

At the communications subsystem level after integration and checkout, the most significant test was the long-form test. This was repeated a number of times before and after environmental testing at the prime contractor's facility. This series of tests was also repeated at the launch site. The test flow for the long-form test included specific functional and performance tests that were conducted during the following spacecraft experiment/operational modes:

- Ranging
- Millimeter Wave (Reference)
- Health, Education, and Telecommunications
- Satellite Instructional Television Experiment
- Very High Resolution Radiometer
- Spacecraft Attitude Precision Pointing and Slewing Adaptive Control
- Tracking and Data Relay Experiment
- Radio Frequency Interference
- Position Location and Communications Experiment
- Antenna Patterns

Each of these modes were actual operational modes that were expected to be used numerous times with the spacecraft when in orbit. For each of these modes, all primary backup and redundant configurations were exercised on command. Thus, every single feature that could be switched was activated and tested at least once. Much detailed data were obtained. The worst-case data involving G/T and e.i.r.p. (Appendix E) were obtained through these tests and by means of calculations involving antenna gain data obtained earlier on an antenna test range. For the long-form tests, a hat coupler was mounted over the prime-focus feed. This permitted coupling signals through the antenna feeds rather than through hard-line coupling directly into the transponder. However, the hat coupler did not permit quantitative data to be obtained involving the antenna feed characteristics.

Most of the detailed antenna data were developed using the prime-focus feed with a 9.14-meter hard aluminum reflector on the antenna range. Separate tests were conducted with individual feeds and the soft furlable 9.14-meter flight reflector. The soft reflector was perturbed to conform to a

“best” contour and a “worst” contour, consistent with the expected thermal variations during flight. The results of these tests are included in Appendix E, which provides both gain and beamwidth for best and worst case reflector contours. Additionally, a number of antenna tests were conducted to obtain data peculiar to monopulse operation, including null depth, null shift, cross-talk, and cross-polarization for the C-band, S-band, and vhf elements. The standard pattern data were good and met all objectives. The monopulse data were also good except at vhf, where it was fair.

For the reported e.i.r.p. and G/T values, all antenna gains, noise figures, and transmitter rf power levels were referred to the same interface point between antenna feed and transponder to account for any intervening passive line losses.

CHAPTER 3
IN-ORBIT PERFORMANCE

INITIAL 30-DAY CHECKOUT (SPECIFICATION/COMPLIANCE)

In the first 30 days in orbit, following launch of the spacecraft on May 30, 1974, the communication subsystem supported the following major experiments:

- Health, Education, Telecommunications
- Television Relay Using Small Terminals
- Position Location and Aircraft Communication Experiment
- Tracking and Data Relay Experiment
- Very High Resolution Radiometer
- Radio Frequency Interference Measurements Experiment

In addition, monopulse operation at vhf, S-band, and C-band was demonstrated.

A summary of this initial communication subsystem performance is presented in Table 3-1. Results correlated closely with prelaunch measurements. The initial calculations of e.i.r.p. based on measurements at 2570 and 2679 MHz were below expected values, but additional tests indicated that measurement techniques and uncertainties needed correction to produce more accurate results. Overall, the communications subsystem performance during the first 30 days of operation showed that the ATS-6 mission requirements for this subsystem were met.

Table 3-1
Communication Subsystem Performance Comparison
(30-Day In-Orbit Checkout)

RECEIVE		Required		In-Orbit*
Frequency (MHz)	Antenna	G/T (dB/K)		G/T (dB/K) (Approx. Peak)
		Peak	FOV	
6350	ECH	-17.0	-20.0	-14.0
6350	PFF	13.5	10.5	-
2250	On-Axis	9.5	-	10.4
1650	Fan	-2.0	-5.0	-2.6 (FOV)
TRANSMIT		E.I.R.P. (dBw)		E.I.R.P. (dBw) (Approx. Peak)
3950	ECH	25.4	24.1	25.7
3950	PFF	48.2	43.5	48.7
2670	S-2	52.3	48.9	-
2570	S-1	52.3	48.7	-
2075	On-Axis	51	-	52.5
1550	Fan	45	42	42.1 (FOV)
860	PFF	51	48	52.6

*Calculated values based on in-orbit measurements.

Experiments and Modes of Operation

Some observations concerning tests conducted in support of specific experiments and spacecraft modes of operation follow. Further details are to be found in the chapters devoted to each experiment.

Tracking and Data Relay Experiment

The Tracking and Data Relay Experiment demonstrated the ability to provide continuous communication for over half of each orbit between a low Earth-orbiting spacecraft and a single ground station control center. The low-Earth satellites planned for this demonstration were Nimbus and GOES. At the time of ATS-6 launch, however, there was no Nimbus spacecraft in low-Earth orbit capable of communicating with ATS-6; so, a Nimbus simulator at Rosman was successfully used to confirm experiment performance. During this operation, Rosman commanded and sent data to the Nimbus simulator by ATS-6, and Nimbus telemetry was similarly sent to Rosman by ATS-6. The Rosman/ATS-6 link was at C-band; the Nimbus/ATS-6 link was at S-band. This test demonstrated the first successful coherent operation of the synthesizer that was locked to the C-band uplink carrier and resulted in a phase coherent S-band transmission from the spacecraft. The ATS-6 bore-sight tracking of a simulated Nimbus low-orbit spacecraft was successfully demonstrated to an accuracy of ± 0.2 degree, compared to a specification requirement of ± 0.5 degree. Later tests with Nimbus-6 proved successful.

Television Relay Using Small Terminals Experiment

The Television Relay Using Small Terminals (TRUST) experiment demonstrated the ability to broadcast from the satellite to small receiving stations located throughout a large geographical area. Although the similar Satellite Instructional Television experiment was to be conducted in India, the Television Relay Using Small Terminals experiment was checked out during this operational period. A 25-MHz bandwidth FM-TV signal was transmitted from Rosman at C-band and successfully received simultaneously at Rosman and Goddard Space Flight Center at 860 MHz using 3-meter ground antennas. Television reception was excellent as indicated by a picture quality of 5 by 5 and a sound quality of 3 by 3.

Position Location and Aircraft Communication Experiment

The Position Location and Aircraft Communication Experiment (PLACE) demonstrated a communication link between ground stations and a large number of aircraft and ships and demonstrated technology for locating these elements. Since there were no aircraft or ships capable of communicating with ATS-6 during the first month of flight, experiment simulators were used at Rosman and Kings Point, Long Island, New York. Communication was successfully demonstrated through ATS-6. The Rosman/ATS-6 link was at C-band; the experiment simulator/ATS-6 link was at L-band. During these tests, it was determined that with up to four simultaneous carriers, the optimum system performance was obtained with the spacecraft configured in the frequency translation (FT) mode. This was later verified during tests with simultaneous users. All communications checkouts with the PLACE simulator were performed using the L-band fan beam.

Monopulse Tracking

The ATS-6 communication subsystem contained three monopulse sensing receivers capable of operating with received signals in the C-, S-band, and vhf frequency regions. The S-band and vhf monopulse receivers were operated at center frequencies of 2250 MHz and 150 MHz respectively in the wideband mode (bandwidth of 40 MHz) and 2253 MHz and 153 MHz respectively in the narrowband mode (bandwidth of 120 kHz). The C-band monopulse receiver was operated at center frequencies of 5950 MHz, 6150 MHz, and 6350 MHz in the wideband mode and at 5953 MHz, 6153 MHz, and 6353 MHz in the narrowband mode.

The three monopulse receivers were checked out as open-loop and closed-loop sensors for the spacecraft X- and Y-axes. All three receivers produced the correct attitude error-signal polarities in the correct axes and were capable of being used by the ACS to actively control the spacecraft attitude about the X- and Y-axes (roll and pitch axes).

Monopulse error curves were obtained for C- and S-band in the wideband mode (C-band at 6150 MHz only) and vhf in the narrowband mode about the spacecraft roll (X) and pitch (Y) axes with the Earth sensor in control of the spacecraft attitude. These error curves are shown in Figures 3-1, 3-2, and 3-3 with "ideal" error curves.

Table 3-2 lists the error curve characteristics and corresponding design goals. At C-band and S-band, the error curve slopes were close to the design goal values with the C-band roll slope about 16 percent low and pitch slope about 4 percent high. The C- and S-band error slopes were acceptable as determined by their closed-loop operation with the attitude control subsystem. The C- and S-band acquisition regions were also close to the design goals as indicated in Table 3-2. It was significant that the C- and S-band monopulse null axes were measured to be colinear within ± 0.004 degree. Tests were also conducted where the C- and S-band monopulse sensors were alternately switched into control of the ACS. It was noted that the spacecraft 3-axis pointing did drift during the transition period, thus requiring that spacecraft commanding be accomplished in the minimum amount of time once the monopulse signal was removed.

The vhf error curves were somewhat disappointing. The vhf slopes were about 70 to 80 percent low and never reached their saturated error voltages. A number of checks were made to determine the cause of the low vhf slopes, but no cause was determined. Both right-hand circular and left-hand circular ground radiation polarizations were used, and it was determined that right-hand circular polarization produced the better received signal level. With right-hand circular polarized radiation, the spacecraft vhf antenna gain was about 14 dB as expected. It now appears that a problem existed in the vhf monopulse receiver error channels at a point common to both the roll and pitch channels that added an excess insertion loss of about 10 to 14 dB. In spite of the low error slopes, the vhf monopulse was capable of serving as a sensor to control the spacecraft roll and pitch axes. When used in the ACS control loops, the vhf null pointing was 0.5° North and 2.0° East of the Rosman ground station as measured by the Earth sensor angles. It is suspected that these large errors are partly due to the low-loop gain resulting from the low monopulse error gains, and that the errors could be reduced by increasing the vhf gains in the digital operational controller.

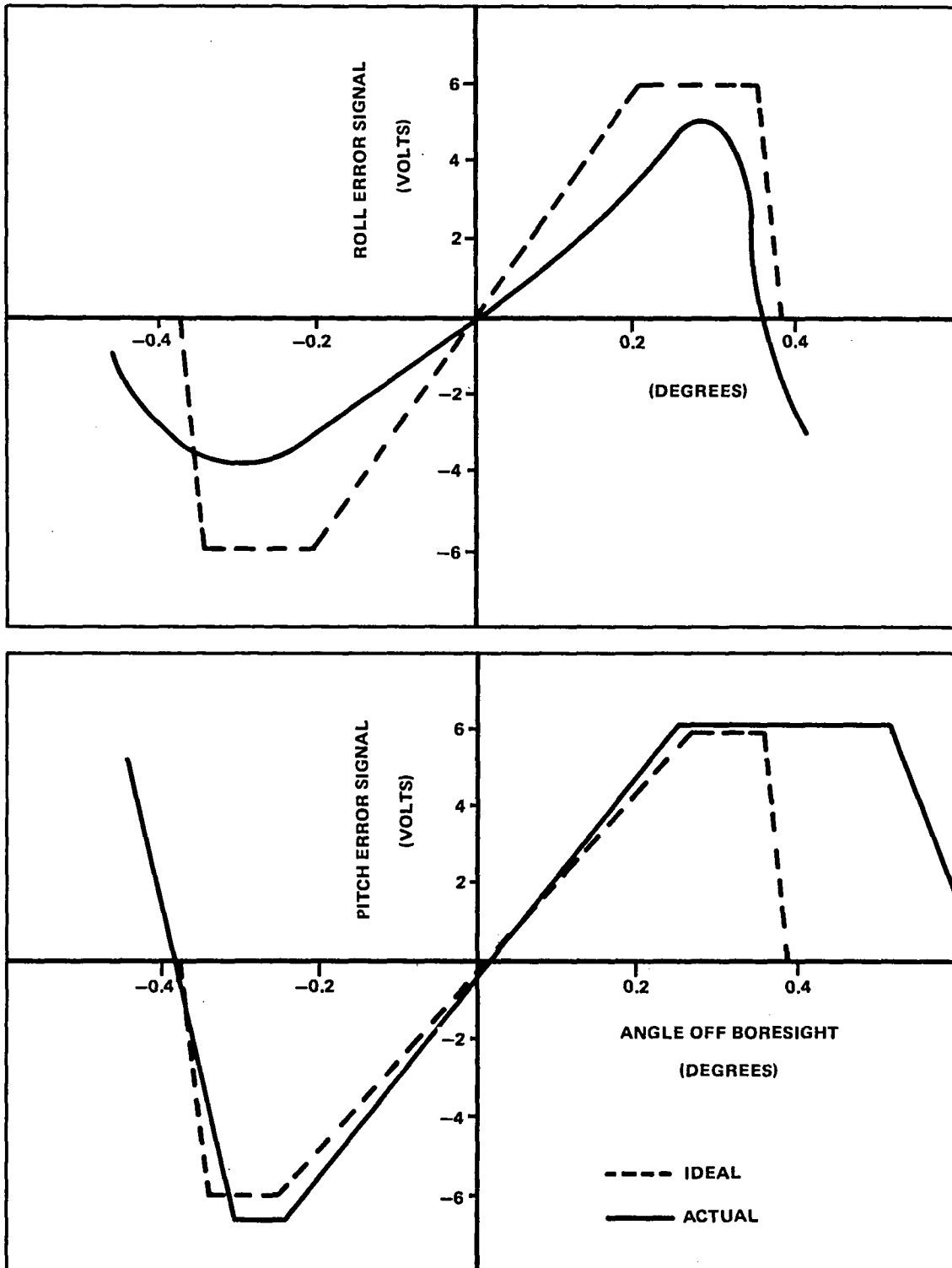


Figure 3-1. C-Band Monopulse Error Curves

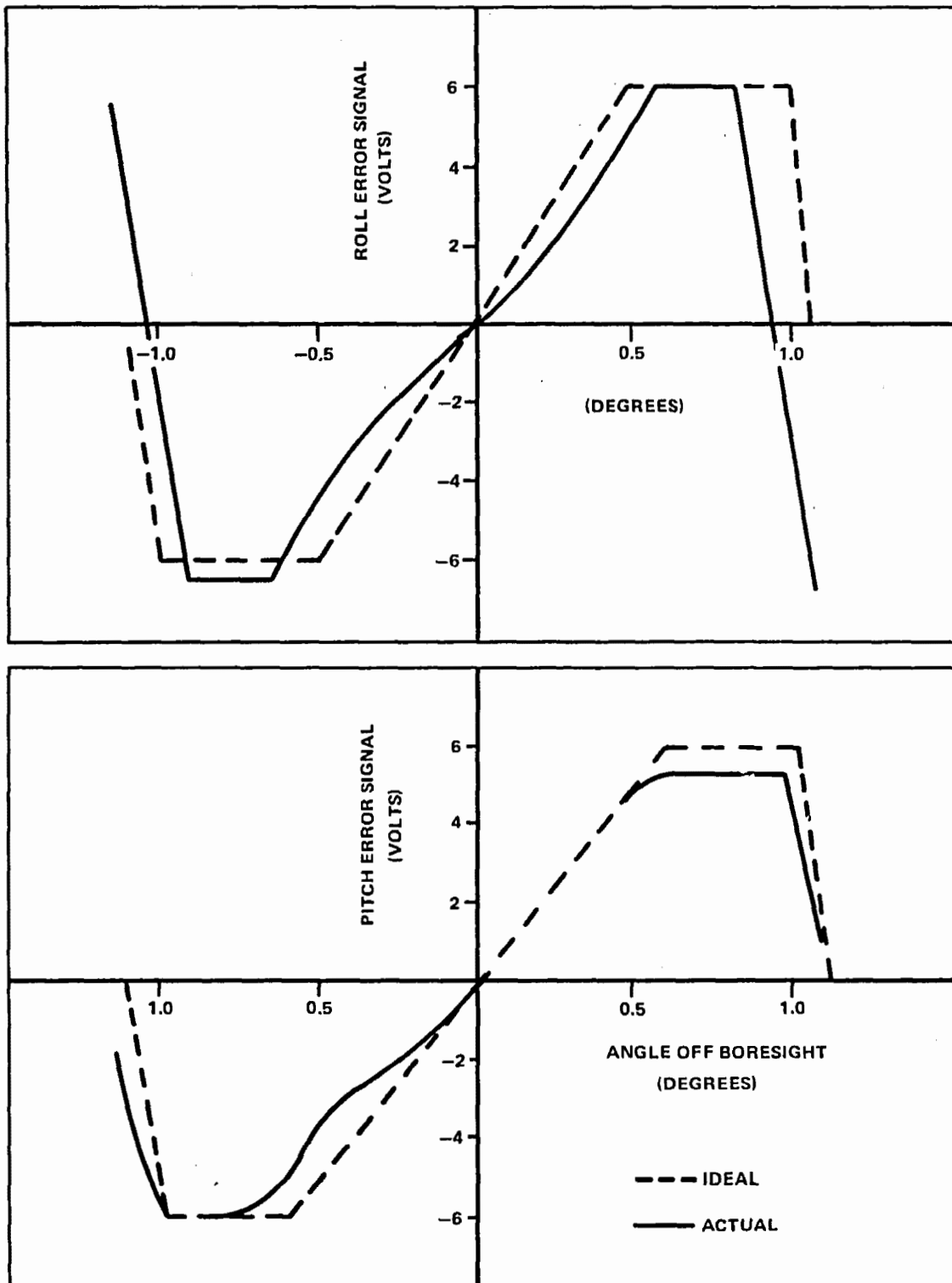


Figure 3-2. S-Band Monopulse Error Curves

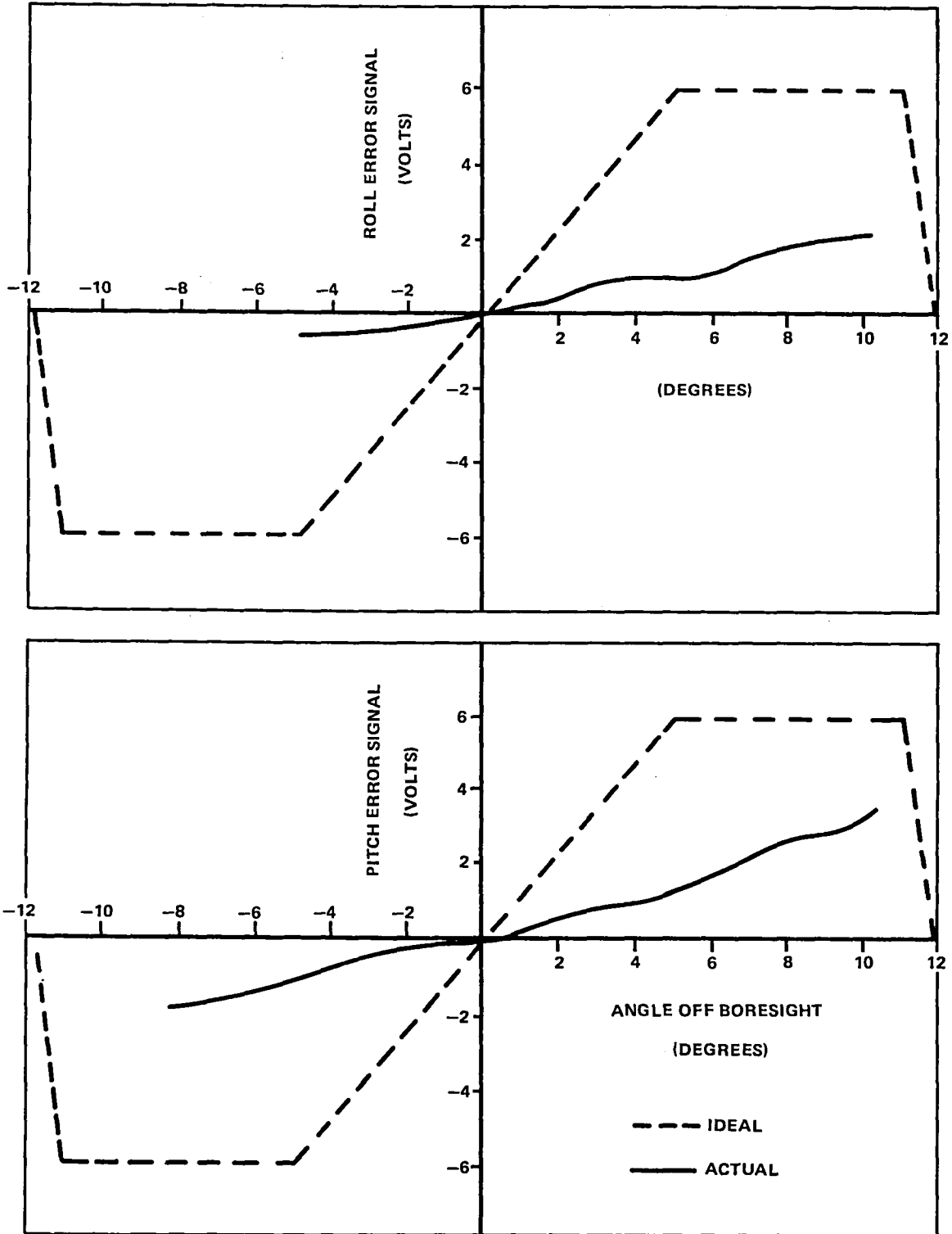


Figure 3-3. VHF Monopulse Error Curves

Table 3-2
Monopulse Error Signal Characteristics

Monopulse Band/Axis	Slopes (Volts/Degree)		Acquisition Range (Degrees)		Null* Offset (Degrees)
	Actual	Goal	Actual	Goal	
C, Roll	20	24	+0.3 -0.3	±0.35	—
C, Pitch	25	24	+0.5 -0.35	±0.35	—
S, Roll	7	8	+0.8 -0.9	±1.0	0.004 S
S, Pitch	7	8	+0.95 -1.00	±1.0	0.004 E
VHF, Roll	0.2	1	>+10 <-5	±11.0	0.5 N
VHF, Pitch	0.3	1	>+10 <-8	±11.0	2.0 E

* The null offset is relative to the C-band monopulse axis for S-band, but relative to the Earth sensor for vhf.

In summary, C- and S-band monopulse sensors worked very well, and the vhf sensor was acceptable.

Millimeter Wave Experiment

The Millimeter Wave (MMW) Experiment obtained data related to the propagation characteristics of the space-to-Earth downlink transmission medium at Ka- and Ku-bands. TV pictures were transmitted to ATS-6 from Rosman at C-band and cross-strapped to both 20 GHz and 30 GHz for retransmission from a 45.7-centimeter (18-inch) parabolic reflector on ATS-6 to a MMW terminal located at Rosman.

COMSAT Propagation Experiment

The COMSAT Propagation Experiment obtained data related to the propagation characteristics of the Earth-to-space (uplink) transmission medium at 12 and 18 GHz. The propagation experiment was operated almost continuously after its initial turn-on. The experiment received signals from many ground stations at both 12 and 18 GHz, and transmitted the signals back to Andover, Maine, at C-band using the spacecraft Earth coverage horn (ECH). The Comsat Propagation Experiment used a separate feed in the ECH to produce a polarization orthogonal to that of the communications subsystem.

Radio Frequency Interference Measurements Experiment

The Radio Frequency Interference Measurements Experiment provided data about the mutual interference between satellite and terrestrial telecommunications systems over a 500-MHz band at C-band. Uplink signals at C-band from known sources were received by the 9.14-meter antenna, frequency translated in the RFIME equipment, and retransmitted to the Rosman RFIME terminal at C-band using the ECH.

Very High Resolution Radiometer

The Very High Resolution Radiometer photographed the Earth's disc from synchronous altitude. The wideband data unit in the communication subsystem successfully modulated high quality video signals both for the infrared and visible spectrums on the C-band downlink carrier. The addition of a multiplexed Interferometer High Speed Data Link (IHSDL) did not degrade the quality of the radiometer pictures. Evaluation of the IHSDL was not completed during the first 30 days, but preliminary examinations indicated that the IHSDL quality was good.

VHF High Gain RF Link

During the first day in orbit, before conducting the yaw flip maneuver, the telemetry and command subsystem was reconfigured from the launch mode into the normal mode. In the normal mode, one command and one telemetry link were switched from one of the telemetry and command omnidirectional antennas to the prime-focus feed. The command link margin improved by 11.5 dB, and the telemetry link margin improved by 1.1 dB. The 9.14-meter antenna gain was measured as 13.6 dB above the omnidirectional antenna gain.

Range and Range Rate

C-band ranging was accomplished during the fourth day in orbit to determine the orbit of ATS-6 and to permit correction of the initial orbit to a final stationkeeping location at $94^{\circ} \pm 0.1^{\circ}$ W longitude. Ranging for purposes of refining the exact orbit parameters for updating the Digital Operational Controller was regularly scheduled once every 2 weeks.

Health, Education, Telecommunications Experiment

The Health, Education, Telecommunications experiment demonstrated the ability to simultaneously broadcast one or two different TV programs by satellite to two different geographical locations. Normal program operation included uplink transmission of an FM TV signal at C-band with translation and retransmission on two S-band downlink frequencies simultaneously (one frequency per antenna beam). The C-band monitor TV signal transmitted from the ECH was also well received. During the checkout period just before the Appalachian Regional Commission (ARC) and Veterans Administration (VA) experiments became operational, the HET S-band receive terminals were reporting excellent quality TV program reception.

TV Camera Reflector Monitor

During the fourth day in orbit, the TV camera reflector monitor was turned on and photographs taken at different times verified the successful deployment of both the reflector and the solar array booms. The TV signal was transmitted using the wideband data unit to modulate the C-band transmitter radiating through the ECH.

Radio Beacon Experiment

During the initial in-flight evaluation period, all RBE command functions were checked out successfully. In addition, special commanding tests were performed to determine if the RBE 140-MHz radiated signal desensitized the spacecraft vhf command receivers. These tests included reducing the ground station e.i.r.p., so that the command receivers operated near their thresholds. No RBE interference was noted.

The output power levels of the three RBE transmitters were measured by telemetry. The ranges of these levels were:

Frequency (MHz)	Level (Watts)
40	1.14 to 1.39
140	1.30 to 1.35
360	1.51 to 1.55

Transponder Signal Characteristics

The correlation between measured and predicted performance of all links was good with differences generally within the measurement and calibration tolerances of ground terminal equipment. Link calculations were performed for each experiment to determine expected performance parameters. A sample link calculation is shown in Appendix A.

The only spurious signals noted during the entire series of tests were observed during transmission of two signals simultaneously as part of the HET experiment. Some ground interferences had been noted during this period. These spurs were not seen in any subsequent HET tests that included other i.f. configurations. Later HET operations were performed with excellent picture transmission.

Antenna Patterns

During the first month of spacecraft operation, antenna patterns were measured using the ATS-6 reflector prime-focus feed at various frequencies. Antenna patterns were measured by pointing the center of the applicable antenna beam at the Rosman ground station and then slewing the spacecraft Z-axis in a predetermined pattern about Rosman, while the received rf signal strength was recorded. The data were later correlated with angle information and conventional antenna pattern plots were produced. The angle information (spacecraft attitude) was generated in real time by the

on-line attitude determination program (ONATT) at ATSOCC and sent to Rosman for recording with the received signal strength.

Antenna patterns made during the prelaunch, postlaunch and end-of-life (EOL) time periods were shown in Appendix F. Calculated and measured values of antenna gain are shown in Appendix E.

OVERALL MISSION PERFORMANCE

The tests conducted during the lifetime of ATS-6 were used primarily to verify operational modes, rather than verification of subsystem designs. However, useful data were generated during the course of the in-orbit testing that directly bore on the major performance characteristics of the communications subsystem.

Specifically, these included the effective isotropic radiated power and the ratio of the receiver gain to the effective system noise temperature (G/T), presented in Appendix E and the antenna patterns, presented in Appendix F.

The e.i.r.p. and the G/T values were the key communications subsystem performance parameters for the downlink and the uplink transmission. The antenna patterns were important, not only because the gain figures were an intrinsic part of e.i.r.p. and G/T , but also because of the field-of-view coverage crucial to satisfying the various experiments. These antenna patterns were used to satisfy desired "footprints" upon the Earth for terrestrial stations, and unique patterns for establishing links to aircraft and low orbiting spacecraft.

IN-ORBIT ANOMALIES

Five anomalies were encountered in the performance of the communication subsystem during the 5 years of continued in-orbit operations. The first, which was observed during initial checkout operations in June 1974, was the occurrence of power dips ("glitches") in the C-band downlink. The second, which occurred in October 1974, was the failure of a HET driver relay. The third, which occurred in November 1976, was the failure of a power transistor in the S-band transmitter. The fourth anomaly involved L-band transmitter noise that was radiated in the L-band receiver band, thus effectively desensitizing the receiver. The fifth anomaly was determined to be due to incomplete AGC calibration curves. Except for these anomalies, which are discussed in the following paragraphs, there was no verified degradation in performance in any component of the communication subsystem.

C-Band Power "Dips"

When the C-band transmitter was first turned on (June 2, 1974), recurring power dips ("glitches") ranging from 0.2 dB to 2.0 dB in C-band downlink transmission were observed on stripchart recordings of the Rosman ground receiver AGC. Initial periodicity ranged between 20 and 120 seconds with power dip widths of approximately 200 milliseconds. There were no indications of any degradation of signal quality. Various causes were hypothesized, including premature traveling wave tube turn-on with insufficient time for outgassing, corona, multipacting and external radio

interference. A series of troubleshooting sequences were run introducing configuration changes involving i.f. amplifiers, synthesizer, transponder command decoder and wideband data unit, but without effect. The use of the onboard wideband data unit eliminated any contributions introduced by the uplink.

Operation at reduced power levels substantially reduced the anomaly. Pending the results of ground simulation tests, it was decided to continue operations at reduced power. A 10-dB i.f. pad was switched in along with a 6-dB pad at the output of the tripler-combiner. With the wideband data unit, only the 6-dB pad could be used.

Statistical observations of the anomaly led to characterizing the probability density distributions of occurrences. Observations were made with both the Earth coverage horn and the prime-focus feed switched in. The resulting curve indicated a Cauchy distribution, which was typical of high-voltage breakdown.

A ground simulation/test effort was initiated at the Philco-Ford facility in California, using a qualification model TWTA and ATS-G C-band output components in a thermal-vacuum chamber. Similar power dips were observed, and attempts to isolate the cause identified an apparent power handling problem in the C-band transmitter output filter. This was later determined to be due to low energy gas discharge caused by residual epoxy contaminants inside the filter. It was then decided that normal transmitter life could be expected if the 6-dB pad were to be left in the output of the tripler-combiner. Due to the nonlinear drive characteristic, the resultant loss in e.i.r.p. was approximately 2 dB. With this pad in use, the glitches were no longer measurable and the impact on experiments involving the C-band transmitter was not significant. The 6-dB pad remained in use for the remainder of the spacecraft's operations during the first 2 years. Subsequent operations were conducted without the 6-dB pad when maximum rf output was required; i.e., for the AIDSAT experiments.

HET-2 Driver Relay

Early in October 1974, it was observed that the HET-2 driver could not be turned off. The problem was attributed to failure of relay function A1A2K1 on the HET transmitter. On October 15, 1974, a corrective procedure was adopted that left this relay on at all times. Fortunately, this relay was in series with relay function A2K2 on the same assembly. Function A2K2 removed power from the drivers as well as the transmitters and since the drivers operated Class C, very little power was dissipated even when they were allowed to remain on in the undriven condition. Along with overriding appropriate interlocks, these changes were incorporated in operating procedures. This failure had no deleterious effects on the ATS-6 mission.

S-Band Transmitter Failure

On November 5, 1976, the S-band output power dropped 2 to 3 dB. The problem was analyzed, and it was concluded that it was due to the failure of one of the four parallel output transistors in the S-band transmitter. Although the spacecraft had a backup S-band transmitter, it was not activated. The degraded prime S-band transmitter was adequate to support the satellite tracking and data relay operations for which it was primarily used. This degraded system was used for the entire

5-year mission and only during the end-of-life tests was the backup transmitter turned on. The backup system worked as specified.

L-Band Transmitter Output Noise

During spacecraft operations that resulted in negative drive S/N at the L-band transmitter, excessive noise was experienced in the L-band receiver input with the following effects:

1. The spacecraft L-band transmitter out-of-band noise coupled into the L-band receiver to effectively lower the receiver sensitivity.
2. The effect of (1) was a function of the amplitude and frequency of the transmitter in-band signal.
3. Because of (1) and (2), L-band receive G/T measurements were meaningful only when the spacecraft L-band transmitter was off.
4. When operating with low level L-band receive signals, it was necessary to provide a relatively large signal in the L-band transmitter to reduce out-of-band transmitter noise.

Apparently, the transmitter bandpass filter was not capable of rejecting the unwanted output noise. This noise was at the input of the L-band transmitter, because low level signals in the i.f. did not drive the AGC adequately to reduce the i.f. gain and thereby reduce the i.f. noise output. For additional information see Appendix D.

Spacecraft I.F. AGC Calibration

During July 1977, it was determined that the multiple calibration curve software at ATSOCC omitted a 5-dB correction required while in the PLACE mode with the 40-MHz filter selected. The 5-dB correction was required because the calibration curve used for this mode was based on the 12-MHz filter configuration.

To verify the ATSOCC multiple calibration curves, the i.f. AGC level was recalibrated and new calibration curves generated for each of the three i.f.'s in both PLACE and FT modes. This recalibration revealed unexpected variances in both FT and PLACE modes with the largest deviation from the accepted "standard" in the PLACE mode (Appendix C).

The calibration look-up tables in the ground computer were not updated because of the lateness in the spacecraft life. To do so would introduce an inconsistency in data from on-going experiments. The new calibration data were recorded and held for reference only.

CONCLUSIONS AND RECOMMENDATIONS

Despite the five cited in-orbit anomalies in the operation of the communications subsystem, all experiment requirements were met or exceeded.

The C-band power dip had negligible effect upon experiments. The problem itself was not attributed to any basic design fault, but rather to contamination of materials.

Monopulse performance at C-band, and particularly at vhf, was not as good as the intended design. The discrepancies were due to several factors:

1. The major assemblies, the prime-focus feed and transponder, were worked on independently for most of the program. When these were integrated, there should have been more detailed ground testing permitting the necessary precise phasing adjustments essentially controlled by the lengths of the transmission lines between the prime-focus feed elements and the transponder receiver front end. This was particularly critical for the more sensitive C-band operation. While vhf operation was understandably of coarser precision, it had excessive ripples and a very poor null.
2. Field tests of the prime-focus feed with the hard 9.14-meter aluminum reflector on the Santa Cruz mountain range had several problems: There were a number of vhf transmitters in close proximity. These interfered with the ability to boresight on the desired test transmitter. The rugged antenna range did not have adequate terrain clearance and, therefore, there were multipath effects as well. Thus, the vhf characteristic for the prime-focus feed was not adequately defined by the quantitative test data, making phase adjustments quite difficult.
3. In addition, the spacecraft configuration with the wrapped truss between the soft reflector and the prime-focus feed perturbed the vhf performance. It was theorized from the linear dimensions that there might have been an effective waveguide filter cut-off phenomenon. This effect showed up both in monopulse operations and the conventional vhf data link operation.
4. There was the common problem of two independent subsystems (attitude control and communications) interfacing shortly before launch for the first time. Both of these were intimately involved in the monopulse performance.

It is recommended that whenever technical performance is dependent upon more than one major assembly, particular attention must be given to overall systems engineering since the interfaces can rarely be that well enough defined to prevent all surprises upon integration. In this instance, the vhf antenna testing could have been improved after integration by using a "fly-by" technique involving either a light plane or helicopter carrying the test transmitter.

The frequency synthesizer exhibited an operational problem achieving lock. To effect phase lock, it was necessary to vary the frequency of the ground signal, and this was both time consuming and difficult. The design for C-band downconverter mixing frequencies was different than that for the upconverter mixing frequencies. For the downconverters, one multiplier chain was used plus a mixer that provided the over and under frequencies with 200-MHz separation. The upconverter frequencies were generated with three separate varactor multiplier chains and the 200-MHz difference frequencies were ignored. These multipliers produced many interference products that had

to be filtered. The design would have been much simpler with two less multipliers if it had been configured like the downconverter mixer frequencies.

During operations requiring C-band on-axis pointing while using the Earth coverage horn antenna, a problem was encountered because of inadequate signal isolation between the PFF and ECH feeds. The poor isolation of these feed systems allowed the signals to add algebraically. The effect of this problem was minimized by selecting the PFF polarizations to be orthogonal to the Earth coverage horn whenever the ECH was selected.

The L-band transmitter had very little out-of-band noise reduction capability. When no discrete signal was driving the L-band transmitter, its noise output extended over a very broad bandwidth that included the L-band receiver band. The transmitter output bandpass filter should have limited the band of noise to about 40 MHz. More care should have been exercised in designing this filter to ensure freedom from noise interference. This problem could have been identified with more extensive prelaunch testing.

The solid-state power amplifiers (uhf, L-band, S-band, and HET) were representative of good conservative designs incorporating appropriate rf power transistors. It is expected that in future designs, new transistors would be incorporated with greater efficiency and fewer devices. This in turn would lead to smaller, more reliable designs.

Part B
Electrical Power Subsystem

CHAPTER 4

INTRODUCTION

The ATS-6 mission demanded a highly adaptable power subsystem that could interface with many experiments, allow multiple operations of these experiments and the operation of the subsystems of the spacecraft without induced or coupled electromagnetic interference. This required that the power subsystem efficiently handle varying loads from the minimum base load of 150 watts to peak power demands of up to 800 watts; i.e., some 200 watts in excess of the solar array capability. Such varying loads also have a significant impact on the design of thermal control systems.

To meet these requirements, a power system with unique features was developed. A shunt-boost power subsystem configuration was used to provide direct power transfer from the solar array to the loads for maximum efficiency. An important feature was the use of shunt power dissipators, not only as a means of power system regulation, but also for thermal control. The shunt dissipators and load interface circuits of the power subsystem were distributed throughout all three modules.

The electrical power subsystem was designed and built by Fairchild Space and Electronics Company, the prime contractor for ATS-6.

POWER SUBSYSTEM REQUIREMENTS

The mission required a power subsystem that could efficiently handle widely varying loads for the simultaneous operation of the various experiments over a minimum 2-year lifetime with a goal of 5 years. Figure 4-1 shows a power requirements profile for the major experiment operational modes. The following were the most significant design requirements placed on the power subsystem.

Mission Normal Power

The peak power available from the power subsystem shall meet that shown in Figure 4-2. The power subsystem shall provide a continuous peak power of 500 watts for a minimum of 4 hours (battery share mode to 50 percent depth of discharge) and a minimum output of 450 watts over the remaining 20-hour operational day throughout 2 years in orbit except during eclipse.

Eclipse/Occult Power

The power subsystem shall provide a minimum of 290 watt-hours for 1.2 hours maximum for spacecraft and experiment operation during the eclipse.

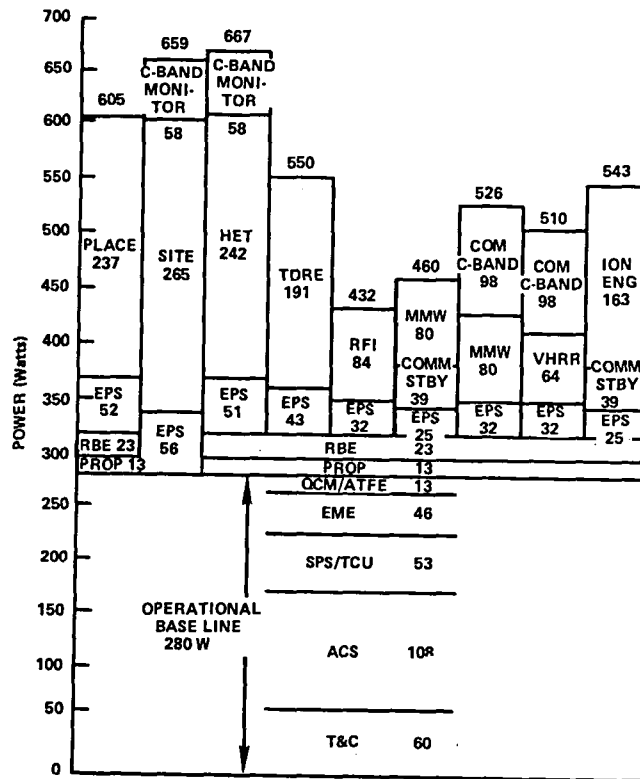


Figure 4-1. Spacecraft Mode Power Requirements

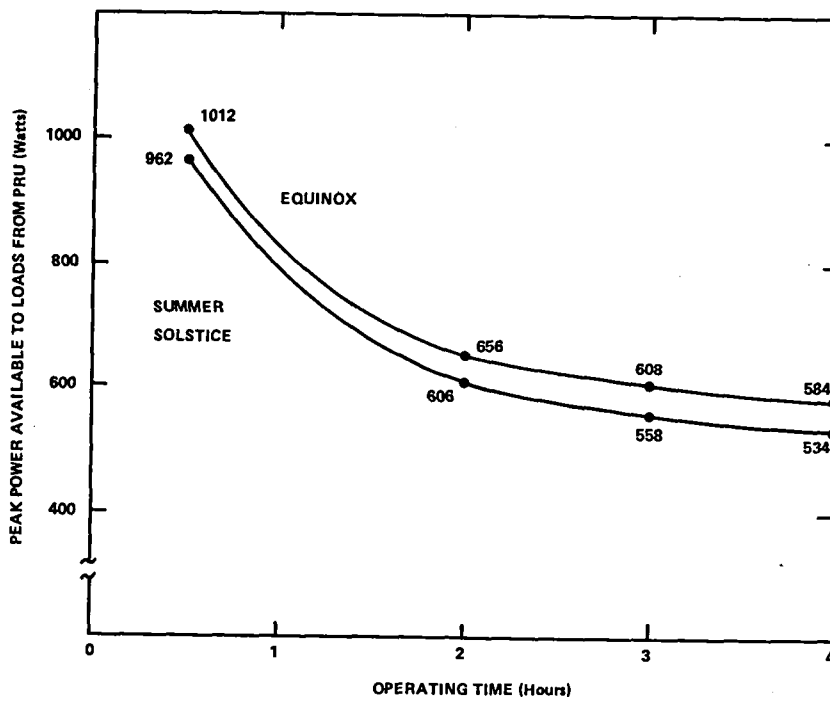


Figure 4-2. Peak Power Available at End-of-Life (Specification)

Bus Voltage Distribution

The following bus voltages shall be provided:

1. Unregulated bus: 19.0 to 28.5 Vdc.
2. Experiment and communication subsystem rf power amplifier regulated buses: 28 Vdc \pm 2 percent.
3. Main spacecraft regulated bus: 30.5 Vdc \pm 2 percent.
4. Command receiver regulated buses: 19 Vdc \pm 2 Vdc.

Protective Features

The following protective features shall be provided:

1. Primary power overload. Disconnect the nonessential loads from the 30.5-Vdc bus, if the bus drops to 28 Vdc \pm 0.5 Vdc for 250 ms \pm 50 ms.
2. Secondary power overload. Disconnect the loads from any 28-volt bus, if the bus drops to 24 Vdc \pm 0.5 Vdc for 500 ms \pm 100 ms.
3. Primary power overvoltage. Limit the maximum instantaneous voltage on the main bus to 36 volts.

Load Control (Experiment and Communication System)

The following shall be provided:

1. Regulated 28-volt \pm 2 percent bus.
2. On/off command control.
3. Adjustable current limit set at 150 percent of load with automatic shutdown.
4. Undervoltage control at 24 volts with automatic shutdown.
5. Line isolation and ripple rejection.

CHAPTER 5

DESIGN DESCRIPTION

The power subsystem chosen was a shunt-boost design that provided the following: (1) excellent use of array power with an 8 to 10 percent increase in efficiency over nonshunt-boost designs, (2) good array-battery static and dynamic load sharing, (3) excellent flexibility to accommodate varying mission requirements, and (4) low electromagnetic interference. Use of this shunt-boost design allowed for optimizing the individual designs of the array, battery, and conversion electronics to achieve the highest power source utilization possible.

A significant area of system optimization was the integration of the shunts into the thermal control system to provide heat input for spacecraft temperature control.

To accomplish this, an array-shunt wiring configuration was used that distributed power equally to the 12 shunts. In addition, the shunt circuit design was compensated for variation in gain to maintain good power balance. This design substantially reduced the range of power dissipation within the spacecraft.

OVERALL DESCRIPTION

The system consisted of two solar array assemblies (paddles), 2 nickel-cadmium batteries, a power regulation unit, a power control unit, 12 shunt dissipators, a squib interface unit, load interface circuits for the experiments, and a 10-meter (35-foot) array harness.

Figure 5-1 shows the functional arrangement of the components of the power subsystem. Figure 5-2 is a basic, simplified block diagram of the shunt-boost design.

The system derived power from the solar array. Energy was stored in the two batteries that were discharged in parallel. The batteries provided electrical power during occult portions of the ascent phase, eclipse periods, and peak loading that exceeded the capability of the solar array.

The power output from the solar array and batteries was regulated to a level of 30.5 Vdc. The design used partial shunt regulation for adjusting the solar array voltage and a boost regulator to obtain 30.5 volts from a 19-cell battery.

The shunt-boost power subsystem design provided maximum use of array power at end-of-life by allowing the array to operate at the fixed voltage where maximum power was available. When the load power exceeded the array power, the array continued to deliver maximum power and the batteries provided the balance of power required (Figure 5-3).

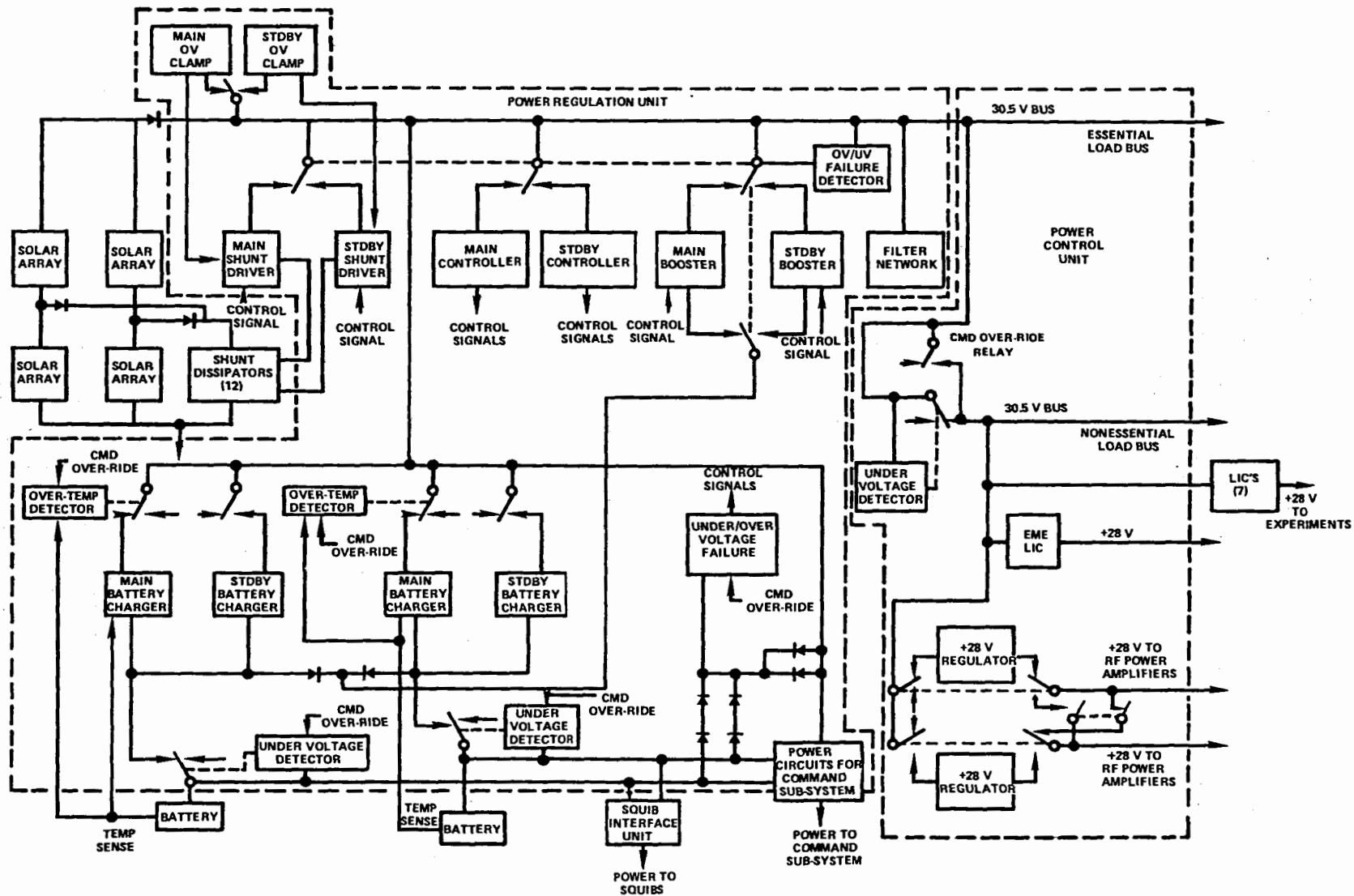


Figure 5-1. Power Subsystem Functional Block Diagram

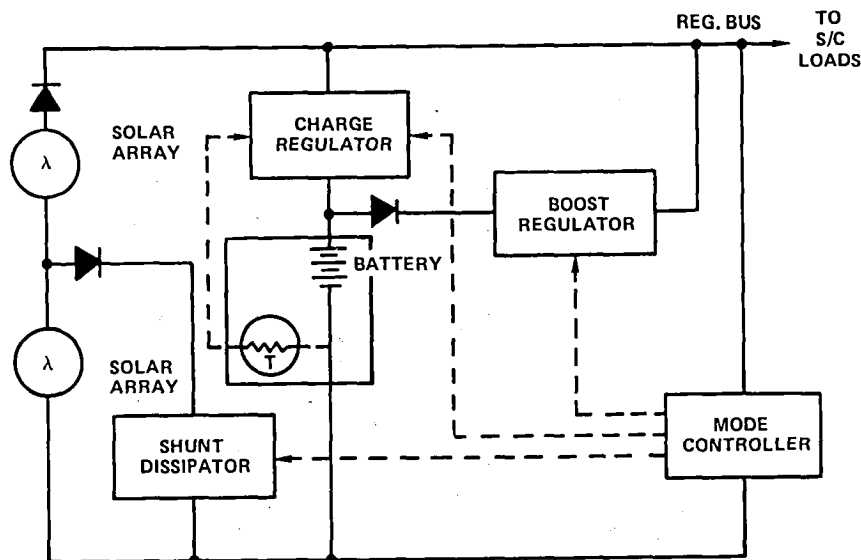


Figure 5-2. Basic Block Diagram Shunt-Boost Subsystem

When excess power was available from the solar array, the battery chargers were enabled to charge the batteries. Each battery had separate charge control circuits and was normally charged with a current limited rate (1.5 A maximum, C/10) with temperature compensated voltage control. When the array power exceeded the load power and battery charge requirements, the excess power was dissipated by shunt circuits.

A common controller provided the necessary error signals for the three major modes of operation: the shunt mode, the charge mode, and the boost mode. These functional modes provided the regulation and charge control for the power subsystem. Figure 5-4 shows these control modes.

Secondary power conditioning at 28 Vdc was provided in the power subsystem for the solid state power amplifiers and for each experiment through individual load interface circuits.

The power subsystem also included a squib interface unit for firing the pyrotechnic devices for spacecraft separation and deployment of solar arrays and reflector. The squib interface unit is described in Volume I, Chapter 6, as part of the spacecraft separation deployment subsystem.

SOLAR ARRAY

The solar array, which was the primary power source, consisted of 21,600 2-cm by 4-cm, 2-ohms-per-cm solar cells distributed on the two hemicylindrical panel assemblies (each weighing 72.7 kg) mounted on booms on the north and south Y-axis of the spacecraft to simulate a cylinder. The solar array assemblies extended beyond the 9.14-meter reflector to avoid mutual shadowing. There were 32 panels in the entire array, arranged in a double row, resulting in a 16-sided prism. The normal of each of these facets was at an angle of 22.5 degrees with respect to the normal of the adjacent facet. With this large number of facets, the power output of the solar array was nearly constant through the day, with geometric factors introducing only ± 0.15 percent variation.

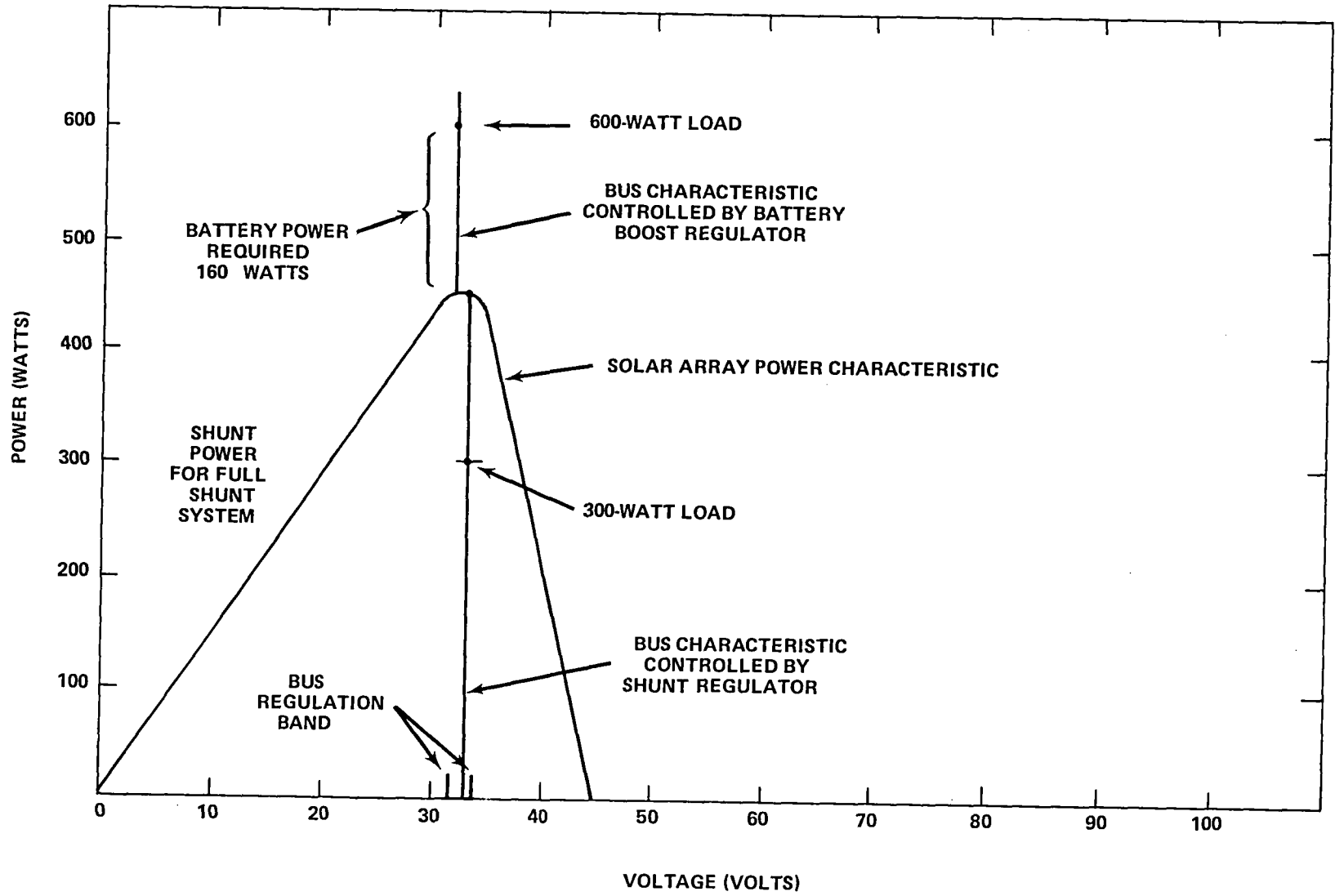


Figure 5-3. Array/Shunt-Boost Power Interface Characteristic

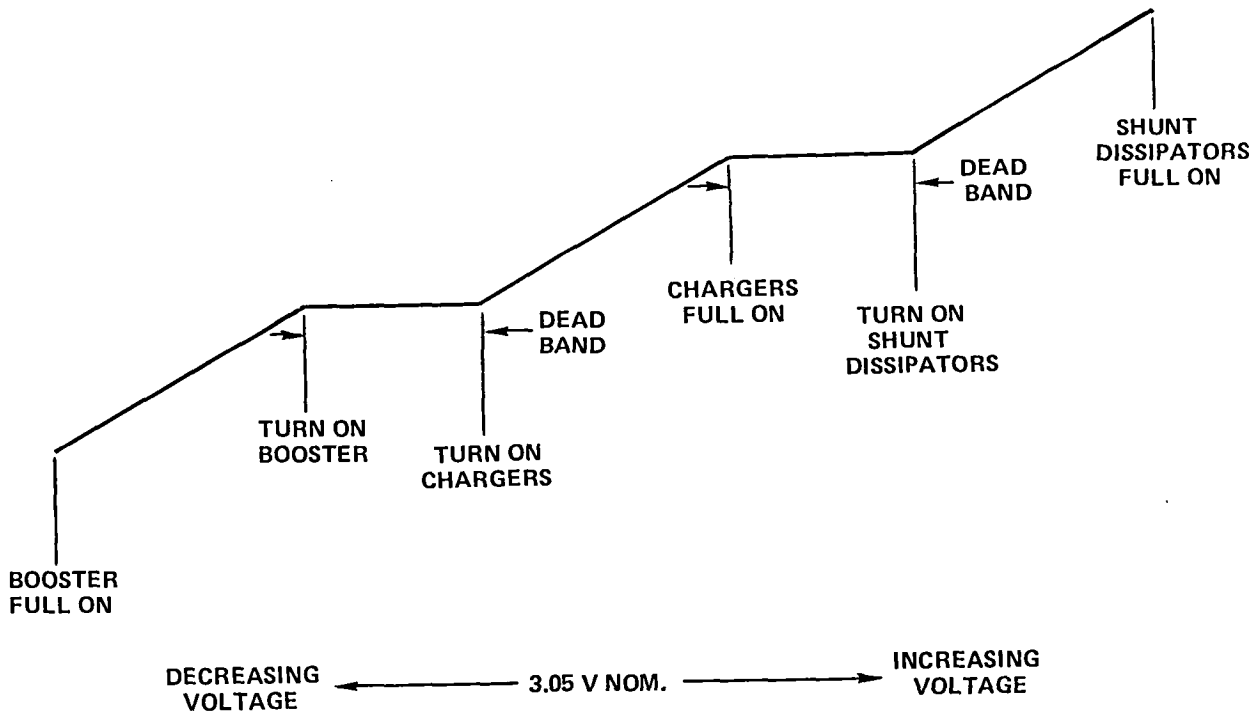


Figure 5-4. Power Subsystem Regulation Control Modes

The solar cells were arranged in 96 series strings of 3-parallel by 75-series cells each, with isolation diodes connecting each string to the power bus. There were three series strings on each panel. The cells were arranged three rows to each string and the direction of current flow was alternated to reduce the external magnetic field and to minimize the interconnecting wiring.

Each panel, which was identical in design and interchangeable with any other panel on any facet, measured 53.3 cm by 119.4 cm and weighed 2.09 kg.

The taps for the shunt dissipators were made at a point that was 50 cells from the negative bus, which corresponded to the end of a row of solar cells. The wiring for each string was twisted to minimize the external magnetic field.

The main power outputs from the solar array were bussed together on the panel assembly. The shunts taps were connected into a matrix, so that one tap out of every 12 was connected to 1 shunt, and each of the 12 shunts drew current from strings located at 45-degree intervals around the cylinder. The net result was that each shunt was connected to eight solar cell circuits and on a projected area basis, so that each shunt handled approximately the same power. Matrixing the shunt connections in this manner tended to even out the individual shunt dissipations as the spacecraft rotated in orbit.

The solar array performance was a function of the radiation damage of the solar array in orbit, the season of the year, and the pointing maneuvers required in orbit. At any given time the power output was maximum at the equinox and minimum at summer solstice because of the effect of Earth-Sun distance and the angle of solar incidence. It was required that the spacecraft be pointed 4

degrees north of the local vertical often; so, the offset Sun/array angle at summer solstice could be as great as 27.5 degrees. This offset angle was used to determine summer solstice performance.

To illustrate typical in-orbit power variations, Figure 5-5 shows the array power output as a function of time for spring equinox launch. The maxima occurred at the equinoxes, and the deep minima at summer solstice. The intermediate minima occurred at winter solstice when the solar constant was about 7 percent higher than at summer solstice.

The solar array design was based on a radiation degradation factor of 20 percent for a 2-year mission with a 6-mil radiation protection cover glass of microsheet.

The temperature history of the end panels on the solar array during the equinox orbit is presented in Figure 5-6. The cool-down and heat-up temperature transients represent the worst any panel on the array experiences. The maximum temperature of 60°C holds for all panels but is time phased according to position on the array. The minimum temperature is approximately -160°C. The various materials shown in Figure 5-7 were selected to meet these temperature extremes.

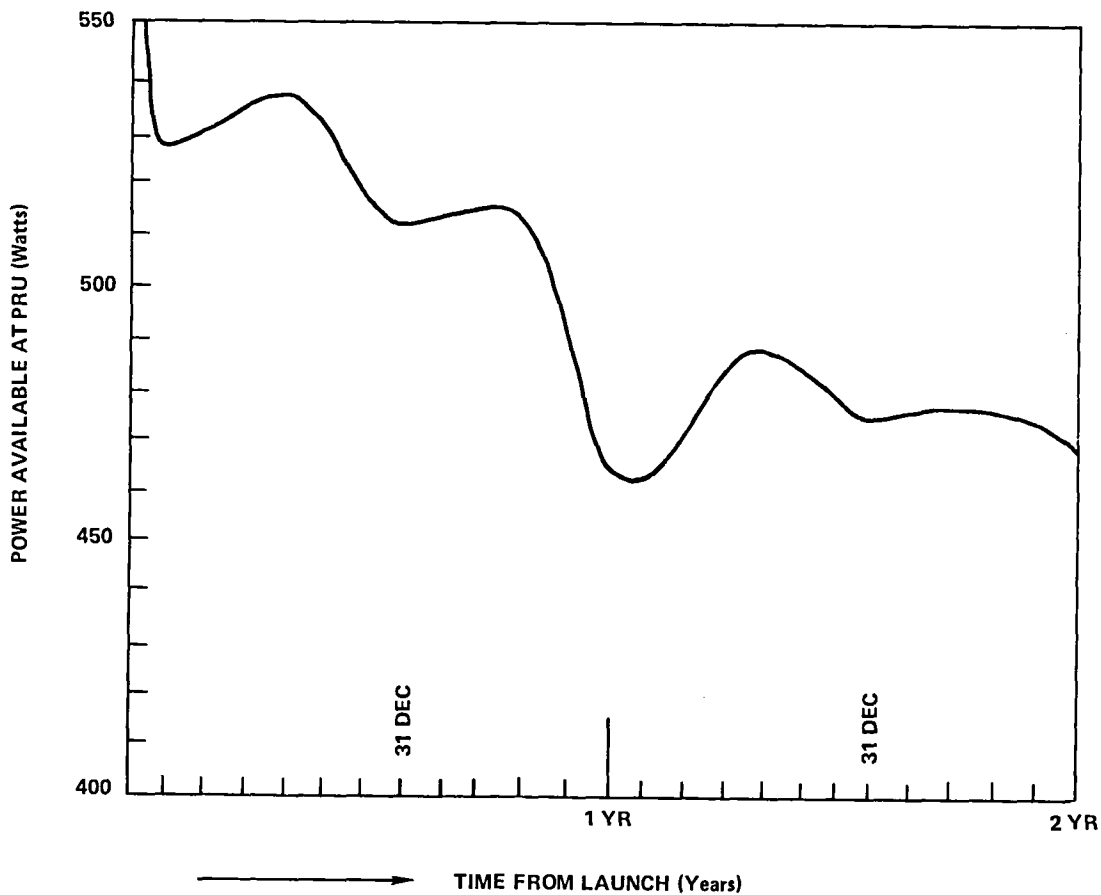


Figure 5-5. Solar Array Capabilities

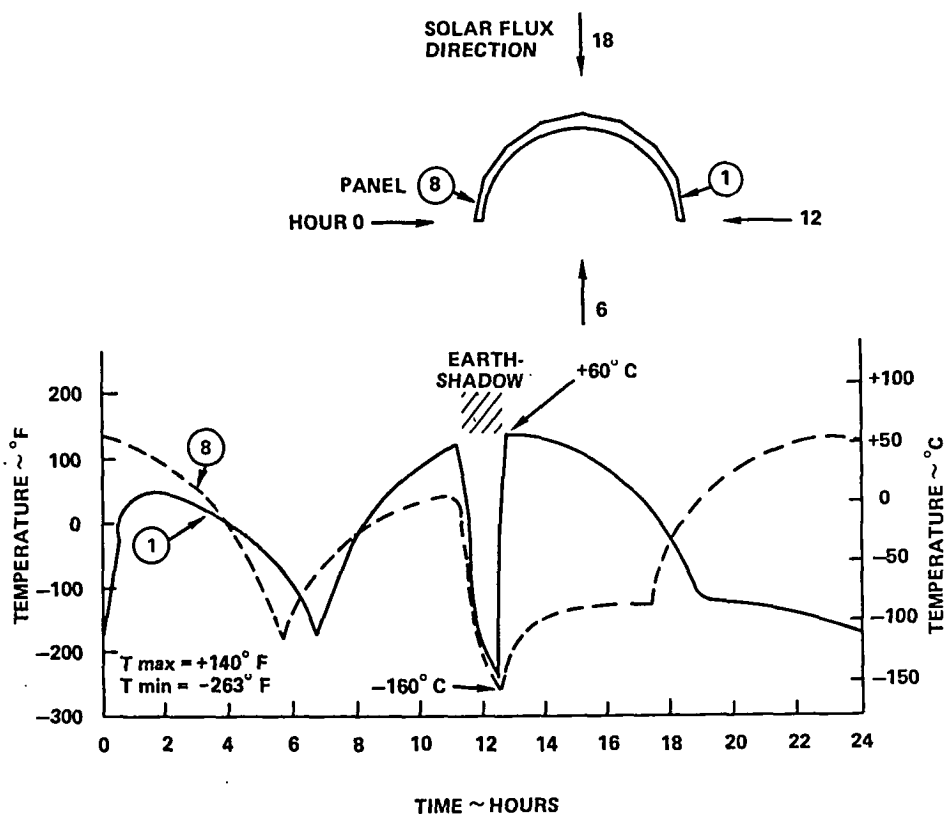


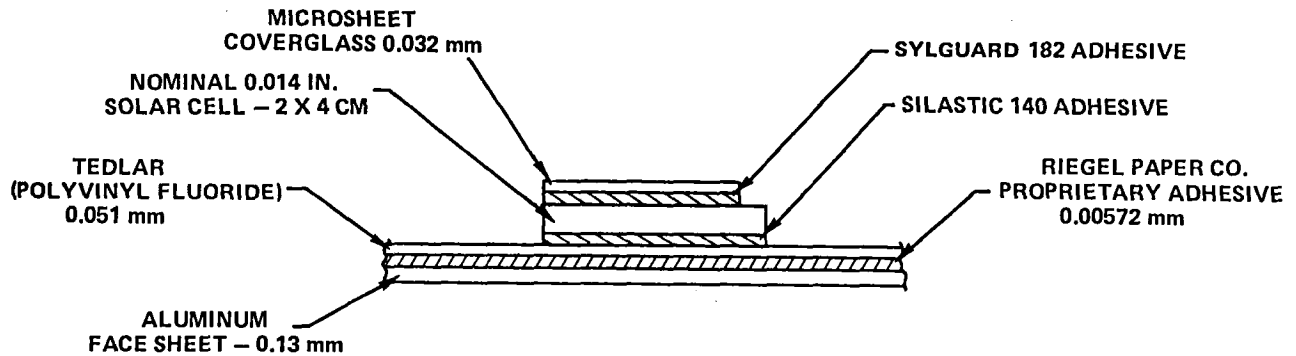
Figure 5-6. Solar Array Temperature versus Equinox Orbit Position

Because of the light mass of the array, the rate of temperature change was extremely fast (25°C per minute). To qualify the design for this rate of temperature change, two qualification panels were subjected to 200 thermal vacuum cycles. In addition, each flight panel was subjected to a minimum of 25 cycles, while some received 50 cycles and others 100 cycles. The test program was graduated from 100 to 50 cycles and then to 25 cycles based on the panel electrical performance and on visual inspection. The temperature range was from -160°C to $+60^{\circ}\text{C}$ with the rate of temperature change on warmup closely simulating the 25°C per minute expected in orbit. Results of this thermal vacuum cycling were good with no major problems occurring.

BATTERIES

The power subsystem contained two 19-cell, 15 ampere-hour, nickel-cadmium batteries. Using these batteries to supplement the solar array, the design could supply up to 1000 watts at peak power demands.

The batteries were sized to provide sufficient power for the occult and load sharing modes without exceeding a 50 percent depth of discharge (170 watt-hours per battery) from rated capacity on a daily basis when operated in the normal two-battery mode for 2 years. The rating of 15 ampere hours was based upon a discharge voltage of 22.8 Vdc (1.20 volts per cell), which was 342 watt-hours per battery.



SUBSTRATE	3.96 mm HONEYCOMB, 0.13 mm A1 FACES
SUBSTRATE INSULATION	0.051 mm TEDLAR 200 BG 30 WH
CELL TO SUBSTRATE ADHESIVE	SILASTIC 140, 50% COVERAGE
COVER GLASS ADHESIVE	SYLGuard 182
SOLAR CELL	2 cm X 4 cm; 0.356 mm THICK, 2 ohm/cm, SOLDER PRESSED Ti-Ag CONTACTS
SOLAR CELL INTERCONNECT	STRESS RELIEF LOOPS, 0.052 mm PHOTO-ETCHED FINE SILVER MESH
COVER GLASS	0.15 mm CORNING 0211 MICROSHEET BLUE FILTER
THERMAL CONTROL COATING	MS-74 WHITE SILICATE PAINT
WIRE	KAPTAN MIL-W-81381/7B

Figure 5-7. Solar Cell Stack

Each battery weighed 17.0 kg and was 22.9 cm long by 30.5 cm wide by 19.1 cm high. The cells were arranged in three rows of seven per row with two rows each using a dummy cell. This configuration allowed for each row to rest on a separate heat pipe for good thermal control. The heat pipes, together with a louver assembly, controlled each battery to a temperature within 0°C to 25°C range for all conditions. Each battery contained separate thermistors for charge control, overtemperature protection, and telemetry.

Each battery cell was hermetically sealed with dual ceramic to metal insulators isolating the terminals. The cases were 304 stainless steel and each cell weighed 690 grams maximum. The cells were sealed with 1/20 atmosphere pressure of helium within to permit mass spectroscopic helium leak testing of both cells and battery. The cells were manufactured by Gulton Industries.

Each battery interfaced with the battery charge function of the power regulation unit. Energy was made available in one of three selectable modes: main constant current— $C/10$ with voltage limit, standby constant current— $C/20$, and trickle charge current— $C/60$.

Figure 5-8 shows the main charger characteristics. When the constant current charge caused the battery to reach its voltage limit (\bar{V}_b) for a given temperature, the battery charger gradually reduced the current (I_c) to the tapered trickle level. The voltage at which charge current taper occurred changed with battery temperature as shown in the figure. The voltage/temperature (V/T) curve was selected from extensive cell characterization tests consisting of repetitive charge-discharge cycling to 50 percent depth of discharge at various cell clamp levels.

The trickle charge mode was used to reduce the overcharge and thermal stress on the batteries when they were fully charged.

Each battery contained a thermistor to sense elevated battery temperature that might occur because of overcharge and to provide a signal to automatically disconnect the battery from its charger. This overtemperature protection circuit was set to operate at 35°C measured internal to the battery. Ground command could override this detector if circuit failure resulted.

To prevent overdischarge of each battery and possible cell reversal, a battery undervoltage detection circuit was provided. Details of this circuit are included in the description of the power regulation unit that housed the undervoltage control circuits.

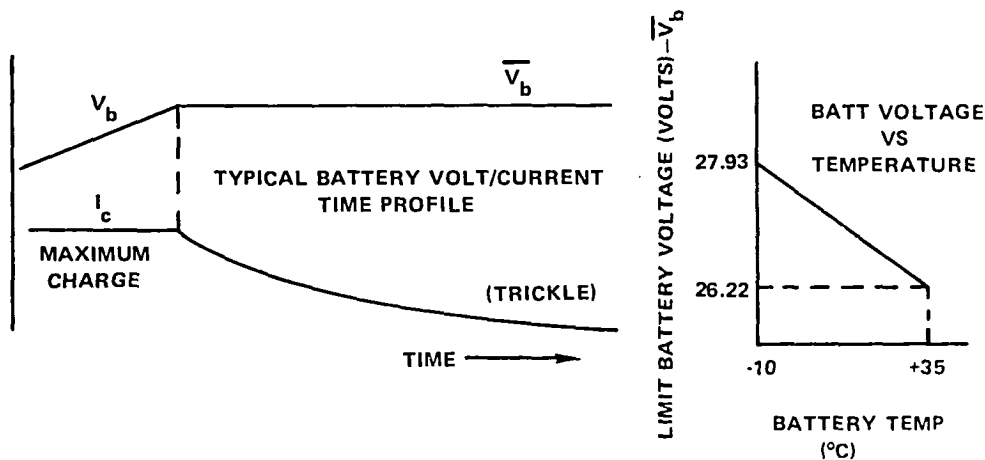


Figure 5-8. Main Charger Characteristics

POWER REGULATION UNIT

The power regulation unit (PRU) was the heart of the power subsystem; it controlled and regulated all primary power used in the spacecraft. The PRU consisted of two redundant units, each containing a battery boost regulator, two battery chargers per battery, shunt driver, controller, and over-voltage clamp. One set of elements (the main unit) were on line controlling the main bus power while the other set was in a standby-off mode. The PRU also contained the bus-failure sensing circuitry to switch to the redundant standby functions in the event of a failure. The PRU weighed 21.4 kg and was 20.3 cm by 43.2 cm by 24.1 cm in size. Details of the functions of components contained within the PRU are described in the following paragraphs.

Controller

The controller consisted of a comparator circuit containing a stable zener-voltage reference and three error amplifiers. Figure 5-9 is a simplified block diagram of the controller. The main-bus output voltage was sampled through a resistance divider network and compared to the stable reference in the comparator operational amplifier. The output from the comparator was a linear voltage that was applied to the inputs of three error amplifiers that were biased at different voltage levels by a single resistance divider network. Depending on the level of this voltage, the amplifiers for either boost regulator control, shunt regulator control, or charge regulator control could be turned "on" as shown in Figure 5-9. A deadband of 150 millivolts was established between the charge regulator turn-on and boost regulator turn-on to ensure that no overlap occurred that could be catastrophic. This deadband was established by the resistance divider network that was common to the three error amplifiers. A single reference was also used to bias all four amplifiers and ensure that the deadband was maintained.

Shunt Driver

The linear error signal from the output of the shunt control amplifier in the controller was applied to the shunt driver, which consisted of a linear amplifier with 12 outputs, one for each shunt dissipator. Each output was capable of a maximum of 28 Vdc, with 150 ohms nominal source impedance. The shunt driver provided drive signals to the shunts when the controller sensed a bus voltage level corresponding to excess power from the solar array. When the error signal increased, the result was a larger drive signal to the shunts from the shunt driver. The shunts then drew more current from the lower (shunted) section of the array thus lowering the voltage of the shunted section, and correspondingly the main bus voltage, to maintain regulation.

Boost Regulator

When the solar array could not provide sufficient power to support the spacecraft loads, additional power of up to 500 watts was provided from the boost regulator that obtained power from the batteries. The boost regulator maintained the bus voltage at a nominal 30.5 Vdc over an input battery voltage range to the PRU of 18.5 to 28.5 Vdc, while providing 0 to 500 watts of load power.

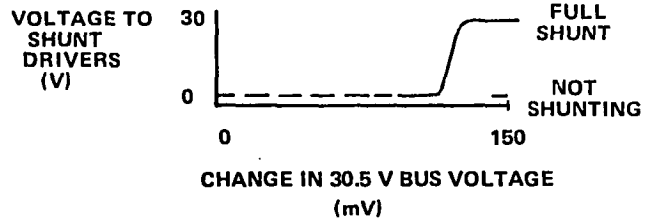
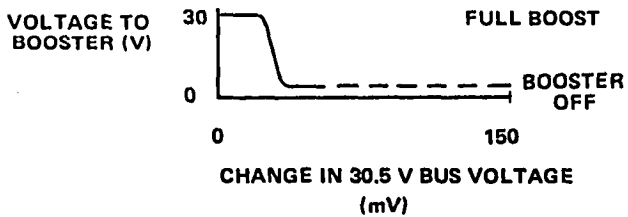
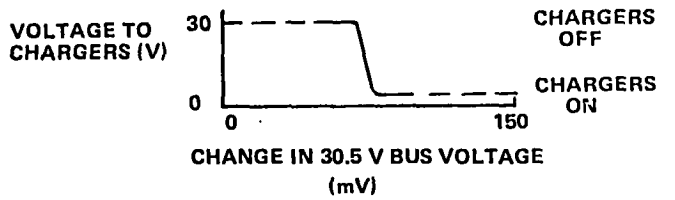
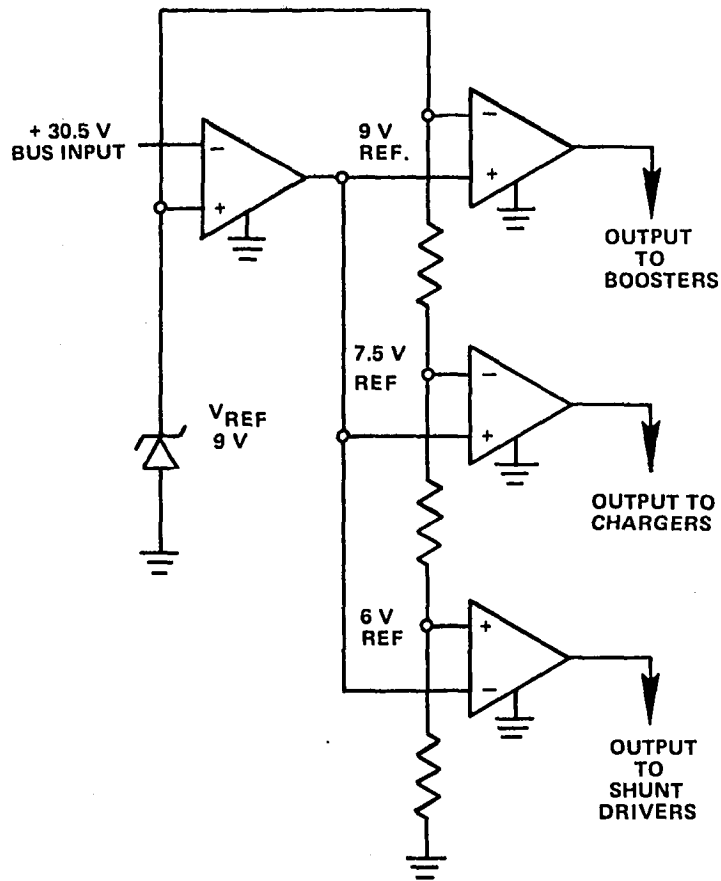


Figure 5-9. Controller Block Diagram

The basic regulator employed a power inverter in series with the battery to provide a voltage boost. The inverter was required to handle and switch only the boost power and not the entire load power, thus offering increased efficiency as compared to other voltage boost power techniques. The inverter used an autotransformer in series with the main battery output. Control of the inverter was provided by a pulse-width modulated drive circuit that was provided with a triangular reference wave and error signal from the controller. The modulator acted as a comparator providing an output pulse whose width was determined by the time period during which the triangular wave exceeded the controller error signal.

An overcurrent protection circuit was provided in the boost regulator to prevent the power transistors from carrying and switching excessive current.

The boost-regulator efficiency ranged from 85 to 89 percent within a 200- to 500-watt range.

Battery Chargers

Each battery had a main charger and a standby charger. These chargers were enabled by the controller, so that during periods of excess energy the solar array charged the respective batteries. During these periods, the chargers could also be turned off by command from the ground.

The battery chargers were capable of operation in any of three different modes identified as (1) constant-current charge (used when the batteries were in a discharged condition), (2) constant-voltage charge (occurred when the batteries approached full charge), and (3) trickle charge (available when needed and upon command from the ground).

When the battery voltage dropped because of discharge, as measured against an accurate reference voltage, the voltage differential was sensed by the main charger and a constant current of up to 1.5 A (C/10) was furnished by the main charger if solar array power was available. When the standby charger was employed, its maximum constant-current charge was 0.75 A (C/20). The constant-current charge continued until the battery voltage reached a predetermined voltage/temperature limit. When this limit was reached, the charger regulated the battery voltage as a function of the temperature sensed by a thermistor embedded in the battery. A highly stable voltage regulation circuit with tight tolerances, controlled the clamp voltage of the charger for temperature variations between -10°C and $+35^{\circ}\text{C}$. Figure 5-8 shows the main charger characteristics.

A trickle charge of 0.25 A may be commanded from the ground stations, but only when the battery voltage exceeded 25.1 Vdc. Normal high-rate (C/10) charging could also be restored at any time by ground command. When the battery was below 25.1 Vdc, the trickle-charge command was overridden by automatic switching circuitry in the charger. This feature was incorporated to prevent a discharged battery from remaining in the trickle-charge mode.

Malfunction Protection

The power regulation unit contained several types of failure detectors. Table 5-1 summarizes the various malfunction protection features.

Table 5-1
PRU Malfunction Protection

Condition	Detector	Action	Reaction Delay Time
30.5-V bus rises above 33.0 V ± 0.6 V	Failure detector	Standby controller, shunt driver, current sensing inverter, and booster used in place of main units. Chargers turned off.	0.1 second, maximum
30.5-V bus drops below 28.0 V ± 0.5 V	Failure detector	(a) Standby overvoltage clamp connected in place of main. Undervoltage failure pulse sent to PCU to open nonessential load breaker. (b) PRU reconfigured as in 33.0 V ± 0.6 V condition.	250 ms ± 50 ms
30.5-V bus rises above 36 V ± 2 V	Overvoltage clamp	Turn shunts full on and inhibit booster operation by overriding controller signals	Immediate
Battery upper section (9 cells) voltage falls below 9 volts, or lower section (10 cells) voltage falls below 10 volts	Battery undervoltage	Remove battery from all loads except command system	1 second minimum
Battery temperature rises above 35°C ± 2 °C	Battery overtemperature detector (one for each battery)	Turn off main battery charger	Immediate

POWER CONTROL UNIT

The power control unit (PCU) was the main distribution point for regulated voltage to the spacecraft loads. A functional diagram of the PCU is shown in Figure 5-1.

The PCU distributed the power to the nonessential loads through the use of two relay circuits arranged in parallel so that either relay could carry power from the essential to the nonessential bus. When both relays were in the open position, the nonessential loads were disconnected.

One of the bus relays could be disconnected by a bus undervoltage signal from either the PRU or internal PCU failure-detection circuits. A low bus voltage of 28 volts for 250 milliseconds would cause the relay to open. The second relay, which was normally open, was controlled by ground command only as an override function.

One of the two 28-volt, 300-watt regulators normally provided power to one of the rf power amplifier buses; however, either regulator could be disconnected and the other regulator could be connected to supply power to both buses and handle the entire load. The configuration was selected by command from the ground. Details on the regulator design will be discussed in the load interface circuit section.

The PCU weighed 7.17 kg and measured 17.8 cm by 20.3 cm by 30.5 cm.

SHUNT DISSIPATORS

There were 12 shunt dissipators that operated in conjunction with the PRU to regulate the solar array output voltage. They dissipated a portion of the power produced by the solar array when it provided more power than could be used by the spacecraft loads or battery chargers. The shunts maintained a constant voltage on the power bus by controlling the voltage at the lower or tapped section of the solar array.

Each shunt was connected to four different strings (on four different panels) of each half-cylinder of the solar array, a total of eight strings in all. Each shunt tap point was at two-thirds of the string length of 75 cells from the negative bus, thereby shunting 50 cells on each array string.

Each shunt dissipator unit was capable of sinking a maximum current of 4 amperes and of pulling the lower section of the solar array down to an operating voltage of 5 volts. Shunt power dissipation design level was 35 watts under normal continuous operating conditions and 50 watts peak for up to 30 minutes.

Each shunt dissipator had a separate control input signal (as shown in Figure 5-10) from the main shunt driver and from the standby shunt driver of the PRU. The two inputs were redundant with either the main or standby shunt driver being capable of operating the shunts. The two control inputs were connected in a dual diode OR configuration and functioned as the base drive signals to the two drive elements that controlled the power control elements of the shunts.

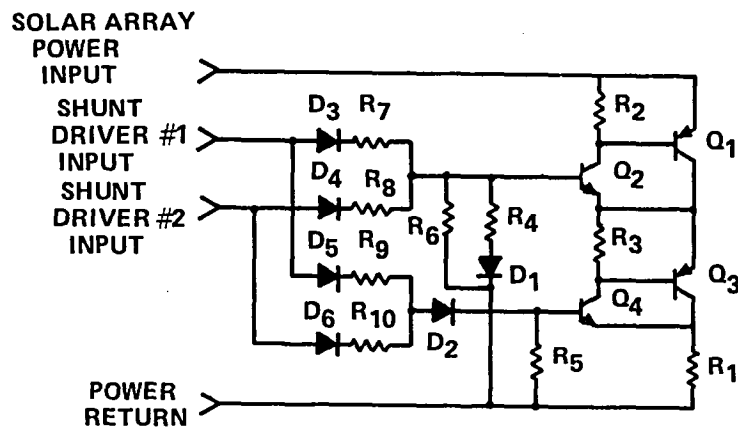


Figure 5-10. Basic Schematic of Shunt Dissipator

The shunts remained operational even if either of the pass transistors suffered an emitter-collector short circuit. The other series-pass element functioned to control the current drain from the shunted array sections.

The solar array current, drawn by each of the shunts, was equalized by the insertion of a resistor in series with the power transistors and the use of low-input impedance networks in the shunts to reduce gain variations. This was done to control the dissipation in each shunt and effect good power sharing among all 12 shunts.

LOAD INTERFACE CIRCUITS

There were seven load interface circuits (LIC) in the electrical power subsystem. Each was located in close proximity to the experiment it powered, to limit the electromagnetic interference coupled to and from experiments. Functional interfaces of the LIC's are shown in Figure 5-1.

Each LIC controlled and distributed the power to its respective experiment load by performing the following functions:

1. Regulated dc voltage to the experiment loads to $28 \text{ Vdc} \pm 2$ percent from the nonessential power bus.
2. Provided short circuit protection to the power system. A shorted output load resulted in the LIC disconnecting the load.
3. Controlled undervoltage by removing the load if the LIC output voltage fell below 24 Vdc .
4. Provided the command capability to turn the experiments on and off.
5. Isolated the experiment load from ripple and noise on the input power line.

The LIC's were of three different power ranges: 15 watts, 60 watts, and 150 watts. The Ion Engine and Millimeter Wave experiments were controlled by 150-watt load interface circuits. The Radiometer and EME were controlled by 60-watt LIC's, and the Propagation experiment was controlled by the 15-watt LIC. The Quartz Crystal Microbalance and Advanced Thermal Control Flight experiments shared a 60-watt LIC. The rf power amplifier regulators in the PCU were similar to an LIC and had 300-watt ratings.

LIC output voltage was regulated to $28 \text{ Vdc} \pm 0.45 \text{ Vdc}$ through the use of a voltage feedback loop. Input voltage to the LIC's could vary from 28.4 Vdc to 38.0 Vdc without causing loss of regulation. A current feedback loop was also provided to limit the output current during start up or if an overload or short circuit occurred in the experiment. The LIC's permitted 150 percent of the nominal current for each power limit to flow through the pass element before initiating current limiting. For relatively short overload durations, the LIC's recovered to normal operating voltage at the end of the overload condition. Figure 5-11 illustrates the regulation characteristics of the LIC.

The rated load current was determined for each LIC, based on its output power rating at 28 Vdc. For the 15-watt LIC, the rated maximum load current was 0.55 A. For the 60-watt and 150-watt LIC, the rated maximum load current was 2.2 A and 5.4 A, respectively. The maximum available load current was set individually for each LIC, based on the maximum power requirements of its experiment load.

Each LIC measured 8.9 cm by 15.7 cm by 10.2 cm. The 15-watt unit weighed 907 grams, the 60-watt unit weighed 953 grams, and the 150-watt unit weighed 1043 grams.

ARRAY HARNESS

Each solar array paddle was connected to the power system through a 10.7-meter external harness. This harness was routed from each paddle along the solar array boom, down the truss assembly and into the service module. Once inside the service module, each harness separated into the main bus harness that went directly to the PRU and the solar array tap harness that was routed to the various shunts.

Because of the tapped array power system configuration, the ground power solar array simulator and umbilical harness became part of the shunt regulation feedback control loop and, as such, its impedance characteristics were important in the overall loop stability and dynamic performance of the power system. A stabilized system was ensured by first incorporating the impedance of the umbilical harness in a mathematical model of the system transfer function and evaluating the stability through gain-phase Bode diagrams. The system was then tested with a solar array simulator and simulated umbilical harness to evaluate the loop stability. Based on these tests, the shunt regulation control loop had adequate stability margins.

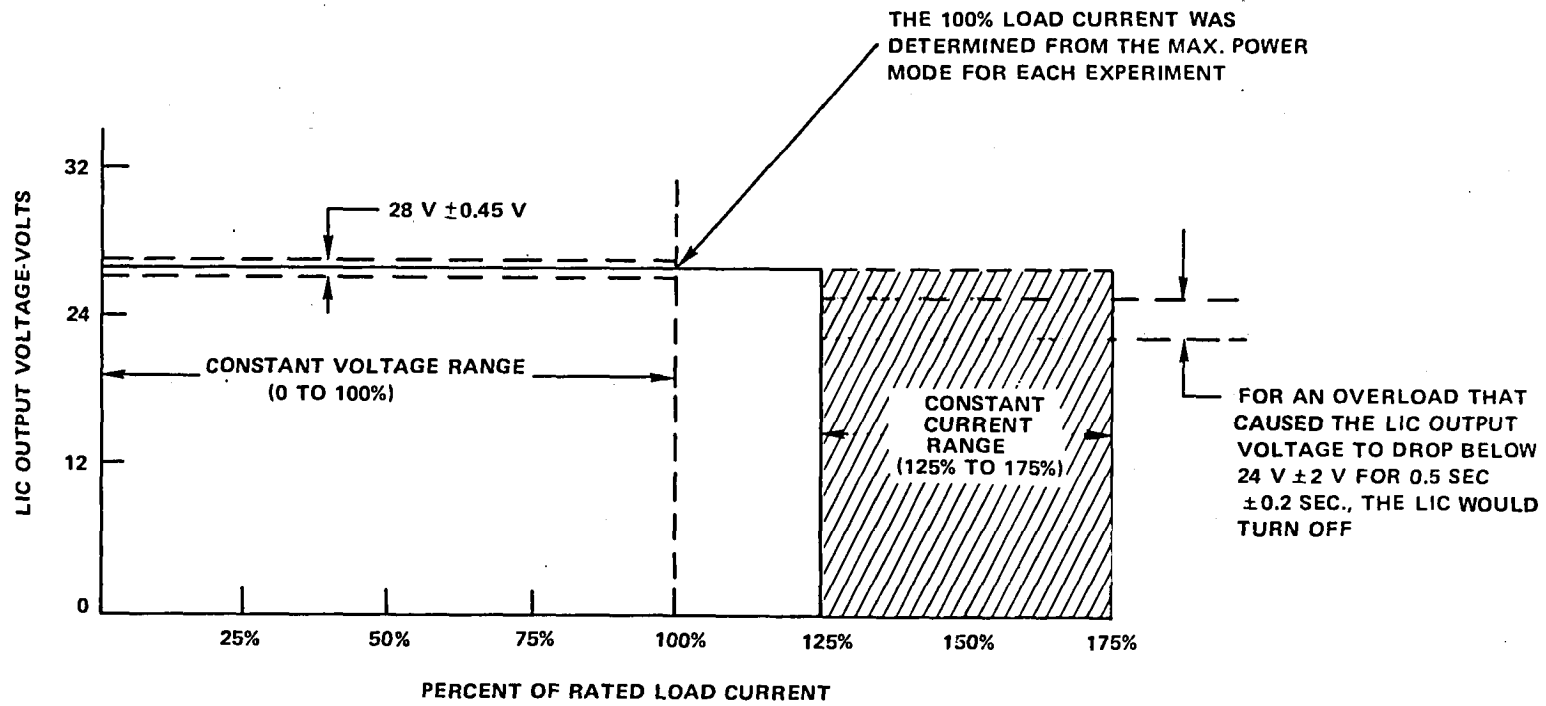


Figure 5-11. LIC Regulation Characteristics

SPECIAL POWER SUBSYSTEM PROTECTIVE FEATURES

Nonessential Bus Undervoltage/Overload Protection

If an overload occurred in the power system that caused the 30.5 Vdc bus voltage to drop to $28 \text{ Vdc} \pm 0.5 \text{ Vdc}$ for 250 milliseconds, nonessential bus relay would open and disconnect all nonessential loads. The signals to open the nonessential circuit breaker were generated from sensing circuits in the PCU and redundantly in the PRU. The circuit breaker could only be reset by command from the ground.

If the 30.5-V bus did not recover to a voltage above 28 V within 500 milliseconds, the power subsystem was automatically reconfigured to the standby units. The signal that caused this switch to the redundant power system units was generated in the power regulation unit (PRU) where the bus voltage was sensed. Up to 1000 watts could be delivered from the power subsystem. During overloads, the battery discharge boost regulator could provide up to 500 watts before the onset of current limiting. An overcurrent turn-off circuit in the booster operated to protect the booster power switching transistors. This circuit did not prevent the battery output from being applied to the regulated bus to provide a high current source for the blowing of fuses or clearing of faults.

Power Amplifier Overload Protection/Experiment Bus Overload

The secondary buses involved were the 28-volt outputs of the load interface circuits and communication system rf power amplifier regulators. If an overload or undervoltage occurred at the output of one of these regulators or load interface circuits that caused the voltage to drop to 24 volts and remain there for 500 milliseconds, the regulator would turn off. If an overload was applied to the regulator or load interface circuit (LIC), the current output would be limited to 150 percent of nominal for the duration of the overload or until the regulator turned off.

POWER DISSIPATION CONTROL

The shunt-boost design provided maximum use of array power at end-of-life by forcing the array to operate at a fixed voltage where the array design could be optimized. Regulation of the array voltage was achieved by using shunt dissipators to control the excess array power.

For active control of array voltage in previous shunt regulator systems, the power dissipating circuits have generally been located external to the spacecraft equipment module. This location was chosen so that the thermal system would not be required to handle the shunt power dissipation. This approach is satisfactory for spacecraft where the load power is fairly constant, such as a single experiment mission. However, on a mission such as ATS-6 where there are many experiment operating modes with power levels that vary from 250 to 800 watts, it is highly desirable to use the excess power in the shunts to limit the power dissipation range within the spacecraft. In addition, it will substantially raise the minimum spacecraft power dissipation.

The use of heat pipes in the ATS-6 thermal design provided good lateral heat transfer. Mounting the shunt dissipators on a heat pipe surface allowed the heat input from the shunts to be distributed along the heat pipe wall for thermal control.

To integrate the shunts into the thermal control subsystem, the power subsystem needed to meet the following requirements:

1. Limit maximum in-orbit shunt power to less than the total array power to lower the maximum power dissipation at beginning-of-life.
2. Distribute shunt power evenly in the three spacecraft Earth-viewing modules.
3. Design shunts to share power with no greater than a 25 percent power differential from lowest to highest power shunts.

To reduce the shunt power dissipation, the tapped array configuration was used. With the tap tie-point located at the 50-cell position of the 75-cell string, the total shunt power varied with load power as shown in Figure 5-12. To a first order approximation, the shunt power varied by the two-third ratio of the excess array power. From the figure, it can be seen that for the minimum load power of 150 watts on the lower array curve, a shunt dissipation of 190 watts results. Thus, for this lower array power case, total dissipation would be 340 watts versus 150 watts without shunt dissipation. For the beginning-of-life maximum array and worst-case peak load condition, the dissipation was 750 watts. When the shunt dissipators were used for thermal control, the power dissipation range was 2.2 to 1 versus 5 to 1 when not used. Thus a substantial reduction in thermal control power dissipation range resulted with the use of the shunt dissipators for heat input.

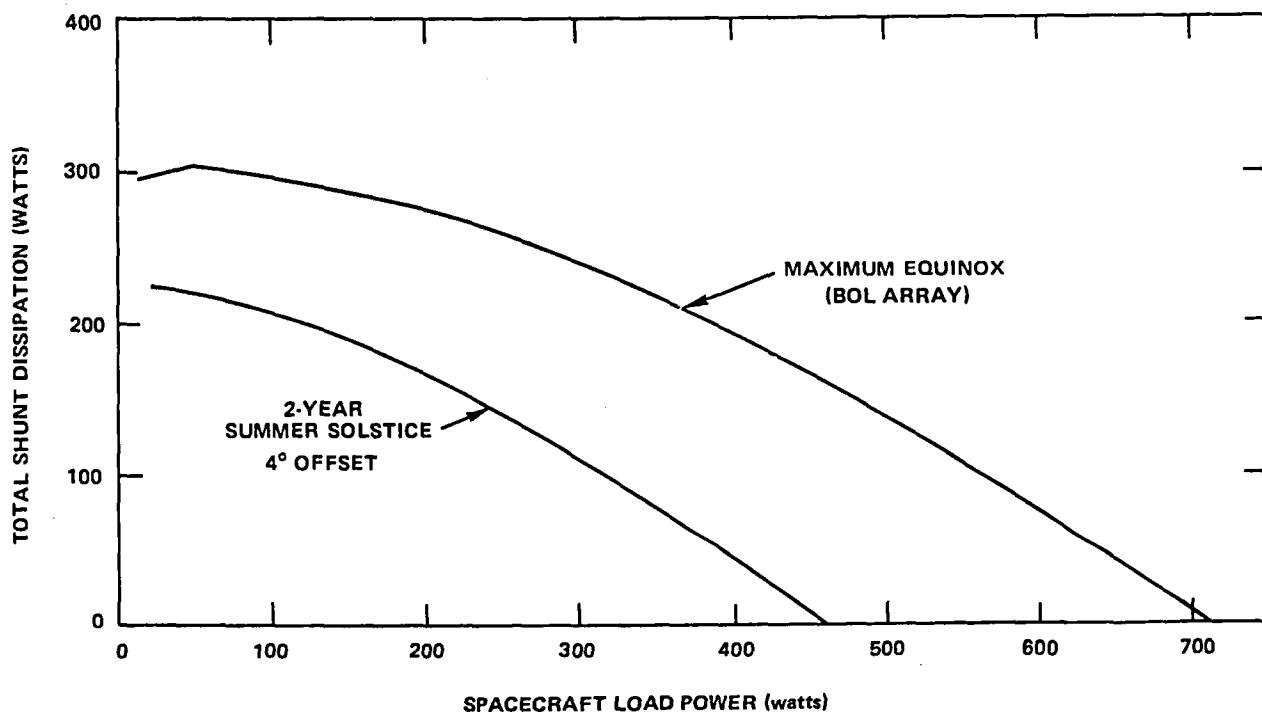


Figure 5-12. Shunt Dissipation

To distribute the shunt power and provide an optimum interface to the solar array, 12 shunts were selected. Each of the three Earth-viewing modules contained four shunts (two mounted on each of the two external heat pipe walls). The array shunt wiring configuration forced the excess array power to be shared equally by the 12 shunts with only a slight variation, since only 6 shunt circuits were connected to the panels on each solar array facet. The adjacent facet provided power to the other six shunts. The shunt power differed slightly from each facet to its adjacent facet because of the small difference in Sun incidence angle and panel temperature.

PERFORMANCE CHARACTERISTICS

Since all spacecraft subsystems interfaced at the power bus, it was here that subsystem interactions could occur due to load current fluctuations and conducted electromagnetic interference. To minimize these interactions, it was important that the power subsystem provide a low impedance bus with fast transient response.

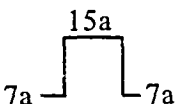
The dynamic characteristics, as obtained by ground tests of the subsystem, are described in the following paragraphs. For these tests, a solar array simulator was used to provide power to the power subsystem. This simulator was designed to provide a current-voltage (I-V) wave shape approximating the actual array characteristics, including the tapped sections for the 12-shunt dissipators.

Dynamic Regulation

Table 5-2 shows the dynamic regulation requirements imposed on the power subsystem.

The transient response of the power subsystem to the instantaneous load change requirements is shown in the sketches traced from photographs and presented in Figures 5-12, 5-13, and 5-14. These figures demonstrate the regulation of the system in the shunt and boost modes. Also shown is the maximum voltage change that occurred for a load change that forces the system from shunt to boost mode and vice versa. For the response evaluation, a steady-state load of 7 A was applied to the system, while the dynamic load applied was a step of 8 A (240 watts), with rise and fall times less than 50 μ s. The load varied from 7 A (210 watts) to 15 A (450 watts) and back to 7 A. The test was performed for three solar array power conditions: 500 watts, 400 watts, and 0 watts.

Table 5-2
Dynamic Regulation Requirements (30.5 V Bus)

Load Current Change: 7 to 15 amp step wave with $t_{\text{rise}} = t_{\text{fall}} < 50 \mu\text{s}$,	Maximum Voltage <u>Overshoot</u>	Maximum Voltage <u>Undershoot</u>	Maximum Response <u>Time</u>
 <p>a. $P_{\text{array}} = 500 \text{ W}$ b. $P_{\text{array}} = 400 \text{ W}$ c. $P_{\text{array}} = 0 \text{ W}$</p>	3.05 V	3.05 V	2 ms

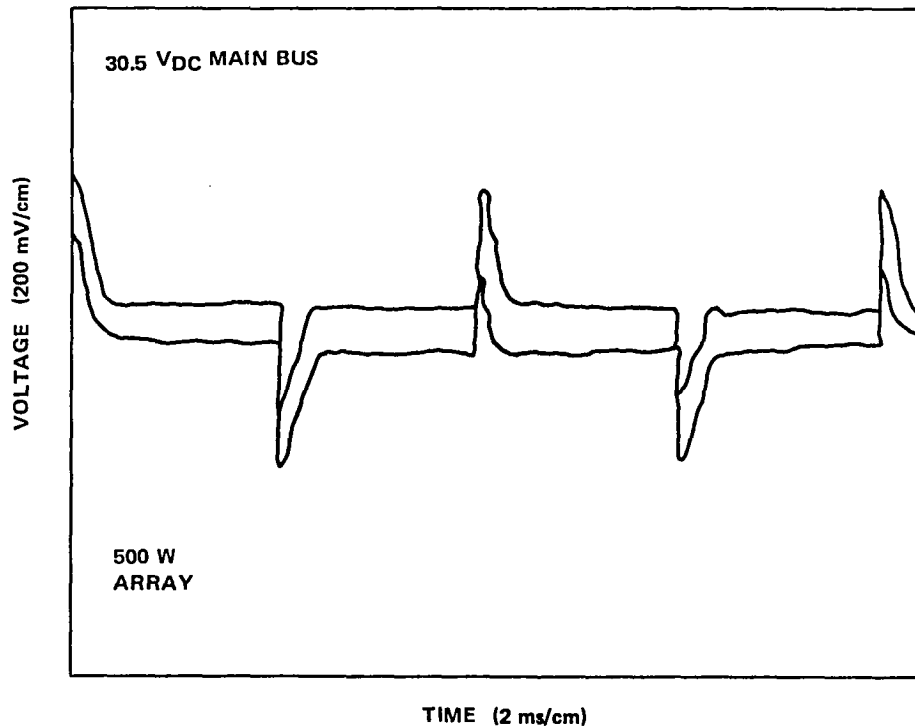


Figure 5-13. Dynamic Regulation (Shunt Mode) 500-Watt Solar Array

Figure 5-13 shows the bus response for the 500-watt array condition. Since the array capability exceeded the maximum load of 450 watts, this test demonstrated the response of the shunt mode. Note from this figure that the application of the 8-A load resulted in an undershoot of 0.3 volt with recovery back to steady state in 0.6 millisecond. The removal of the 8-A load resulted in an overshoot of 0.32 volt with recovery in 0.6 ms.

Figure 5-14 shows the bus response for the 400-watt array condition. For this test, the dynamic load requirement of 450 watts (15 A) exceeded the capability of the array and the boost regulator had to turn on and supply the additional energy from the batteries. This test shows the worst-case voltage change on the bus, from shunt through charge to boost mode and back to shunt.

The application of the 8-A load did not result in any measurable undershoot. The change in steady-state value was due to the 0.15 volt dead-band separating the boost mode from the charge and shunt modes. The overshoot that occurred on removal of the 8-A load was 1.4 volts with recovery in 1.2 milliseconds.

Figure 5-15 shows the bus response to a zero-watt array. For this condition, only the boost mode was active with the battery supplying the load through the boost regulator. The application of the 8-A load resulted in an undershoot of 0.66 volt with recovery in 0.6 ms. An overshoot of 0.9 volt with recovery within 0.6 milliseconds resulted from the removal of the 8-A load.

These figures show the excellent dynamic regulation and transient response of the power subsystem. This performance was achieved by providing fast responding feedback loops in the shunt, charge,

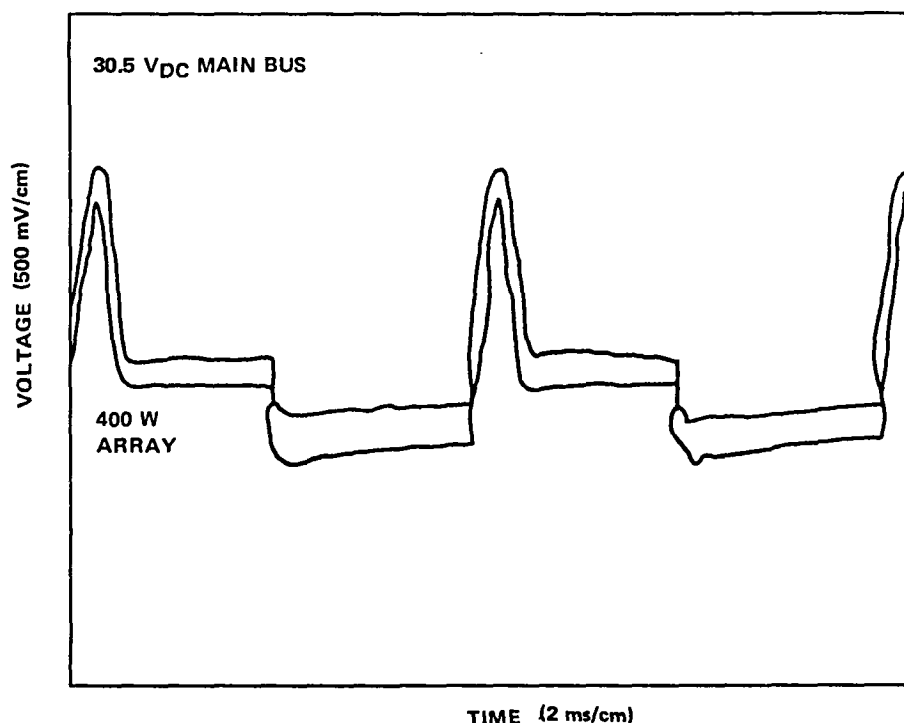


Figure 5-14. Dynamic Regulation (Shunt/Boost Mode) with 400-Watt Solar Array

and boost modes. Gain crossover for the shunt loop was set at 20 kHz, the charge-loop crossover was set at 5 kHz, while the boost-loop crossover was 2 kHz. In addition, the linear shunt circuit configuration and the autotransformer boost circuit also provided fast response to the feedback error signals. Since the shunt and boost regulator designs and the feedback bandwidths provided excellent response, the main bus capacitors needed for energy storage could be minimized. Only 2000 microfarads of capacitance were used, resulting in a substantial reduction of weight and volume.

With this capacitance and regulation, a maximum of 50 mV of ripple voltage occurred on the main bus in the boost mode (eclipse operation). That compared to a specification maximum of 150 mV. In the shunt mode (operation in sunlight), where the system operated most of the time, a ripple voltage of less than 10 mV occurred.

Output Impedance

The output impedance of the power subsystem is shown in Figure 5-16 for the primary modes of operation—shunt and boost. The impedance for both modes is quite low—well below 0.1 ohm, which accounts for the excellent dynamic performance. A close look at the curves shows the maximum impedance of 0.06 ohm occurred at about 2 kHz, the 0 dB gain crossover for the boost feedback loop. For the shunt mode, which had higher loop gain and bandwidth, a maximum impedance of 0.035 ohm occurred.

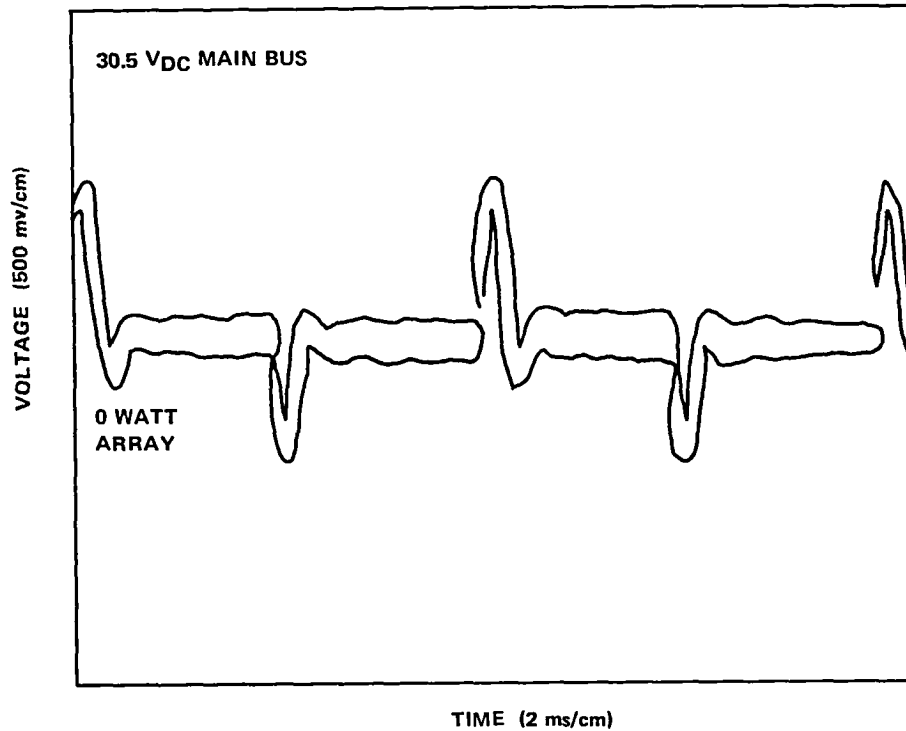


Figure 5-15. Dynamic Regulation (Boost Mode) with 0-Watt Solar Array

Overload Protection

To protect the spacecraft subsystems from bus transients due to the occurrence of an overload or short in any load, a unique protection feature was incorporated into the power subsystem. If an overload (over 1000 watts in sunlight and 500 watts in occult) occurred, the boost regulator cycled off for 90 milliseconds and linearly on for 10 milliseconds to sample for presence of the overload. During the 90 milliseconds that the boost regulator was off, the bus was clamped to the battery. If the overload continued for 250 milliseconds, the nonessential relay opened disconnecting the nonessential loads. Should the overload remain, the regulator continued to cycle on and off linearly until an additional 250 milliseconds had elapsed. At that time the power system was automatically reconfigured to its standby redundant units. Should the overload or fault continue, it could be cleared by the battery since the battery was applied directly to the regulated bus to provide a high current source for clearing faults. Figure 5-17 shows the power regulation unit (PRU) and power control unit (PCU) fault signals generated to control removal of nonessential loads and switchover to the standby redundant units.

Figures 5-18 and 5-19 show the actual performance of the power subsystem to both nonessential and essential bus faults. Note the smooth linear rise and fall of the bus voltage and the absence of

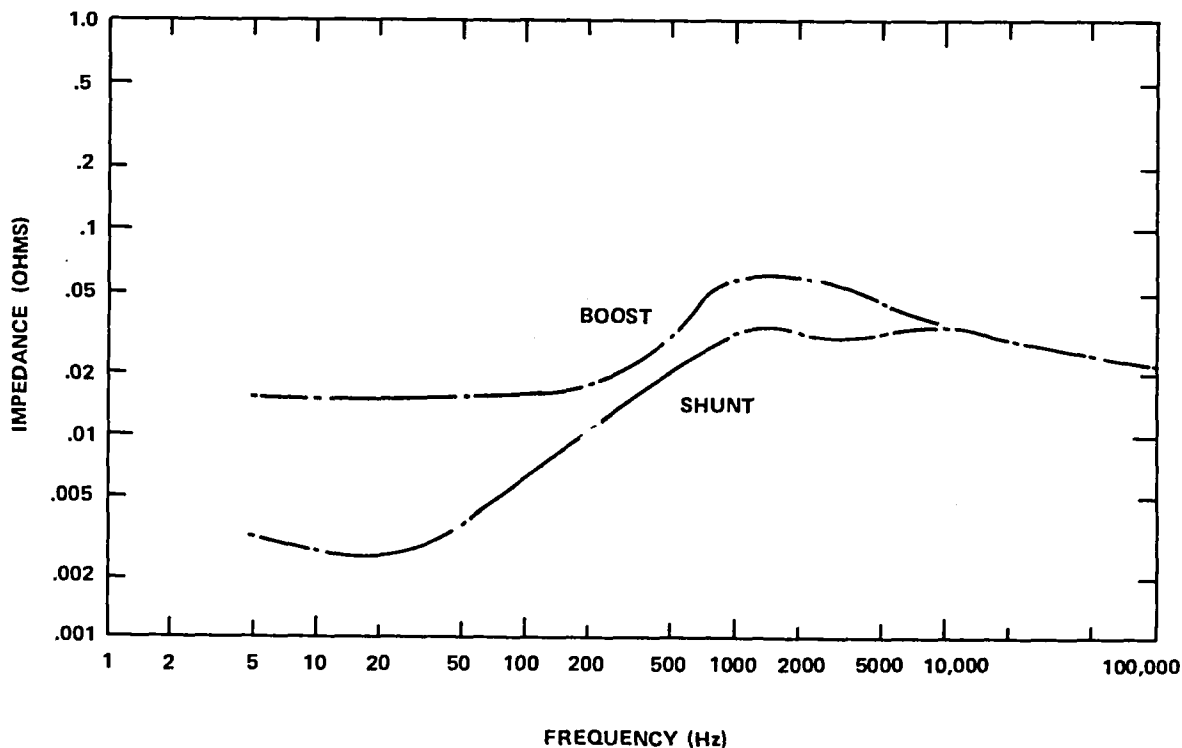


Figure 5-16. Output Impedance

any fast bus voltage transients. In Figure 5-18, the opening of the nonessential bus relay removed the overload and the bus voltage smoothly recovered to the regulated level of 30.5 Vdc. Transfer to the standby regulation units did not occur as evidenced by the absence of a 5-volt level change in TP39 (telemetry signal indicating on/off status of redundant units in the PRU). In Figure 5-19, the overload was removed after 650 milliseconds. For transfer to standby units, 500 milliseconds was required. The change of 5 volts in the level of TP39 shows the transfer of the system to the redundant units. A smooth voltage recovery is again evidenced.

Load Interface Circuits

The current-voltage (I-V) characteristics of the output of each LIC is shown in Figure 5-11. This characteristic shows the voltage regulation mode, constant current mode for overload protection, and undervoltage protection mode.

Line isolation of noise and ripple voltage was provided by the ability of the LIC's to attenuate input variations over a broad frequency range. Input ripple rejection as a function of frequency for a 300-watt LIC is shown in Figure 5-20.

Output impedance characteristics of a 300-watt LIC is shown in Figure 5-21.

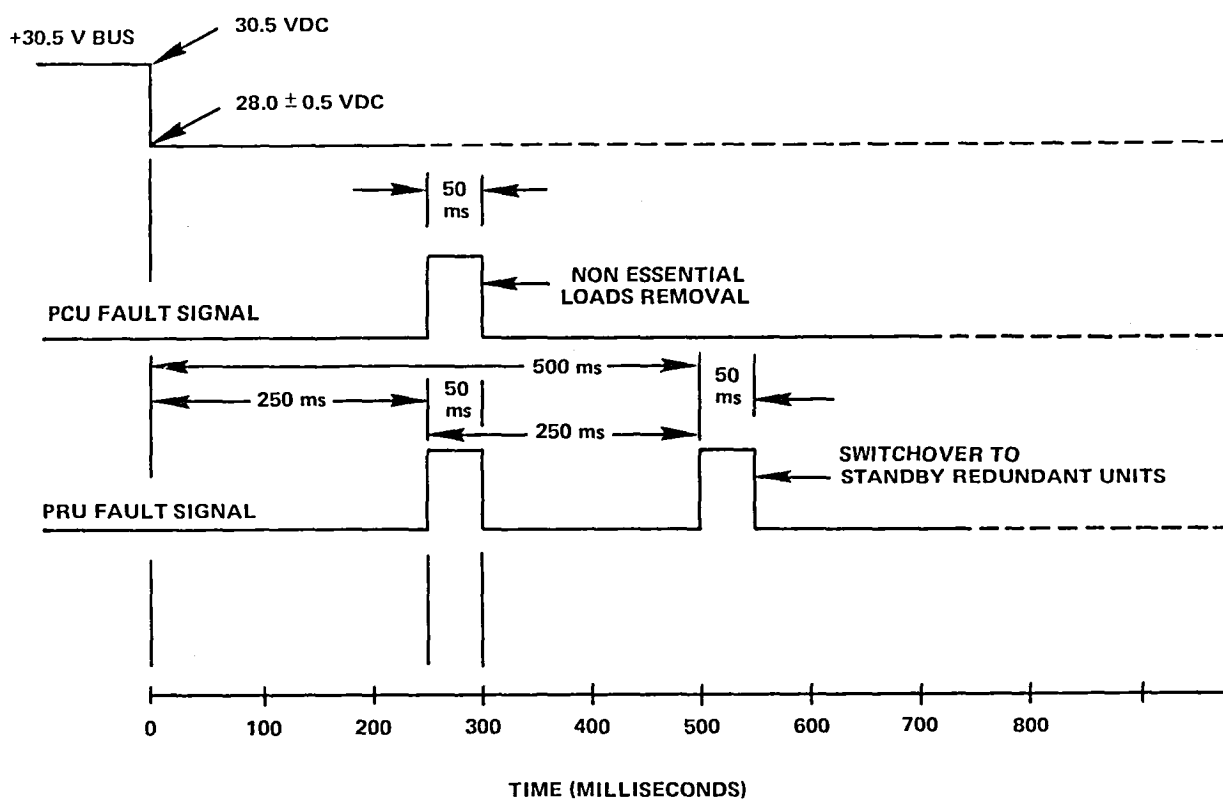


Figure 5-17. PCU/PRU Timing Scheme for Bus Protection

ELECTRICAL POWER SUBSYSTEM TEST REQUIREMENTS

The electrical power subsystem was qualified, first at the component level, and then as a subsystem following integration into the spacecraft with the flight harness. Component test flow was as follows:

- Weight and center of gravity
- Leakage (batteries only)
- Performance
- Vibration, sine and random
- Performance
- Thermal-vacuum

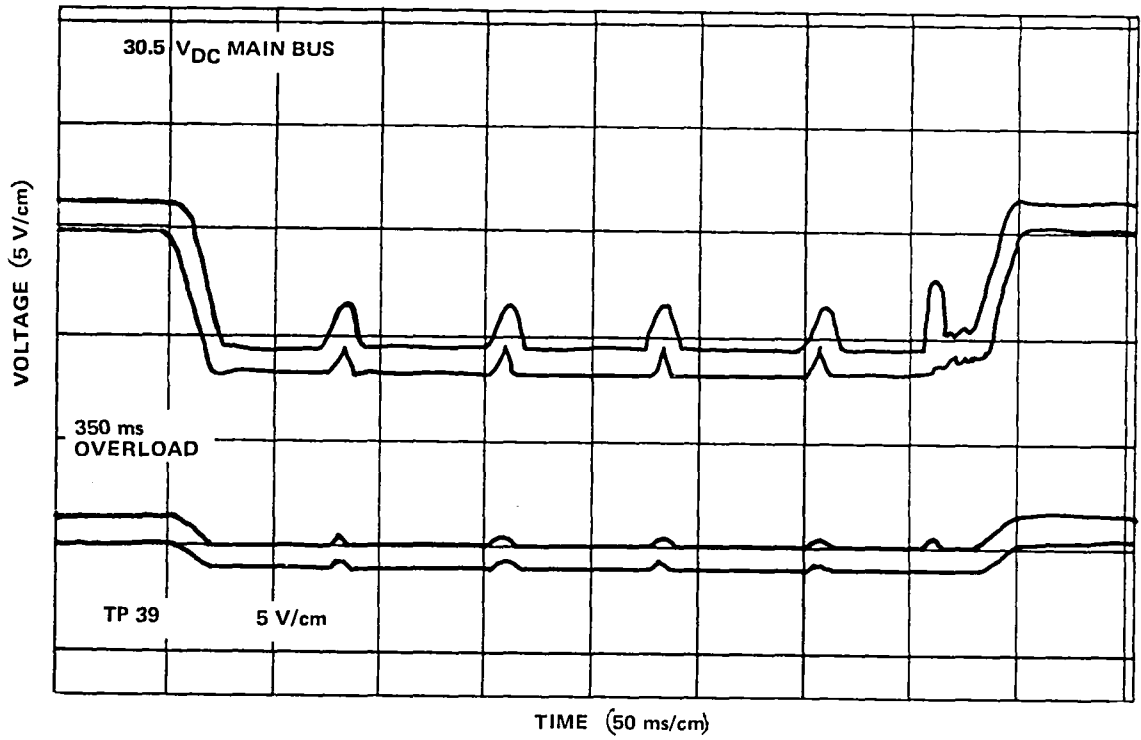


Figure 5-18. Bus Response to Nonessential Bus Overload

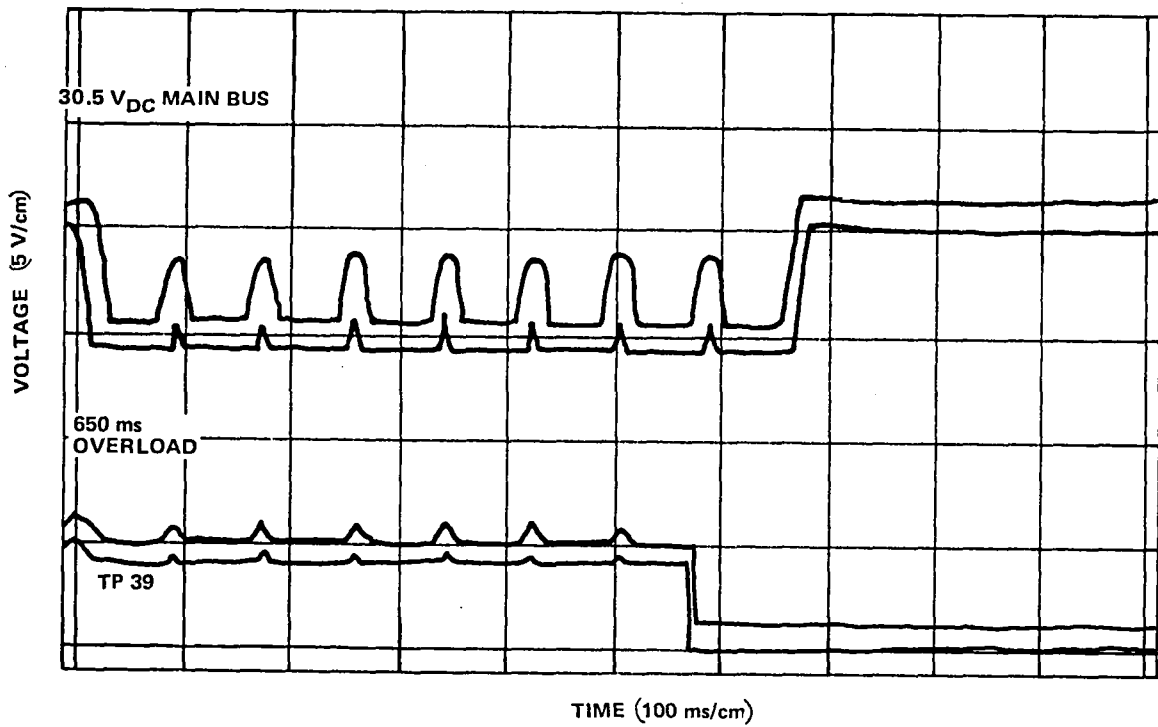


Figure 5-19. Bus Response to Essential Bus Overload

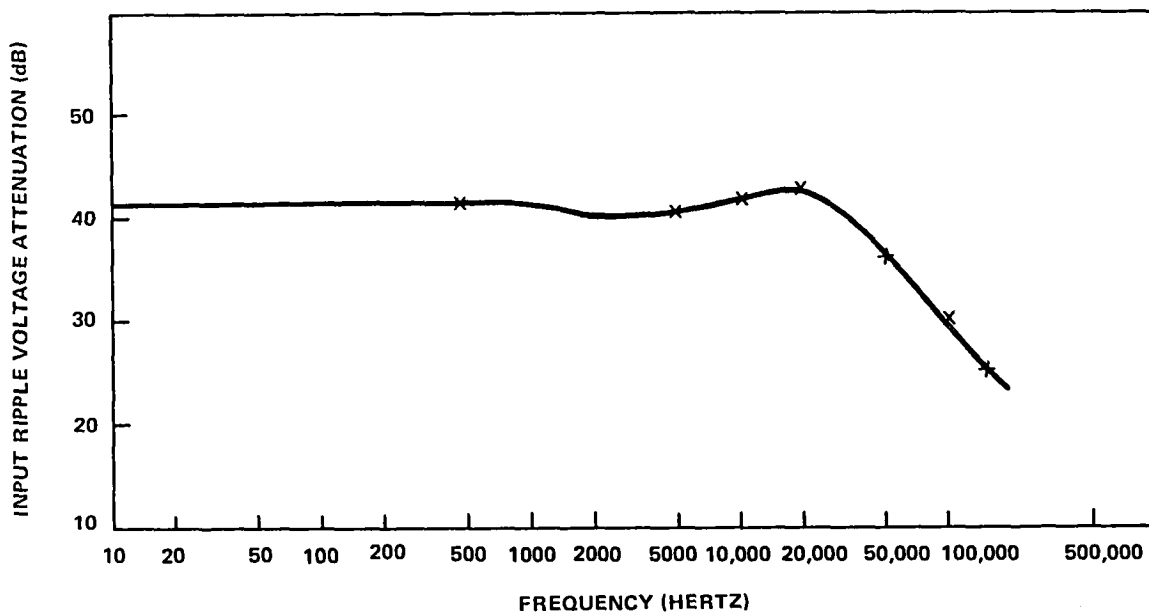


Figure 5-20. LIC Input-Ripple Voltage Attenuation versus Frequency (300-Watt Unit)

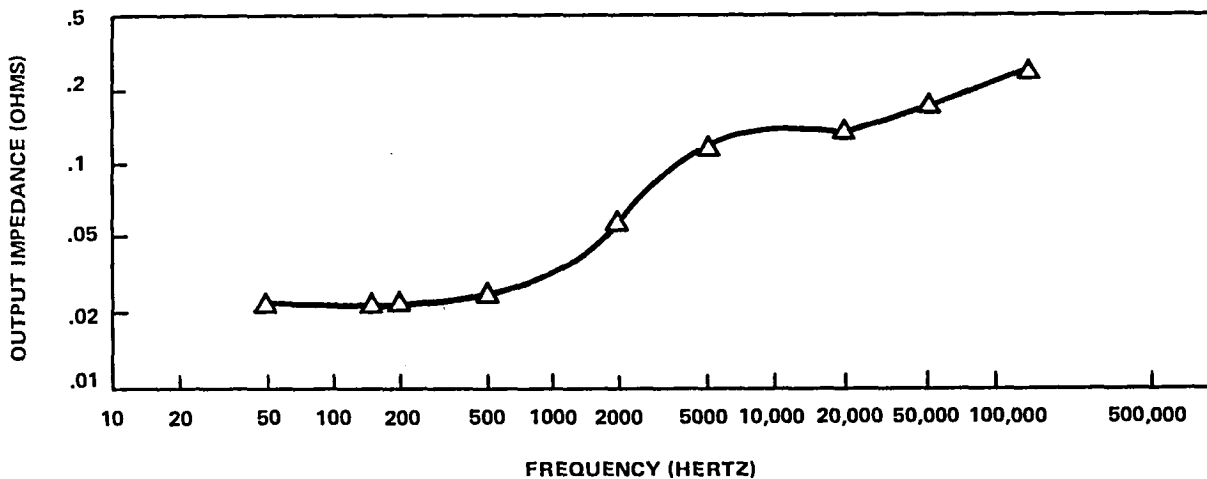


Figure 5-21. Load Interface Circuit Output Impedance (300-Watt Unit)

- Performance
- Spacecraft integration

The electrical power subsystem was not tested at the system level until it was integrated into the flight spacecraft. Performance tests were conducted at the system level during installation and integration of subsystem and experiment instrumentation in the spacecraft during spacecraft integration. System level performance tests were then conducted following spacecraft environmental tests. Since the Earth-viewing module, as a single assembly, was subjected by itself to thermal-vacuum tests, the solar arrays and all spacecraft harnesses were not installed or connected. Therefore, system level tests during thermal-vacuum testing did not include these elements.

The following sections describe special tests and operations that were unique to the electrical power subsystem and the spacecraft.

SPECIAL TESTS AND OPERATIONS

Solar Array Panel Environmental and Performance Tests

A program was incorporated into the spacecraft test flow that minimized spacecraft test disruption while adequately testing the array. The large size of the array posed a significant challenge for testing the array while mounted on the spacecraft. In addition, test accuracy and repeatability were very important to analyze and evaluate the pretest and post-test data after each major spacecraft environmental test.

The solar array test program was structured to provide the highest practical assurance that the solar array would meet its objectives. There were two levels of test. The first level was on the individual panel where thermal cycling of the panels was performed to ensure that good quality panels were delivered to the spacecraft. The second level was on the spacecraft where a highly uniform flash illuminator was used to test each panel.

The prime driver behind the panel thermal cycling test was the extreme low-temperature limit of -160°C (Figure 5-6). A parametric thermal cycling test program was developed to determine the number of thermal cycles required to verify acceptable panels for the synchronous orbit temperature range. An inadequate number of thermal cycles might not sufficiently stress the hardware and, therefore, not expose manufacturing defects. An excessive number of cycles might reduce the life of the hardware.

The structure of the thermal cycle test program had to resolve this conflict by providing high confidence at minimum risk. The first step was to segregate a randomly selected lot of 40 panels (32 required for one spacecraft plus 8 spares) into 5 groups of 8 panels each. The first group of 8 panels was subjected to 100 cycles from -160°C to $+60^{\circ}\text{C}$; the second group was subjected to 50 cycles and the third group to 25 cycles. Their (I-V) curves were recorded and visual inspections made before and after the thermal cycling. Based upon a comparative analysis of all groups, all the remaining panels were then subjected to the minimum number of cycles required to ensure that most

of the manufacturing defects would be detected and corrected. One of the conclusions drawn from the parametric thermal cycle test was that 25 cycles over the synchronous orbit temperature range were sufficient to disclose workmanship defects. Figure 5-22 shows electrical degradation as a function of cycles. As shown in this figure, a point was reached between 25 and 50 cycles where the degradation rate began to flatten out. Increased degradation would not be expected until the design-life point is reached and fatigue would dominate the performance characteristics.

Comparison of the visual inspection data with the electrical data showed that the panels that experienced the greatest electrical degradation also had the largest number of mechanical defects. Within the 25- to 50-cycle range, the panels with workmanship problems were effectively identified. A precision flash illumination system, the TRW large area pulse solar simulator, was used for testing the solar array at the panel string level while mounted on the spacecraft. The system consisted of a pulsed 3-megawatt xenon flash unit and a temperature-intensity correcting data acquisition console. The data acquisition console automatically plotted and printed on paper tape a ten-point I-V curve from open-circuit voltage to short-circuit current with eight adjustable load points to show the I-V knee characteristics. The flash illumination uniformity was better than 1.0 percent over a target area of 0.74 m² (8 sq. ft.) and a distance between flash unit and panel of 9.1 meters (30 feet).

When tested on the spacecraft, the array was in the stowed position as shown in Figure 5-23. Every panel and each string on every panel were tested by rotating the spacecraft one time on the Goerz table in 22.5-degree steps to place the panels under test normal to the illumination. The total time to completely check the I-V characteristics of all 32 panels, including setup, was approximately 4 hours. When the I-V characteristics of all 3 strings on each panel were taken and an I-V curve plotted for the panel itself, for a total of 128 I-V curves, the total test time was less than 12 hours. This technique minimized the interruptions to the spacecraft test flow.

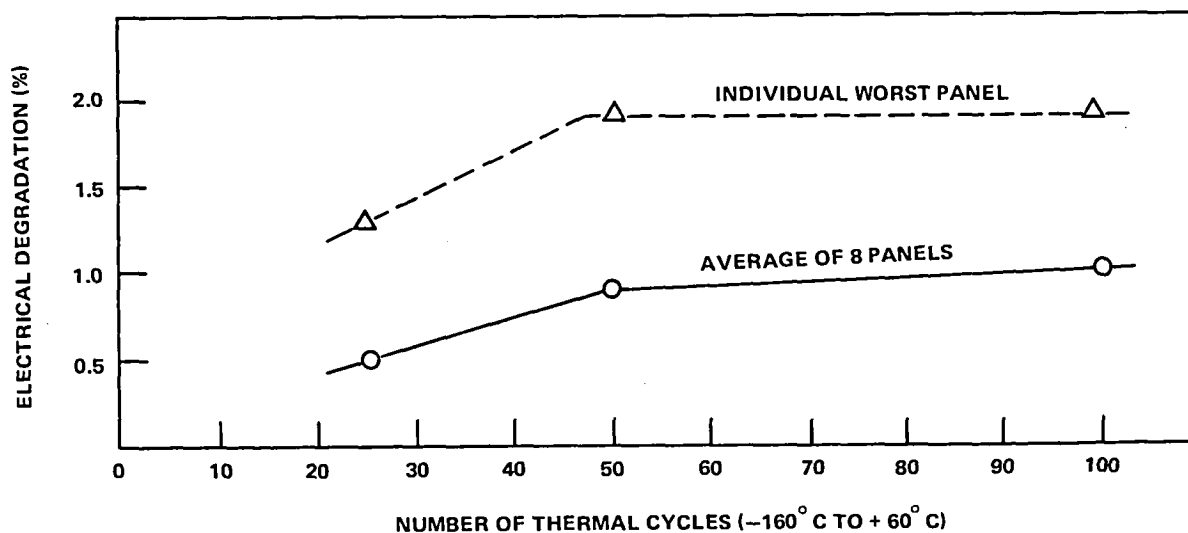


Figure 5-22. Panel Electrical Performance versus Thermal Vacuum Cycles

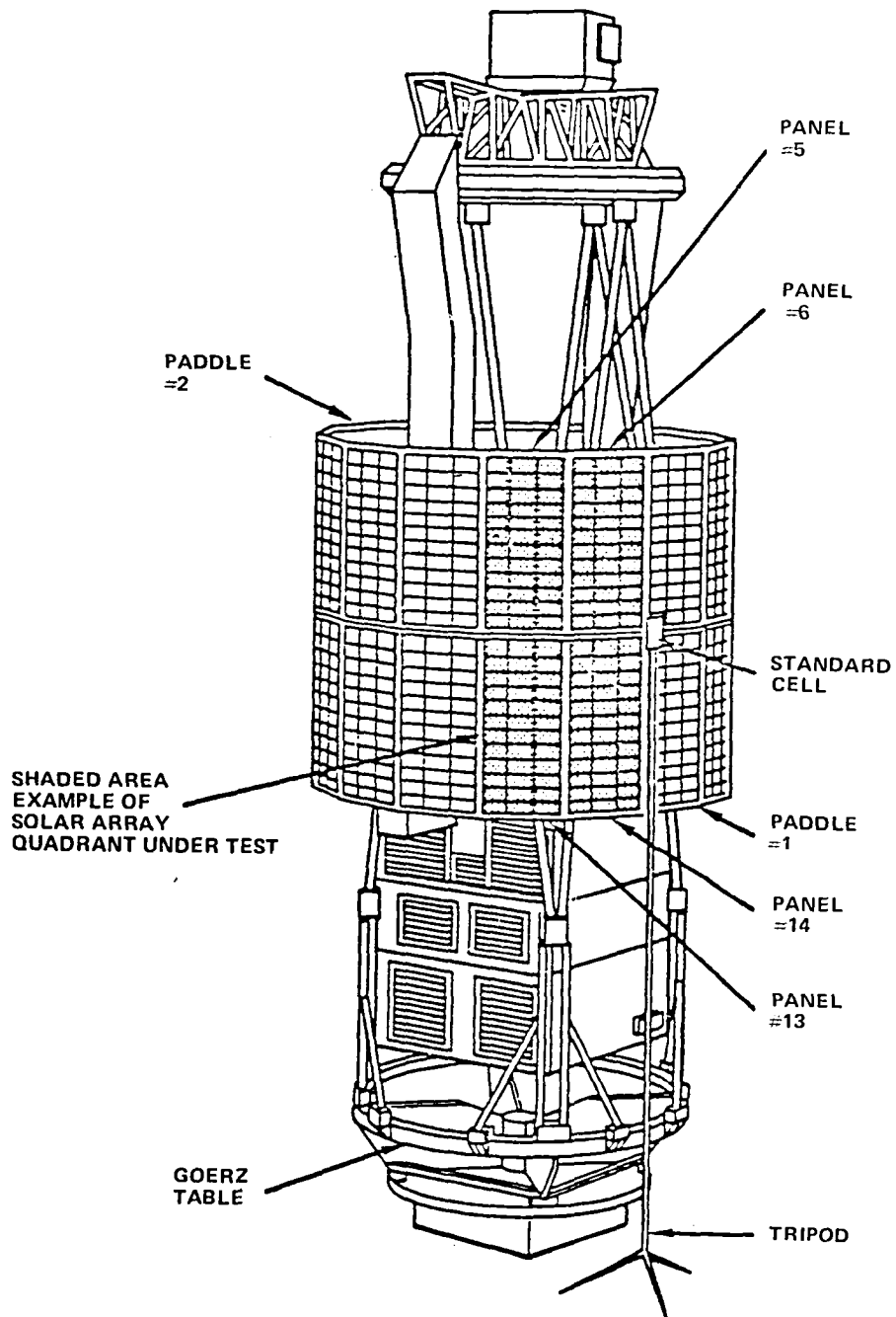


Figure 5-23. Spacecraft Setup for Solar Array Flash Allumination

Solar Cell Cleaning Operations

Except for specific spacecraft tests, the array panels were covered for protection. After the solar panels had been on the spacecraft for several months, inspection showed that small amounts of film had collected on the surface of the coverslides. The presence of this film was of concern because, when exposed to ultraviolet radiation in space, the film could darken and cause a decrease of solar array power output (possibly as much as 5 percent).

The fragile nature of the solar cell strain relief interconnect design made cleaning of the coverglasses an operation that was very hazardous to the solar panel. Also, the area of the solar array (20 m²) made the cleaning operation a large task. The considerable risk and effort involved in the cleaning task had to be weighed against the improved performance to be attained.

The first concern was to determine if there was sufficient film on the coverslide to warrant cleaning. Because of the accuracy and repeatability of solar testing with the flash illumination system, it was decided to clean and test the smallest testable unit on the array. Therefore, one series string (75 cells) on three separate panels was cleaned prior to shipment to the launch facility. An I-V curve (Figure 5-24) was taken of each of the strings before and after cleaning. The data were consistent for all three strings and showed that the film on the string of coverslides had reduced the string power output by 1.7 percent. The decision was made to clean the panels at the launch facility, using a trichlorethylene solution and cotton swabs.

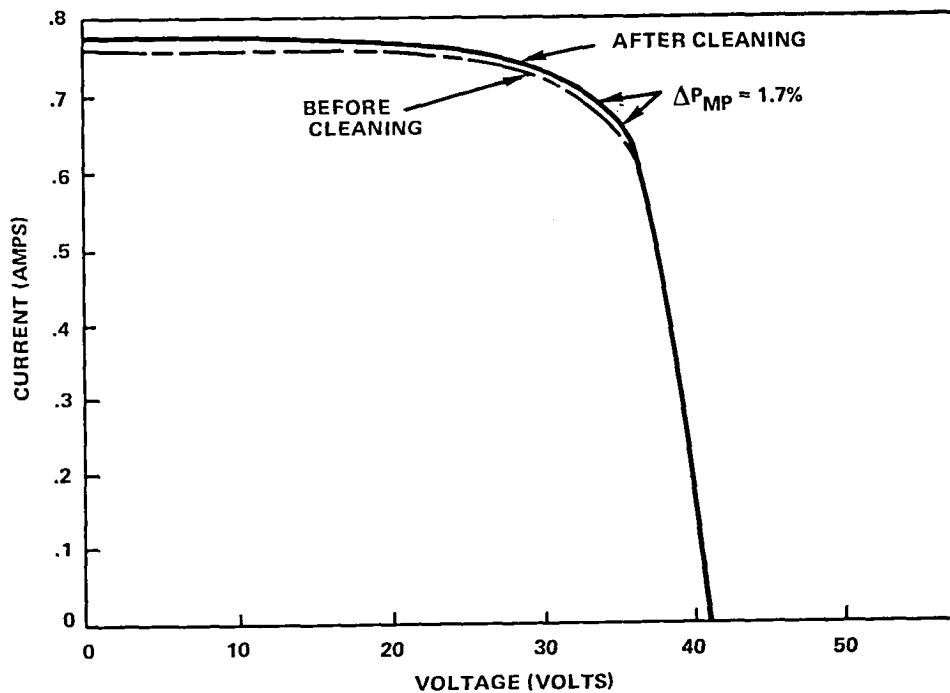


Figure 5-24. String I-V Curve

Squib Interface Unit/Titan Timing Test

On the ATS-to-Titan separation system, the time delay between the firing of the separation bolts on the spacecraft side and the firing of the separation bolts on the Titan side was very critical. If the time delay was too long (in the millisecond range), then, depending on possible failure conditions, ATS-6 would be subjected to large asymmetrical separation forces that could cause hang-up and prevent separation. To ensure the adequacy of the squib interface unit (SIU) designs and the Titan design, a compatibility test was performed early in the program with the SIU breadboard and a Titan at Cape Canaveral. The test results showed that the time delay was within acceptable expected limits.

Shunt Regulator Dynamic Response Test With Simulated Umbilical Cable

The power subsystem used a partial shunt regulator for controlling the solar array voltage to 30.5 volts. During ground power operations, a solar array simulator containing 12 I-V shapers was used for simulating a tapped solar array. At the launch site, this solar array simulator (ground power unit) had to be located over 300 feet from the spacecraft power regulators. Since the spacecraft shunt regulator is an active regulation system, the characteristic impedance of the umbilical cable became important to the shunt regulator loop stability. This effect was included in the shunt regulator analysis, and interface control was imposed on the characteristic impedance of the Titan umbilical cable. The power subsystem stability was confirmed by dynamic testing using an umbilical cable simulator designed with air inductors, resistors, and capacitors.

Solar Array Bus Electromagnetic Interference Filtering

Since the very high frequency (vhf) omnidirectional antennas were mounted on the outboard ends of the solar arrays and there were long power cable runs (>10 m) between the solar arrays and the Earth-viewing module, there was concern that electromagnetic interference could be conducted into the Earth-viewing module through the long power cables. Tests were performed on an individual solar array panel to evaluate the effects of the high vhf radiation levels. The high vhf radio frequency (rf) levels did not have an effect on the panel, and an effective attenuator of the rf energy that did enter the Earth-viewing module was found to be the bus filter capacitors within the power regulation unit. Therefore, as a result of testing and analysis, it was not considered necessary to add a separate electromagnetic interference filter to the solar array power leads.

Battery Cell Characterization Tests

Fairchild performed two different characterization tests on the batteries for ATS-6. The first test characterized all the cells of the lot that would be used for battery fabrication and established the voltage/temperature curve for the charger design. The second test characterized groups of 25 cells with regard to cell voltages and capacities. The 19 cells that were selected from each group of 25 cells for fabrication of a battery had the best match of these characteristics.

END-OF-MISSION TESTS

The performance of the electrical power subsystem throughout the 5-year mission of ATS-6 was characterized by near perfect operation. Redundant components were not required to support spacecraft operations except for the use of the battery standby charger (C/20 rate) to obtain total recharge of the batteries. Operating philosophy required that the system be maintained in the primary mode at all times and that alternative (redundant or backup) operating modes not be used unless a failure occurred in the primary mode. For this reason, the redundant and backup operating modes were never exercised prior to initiation of spacecraft shutdown operations.

During spacecraft final operations, a complete check of all electrical power subsystem alternate and redundant modes of operation was performed. All modes were brought on-line and exhibited nominal operating characteristics. The subsystem was then reconfigured to its normal operating mode for spacecraft terminal shutdown operations.

CHAPTER 6

IN-ORBIT PERFORMANCE AND OPERATIONS

SOLAR ARRAY

The solar array performance in orbit was a function of radiation damage, thermal cycling effects, the season of the year, and the pointing maneuvers required in orbit. At any given time, the power output was maximum at the equinox and minimum at summer solstice, because of the effect of the distance between the Earth and the Sun and the angle of solar incidence. The array temperature profile was as predicted. The severe temperature extremes of -160° to $+60^{\circ}\text{C}$ occurred during the eclipse seasons, and no unexpected degradation of the array occurred because of this thermal cycling. However, three of the four temperature sensors mounted on the back of the array ceased to function, probably because of thermal cycling.

The power output of the solar array during the 5 years in orbit is shown in Figure 6-1. As can be seen by examining this figure, the actual array power tracked the predicted array power remarkably well. An average degradation of 18.5 percent occurred after 2 years compared to 20 percent predicted. After nearly 3 years in orbit, a degradation of 19.2 percent occurred versus 22 percent predicted. After 5 years of orbit operations, solar array degradation was 26.8 percent versus 28.9 percent predicted. The level shown was the power available at the terminals of the power regulation unit, accounting for isolation-diode and harness-resistance losses.

Since the array was composed of two semicylinders that behaved as a cylinder with axially displaced halves that rotated once a day, a relatively constant solar array power was provided throughout the orbit. All the data for the figure, however, were taken at 6 a.m. and 6 p.m. (spacecraft time) when only the south or north array was illuminated. This allowed for the evaluation of total power out of each half array (each semicylinder). As shown, both array halves initially performed as predicted. The north array experienced somewhat more degradation than the south array with the south array delivering about 30 watts more than the north array.

The north array experienced a loss of approximately 20 watts in power capability near June 8, 1976. The failure mode was not determined. This "step function" accounted for the major difference in degradation between the two arrays.

The yearly seasonal variations are apparent in the figure. The maxima occurred at the equinox, and the deep minima at summer solstice. The intermediate minima occurred at winter solstice, when the solar constant was about 7 percent higher than at summer solstice.

SYMBOLS

- SOUTH PANEL OF SOLAR ARRAY - 0600 S/C TIME
- NORTH PANEL OF SOLAR ARRAY - 1800 S/C TIME
- ▽ PREDICTED VALUES

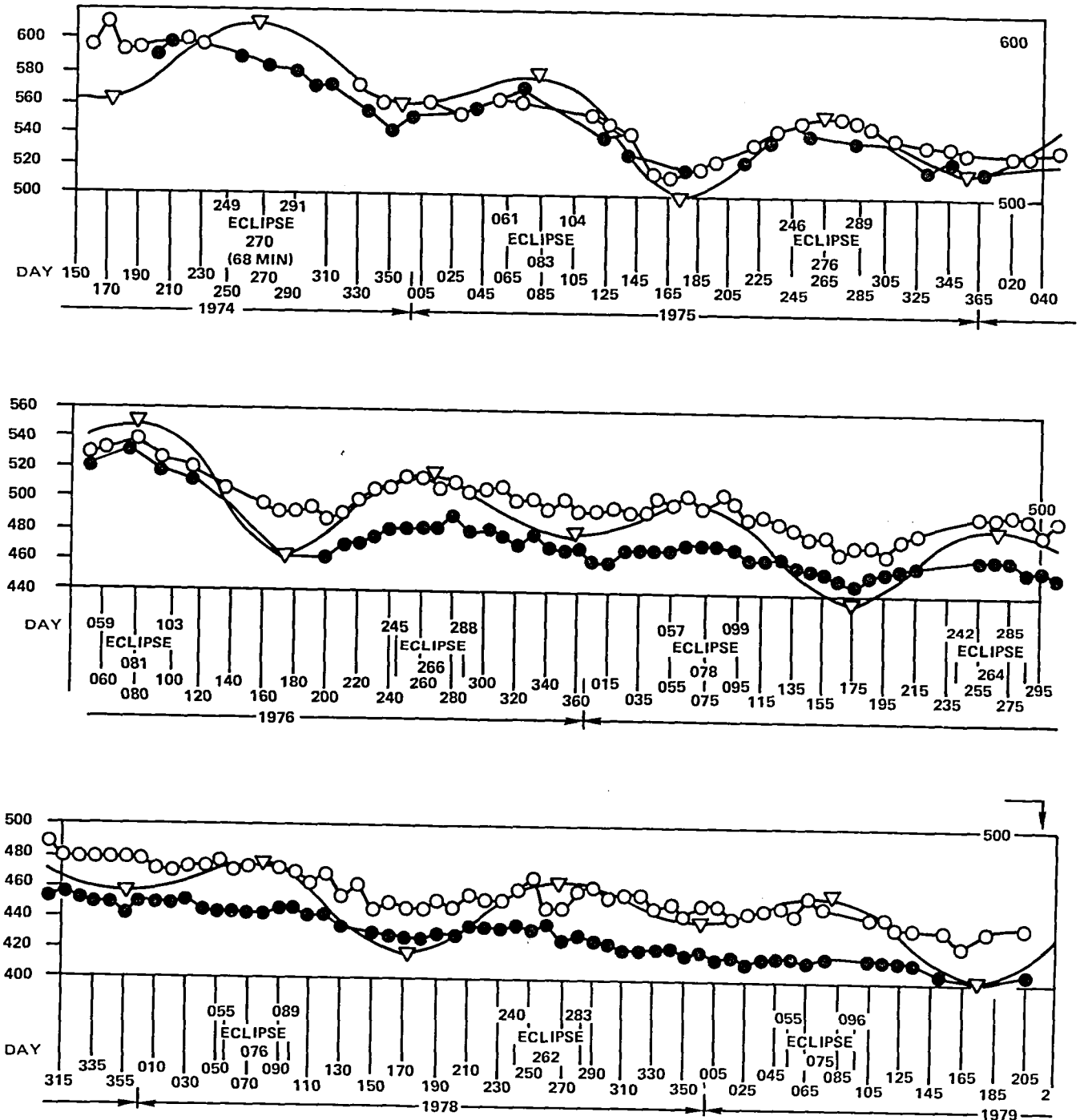


Figure 6-1. ATS-6 Available Power

ELECTRONICS

After launch of the spacecraft on May 30, 1974, the power subsystem electronics performed well within all specifications, fully satisfying the design requirements. Although redundancy was incorporated in the power subsystem electronics to avoid single-point failures, switch over to a redundant unit was only necessary for flexibility in battery charging.

Table 6-1 is a specification compliance matrix showing the performance of the major parameters and components of the power subsystem.

Power Control Unit and Load Interface Circuits

The performance of the power control unit and the load interface circuits were well within specifications. Table 6-1 shows the performance of the regulated bus voltages of these circuits.

Table 6-1
Electrical Power Subsystem: In-Orbit Performance

Component/Parameter	Specification	In-Orbit Performance
Spacecraft bus voltage	30.5 V \pm 2%	30.5 V $\begin{matrix} +0.3\% \\ -0.9\% \end{matrix}$
Battery 1 charge current limit	1.5 A $\begin{matrix} +0.15 \text{ A} \\ -0.08 \text{ A} \end{matrix}$	1.5 A $\begin{matrix} +0 \text{ A} \\ -0.03 \text{ A} \end{matrix}$
Battery 2 charge current limit	1.5 A $\begin{matrix} +0.15 \text{ A} \\ -0.08 \text{ A} \end{matrix}$	1.5 A $\begin{matrix} +0 \text{ A} \\ -0.03 \text{ A} \end{matrix}$
Battery 1 V/temp	26.88 V \pm 0.2 V @ 17.4°C	26.9 V @ 17.4°C
Charge taper performance	26.58 V \pm 0.2 V @ 22.8°C	26.6 V @ 22.8°C
Battery 2 V/temp	26.88 V \pm 0.2 V @ 17.4°C	26.8 V @ 17.4°C
Charge taper performance	26.58 V \pm 0.2 V @ 22.8°C	26.5 V @ 22.8°C
LIC (QCM)	28.0 V \pm 0.45 V	27.9 V
LIC (VHRR)	28.0 V \pm 0.45 V	28.0 V
LIC (MMW 1)	28.0 V \pm 0.45 V	27.9 V
LIC (MMW 2)	28.0 V \pm 0.45 V	27.9 V
LIC (PROP)	28.0 V \pm 0.45 V	28.0 V
LIC (ION 1)	28.0 V \pm 0.45 V	28.1 V
LIC (ION 2)	28.0 V \pm 0.45 V	28.0 V
PCU regulator 1	28.0 V \pm 0.45 V	28.1 V
PCU regulator 2	28.0 V \pm 0.45 V	28.2 V
PCU LIC (EME)	28.0 V \pm 0.45 V	28.0 V

Power Regulation Unit

The performance of the power regulation unit (the heart of the electrical power subsystem) was monitored in its major operating modes. These major modes of operation are shown in Figure 6-2, which is a typical plot of the static load performance of the power system bus. The telemetered data shown were taken with the system in the boost mode, boost/charge deadband, charge mode, and shunt mode. The beginning-of-life bus I-V curve is also shown in this figure. The entire regulation occurred within a band of 30.2 V to 30.6 V (ΔV of 0.4 V), which is well within the bus specification of 30.5 Vdc \pm 2 percent (ΔV of 1.22 V). In addition, there were no indications of overlapping modes or excessive spreads in the deadbands since the modes of operation were close to the predicted voltages.

A tracing of a photo of the preflight main bus excursion through the three modes—shunt, charge, and boost—is shown in Figure 6-3. Note that the deadband between shunt and charge was 30 millivolts and between charge and boost was 150 millivolts.

Shunt Dissipators

Table 6-2 shows how uniformly the 12 partial dissipators shared the excess solar array power. Two cases are tabulated: (1) low shunt dissipator current ($I_{sh} = 1.7$ A), and (2) medium shunt dissipator current ($I_{sh} = 10.4$ A). Since total shunt dissipator current was telemetered, instead of each of the 12 individual shunt currents, the assumption was made that each shunt current was 1/12 of the total. This is reasonable since the ground test data on all the shunt dissipators showed close current sharing. The tap voltages shown in Table 6-2 were telemetered data.

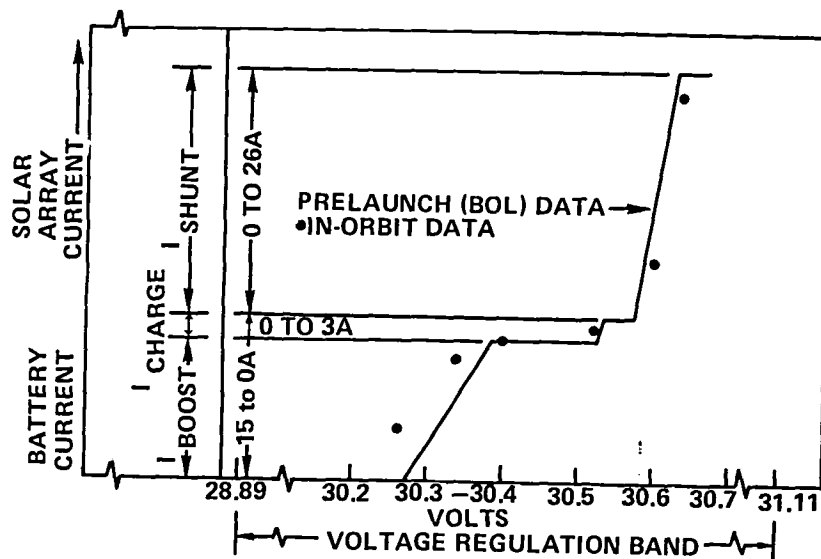


Figure 6-2. Regulated Bus Data

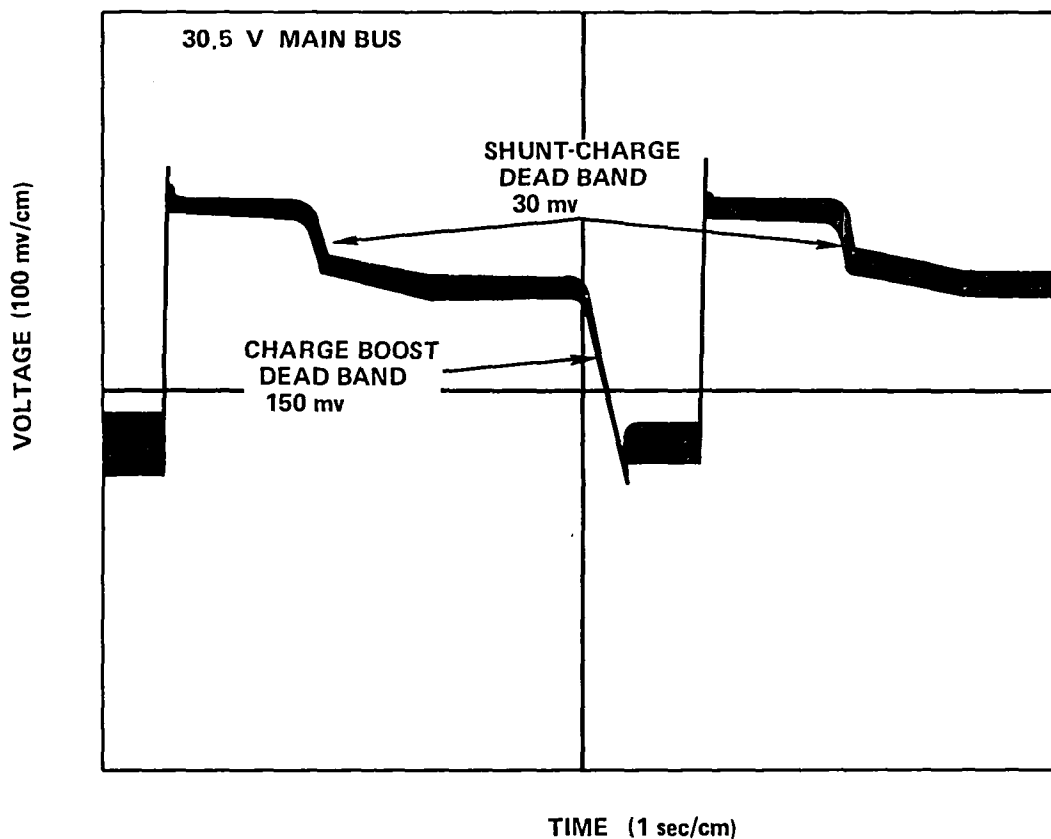


Figure 6-3. Preflight Deadbands

BATTERY PERFORMANCE

The ATS-6 mission resulted in a unique battery cycling regime for synchronous orbit. The batteries were discharged to varying depths from 5 to 60 percent during each eclipse. In addition, during the second year, discharges occurred twice a day to depths of up to 35 percent and 45 percent respectively. Normally for synchronous orbit, batteries are required to support the spacecraft during the eclipse seasons only. However, on ATS-6, an early decision was made to use battery power to supplement the array for peak loads rather than increase the array size and weight. This decision was also based on the fact that the power system design would provide the highest overall system efficiency by forcing the array to supply all available power and requiring that the battery supply only the deficiency.

Data were recorded for the battery discharge cycles that occurred during the first and second years and part of the third year of operation. Table 6-3 shows the number of discharge cycles versus the depths-of-discharge (DOD) range for nearly 3 years of operation including six eclipse periods.

The second year of operation subjected the batteries to greater depths of discharges and more frequent discharge cycles. In the second year, for example, the Satellite Instructional Television

Table 6-2
Shunt Dissipator Power Sharing

Shunt Dissipator	$I_{SA} = 17.8 \text{ A}$ $I_{SHUNT} = 1.7 \text{ A}$			$I_{SA} = 10.2 \text{ A}$ $I_{SHUNT} = 10.4 \text{ A}$		
	Tap Voltage	Dissipator Current	Dissipator Power	Tap Voltage	Dissipator Current	Dissipator Power
A419	19.2	0.14 A	2.68 W	17.2	0.9 A	15.5 W
A420	19.6	0.14 A	2.74 W	17.6	0.9 A	15.8 W
A421	19.3	0.14 A	2.7 W	16.9	0.9 A	15.2 W
A422	19.1	0.14 A	2.67 W	16.8	0.9 A	15.1 W
A423	19.3	0.14 A	2.7 W	16.9	0.9 A	15.2 W
A424	19.9	0.14 A	2.79 W	16.7	0.9 A	15.0 W
A425	18.8	0.14 A	2.63 W	16.8	0.9 A	15.1 W
A426	19.5	0.14 A	2.73 W	17.5	0.9 A	15.8 W
A427	19.1	0.14 A	2.67 W	16.9	0.9 A	15.2 W
A428	19.7	0.14 A	2.76 W	16.7	0.9 A	15.0 W
A429	19.5	0.14 A	2.73 W	17.5	0.9 A	15.8 W
A430	19.2	0.14 A	2.68 W	16.9	0.9 A	15.2 W

Table 6-3
Battery Discharge Cycles for First 2½ Years of Operation

Depth of Discharge	No. of Discharge Cycles			Total Number Cycles May 30, 1974 to April 12, 1977
	May 30, 1974 to July 1, 1975	July 1, 1975 to August 19, 1976 (SITE Operation Period)	August 19, 1976 to April 12, 1977	
5 to 10%	102	5	31	138
10 to 20%	129	90	31	250
20 to 30%	68	324	26	418
30 to 40%	54	324	37	415
40 to 50%	54	91	24	169
50 to 60%	5	2	0	7
80 to 90%	0	3	1	4
Total	412	839	150	1401
Eclipse Cycles	88	88	88	264
Noneclipse Cycles	324	751	62	1137

Experiment (SITE) in India was operated twice a day. During this operation, the combination of experiment loading combined with the SITE operation exceeded the power out of the array, requiring the battery to provide power for the additional load. The battery discharge profile for SITE operations is shown in Figure 6-4. Note that twice daily discharges of 35 percent and 45 percent DOD during the noneclipse season were routine. During the eclipse seasons, discharges occurred three times a day: i.e., the eclipse discharge (peak of 50 percent DOD) and the two SITE discharges (reduced to 15 percent and 25 percent DOD).

Table 6-3 shows the dramatic increase in the number of discharges in the 20 to 30 percent and 30 to 40 percent ranges caused by SITE operations. Also note that of the 1401 total discharge cycles, 1013 were at depths of greater than 20 percent and 1137 were noneclipse discharges.

Concerning battery performance, Figure 6-5 shows the discharge characteristics for eclipse seasons 1 through 8 for the maximum shadow of 72 minutes.

The end-of-discharge voltage for eclipse season 3 appeared to be lower than expected. The reason for this was insufficient pre-eclipse battery charging. By increasing the charge to the batteries prior to the fourth eclipse season, the end-of-discharge voltages for eclipse season 4 remained as high as those previously found for eclipse season 3. Discharge characteristics for eclipse seasons 5 through 8 show some additional degradation; however, battery performance continued to be excellent. The minimum battery voltage of 21.3 volts, after 4 years of daily discharges and eclipse cycling, still remained well above the 19-volt minimum required for power subsystem operation.

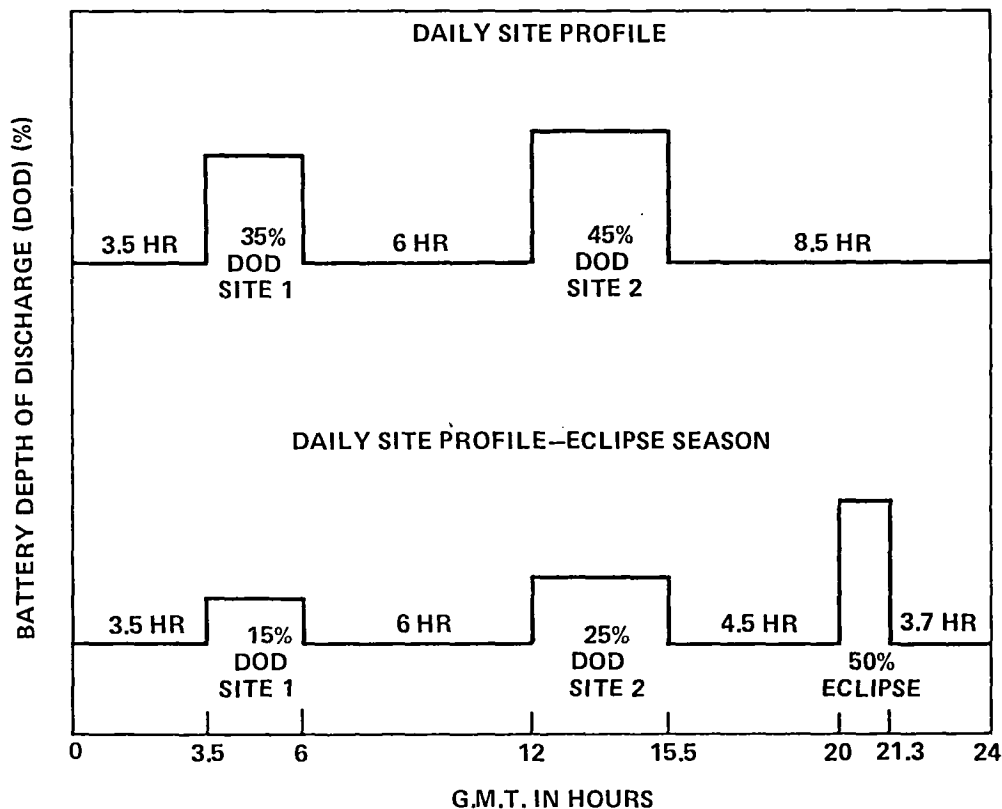


Figure 6-4. Battery Discharge Profile for SITE Operations

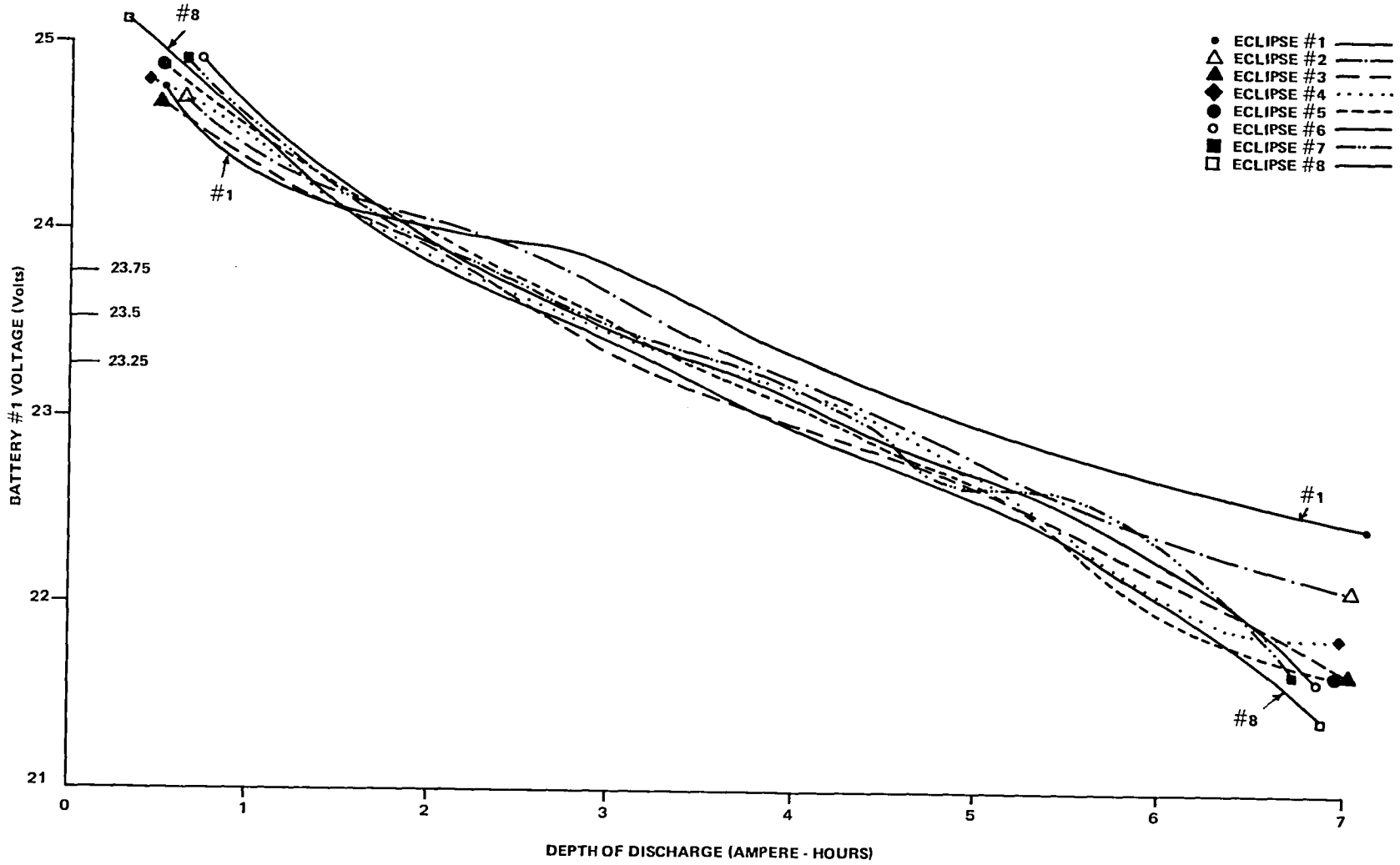


Figure 6-5. Battery Discharge Curves for Eclipse Seasons 1 Through 8

Battery capacity was evaluated by extending the SITE 2 experiment on February 22, 1976, which allowed the batteries to be discharged to 19.5 volts (1.02 V per cell) at an average discharge rate of approximately 2.5 A (C/6). The battery discharge characteristics for this test are shown in Figure 6-6. A capacity of 13 ampere-hours was measured from this test. A similar simulated flight test was performed on a group of five equivalent cells at NAD Crane. The results of this test are also shown in this figure.

A comparison of the Crane flight equivalent cells to the spacecraft battery cells shows that additional degradation occurred on the spacecraft batteries. This was probably due to the additional noneclipse cycles the spacecraft batteries were subjected to that the Crane flight cells were not. A second deep discharge test was performed on April 30, 1976, following the fourth eclipse, about 70 days following the initial test. The results of that test are also shown in Figure 6-6. While there were approximately 200 discharge cycles between the two tests, no appreciable degradation in capacity occurred. This may be an indication that the rate of capacity loss had decreased significantly.

While the Crane cells experienced some degradation, they did not experience the equivalent degradation of the flight cells, since they were subjected to only 300 total discharge cycles. Of this total, 170 cycles were noneclipse discharges that simulated the actual profile experienced by the flight cells during SITE operations.

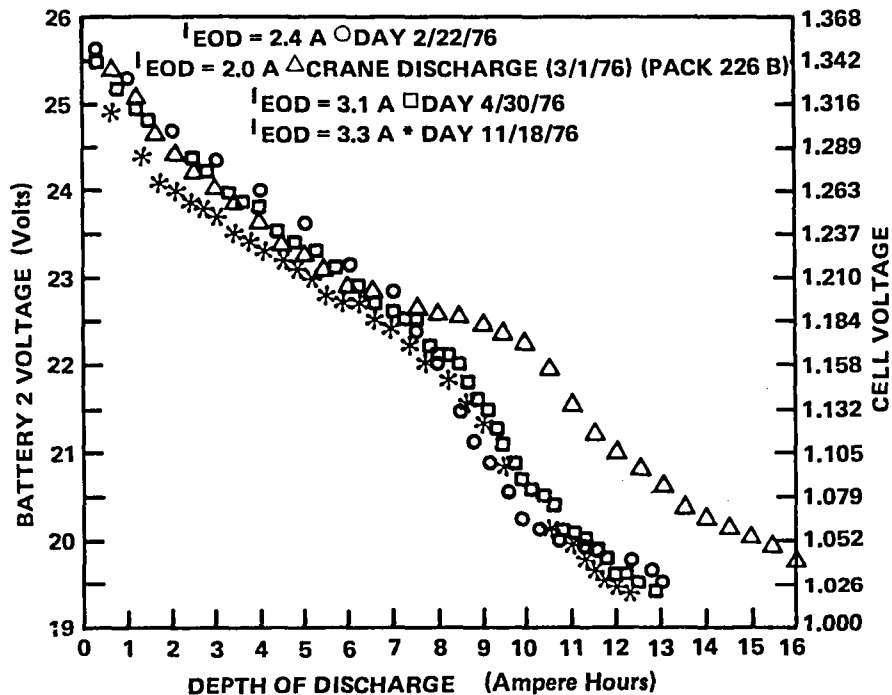


Figure 6-6. Battery Discharge Characteristics

A third deep discharge test was performed on November 18, 1976, following the fifth eclipse season and the conclusion of the SITE experiment. Figure 6-6 shows this discharge characteristic. A capacity of 12 ampere-hours was measured. There was only a slight reduction of capacity in spite of the occurrence of an additional 275 cycles of discharge.

A deep discharge test was performed on July 27, 1979, five days before spacecraft operations were terminated. The test results for both batteries are shown in Figure 6-7, together with the Battery No. 2 test results obtained 41 months earlier for comparison. At the end of 5 years, both batteries were tracking within 0.2 V and load-sharing within 0.1 A and had approximately 10 ampere-hours capacity (at 19.5 volts end-of-discharge). Furthermore, when the deep discharge tests were performed, Battery 1 and 2 voltages continued to track within 0.2 volt until the tests were terminated at 19.5 volts. This indicated that the cells were still well matched with no apparent cell divergence.

The battery temperature varied daily between 10°C and 25°C with average temperatures of +18°C. Battery 1 and 2 temperatures tracked within 1°C, and the batteries voltages continued to share loads within 0.1 A over this temperature range.

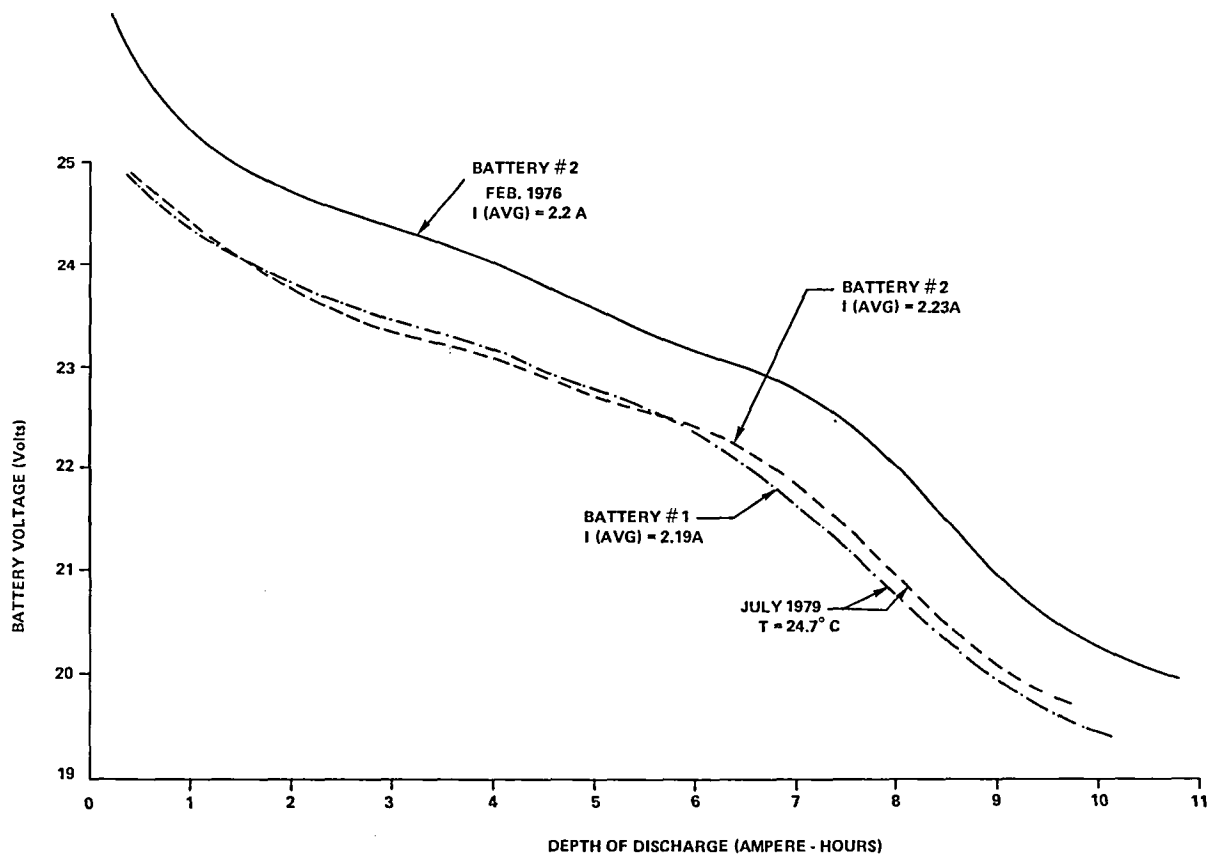


Figure 6-7. Discharge Characteristics

CHAPTER 7

IN-ORBIT ANOMALIES AND CONCLUSIONS

BATTERY END-OF-CHARGE TERMINAL VOLTAGE

The batteries were charged by the primary charge system that provided a constant current (C/10) until the battery terminal voltage reached a predetermined level as a function of temperature. At this point, the battery current tapered, maintaining a fixed battery voltage. From the battery cell characterization test program, it was decided to set the battery voltage/temperature curve so that 95 percent ampere-hours of charge would be restored before the onset of taper. This minimized overcharge while allowing the batteries to become fully charged. Actual flight data of the battery charge characteristics for eclipse season 1 and eclipse season 4 are shown in Figure 7-1. These data show that for eclipse season 4, the battery was starting taper after only 80 percent of the ampere-hours had been returned. From these data, it was evident that the battery end-of-charge terminal voltage had increased causing premature taper. A contributing factor to this change in characteristic may have been the large number of heavy noneclipse discharge cycles. Recognizing that premature taper was occurring, the recharge problem was solved with the standby (redundant) charger.

The standby battery charger provided a constant current of C/20 (0.75 A) to the battery and did not have voltage/temperature taper charge control. The power system had the flexibility to charge the battery from the primary charger, the standby charger, or by the parallel combination of both chargers. The batteries were charged initially from the main charger (C/10 rate) and the charge current was allowed to taper as normal; however, when the taper current reached the C/20 rate, the charge control was switched to the standby charger to maintain the constant rate of C/20. Battery charging was completed on the standby charger.

While use of the standby charger with its constant current rate resolved the charging problems, a multiple V/T level system would do the same. In addition, multiple V/T levels would provide added flexibility to accommodate further change in battery charge characteristics without sacrificing the charge taper characteristics.

SOLAR ARRAY REDUCED OUTPUT

In the period between May 14 and June 8, 1976, the north solar array power output suffered a degradation of approximately 20 watts. This was apparently a single event, the cause of which was not determined. Following this event, the north and south arrays continued to exhibit similar gradual additional degradation while maintaining the approximately 20-watt difference in power output. (Refer to Figure 6-1.)

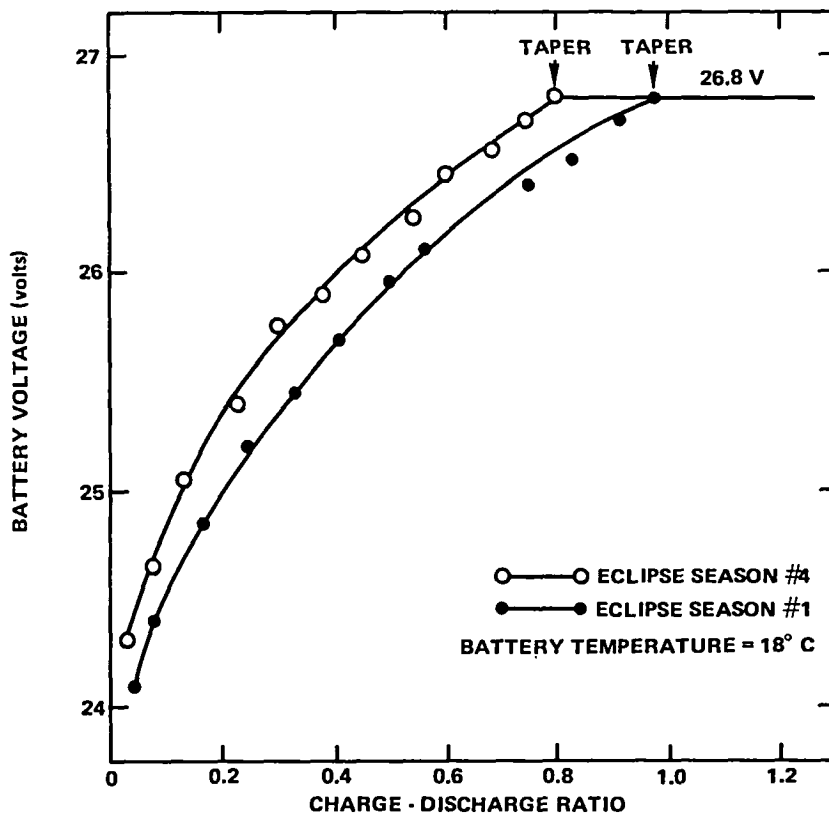


Figure 7-1. Battery Charge Characteristics

OTHER MINOR ANOMALIES

None of the other anomalies impacted flight operations and six of the reported anomalies were related to either one of two general types of anomalies; i.e., high shunt tap voltages, or high solar array temperature sensor readings. Details for the period May 30, 1974 to May 20, 1976 concerning each anomaly are summarized as follows:

Description	Comments
High solar array shunt tap voltages (3)	The shunt tap voltages read high (25 to 26 volts versus normal 2 to 23 volts) at certain times during summer solstice seasons. This condition had no impact on flight operations. Both solar arrays and power conditioning components continued to function normally.
Solar array temperature sensor failures (3)	Three solar array temperature sensors failed in an open condition resulting in a high count reading to each sensor telemetry channel. Appropriate changes were made to the ATSOCC data base to eliminate CRT errors. Since all three sensors failed during either the summer solstice or eclipse season, the principal cause of this type of failure is attributed to temperature cycling.
Battery 1 overtemperature detector turn off	Battery 1 overtemperature detector turned off without being commanded. The detector was commanded on and remained on without any anomalies.

There were no other anomalies reported during the last 3 years in orbit.

CONCLUSIONS AND RECOMMENDATIONS

Electrical Power Subsystem Design

For more than 5 years in orbit, the design performance of the electrical power subsystem was excellent. All components of the electrical power subsystem, including the solar arrays, batteries, and power conditioning/distribution components, successfully provided uninterrupted power to all spacecraft subsystems. No failures pertinent to the generation, conditioning, and distribution of electrical power on the spacecraft occurred, except for the 20-watt step-degradation of the north solar array. This degradation did not adversely affect performance of mission operations.

Battery Temperature Control

In-orbit operations during winter solstice seasons have shown that with the present thermal design battery, peak temperatures can exceed 30°C. Since battery life can be enhanced by restricting peak temperatures to 30°C or less, future spacecraft designs should include a thermal design that will ensure that battery peak temperatures do not exceed 30°C.

Noneclipse Cycling of Synchronous Orbit Batteries

With the continued success of ATS-6 mission operations, increased demands (beyond prelaunch expectations) were placed on the batteries. While concern for potentially increased battery degradation existed as load levels increased, sufficient data did not exist from previous satellite programs to cause immediate load reductions to be made. Consequently, after 2 years of in-orbit operations, the capacity of the batteries was reduced to a level (12 A-h at 19.5 V) that required absolute minimal use during noneclipse periods in the remaining 3 years of the 5-year spacecraft operations. In 5 years, the capacity of each battery was reduced to approximately 10 ampere-hours capacity at 19.5 V end-of-discharge.

Two important conclusions that can be drawn from ATS-6 operations concerning the use of synchronous orbit satellite batteries during noneclipse periods are as follows:

(1) *Batteries are a limited resource* and their use during noneclipse periods must be *carefully* evaluated against the battery design and mission life profile of the spacecraft. If the batteries are designed and sized to support only eclipse loads, their use during noneclipse periods will increase capacity degradation. This degradation, which is dependent on the number of depth of noneclipse cycles, may be such that the capacity of the batteries may fall below eclipse requirements before the end of the spacecraft design life. Thus, the use of the batteries during noneclipse periods to support extra spacecraft loads during early mission phases must be weighed against the loss of spacecraft power that occur should battery capacities fall below eclipse load requirements.

(2) Long-term relationships between the number of discharge cycles and their depth on battery capacity were established and the relative advantages that can be gained by making moderate load reductions were demonstrated.

Conclusions

The excellent performance and flexibility of the ATS-6 power system contributed significantly to the successful operation of the spacecraft in carrying out its full complement of unique experiments. For more than 5 years, the power subsystem exceeded all operational requirements.

Of particular note are the following design and performance conclusions concerning the power subsystem:

- The power subsystem shunt boost configuration was selected for efficient use of the array and battery power. It also provided a low impedance bus with excellent static and dynamic regulation. This characteristic was necessary to minimize load interactions and electromagnetic interference and permit the successful operation of multiple experiments.
- The array power degradation at the end of 5 years was 26.8 percent compared to the 28.9 percent predicted. This performance resulted in spite of the extreme eclipse cycling of -160° to $+60^{\circ}\text{C}$ and the daily self-shadowing cycling of -100° to $+60^{\circ}\text{C}$. Therefore, the adequacy of the array design and fabrication for a deployed array in synchronous orbit was verified.
- In the area of test, the large size of the solar array, consisting of 32 panels, posed a significant challenge for evaluating the array with accuracy and repeatability throughout the spacecraft test flow. A xenon-flash illuminator coupled with a data-evaluation system provided an improved method of solar array testing that allowed testing at the array, the panel, and the string level while the array was mounted on the spacecraft.
- The ATS-6 mission often required battery load sharing with the array on a daily basis. The batteries were discharged to varying depths from 5 percent to 60 percent. Normally, for synchronous orbit, the batteries are required to support a spacecraft during the eclipse seasons only. The battery performance for the ATS-6 cycling regime was good. There was a small decrease in end-of-discharge voltage and a slight increase in end-of-charge voltage. Insufficient battery recharge resulted from this increase of end-of-charge voltage; however, with the flexibility designed into the charge system, reverting to the standby solved the problem and accommodated further change in battery charge characteristics. Battery capacity was evaluated through deep discharges to 1.02 V per cell at three different times during the second year of operation and again at termination of spacecraft operations. The last test showed that the batteries had degraded to a capacity of about 10 ampere-hours at 19.5 volts end-of-discharge. While this represented a marked reduction in their initial capacity, it still was adequate to handle minimum necessary eclipse loads at the end of the ATS-6 mission. Thus, the use of batteries for handling peak load demands in addition to eclipse loads is practical, with a proper match of mission load demand cycles and battery design.

Part C
Telemetry and Command Subsystem

CHAPTER 8

INTRODUCTION

FUNCTIONAL REQUIREMENTS

The Telemetry and Command Subsystem (T&CS) provided the primary communication link between the ground operations controllers and ATS-6. The T&CS command capability included receiving, decoding, and distributing discrete and data word commands to the spacecraft subsystems and the spacecraft experiments. The T&CS also provided the command link between the ground station computers and the spacecraft attitude control subsystem during the ground attitude control experiment (SAPPSAC).*

The telemetry capability included the multiplexing, formatting, and transmitting of analog and digital data from the spacecraft subsystems and the experiments.

A special data link was provided for voice-bandwidth analog data communication between ATS ground stations, and a wideband data link was provided for the Interferometer Experiment as described in Chapter 3, Volume II.

The telemetry and command subsystem was designed and built by IBM under the direction of Fairchild Space and Electronics Company, the prime contractor for ATS-6.

DESIGN DESCRIPTION

The antennas used by the telemetry and command subsystem included two omnidirectional antennas, located on the solar panels and the prime-focus feed antennas (part of the communications subsystem) associated with the parabolic reflector. In addition, the telemetry and command subsystem had a switchable backup capability of accepting commands through the C-band receiver and telemetering through the use of the C-band transponder. Both of these C-band elements were part of the communications subsystem.

The design provided high reliability and protection against single failures preventing commanding or telemetering any of the spacecraft functions. In many areas, the nature of the configuration provided multiple failure protection; e.g., four transmitters plus the C-band transponder. The design met the Aerospace System Standards and also provided special mission support for the SAPPSAC experiment, the special data link, and the high-speed execute (HSE) mode. The T&CS could be commanded into either the ground attitude control (GAC) mode associated with the SAPPSAC experiment or the high speed execute mode by a normal discrete command. GAC mode commands provided control pulses to the attitude control subsystem wheels or jets. The HSE mode provided the capability of executing normal discrete commands at a higher rate than the normal execute command (up to 44.5 per second) and also provided an unlimited time duration execute pulse width.

*SAPPSAC—Spacecraft attitude precision pointing and slewing adaptive control

The subsystem was operationally similar to the ATS-1 to ATS-5 series spacecraft subsystems and offered a data-word command capability, discrete command, or voice-bandwidth analog modulation of the command carrier, and simultaneous transmission of normal telemetry, Environmental Measurements Experiment data, and voice-bandwidth analog data on the telemetry carrier. The subsystem employed standardized outputs from the command decoder and distribution (CDD) unit and standardized inputs to the data acquisition and control unit, and also satisfied specialized subsystem requirements, such as unique data-word transfer to the digital operational controller (DOC), telemetry synchronization pulses to the attitude control subsystem and interferometer, timer function for the experiments, and time code generation.

A block diagram of the T&CS is shown in Figure 8-1. The diagram illustrates the redundancy approach used to satisfy the reliability and single-failure protection requirements. Multiple simplex units were used throughout to provide functional redundancy at the subsystem level. For example, two redundant CDD's were provided; each had its own spacecraft address, and only one was activated at any one time. An rf switch block diagram of the T&CS is given in Figure 8-2.

Command Function

The functional parameters of the command subsystem are highlighted in Table 8-1. The command subsystem received, decoded, and distributed discrete and data-word commands to the spacecraft subsystems. It had a capacity of 512 discrete command addresses and 45 data-word addresses. Each data-word transmission carried nine bits of data. It employed a very high frequency (vhf) carrier which was amplitude modulated by the frequency shift keying (FSK) "0" and "1" command tones. The "0" and "1" tones were 50-percent amplitude modulated by a 128-hertz (Hz) sine wave clock, which was demodulated in the CDD and used for all timing within the CDD and for data-word transfer to the subsystems. Before command execution, ground personnel verified that the proper command was received by the CDD from telemetering of the 6-bit data-word address/discrete function, 9-bit command word/9-bit discrete address, 1-bit address check, and 1-bit command-load indicator. Two redundant CDD's were employed, each with its own spacecraft address, so that only one was activated at any one time. Execution of all normal discrete and data-word commands occurred only upon receipt of an execute command from the ground.

In a special mode, a second pair of FSK "0" and "1" tones, amplitude modulated by a 1200-Hz sine wave clock, were used to provide the GAC and high-speed execute (HSE) command capability. The GAC and HSE commands were executed immediately without ground verification. The CDD performed an address check and a parity check on the command before issuing the GAC discrete execute pulse. Discrete commands (1 each) were used to enable the GAC or HSE modes and a discrete command was used to disable both GAC and HSE modes. A safety feature was included in the CDD-GAC decoder that disabled either the GAC or HSE mode upon the loss of the GAC tones and clocks for 3 seconds and the loss of normal tones and clocks for 1 second. The presence of either normal or GAC tones and clocks maintained the enable state of the GAC decoder, and allowed GAC and normal commands to interleave freely. A similar safety and interleaving feature was implemented for the CDD-normal decoder to reset or maintain its registers. A functional block diagram of both normal and GAC decoders in the CDD is shown in Figure 8-3.

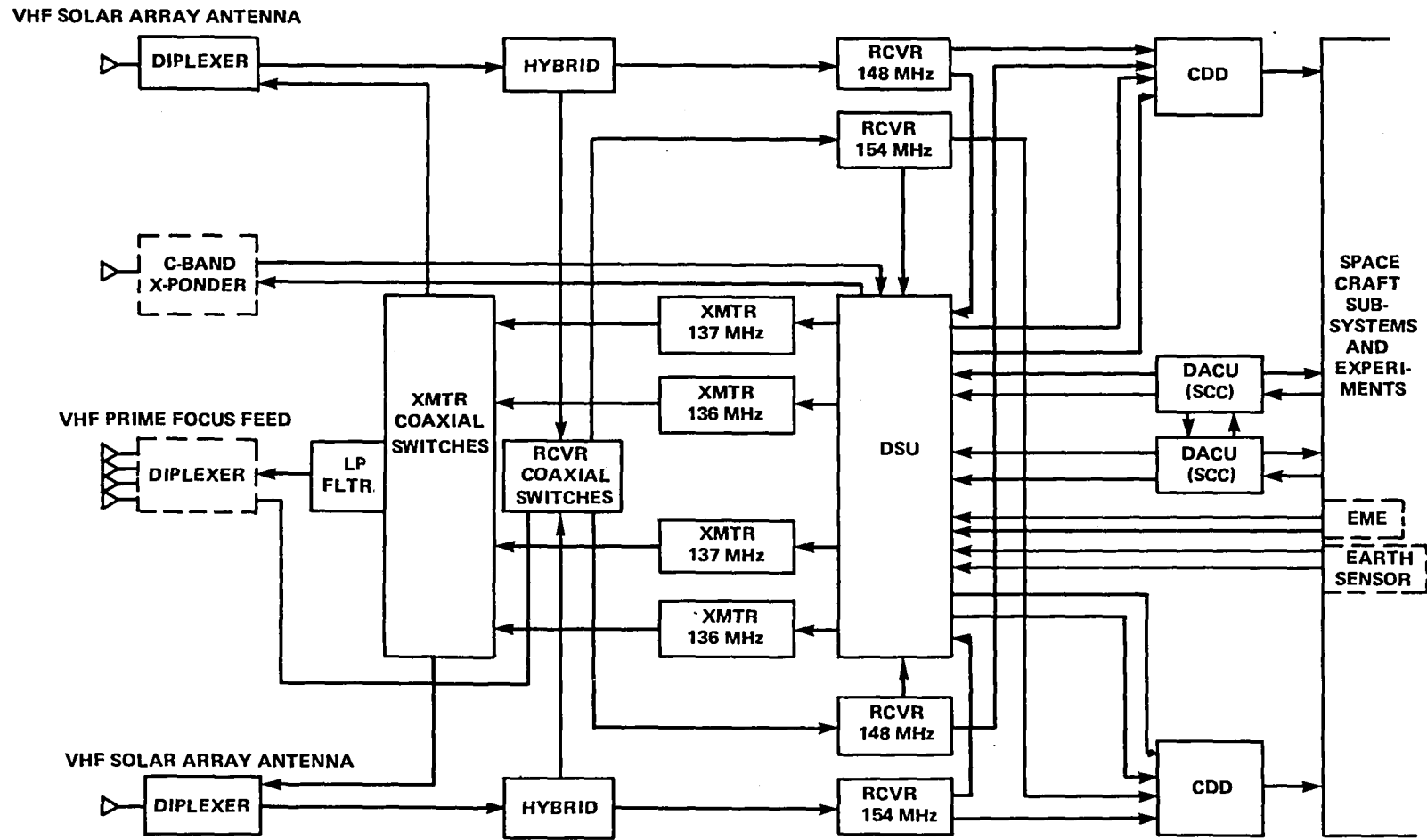


Figure 8-1. ATS-6 Telemetry and Command Subsystem Block Diagram

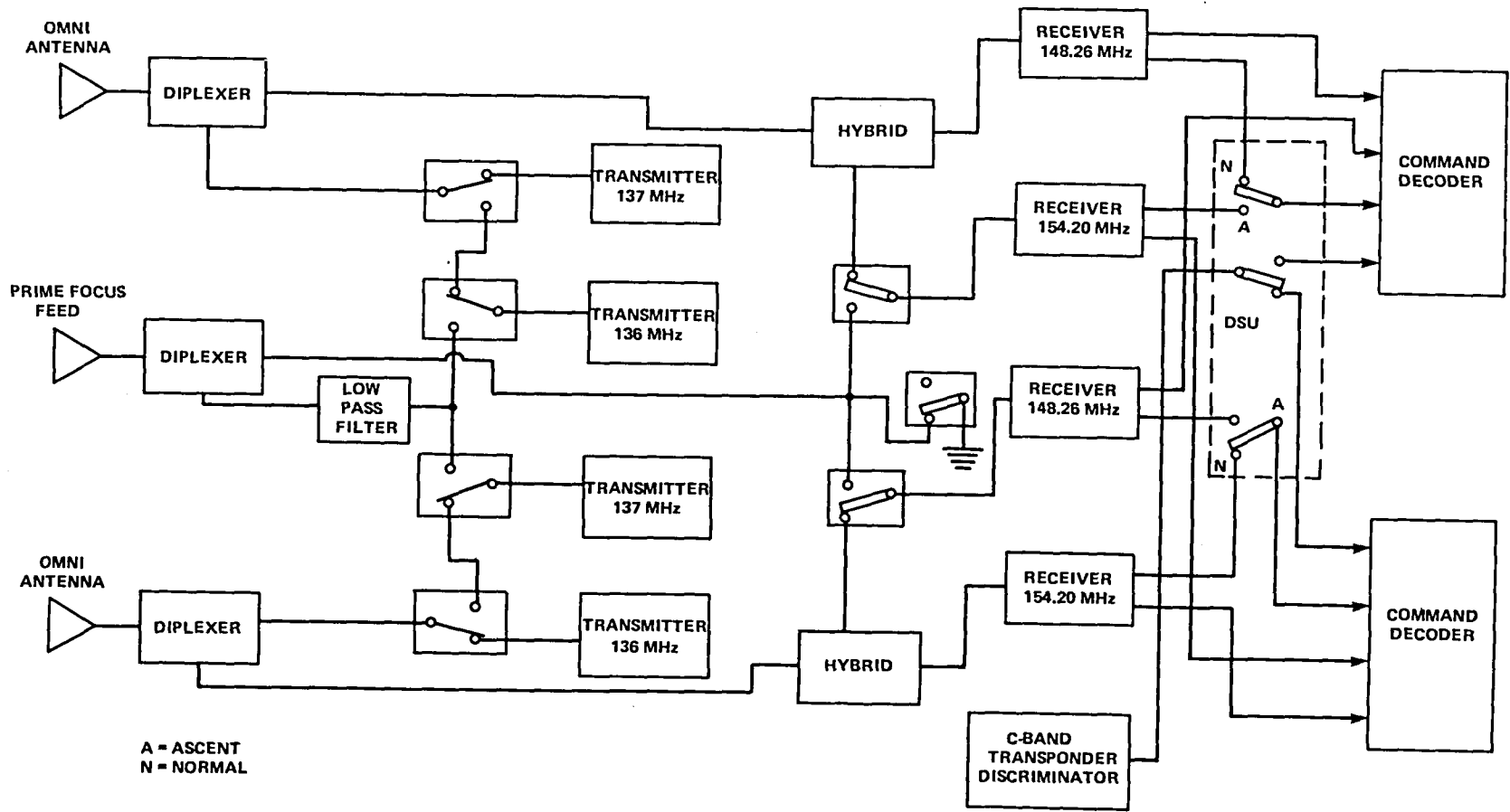


Figure 8-2. Telemetry and Command Subsystem Functional Block Diagram

Table 8-1
ATS-6 Command Characteristics

Item	Characteristics	
	Normal Command and Execute	GAC Command
Modulation:	PCM/FSK/AM/AM at vhf PCM/FSK/AM/FM at C-band	Antennas: 2 solar panel omnidirectional (vhf); vhf prime-focus feed; C-band Earth coverage horn
Frequencies:	154.20 MHz, prime 148.26 MHz, standby C-band, switchable backup	
Verification	Ground via telemetry	Decoder address and parity
Execute	Digital command	Execute as received
FSK tones	Logic "0" 7296 Hz Logic "1" 7808 Hz	Logic "0" 8700 Hz Logic "1" 11,900 Hz
Bit rate	128 bps	1200 bps
Decoder address	9 bits	7 bits
Frame length	28 bits	13 bits
Discrete commands	512	—
Data word addresses	45	—
Data word length	9	—
ACS configuration addresses	—	32
Normal command execute options	a) Execute and clear b) Execute and hold	High speed execute of normal command
Execute pulse width	a) 56 ms, nominal b) 253 ms, nominal	11 ms, nominal
Maximum command rate	2.2/s for 56-ms commands; 1.4/s for 253-ms commands; any rate up to 1.4/s for either pulse width; none between 1.4/s and 2.2/s.	92.3/s
Maximum repetitive	4.6/s for 56-ms commands; 2.1/s for 253-ms commands; any rate up to 2.1/s for either pulse width; none between 2.1/s and 4.6/s	44.5/s (high speed execute mode)
Time duration command resolution	253 ms	11 ms
Command distribution	a) Array for support subsystem b) Dedicated to experiments c) Remote distributor for transponder	Dedicated to ACS only —
Redundancy	Complete redundancy	Complete redundancy

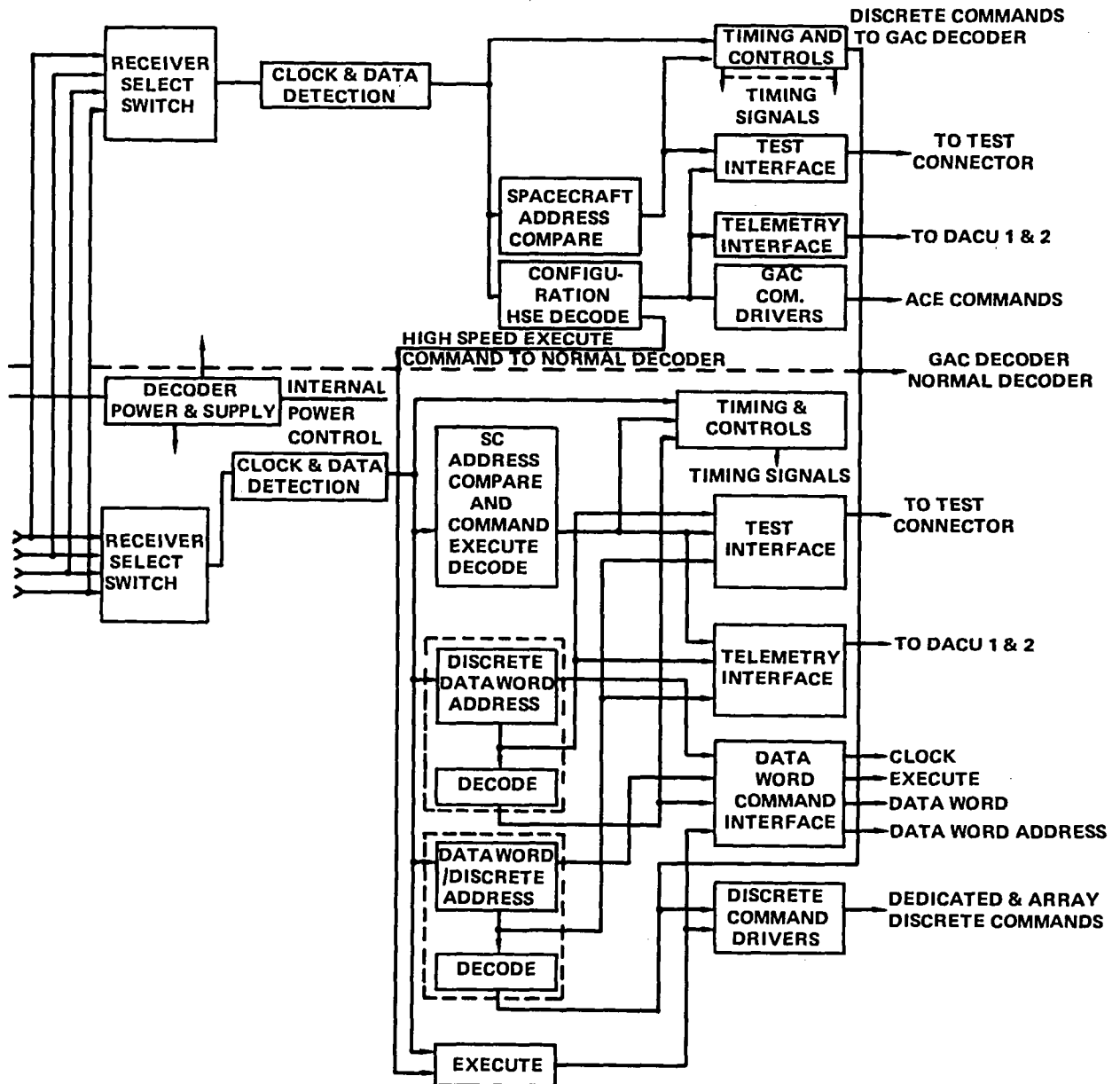


Figure 8-3. Command Subsystem Functional Block Diagram CDD Expanded

A third signal (command carrier), amplitude modulated by a voice-bandwidth-analog signal (special data-link mode), could be received by the vhf receiver or the C-band receiver. The signal was demodulated by the command receiver connected to the prime-focus feed and switched by the data switching unit (DSU) frequency division multiplexer (FDM) to a telemetry transmitter for retransmission to the ground by the prime-focus feed antenna. This signal did not activate the CDD's. This mode of operation provided for simplex push-to-talk voice coordination between ground stations, as required in support of some operations.

Command word formats are shown in Figure 8-4.

Telemetry Function

A functional block diagram of the telemetry subsystem is shown in Figure 8-5, and the functional parameters of the subsystem are highlighted in Table 8-2. In the normal telemetry mode, one of the two data acquisition and control units (DACU's) was commanded on, along with one of the two master oscillators and both time-code generators. The DACU sampled the input lines from the digital and analog telemetry points in a predetermined sequence, digitized the analog levels sampled in a 9-bit analog-to-digital converter, and serialized the digital bits into a nominal 391-bps biphasic bit stream, which was switched by the data switching unit to the frequency division multiplex unit or one of the four transmitters under control of ground command.

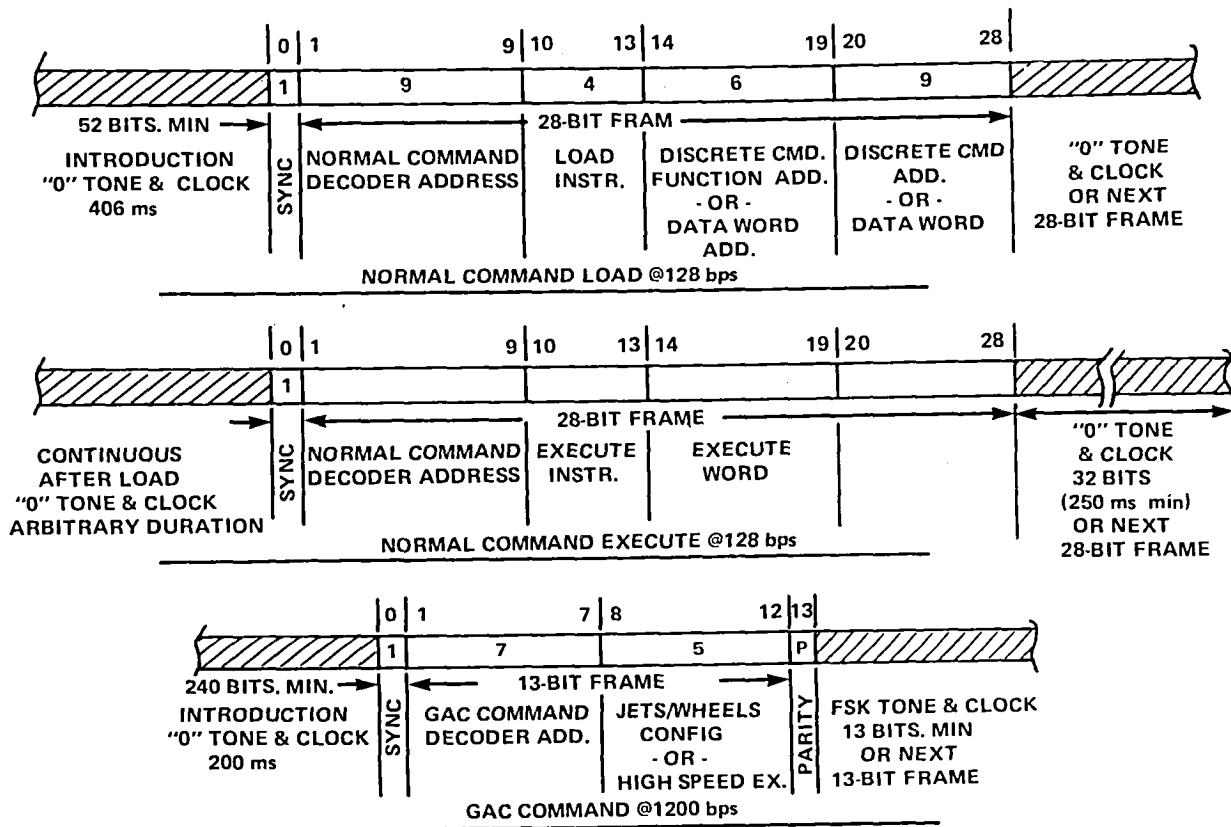


Figure 8-4. Command Word Formats

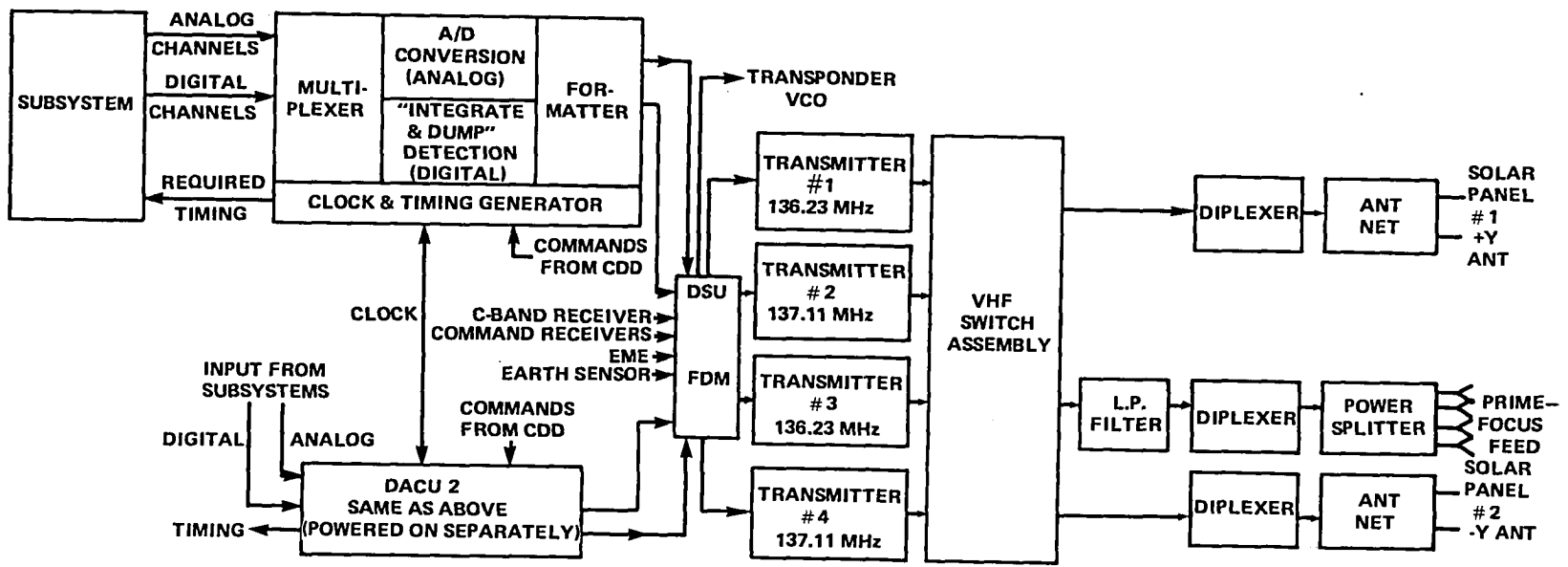


Figure 8-5. Telemetry Subsystem Functional Block Diagram

Table 8-2
ATS-6 Telemetry Parameters

Item	Characteristics
Frequencies	136.23 MHz, 137.11 MHz
Spacecraft Antennas	Near omnidirectional mounted on solar arrays, directional via prime-focus feed and parabolic reflector
Modulation	PCM/PM on omnidirectional-associated transmitters PCM/FM/PM or PM on prime-focus feed-associated transmitters.
Formatting	Fixed format with dwell capability; data format Manchester II +180
Bit Rate	391 bps normal
Word Length	9 bits
Minor Frame Length	128 words
Minor Frame Period	Approximately 3 seconds
Subcommutation	Last 16 words, 16 words deep
Total Format Capacity	368 nine-bit words; each word carries one digitized analog telemetry point or nine digital telemetry points.
Analog Channels	276
Digital Channel (Bits)	783 (87 nine-bit words)

The DACU was a fixed-format encoder with dwell capability. It accepted digital and analog data from the spacecraft subsystems and experiments, digitized each analog sample in a 9-bit analog-to-digital converter, and sequenced each telemetry point into its preassigned position in the telemetry format. The DACU included the spacecraft clock that provided the time code, 0 milliseconds through 365 days, for insertion into the DACU telemetry data stream; the 6-hour timer used to satisfy spacecraft special timing functions; and the 100-kHz clock also used to satisfy spacecraft special timing requirements. The DACU used the 800-kHz output from the spacecraft clock as an input to frequency dividers and logic functions that generated the switching functions required to establish the telemetry format. In the dwell mode, the first 16 words were repeated in each minor frame irrespective of which word was being dwelled upon. Thus, synchronization, status, calibration, command verification, and other telemetry points of prime importance were present for ground station use in each minor frame, independent of the DACU mode of operation.

Four telemetry transmitters were employed: two at each of the two assigned frequencies. Two transmitters could be switched to an omnidirectional antenna or to the vhf prime-focus feed. The other two transmitters were hardwired to omnidirectional antennas. The transmitters were individually commanded on or off from the ground.

The prime mode of operation was frequency modulation/phase modulation, with normal telemetry (DACU), the Environmental Measurements Experiment (EME), and voice-bandwidth-analog data, frequency-division multiplexed onto the carrier of one of the two transmitters associated with the prime-focus feed. This mode took advantage of the high-gain parabolic antenna to give both the EME and voice-bandwidth-analog channels adequate margin for high quality link performance. Normal telemetry or EME data could modulate either of the omnidirectional-associated transmitters or the prime-focus feed-associated transmitters directly in backup modes. Telemetry data could also use the C-band transponder as a backup downlink.

Overall Subsystem Operation

This section describes the functional operation of the telemetry and command subsystem when operating from discrete commands, data word commands, the high speed execute mode, the ground attitude control (GAC) tone mode, normal and dwell telemetry modes, the high-rate EME telemetry mode, and the special data mode (voice-bandwidth-analog channel).

The telemetry and command subsystem shown in Figure 8-1 employed two vhf command frequencies (148.26 MHz and 154.20 MHz) and two vhf telemetry frequencies (136.23 MHz and 137.11 MHz). One vhf command receiver at each frequency was wired directly to an omnidirectional antenna. The second vhf command receiver at each frequency was switchable between the opposite omnidirectional antenna and the prime-focus feed antenna. This configuration assured continuous command capability while taking advantage of the high command link margins afforded by the prime-focus feed antenna when available (parabolic reflector in an Earth-oriented attitude). Both vhf command and telemetry frequencies were useable through the omnidirectional antennas and through the prime-focus feed antenna.

The primary telemetry link was a frequency-division-multiplexed link associated with transmitter 2 or 3 and the prime-focus feed antenna. The frequency division multiplex unit was designed to multiplex normal data (output of the data acquisition and control unit [DACU]), EME data, and the special data functions onto one downlink carrier (136.23 MHz if transmitter 3 was used, and 137.11 MHz if transmitter 2 was used).

The scheme allowed simultaneous transmission of the EME and special data functions. Without the frequency division multiplex (FDM) feature, only one function at a time could be transmitted over the parabolic antenna. Adding the normal telemetry function to the multiplexed channel also augmented the link margin for this function. When the spacecraft was maneuvered, so that the directional beam was no longer pointing toward the Earth, the normal telemetry was switched by ground command for transmission to Earth via the omnidirectional antennas. The data switching unit (DSU) could also be commanded to switch the EME to another transmitter (one not being used for the normal telemetry function) for transmission to Earth. The special data function would not

normally be switched to the omnidirectional-associated transmitters, since the link was marginal for a voice-bandwidth analog signal.

The FDM unit was housed in the DSU. In case of a failure in the FDM unit, the normal telemetry data (DACU) and the EME data could be switched directly into the vhf transmitters; e.g., the DACU on transmitter 1 into omnidirectional 2 and the EME data on transmitter 2 on the prime-focus feed.

A DACU entered the dwell mode under control of ground command, which used a data-word command to select the DACU dwell word. In this mode, the first 16 words of the 128-word minor frame were still telemetered as in normal mode (to retain synchronization, status, calibration, and command verification), but the remaining 112-word positions were repetitions of the word dwelled upon. When this was a minor frame word, the selected word was repeated 112 times each minor frame (3 seconds). In the case of dwell on a subcommutated word, the 16-word subcommutation was repeated 7 times in the 3-second minor frame period. The DACU returned from the dwell mode to normal mode upon command from the ground. Both DACU's could be activated simultaneously, and if desired, one could be in normal mode while the other was in dwell, both could be in normal mode, or both could be in a dwell mode on the same or different words and transmitted by different telemetry transmitter frequencies. Certain timing difficulties might be encountered if both DACU's were in normal mode or both in dwell at the same address.

High rate (1800 bps) telemetry data from the EME and voice-bandwidth analog (special data link) data also modulated the downlink carriers. The prime mode of operation employed a frequency division multiplexed combination of the three modulation sources. The frequency division multiplex signal phase modulated one of the vhf transmitters (normally one associated with the prime-focus feed) or could be switched to the C-band wideband voltage-controlled oscillator input. In backup modes, the normal telemetry and EME data could modulate the vhf transmitters directly.

The telemetry format is shown in Figure 8-6. The 128-word minor frame had the final 16 words subcommutated 16 words deep. The dwell mode formats, while dwelling on a minor frame word or a subcommutated word, are also shown.

The telemetry-receive ground sites had wide flexibility in providing various polarization diversity configurations as follows:

- Circular Dual Polarization Diversity

Omnidirectional-antenna/transmitter 1

$$RCP_1 + LCP_1$$

or

Omnidirectional-antenna/transmitter 2

$$RCP_2 + LCP_2$$

- Circular Quadruple Polarization Diversity

$$RCP_1 + LCP_1 + RCP_2 + LCP_2$$

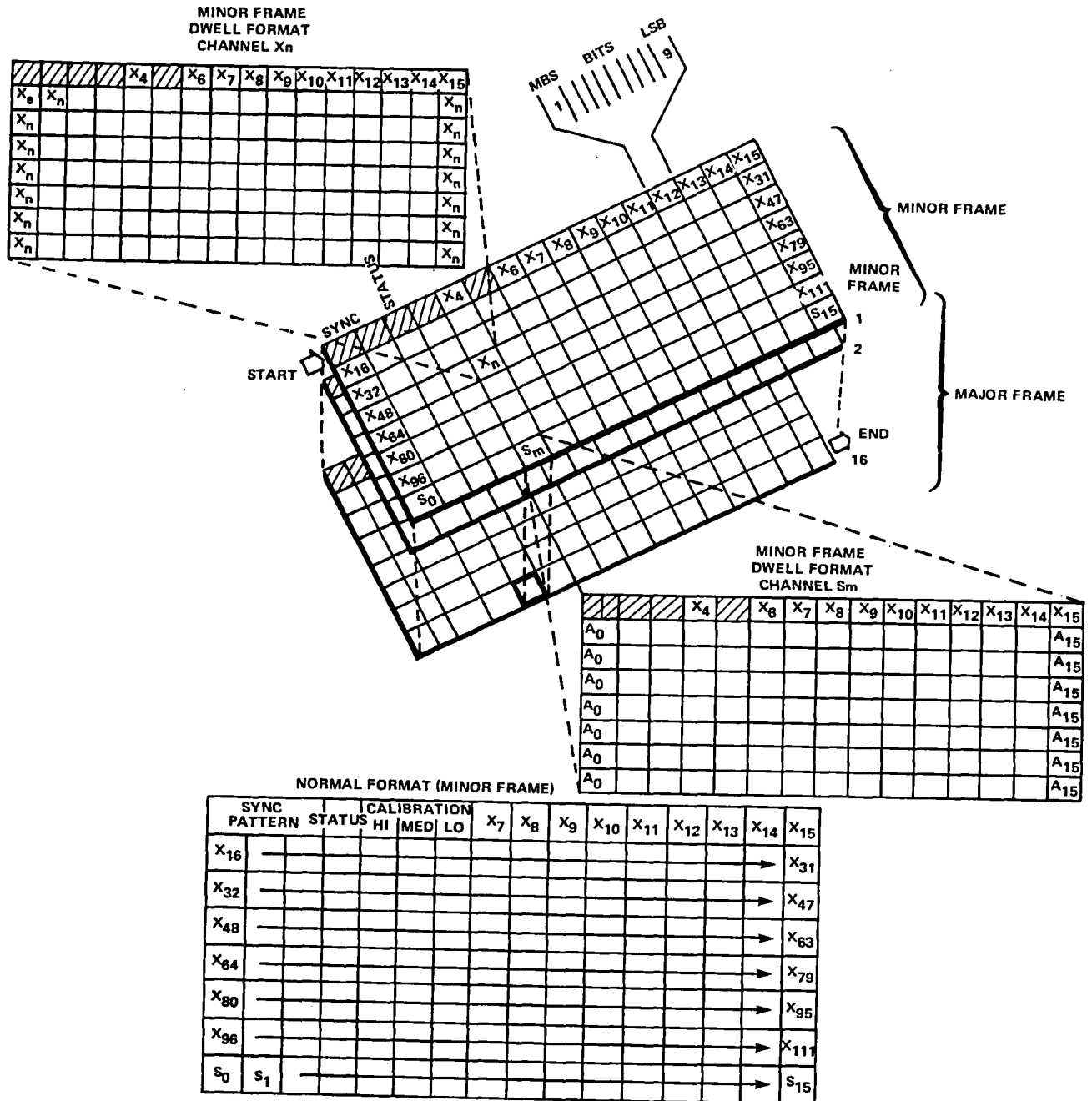


Figure 8-6. Data Acquisition and Control Unit

- Linear Dual Polarization Diversity

Omnidirectional-antenna/transmitter 1

$$V_1 + H_1$$

or

Omnidirectional-antenna/transmitter 2

$$V_2 + H_2$$

- Linear Quadruple Polarization Diversity

$$V_1 + H_1 + V_2 + H_2$$

Each of the indicated dual-diversity configurations represents telemetry reception from one spacecraft omnidirectional antenna and its associated transmitter; i.e., using polarization diversity. The quadruple diversity involves reception from both transmitting systems simultaneously, operating at two different frequencies.

Command reception was at one of the two possible vhf frequencies. The onboard detection element selected the stronger (viable) signal being received from one or the other of the two omnidirectional antennas. Since the two omnidirectional antennas were mounted at the extreme ends of the two solar panels, the selection of the stronger signal under these conditions constituted space diversity combining.

Component Description/Function

The telemetry and command subsystem consisted of the following major assemblies:

- 2 Data acquisition and control units (DACU)
- 4 Vhf telemetry transmitters
- 2 Vhf diplexers
- 2 Vhf hybrids
- 4 Vhf command receivers
- 2 Command decoder and distribution (CDD) units
- 2 Vhf antennas
- 1 Data switching unit
- 1 Low pass filter
- 7 Vhf relays (single pole, double throw).

The DACU selected data from a fixed number of analog and digital data sources in a sequential manner, formed 9-bit telemetry words, and arranged them into a 128-word minor frame. This operation and the order of its execution were controlled by the program generator, with an 800.0-kHz clock being received from one of the master oscillators. The major components of the DACU were the digital multiplexer, analog multiplexer, 9-bit analog-to-digital converter, and the program

generator. The digital multiplexer consisted of 783 channels that were sensed one at a time under control of the program generator. The analog multiplexer served 276 channels; the selected channel was gated into the 9-bit analog-to-digital converter whose output was then placed into the 128-word telemetry format. The program generator controlled the arrangement of data into the telemetry format and controlled the subcommutation of the last 16 words in the format. The last 16 words were subcommutated 16 deep.

The DACU had a dwell capability that allowed a selected minor frame channel (single word or subcom) to be telemetered exclusively. The dwell mode was controlled by ground commands processed through the CDD and the dwell address was inserted into the DACU dwell control circuitry. This address was used by the DACU to select the data word to be transmitted at the higher rate. An execute command from the CDD then initiated this mode of operation.

The DACU also had an internal backup clock that was enabled only when the clock select logic sensed no signal from either of the master oscillators. Finally, the DACU circuitry included a spacecraft clock that was electrically independent of the remaining DACU electrical hardware.

The vhf transmitter was a solid-state unit capable of phase modulating a radio frequency (rf) carrier (frequency of 136.23 MHz or 137.11 MHz) with either 391-bps or 1800-bps telemetry data or a voice-bandwidth-analog signal. Four identical transmitters were used in the telemetry subsystem: two at 136.23 MHz (standby frequency) and two at 137.11 MHz (prime frequency). A low-pass filter was provided between the last power amplifier and the transmitter output to reduce the spurious output signals. An isolator was provided in the final stage to ensure that the transmitter could not be damaged as a result of improper antenna loading. The output rf power was nominally two watts from each transmitter. The transmitters were commanded on or off individually by ground command to the power interface circuits located in the data switching unit.

The vhf diplexer isolated one of the transmitters at either 136.23 MHz or 137.11 MHz from one of the receivers at 148.26 MHz or 154.2 MHz when sharing a common antenna.

The vhf coaxial switches switched the inputs to the vhf receiver or the outputs from the vhf transmitters from the omnidirectional antennas to the prime-focus feed or vice versa.

The solar panel vhf antenna units were capable of transmitting and receiving circularly polarized rf energy at frequencies ranging from 136 MHz to 155 MHz. The antennas had gain patterns that provided the capability of establishing and sustaining communication over the sphere enclosing the spacecraft. There were two antenna assemblies, one mounted on each of the solar panels, each connected to an independent command receiver to effect space diversity reception. The low-gain region of one antenna assembly did not coincide with the low-gain region of the other, thus allowing omnidirectional coverage. Each antenna unit consisted of a pair of vhf whips in an orthogonal configuration and a wire line hybrid power divider. The power received from the vhf transmitter was divided in half by the power divider with output signals, now 3 dB down from the input signal, going to each monopole of the monopole pair antennas. These signals were 90 degrees out of phase, causing circularly polarized radiation.

The vhf command receiver was a solid-state, single-conversion amplitude-modulated (AM) receiver. The receiver demodulated the command signals received from the vhf antennas and provided an audio output for the command decoder. The received command signal was an FSK-AM/AM signal at a carrier frequency of 154.20 MHz or 148.26 MHz. The received rf signal was filtered, amplified, and downconverted to a 10.2-MHz intermediate frequency (i.f.) by a crystal controlled oscillator. The i.f. signal was filtered by a crystal filter and amplified by a four-stage i.f. amplifier. The output level of the i.f. stages was fed back to the i.f. stages and rf amplifier by the automatic gain control circuits. The audio output was fed into audio amplifiers that provided the required audio levels.

The receiver provided resistor-isolated audio outputs, so that a shorted output would not affect the other outputs by more than 10 percent. Two audio outputs from each of the two primary receivers ($f = 154.20$ MHz) contained the demodulated command signals at the audio frequencies (Table 8-1) and were connected to each of the two command decoders. Audio outputs from the prime-focus feed associated receivers were connected through the DSU-FDM to transmitter 2 or 3 for direct relay transmission of the voice-bandwidth analog signal to the ground. The receiver was provided with automatic gain control, so that the audio output level was reasonably constant over a wide signal input dynamic range. A telemetry output was provided for monitoring the automatic gain control voltage. All four receivers were connected to the essential loads 28-volt power bus through dedicated regulators, and could not be commanded off.

The command receiver output interconnection to the command decoder distributor is shown in Figure 8-7. In addition, the prime-focus command receivers could be switched to the DSU frequency division multiplex to provide the special data link capability.

The CDD receiver select logic connected the CDD to the command receiver that had a valid signal output; i.e., "0" or "1" tones modulated by the 128-Hz clock for normal receiver select circuits. The detected clock was used in the timing and control of the command data into the appropriate CDD registers. The CDD decoded the data as defined by the command format shown in Figure 8-4.

The "normal command load" command was decoded to provide a total of 512 discrete commands consisting of 144 dedicated commands with 56-ms (nominal) duration; 160 matrix commands with 252-ms (nominal) duration and 208 matrix commands (16X by 13Y) with 56-ms (nominal) duration. The "normal command load" command was also decoded to provide a total of 45 data-word transfer addresses to which the 9-bit data word could be loaded. The data word transfer addresses included 20 dedicated and 25 matrix addresses (5X by 5Y).

The "normal command execute" command was decoded to provide either an "execute and clear" the CDD register contents or an "execute and hold" CDD register contents (retained the last "normal command load" in the CDD registers). The "GAC command" was both a load and an execute command. An address and parity check was performed on this command, and the command was executed immediately upon successful check. The "GAC command" was decoded to provide 27 combinations of positive/negative/off commands to roll, pitch, and yaw torquers (wheels or jets as previously selected by ground command), plus 5 discrete commands.

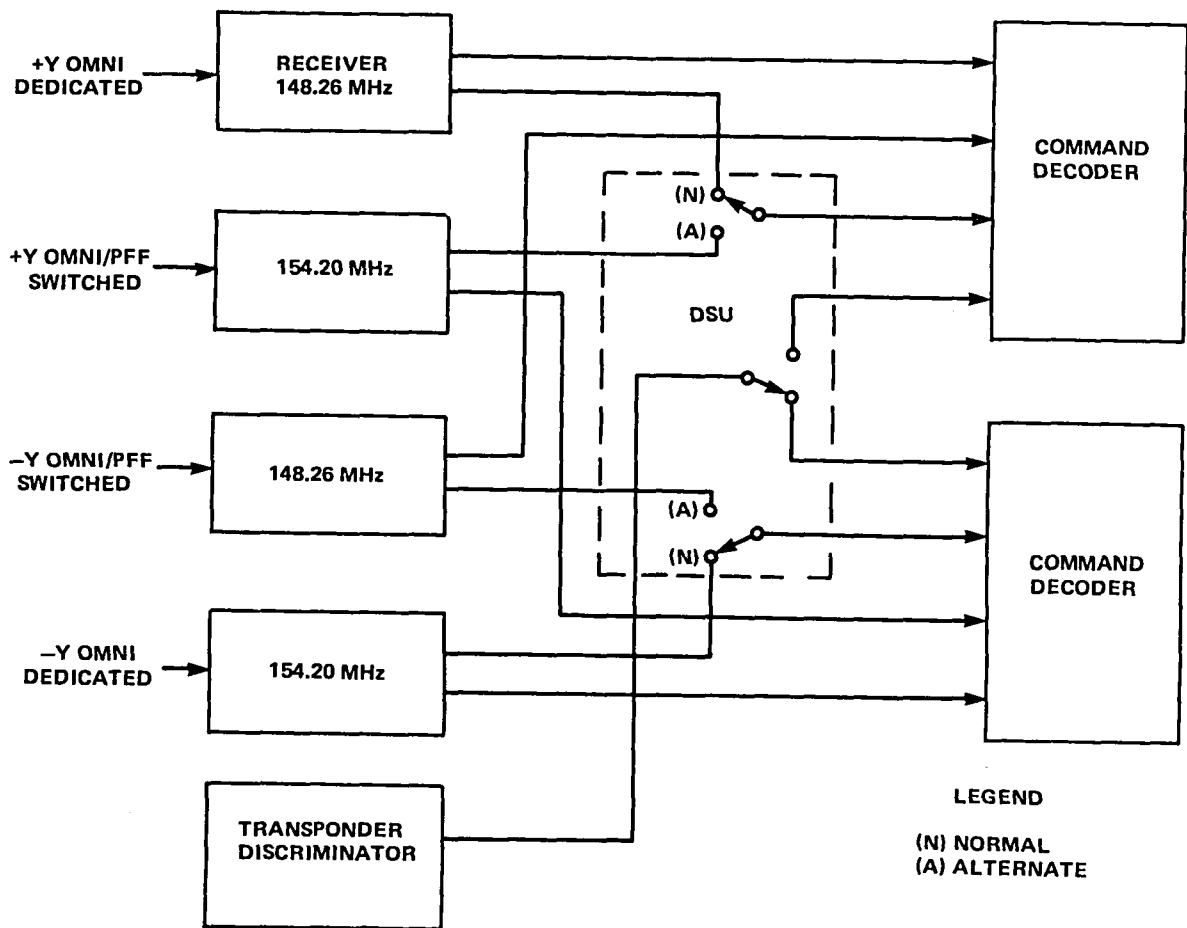


Figure 8-7. Command Receiver/Decoder Interconnections

The DSU connected data sources to the four vhf transmitters and to the C-band wideband, voltage-controlled oscillator input. In addition, switching was provided between the vhf receivers and C-band receiver to the CDD's. The DSU also contained a frequency division multiplex to multiplex three data sources (EME, DACU, and special data link data) on to one telemetry downlink at either vhf or C-band. The power interface circuits for the vhf transmitters were located within the DSU and were controlled from the DSU command matrix.

DESIGN VALIDATION

Telemetry and command hardware previously qualified for space application was selected for use on ATS-6 where design requirements could be satisfied. All rf components except the vhf omnidirectional antennas were in this category, i.e., the command receivers, telemetry transmitters, diplexers, low-pass filters, rf switches, and hybrids. Only minor modification to these components was necessary. Data handling equipment was developed specifically for ATS-6: command decoder and distribution unit, data acquisition and control unit, and the data switching unit. The subsystem design, essentially completed in the ATS-F and -G Phase B/C effort, identified those specific areas that

required new designs. A significant level of activity to trade-off technical approaches, and to develop and verify performance of these new designs began early in the Phase D program, culminating in engineering model fabrication, test, and evaluation. Analytical methods were used for design verification in many areas, including parts stress and reliability, mechanical design, and rf link performance. Parallel development of bench test equipment and aerospace ground equipment provided good program visibility as designs were verified and changes were implemented in preparation for flight equipment development and component qualification. Simplex telemetry and command subsystem tests, using engineering models, demonstrated interface compatibility, specification compliance of major parameters, and operating margins. Subsequent to qualification, telemetry and command components were integrated for electromagnetic interference testing. Spacecraft level integration of all subsystem components, with ground support equipment and flight software, provided exhaustive verification of function/performance at the subsystem level, in addition to those operating parameters that could be verified directly during normal and troubleshooting tests. At every stage, feedback to the design and operations planning activities improved the hardware and lowered the risk in succeeding phases. Special tests were implemented at several points in the program to resolve technical questions of importance. The following paragraphs describe a representative sample of the design verification testing activity during the development of the subsystem.

Development

Command Interface Circuits

During Phase B/C, it was determined that a low impedance, low-level command driver/command termination approach was best suited to ATS-6 applications from the standpoints of high functional reliability and immunity to high noise levels that might be encountered on board the spacecraft. Design of fault-tolerant, totem-pole common emitter PNP driver and NPN terminator configurations was completed and breadboard tested. All fail-safe and interference immunity objectives were satisfied; i.e., proper operation at tolerance limits, shorted or opened parts, no false commands with open or shorted interface wiring, and no false commanding with up to 10 amperes at 95-volt pulses (56 ns rise time) present in adjacent pairs of an unshielded 15-meter long interface cable. Complete absence of command anomalies attributable to this interface in component, spacecraft ground test, and flight operations was due at least in part to the standard interface used throughout the spacecraft for both discrete and serial magnitude command distribution.

Command Detector Circuits

The command decoder distributor command detector circuits were breadboarded early in Phase D to prove bit-error rate performance over temperature and to determine clock acquisition times, dynamic range, and stability of its active filters. Bit-error rate performance of this noncoherent FSK detector design was found to be within 2 decibels of theoretical over most of the input range.

Vhf Antenna Coverage

The telemetry and command vhf omnidirectional antenna design was scaled and tested with a spacecraft structure mockup on the International Business Machines (IBM) Huntsville antenna range, and

antenna patterns were recorded. These patterns verified the antenna subsystem performance for seven possible configurations from launch through injection (Figure 8-8). Performance reflected the inherent system space and polarization diversity provided to the ground stations because of their ability to select any one of four polarizations. The pattern format was a contour plot of the complete sphere about the spacecraft representing the gain of the antenna subsystem in any direction relative to the spacecraft.

Table 8-3 lists the telemetry and command antenna subsystem coverage based upon a minimum allowable gain of -10 dBi (gain relative to an isotropic antenna). The coverage is listed for each of the seven configurations assuming full ground station polarization diversity, first with one spacecraft antenna available and then with both antennas available. (Note that both of the antennas are independent in the subsystem.)

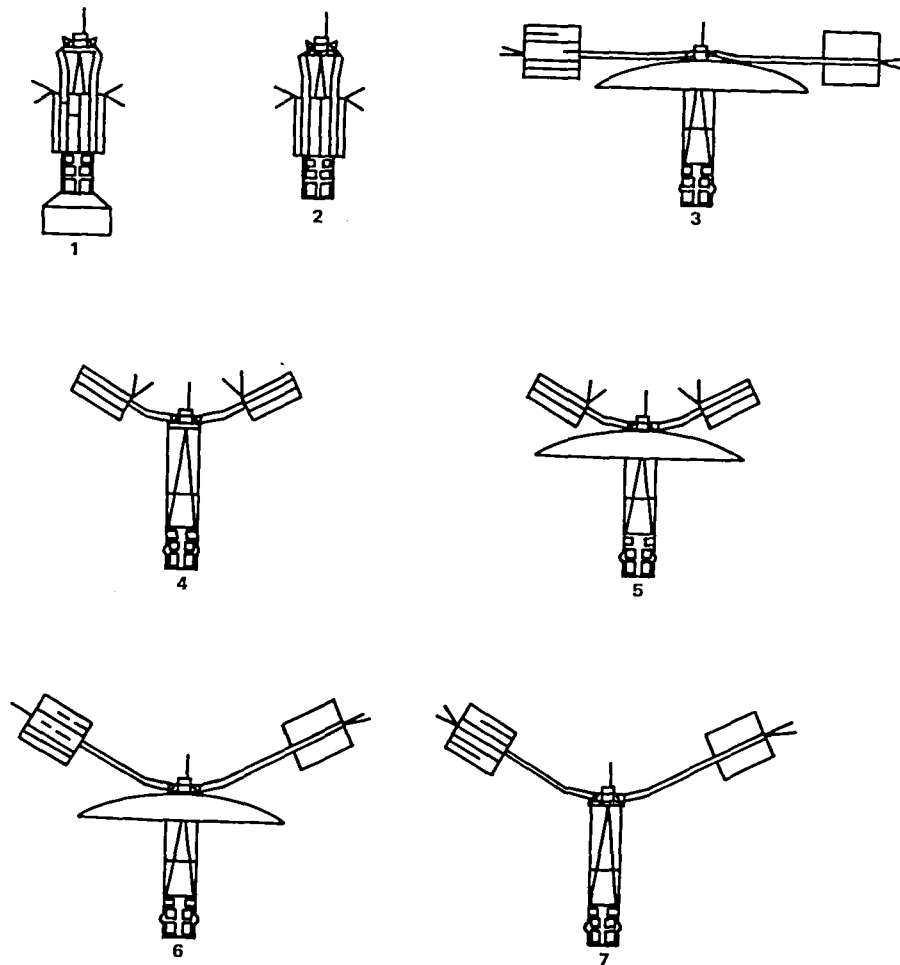


Figure 8-8. Spacecraft Test Configuration

Table 8-3
Percent of Sphere Having Gains of -10 dBi or Better

Configuration	One Antenna (%)	Two Antennas (%)
1	92	99
2	94	100
3 (Normal operational case)	95	100
4	92	98
5 (Failed panel deployment case)	74	86
6	97	100
7	95	100

Subsystem Level

After completion of the subsystem engineering model components, a simplex configuration of the subsystem was assembled to verify operating characteristics and interface compatibility, and to establish certain electrical test limits for qualification test procedures. No significant problems were encountered. One of the results of this test was a modification to the gain constants in the frequency division multiplex assembly of the data switching unit to produce the desired modulation indices at the telemetry transmitter.

During the same period, interface compatibility with the transponder command distributor and digital operational controller was demonstrated.

Following component qualification, a telemetry and command system configured largely of the qualification components in a simulated Earth-viewing module was integrated to test for electromagnetic interference. Additional tests were conducted for command receiver susceptibility as a result of the subsystem electromagnetic interference test.

During the thermal structural model mating check at Kennedy Space Center, the engineering model omnidirectional antenna was mounted in the launch position to verify the viability of prelaunch telemetry and command communications links through service tower parasitic antennas.

Spacecraft Level

All-up spacecraft testing used the subsystem in all of its modes to support tests of experiments and other subsystems. Exposure to the high rf fields involved, in addition to local interference, proved to be a good test of flight worthiness. Two results should be mentioned.

During initial test with the Radio Beacon Experiment operating, command thresholds for the 154.2-MHz receivers were found to have increased by about 9 dB; all tests were purposely run with command levels within 6 dB of the threshold to reveal any desensitization problem. An intermodulation analysis and confirming spectrum analysis showed the interference to be due to a fifth order product caused by mixing of the third harmonic of the 40.017-MHz carrier of the Radio Beacon Experiment with the 137.11-MHz telemetry transmitter second harmonic. The resulting spurious signal at 154.169 MHz was only 31 kHz from the 154.2-MHz receiver passband center frequency. Shielding of telemetry lines extending from the Earth-viewing module into the hub area corrected the problem.

Another unexpected anomaly was out-of-band emissions from the telemetry transmitters that were due to command decoder distributor power line conducted noise coupled to the transmitters through the power interface circuits in the data switching unit. High transmitter modulation sensitivity to conducted power line noise was discovered. It was due to unbalanced stray capacitance from the modulation circuit to the housing. This problem was corrected by grounding the power return bus close to the transmitter power and signal connector.

CHAPTER 9
IN-ORBIT PERFORMANCE AND OPERATIONS

INITIAL THIRTY-DAY CHECKOUT

The telemetry and command subsystem performed without a flaw during prelaunch, launch, and orbital phases. Tables 9-1, 9-2, and 9-3 contain data from the initial 30-day telemetry and command tests. Compliance with the specification requirements for the telemetry and command subsystem was satisfied in every area by a comfortable margin. Though not shown in the tables, successful operation in normal/dwell telemetry, downlinking at baseband or frequency division multiplexing, use of the omnidirectional and prime-focus feed antennas, transmitter switching, and commanding, command receiver automatic gain control levels, etc., were verified during normal spacecraft operations.

Table 9-1
Telemetry and Command Subsystem Performance Comparison

Parameter	Specification	Inflight Performance
Transmitter Frequency	A1 136.23 ±0.003%	136.231469 +0.0011%
	A2 137.11 ±0.003%	137.109984 -0.000%
	A3 136.23 ±0.003%	Was not powered on launch
	A4 137.11 ±0.003%	137.107742 -0.0017%
E.i.r.p. Power	-3 dBW min.	E.i.r.p. not measured; bit-error rate < 10 ⁻⁵
DACU Bit Rate	390.625 ±0.00015%	7-day check < 0.00005%
DACU Analog Calibration Voltage	Low 0.265 ±0.005 Vdc	0.265 V ± 0
	Med 2.565 ±0.005 Vdc	2.565 V ± 0
	High 5.095 ±0.005 Vdc	5.095 V ± 0
FDM		FDM multiplexing of combined EME data, DACU normal data, and Earth sensor data, were successfully demultiplexed at both ground stations after first day of flight, via the prime-focus feed/9.14-m parabolic reflector.
Receiver/CDD	-107 dBm	Actual margin above threshold was 15 to 27 dB with BER < 10 ⁻⁵

Table 9-2
Uplink Command Receiver Signal Levels

Conditions With Spacecraft in Local Vertical – Reference Orientation	Receiver 1 Omni-1* (+Y)	Receiver 2 Omni-1 (+Y)	Receiver 2 Prime- Focus Feed	Receiver 3 Omni-2 (-Y)	Receiver 4 Omni-2 (-Y)
Spacecraft orbital data AGC level	-90 dBm	-92 dBm	-80 dBm	-88 dBm	-90 dBm
Receiver threshold measured in ground test	-118.0 dBm	-119.4 dBm	-119.4 dBm	-116.5 dBm	-119.7 dBm
Approximate margin above threshold	28 dB	27 dB	39 dB	28 dB	30 dB
Margin above specification	17 dB	15 dB	27 dB	19 dB	17 dB

*Omnidirectional antenna

Table 9-3
Downlink Performance

Conditions with Spacecraft in Rosman Pointing – Reference Orientation	136 MHz XMTR 1* Omni-2 (-Y)	137 MHz XMTR 2 Prime-Focus Feed
Receiver input signal level at Rosman Ground Station	-116 dBm	-107 dBm
SATAN receiver antenna gain	+19 dB	+19 dB
Space loss (35,800 km)	168 dB	168 dB
E.i.r.p. at spacecraft	+33 dBm	42 dBm
PR-2000 min. spec. e.i.r.p.	+27 dBm	NA
E.i.r.p. predicted from prelaunch measurement	+31 dBm	41 dBm

*XMTR – Transmitter
Omni – Omnidirectional antenna

OVERALL MISSION PERFORMANCE

The telemetry and command subsystem successfully provided spacecraft command control and telemetry functions throughout its 5 years in orbit. With the exception of anomalies (Chapter 10) relating to performance of the data acquisition and control unit (DACU), performance of the subsystem was excellent during all mission phases including critical drift-phase operations. All redundant units (except DACU-1) remained in a standby status. Major performance parameters, verified during inflight operations, are summarized in Tables 9-1 through 9-5.

These exhibits not only show compliance with initial specifications, but also indicate excellent stability over the 5-year period of operations.

Table 9-4
Telemetry Transmitter Frequency Performance

Specification	30-Day Test	July 1979 Test	Change
136.23 MHz \pm 0.003%	136.231469 MHz	136.2311 MHz	-0.00027%
137.11 MHz \pm 0.003%	137.109984 MHz	137.1118 MHz	+0.0013%
136.23 MHz \pm 0.003%	Not measured	136.2305 MHz	—
137.11 MHz \pm 0.003%	173.107742 MHz	137.1092 MHz	+0.0011%

Table 9-5
Telemetry Downlink Performance*

	30-Day Test		July 1979 Test	
	136.23-MHz Omni-2**	137.11-MHz PFF***	137.11-MHz Omni-2	136.23-MHz PFF
Rosman receiver input level	-116 dBm	-107	-118	-106
SATAN receive antenna gain	+19 dB	+19	+19	+19
Space loss (35,800 km)	168 dB	168	168	168
Spacecraft e.i.r.p.	+33 dBm	+42	+31	+43
Specification minimum	+27 dBm	N/A		
Prelaunch e.i.r.p. estimate	+31 dBm	+41		

*Spacecraft pointed at Rosman

**Omnidirectional antenna

***Prime-focus feed

Following the 3σ -day in-orbit checkout, system status was again verified in December 1974. The subsystem performed successfully, providing normal and dwell telemetry of experiment and support subsystem data, downlinking of the Environmental Measurements Experiment data, and processing and distributing commands throughout the spacecraft. Primary characteristics monitored during the period were:

- Downlink Characteristics
 1. Telemetry signal quality including frequency division multiplex operations
 2. Telemetry time base accuracy
 3. Transmitter power output and frequency
 4. Normal and dwell data acquisition and control unit (DACU) operations
- Uplink Characteristics
 1. Normal command operations
 2. Ground attitude control command operations
 3. C-band command operations.

The telemetry subsystem configuration (Figure 9-1) that supported ATS-6 operations used the frequency division multiplex unit to provide both DACU-2 normal and environmental measurements experiment (EME) telemetry to the 137.110-MHz telemetry transmitter for downlink transmission through the prime-focus feed/9.14-meter parabolic antenna. Dwell telemetry was provided by DACU-1 and the 136.231-MHz telemetry transmitter through its associated omnidirectional antenna.

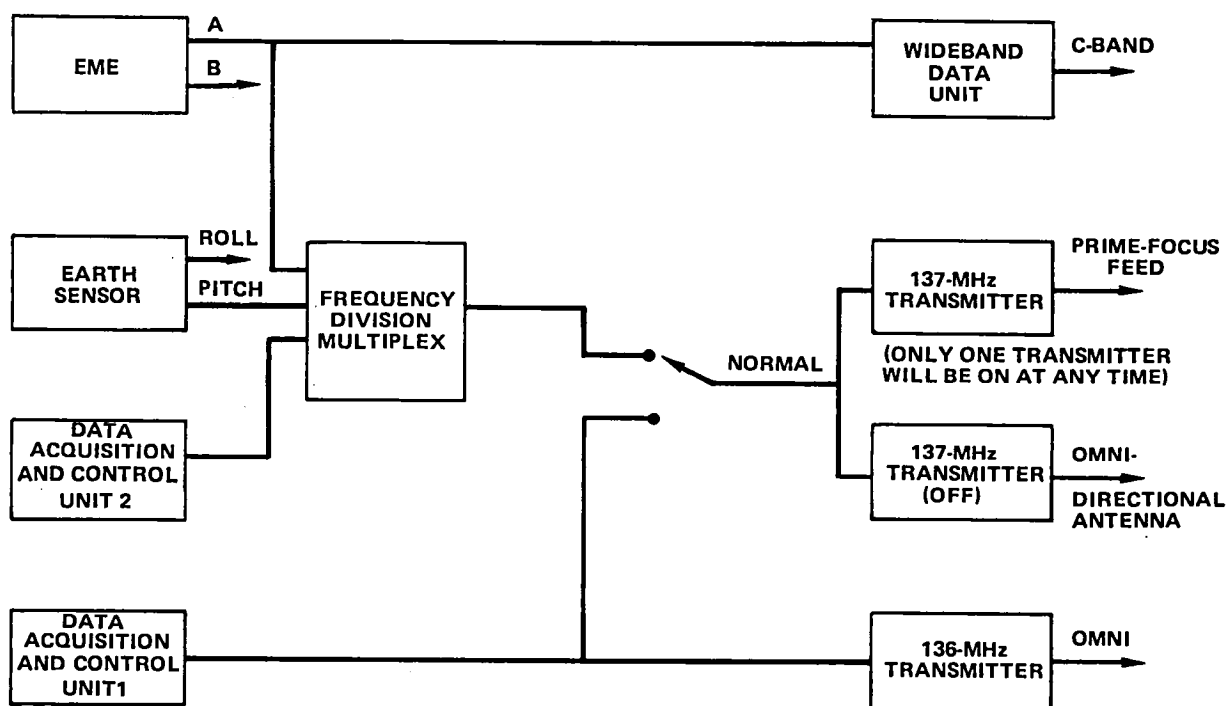


Figure 9-1. Telemetry RF and Baseband Configuration

The redundant 137.105-MHz telemetry transmitter was not powered on after the 30-day check-out, and the 136.23-MHz transmitter after launch, until the final engineering tests at the conclusion of normal mission operations.

Figure 9-2 shows the command configuration used to support ATS-6 operations. The majority of commands uplinked to the spacecraft were sent by the prime-focus feed/148-MHz receiver command decoder distributor-2 (CDD-2) command link.

FINAL ENGINEERING TESTS

Prior to the deactivation of ATS-6 on August 3, 1979, telemetry and command subsystem engineering tests were conducted to measure principal end-of-life operating parameters of the system. Results are presented in Tables 9-4 and 9-5. These tables show both the 30-day and end-of-mission test results. All transmitters stayed well within the specification range, operating within 0.0013 percent of the specification frequencies. Maximum change over the 5-year orbital period was also 0.0013 percent.

Allowing for output variations in transmitter power, potential measurement errors, and some differences in cabling losses, calculated telemetry e.i.r.p. values shown in Table 9-5 agree with 30-day test results. This agreement indicates no significant degradation in the system rf transmission losses (coaxial cables, diplexers, rf switches), antenna gains, or transmitter power output during the 5-year period.

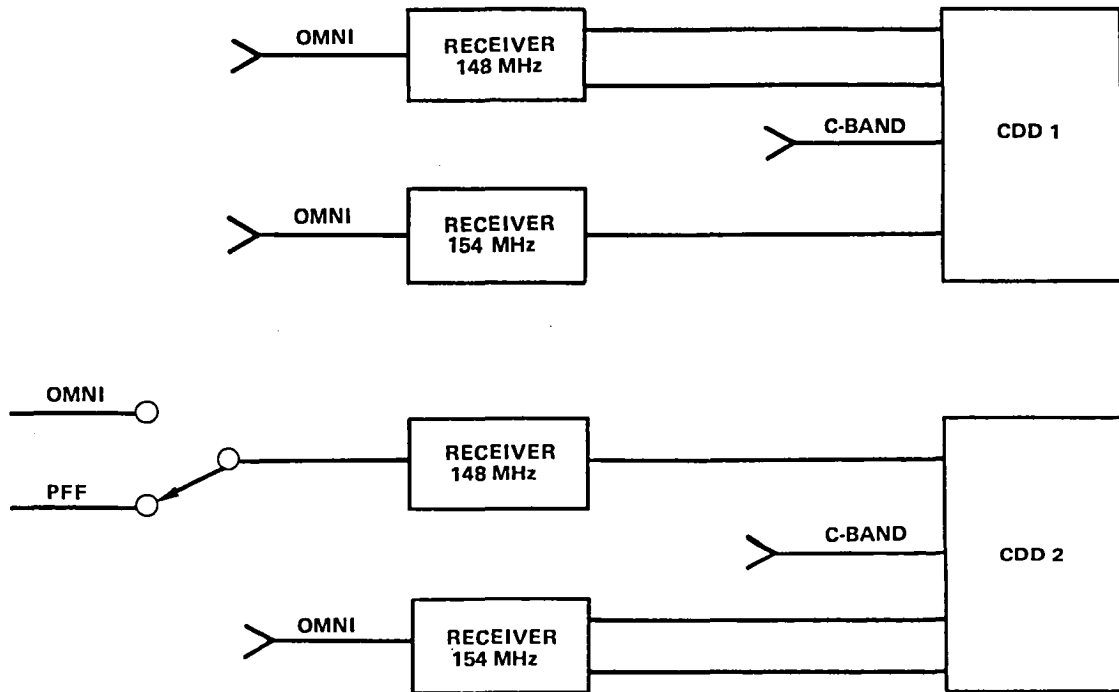


Figure 9-2. Command Configuration

In addition to the tabulated data, the downlink bit rate was measured and found to have remained at 390.6 bits per second (bps). Command threshold at 154.2 MHz was measured to be -119 dBm, which is in excellent agreement with the -119.4 dBm obtained during prelaunch command tests. While comparative data for the remaining three receivers were not collected during the July 1979 test, both uplink frequencies were used successfully during the mission.

Spectrum analysis of the 137.11-MHz downlink with DACU-2 modulation and the 136.23-MHz downlink with FDM showed no abnormalities.

IN-ORBIT ANOMALIES

DACU-1 Anomaly

Description

On November 30, 1974, at 00:33:19 G.M.T., ATS ground stations lost lock on the data acquisition and control unit-1 (DACU-1) telemetry downlink approximately 4 minutes after it had been commanded to dwell on channel 113. During a brief series of subsequent checks by flight operations personnel, it was determined that the ground stations were able to lock on DACU-1 when in "normal" or when dwelling on even-numbered telemetry channels, but lost lock whenever DACU-1 dwelled on an odd channel. DACU-1 was turned off at 02:47 G.M.T. and left off until 19:18 G.M.T. on December 2, 1974, at which time a series of special tests were conducted to investigate the anomaly. After these tests were completed, the data acquisition and control unit was again turned off until December 27 at 17:21 G.M.T., when it was turned on to determine its status. On that date, a decision was made to leave the DACU on permanently.

DACU-1 performance in the normal mode was excellent until August 7, 1975, when some of the format anomaly symptoms began to reoccur. Initially, the only errors occurred in words 0, 2, and 21 and seemed to be related to spacecraft configuration (i.e., errors were more frequent with the propagation experiment on). The errors caused no significant problem at ATSOCC, and DACU-1 continued to function as the primary data source.

However, during the 4-month period from August to December, 1975, DACU-1 gradually continued to degrade, so that by December 18th, seven telemetry words were providing erroneous data on one or more minor frames of each major frame. Therefore, to avoid unnecessary problems at ATSOCC, on December 18, 1975, (approximately 1 year from the time of the initial anomaly), DACU-1 was placed in standby, and DACU-2 was used as the primary data source at ATSOCC. Although DACU-1 remained on and in standby, data were to be transmitted and recorded only on a periodic basis to monitor degradation status.

Subsequently, DACU-1 was turned off during the February 29 to April 12, 1976 eclipse season to conserve spacecraft power. Reactivated periodically when DACU-2 was operated in the dwell mode, valid data were received. Backup utilization for periods of up to 24 hours at a time continued through to the end of the mission. Normal operation was obtained on each occasion, spacecraft operation being totally dependent on DACU-1 during DACU-2 anomaly periods. Details of the anomaly conditions and chronology are presented in the following paragraphs.

Initial DACU-1 Anomaly, November 30, 1974—On November 30 at 00:29:26 (0 hours, 29 minutes and 26 seconds) G.M.T., DACU-1 was operating properly, providing dwell data on channel 116. Since the first weeks of flight, DACU-1 had been used primarily to dwell on channel 116 to enable attitude control subsystem operations personnel to closely monitor the performance of the Polaris tracker, occasionally being commanded to “normal” or another dwell channel for supplemental data.

At 00:29:29 G.M.T. (all subsequent times will be given in G.M.T.), DACU-1 was commanded to dwell on channel 113. The switch was accomplished without incident and good data were obtained. At this time, the spacecraft was in a nominal configuration, pointing at Rosman with -2.6 degree roll, and conducting an L-band PLACE* experiment. All other experiments were off except the Environmental Measurements Experiment, the Advanced Thermal Control Flight Experiment, and the Quartz-Crystal Microbalance Experiment. Accordingly, the communications subsystem was configured so that the L-band and C-band driver and power amplifiers were on and the uhf and S-band units were off (i.e., com-status word 4 = octal 463). Three minutes and 11 seconds later at 00:32:40, during the fourth minor frame, two anomalies occurred in DACU-1 (as seen in subsequent tape playback data**): the first sync word (word 0) changed from octal 765 to 775, and the com-status word (word 4) changed from 463 to 000. No apparent anomalous changes occurred in the DACU-2 data at this or any other time during this period. Furthermore, no spacecraft commands were transmitted or executed during this period. Four frames later at 00:32:52, word 4 shifted from 000 to 475 (and remained at that value until frame sync was lost at 00:33:16). At 00:33:13 (frame 15), word 0 shifted from 775 to 514 and after 2 frames; sync lock, and therefore DACU-1 data, was lost. Bus voltage was 30.40 and steady and DACU temperature was 26°C.

At 00:52:32, DACU-1 was commanded back to dwell on channel 116. Sync lock was obtained immediately and no anomalies were present (i.e., word 0 was 765 and word 4 was 463). During the interim period, the only command transmitted and executed was 03106. “IF 2 beacon power on.” At 00:54:30, after 2 minutes of proper operation, DACU-1 was again successfully commanded to dwell on channel 113. At 00:55:11, after only 41 seconds of proper operation, the malfunction symptoms described above reappeared and at 00:55:23, sync lock was lost after two consecutive frames where the first sync word was 514.

DACU-1 was then commanded through a series of dwell configurations as summarized in Table 9-6. Note that the DACU operated properly when dwelling on even channels, but lost sync after short periods of dwelling on odd channels.

At 01:50, DACU-1 was commanded into the “normal” mode. Sync lock was obtained almost immediately, and all data appeared to be valid. Good data were provided for a period of 57 minutes at which time the DACU was commanded to dwell on channel 116 for 2 minutes and was then turned off pending analysis of the malfunction indications encountered in the dwell mode.

*Position Location and Aircraft Communication Experiment

**These data were played back subsequent to the special test conducted December 2, so the details of the format anomalies discussed were not known at the time of the test.

Table 9-6
DACU-1 Operation—November 30, 1974

Time	Command/Operation	Comments
01:00	Dwell on 116	Proper operation
01:04	Dwell on 113	Lock lost after 1½ min
01:07	Dwell on 114	Proper operation
01:14	Dwell on 115	Lock lost after 2 min
01:19	Dwell on 117	Would not lock
01:20	Dwell on 118	Proper operation
01:25	Dwell on 117	Lock lost after 2 min
01:32	Dwell on 116	Proper operation
01:33	Dwell on 113	Lock lost after 2 min
01:35	Dwell on 116	Lock lost after 2 min

DACU-1 Dwell Anomaly Investigation, December 2, 1974—On December 2, at 19:18:31, DACU-1 was turned on to conduct a special test to investigate the dwell anomalies encountered on November 30. The test was divided into three phases as follows:

- Phase I: DACU in normal mode for 15½ minutes
- Phase II: DACU alternately dwelling on channels 49 and 70 for a period of 1 hour and 58 minutes
- Phase III: DACU back in normal for 21 minutes.

DACU-1 operating characteristics during these phases are presented in the following paragraphs.

- *Phase I: DACU-1 in Normal*—DACU-1 was turned on at 19:18:31 on December 2, after being off for approximately 2 days and 16½ hours. No real-time data were obtained during this period, since the sync pattern was unknown at the time of the test. However, during a subsequent playback of the Rosman analog tape using the information gained during the Phase II dwell mode portion of this test, sync lock was obtained on 514 514 xxx at 19:23:18 where xxx (word 2) was acting as a frame counter, i.e., like word 3. At this time, there were a minimum of 34 “doublets” wherein an even numbered channel assumed the value of the next odd numbered channel, that is:

word 4 = word 5
word 8 = word 9
word 10 = word 11
word 12 = word 13
etc.

There may have been more, since there were a number of sets that read 000, where 000 was also a correct value for the even word. After 11 minutes, DACU-1 was cycled off/on, with no apparent change, as the number of proven doublets varied between 33 and 37. After a total of 15 minutes and 26 seconds, the DACU was commanded to dwell on channel 69.

- *Phase II: DACU-1 in Dwell*—DACU-1 was commanded to dwell on word 69 at 19:33:57. Word 69 was selected, because it is a CDD status word that already read 000 unless GAC commands were being executed. Therefore, the only channels with data at this time were the first 16 words of each minor frame. By displaying the initial portion of the resultant bit pattern on a scope at ATSOCC, telemetry and command subsystem engineers were able to determine that DACU-1 had apparently shifted to a new sync pattern, 514 514 xxx. Subsequent analysis revealed that the new pattern was actually a symptom of a much broader condition, whereby the even channel words (i.e., 0, 2, 4, etc.) tended to duplicate the value of the succeeding odd channel words (i.e., 1, 3, 5, etc.). Word 0, therefore, duplicated word 1, and read 514 instead of 765. Word 2 duplicated word 3, and read frame count instead of 600. Since this pattern was consistent and repeatable, ATSOCC was able to lock up on the resultant 18-bit pattern of 514 514, and the remainder of the bit stream could be decoded and printed. The first available full-frame octal printout was obtained approximately 15 minutes after switching to word 69 and the data showed that all of the first 16 words were paired, resulting in 8 doublets. The balance of the minor frame read all 000's. This condition prevailed for the remaining 15 minutes that DACU-1 dwelled on word 69.

At 20:00:47 DACU-1 was commanded to dwell on word 70, which also always read 000 unless CDD-2 GAC commands were being executed. Initially, the first 16 words appeared as 8 doublets; however, during the seventh frame, the doublets started to disappear and after 1 minute of dwelling on word 70, the condition had cleared and the data format was correct.

At 20:02:21 DACU-1 was commanded to dwell on word 69. After 12 seconds, word 0 shifted to 775, and after 21 seconds doublets started to appear.

At 21:32:00, DACU-1 was commanded back to the normal mode after dwelling on channel 69 for 1 hour and 11 minutes.

- *Phase III: DACU-1 in Normal*—Approximately 1 minute after being commanded back to normal, sync lock was obtained on 514 514 xxx, with 27 doublets in the major frame. However, almost immediately, the number of doublets started to decrease rapidly, so that approximately 2½ minutes after switching to normal, there were only two left (words 0 and 1, and 48 and 49). Approximately 18 seconds later, word 3 read 600 (instead of frame count) for one minor frame, and 20 seconds after that, word 0 read 775 instead of 514. However, 1 minute later at 21:35:36, DACU-1 was cycled off/on, and at 21:36:21 there were 39 doublets. Again, the number of doublets decreased rapidly so that 2 minutes later there were only two left (again, words 0 and 1, and 48 and 49). During the next 3 minutes,

the frame sync pattern intermittently (almost reluctantly) shifted from 514 514 xxx to 765 514 600 and by 21:43:20, the proper pattern predominated with an occasional occurrence of 775 or 514 in word 0, instead of 765. Word 48 started to read correctly at 21:37:40, and no other doublets, except for words 0 and 1, were observed thereafter. By 21:44:19 (12 minutes and 19 seconds after being commanded from dwell to normal and 8 minutes after being cycled off/on), the sync pattern was consistently 765 514 600, except for the 16th minor frame of every other major frame, wherein word 0 momentarily shifted to 775. The test was terminated at 21:53:08 when DACU-1 was turned off.

DACU-1 Status—December 27, 1974—At 17:21 on December 27, 1974, DACU-1 was turned on for a status check after being off for 3½ weeks. The system came up in the anomalous mode. Sync lock was obtained at ATSOCC approximately 2 minutes after turn-on using 514 514 xxx. There were 33 proven doublets in each major frame. After approximately 17 minutes of operation, the number of doublets gradually started to decrease. The system continued to improve and at 18:16, 55 minutes after turn-on, DACU-1 had completely “healed” itself, as frame sync held solid at 765 514 600; there were no doublets, and all data looked good. A brief chronological sequence of the healing process is presented in Table 9-7. It was decided to leave DACU-1 on indefinitely, pending final analysis of the data.

Subsequent to the status check, on Saturday, December 28, 1974, ATSOCC operations switched from DACU-2 (which remained on) to DACU-1, as the primary data source. Thereafter, DACU-1 provided continuous good data with no anomalies encountered until the latter part of 1975.

Table 9-7
DACU-1 Operation—December 27, 1974

Time	No. of Doublets	Frame Sync
17:38	32	Solid 514 514 xxx
17:40	26	Solid 514 514 xxx
17:41½	22	Solid 514 514 xxx
17:43	16	
17:45	6	1 frame 775 514 600
17:51	4	1 frame 775 514 600
17:57	1	Intermittent 775 514 600 514 514 xxx 765 514 600
18:07	1	Last occurrence of 514 in word 0
18:08		Frame sync correct except for 775 in word 0 every 16th frame
18:15		Frame sync solid at 765 514 600

DACU-1 Status—December 19, 1975—Table 9-8 shows the error status of DACU-1 on December 19, 1975. Note that most of the seven errors occurred on a predictable basis, and could be compensated for by the ATSOCC computer, if required. For example, the com-status (word 4) was only in error in frames 0, 2, and 4 and could be masked out to avoid causing an erroneous cathode-ray tube (CRT) display. However, since DACU-1 was apparently still degrading, and DACU-2 was available, DACU-1 was replaced by DACU-2 as the primary data source at ATSOCC, but was not turned off.

DACU-1 Status—February 9 and 10, 1976—On February 9, 1976, ATSOCC attempted to switch back to DACU-1 temporarily for normal data to use DACU-2 to obtain dwell data in support of a special test. However, the Hybrid Ground Station at Madrid, Spain, could not obtain frame sync lock on the DACU-1 bit stream, and DACU-2 was left in normal. As a result of subsequent lock-up attempts and adjustment of the ground station data handling equipment, frame sync lock was ultimately obtained and DACU status could be determined. The data revealed that the DACU-1 output format had degraded significantly since December 19. There were one or more errors in a majority of data words in a 48-second major frame period. The reason that frame sync lock was not readily accomplished was because word 3 (frame count) was being substituted for word 2 (third frame sync word) in just about every frame, instead of just frame 0, as before. Furthermore, words 0 and 1 (frame sync words 1 and 2) also contained one or more errors per minor frame.

Table 9-8
DACU-1 Error Status—December 19, 1975

Word	Description	Error Observed	Occurrence
0	Frame Sync	Read octal 775 versus 765	All frames
2	Frame Sync	Substituted word 3 value for word 2	Frame 0
4	Com Status	Read erroneous value	Frames 0, 2, and 4
40	RGA Yaw Rate	Read erroneous value	Frames 2 and 4
56	Battery 1	Substituted word 58 value for word 56	Frame 2, intermittently
64	Solar Array Shunt Current	Read erroneous value	Frames 6, 7, 14, and 15
80	+Yaw on Time	Substituted word 81 value for word 80	Various frames, intermittently

An octal dump comparison printout for DACU-1 versus DACU-2, which was obtained at 3:14 G.M.T. on February 10 approximately 6 hours after frame sync lock was obtained, showed that there were more than 50 errors in 7 of the first 8 frames of the major frame (frame 4 was not printed out), not including word 0, which consistently read octal 775 instead of 765. The following items are noted from the printout:

- Errors were more prevalent in the first three frames.
- Errors were more prevalent in even-numbered channels.
- Most of the errors appeared to be due to erroneous bits within a word and not to whole word repetition, which was a strong characteristic of the original anomaly (i.e., the doublet pattern).

Due to a requirement to reduce spacecraft loads during the February 29 to April 12, 1976 eclipse season, DACU-1 was turned off.

Assessment

The most probable cause of the anomaly was identified as a change in the threshold voltage of the MOS semiconductor device in the least significant bit address lines inside the read-only memory used as the minor frame and instruction memory SCI part number 2854108-1. This condition was attributed to possible ionic contamination (probably sodium) introduced during the MOS manufacturing process that could account for the malfunction symptoms, including the "healing" effect by ionic migration. Since other identical circuits in the read-only memory did not show the same malfunction symptoms under similar stress conditions, the problem was considered a random failure and not indicative of a design or application deficiency.

A September 1975 review of frame synchronization problems led IBM to conclude that the DACU-1 anomalies were essentially identical to those that occurred in November to December 1974 and were due to the same suspected cause: "A change in the threshold voltage of the MOS semiconductor device(s) . . . (due to mobile ionic contamination) inside the read-only memory." As stated in an earlier IBM report, it is the type of mechanism that can continue to degrade. IBM did not feel that it would be worthwhile to conduct additional studies or bench tests. They did suggest the possibility that prolonged dwelling on an odd channel might counteract the effects of the previous extended periods of dwelling on even channel 116 and at least partially cure the DACU. However, no one could be sure that this would help or whether it would, indeed, further degrade the unit.

Operational experience, until the spacecraft was powered down on August 3, 1979, remained consistent with the initial failure hypothesis. An operational constraint was imposed on the use of DACU-1 after April 1976; namely, that it should be turned on for short periods only when needed and only in the normal mode. DACU-1 was used successfully in this manner a number of times thereafter. In particular, when the DACU-2 anomaly occurred in May 1979, DACU-1 was operated successfully in this manner many times, for continuous periods of 24 hours and more, with no evidence of anomalies.

DACU-2 Anomaly*Description*

On May 9, 1979, telemetry of four minor frame analog channels from DACU-2 became intermittent 000_g. The anomaly progressed during 1 hour until 42 analog channels were affected, suddenly all recovered, then again became all zeros. Over a period of about 2 hours, data again became near normal, except for midscale calibration which remained 10 millivolts (mV) low. Digital channels were unaffected. DACU-1 data were verified to be normal during the period. On May 11, ten additional channels became intermittent zeros; this time, digital words were also affected. DACU-2 was turned off on May 14 and reactivated May 23; data anomalies were still present in both normal and dwell modes. On May 24, all data became valid, then suddenly both digital and analog channels previously affected dropped to zero; gradual recovery followed, all digital first, then, analogs. This intermittency characteristic was repeated several times; all data finally became valid on May 25 and remained so until June 15 when all channels previously affected were again anomalous. The anomaly condition prevailed until June 25 when all channels suddenly returned to normal and remained so for approximately 2 hours; in the next hour, anomalies progressed until previously affected channels were again invalid. On July 12 the anomaly again suddenly disappeared, but reappeared July 26.

Table 9-9 shows the chronology of events and affected channels.

Table 9-9
DACU-2 Anomaly Chronology

Day	Date	Event
129	May 9, 1979	41 DACU-2 analog words become 000 _g . (Words 5, 24, 41-58, 63, 76-81; subcom 114/0-3, 5; 114/4-8, 11, 13-15)
131	May 11	10 additional DACU-2 words, intermittent on May 9, become 000 _g . (Digital words 26-30, 33; subcom analog words 114/0-3)
134	May 14	DACU-2 turned off
143	May 23	DACU-2 turned on; dwell on word 42. Data remained anomalous
145	May 25	All DACU-2 data became normal
166	June 15	DACU-2 data anomalies reappeared
176	June 25	DACU-2 data recovered for about 2 hours then failed again
193	July 12	DACU-2 data became normal
207	July 26	DACU-2 data anomaly reappeared

Data Review

History tape data was reviewed for minor frame words 5, 24, 41 to 58, 63, 76, 78, 80 (analog); 26 to 30, 33 (digital); and subcom words 113, 114 (all analog, except 114 words 9 and 10, which were digital). Periods covered by the data were selected intervals on May 9 and 10, May 24, June 25, and July 12. Primary objectives of the data review were to identify any similarity with the DACU-1 anomaly and to characterize the anomaly and transition periods. Table 9-10 presents anomaly trends observed in the data.

Figure 9-3 portrays analog words 49, 54, 57, 58 major frame error frequency as a function of time during a typical transition from good to bad data on May 9, 1979. The data covered a 1-hour, 42-minute interval or about 130 major frames. General correlation is evident; however, no specific pattern was found that governed either the degradation or recovery sequences. This feature is in contrast to the earlier DACU-1 anomaly that exhibited strong error pattern characteristics. Primary findings drawn from the data reviewed were as follows:

1. Telemetered values of affected channels became lower than normal or 000_g .
2. Both analog and digital channels were affected.
3. Both main and subcom locations were affected.
4. Review of data covering 30 main and 2×16 subcom words showed that 1 analog and 2 digital words were never affected (word 63 and subcom 114, words 9 and 10). When the anomaly was most pervasive, all other data became 000_g .
5. In transitions from valid to anomalous data, analogs failed first, then digitals. When recovery was gradual, digitals recovered first, then analogs. Some transitions were abrupt.
6. Duration of anomaly and normal periods varied considerably.
7. No specific failure or recovery sequence was evident in the review data, although the higher numbered word locations generally failed first, recovered last.
8. Word 5 (analog-to-digital converter midscale calibration) nonzero anomalous data sometimes correlated with other analog channel anomalies in the same minor frame; i.e., scale factor adjustment based on word 5 sometimes "corrected" other analog data. Usually, they were uncorrelated. Since the sampling rate for a given minor frame word was 1 per 2.95 seconds, the anomaly condition was found to change in 1-word time or less.

Assessment

DACU-2 data anomalies were not produced by the same defect that caused earlier DACU-1 anomalies. The observed DACU-2 anomalies were due to an intermittent failure affecting both analog and digital MOSFET multiplexers in a manner that effectively opened some of the signal paths to the analog-to-digital converter and digital comparator. The analog-to-digital converter, digital comparator, data formatter, and timing functions were not implicated. Intermittent gate-drive level or duration produced the observed effects. High MOSFET switch resistance during a data sampling interval, or a shortened gate pulse lowered digitized analog values and effectively raised the digital comparator

Table 9-10
DACU-2 Anomaly Trends in Review Data

Date	Hr:	Min:	Sec:	Comments
May 9, 1979	22:	44:	00	Words 41, 43, 48, 54 started showing intermittent zeros. Word 5 (midscale calibration) data showed intermittent low values, 377 octal predominant.
	23:	03:	22	Anomaly progressed, causing all-zero data in all analog channels reviewed except word 63 (words 5, 24, 41 to 58, 76, 78, 80, 113 and 114/0 to 8 and 11 to 15). All digital channels (words 26 to 30, 33, 114/9 and 10) normal.
	23:	04:	51	All analog channels suddenly recovered.
	23:	05:	38	Word 5 became zero; some analog channels and all digital normal.
	23:	16:	38	Word 5 zero; all analog except word 63 became zero; digital normal.
May 10, 1979	23:	21:	57	Word 5 intermittent low; other analogs recovered intermittently; digital normal.
	00:	56:	13	Word 5 became zero or intermittently low; other analogs intermittently zero. Digital remained normal.
May 24, 1979	01:	05:	48	Word 5 recovered to intermittent low values; other analogs recovered to normal. Digital remain normal.
	14:	55:	26	All channel data normal.
	15:	20:	48	All analog and digital channels suddenly zero except analog word 63 and digital 114/9 and 10.
	15:	25:	07	Digital channels began intermittent recovery; analogs remained zero except word 63.
	15:	25:	49	Digital channels fully recovered; analogs still zero except for word 63.
June 25, 1979	16:	06:	33	Intermittent analog recovery began; all digital normal.
	16:	26:	40	All analogs failed to zero except word 63; all digital normal.
	06:	55:	08	All analog except word 63 and all digital except word 114/9 and 10 read zero.
	07:	37:	57	Suddenly all channels became normal.

Table 9-10
DACU-2 Anomaly Trends in Review Data (continued)

Date	Hr:	Min:	Sec:	Comments
June 25, 1979 (cont)	09:	38:	34	Word 5 dropped to 377 octal; all analog channels except word 63 intermittent. Digital normal.
	09:	51:	18	Word 5 became normal; all analog and digital were normal.
	10:	15:	50	Word 5 dropped to 377 octal; all analogs intermittent. Digital normal.
	10:	18:	41	Word 5 became zero with all analogs except word 63. Digital remained normal.
	10:	19:	04	All words were zero, except analog 63 and digital 114/9 and 10.
July 12, 1979	05:	25:	35	All words zero, except analog 63 and digital 114/9 and 10.
	05:	40:	35	All words suddenly became normal.
	10:	00:	12	All words remained normal.

threshold; the digital circuits were generally more tolerant of such defects up to the 1/0 logic threshold. Since the analog and digital multiplexers were on different circuit boards, using individual mother-board connectors, the fault was likely to be on the multiplex address decode and gate drivers board that generated gate-drive signals for both. Gate-drive circuits used a multiplicity of 2N2484 and 2N2907A discrete transistors; due to the number of channels affected and the absence of any specific pattern, these active devices were not suspect. However, noise on the +5, +2.4, or -20 Vdc power buses on the board, or intermittents in the multilayer (MIB) printed circuit board itself could have produced the anomalies. Since some data channels were unaffected throughout the failure periods, an intermittent defect in MIB 2854072 was the suspect fault.

Affect of Anomalies

During DACU anomaly periods, the alternate unit always provided accurate telemetry data for operating support. Restrictions on DACU-1 operating mode and on-time (see paragraph titled DACU-1 Anomaly) did, however, increase operations tasks following the onset of DACU-2 anomalies in May 1979 (see paragraph titled DACU-2 Anomaly).

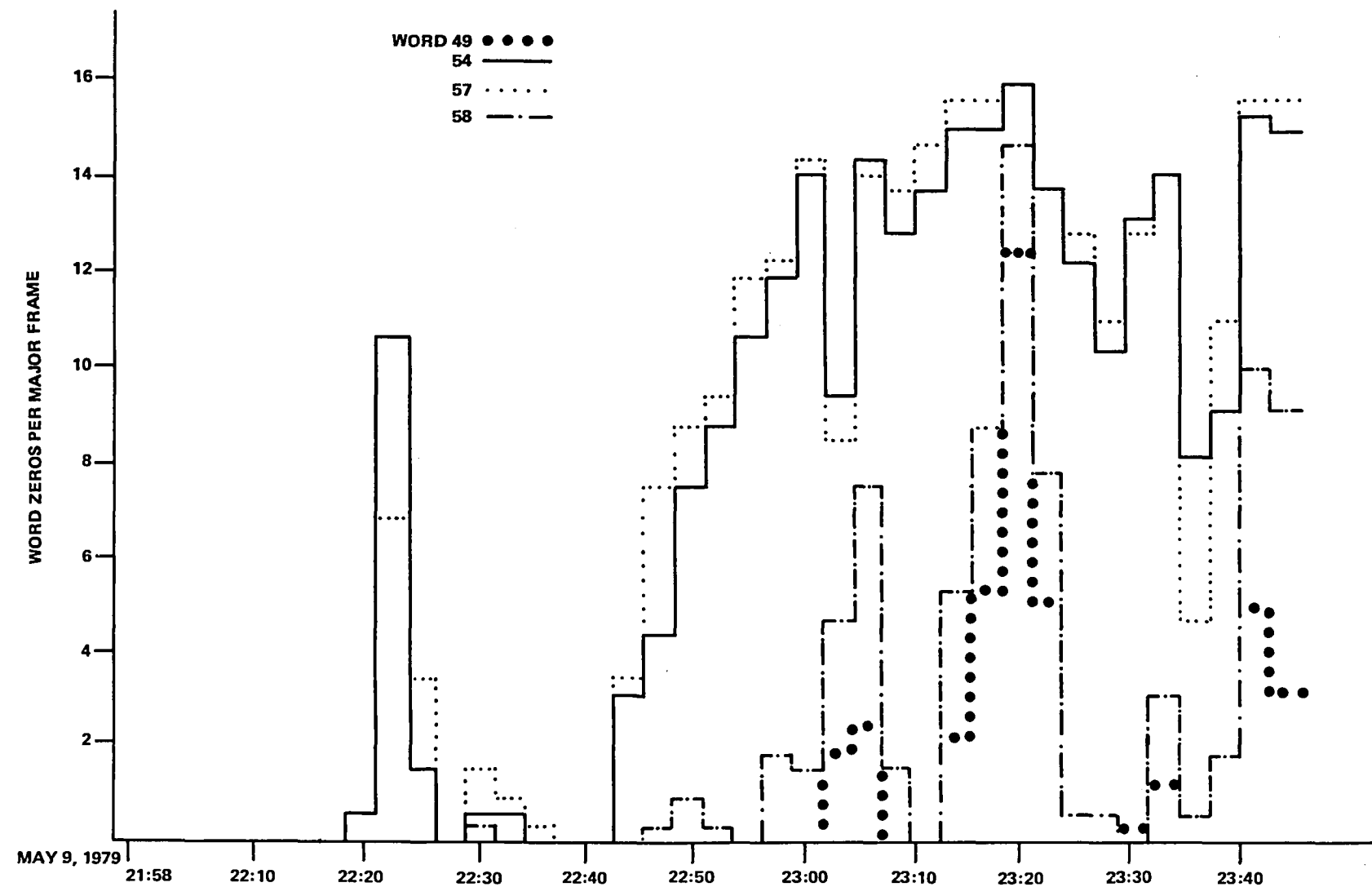


Figure 9-3. DACU-2 Typical Telemetry Anomaly Frequency

IN-ORBIT OPERATIONS

In addition to providing housekeeping command and control functions, the telemetry and command subsystem also successfully supported several experiment and special test operations including:

- *Remote Command Checkout*—A special test was conducted on April 17, 1975, to determine the feasibility of commanding ATS-6 by relaying both commands and telemetry through another spacecraft (ATS-3). During this test, commands and telemetry were successfully relayed between ATSOCC and ATS-6 through the Rosman/ATS-3/Mojave/ATS-6 link depicted in Figure 9-4. Results of the test indicated that ATS-6 could be controlled by remote satellite and ground station links, if required, during emergency situations.
- *Special Data Link Operations*—During drift phase and the Satellite Instructional Television Experiment (SITE) operations, the special data link was used periodically (once per week) to provide voice communications between supporting ground stations via ATS-6. During these periods, the special data link provided reliable communications with no reported anomalies. Figure 9-5 depicts the spacecraft equipment configuration used to support special data link operations.

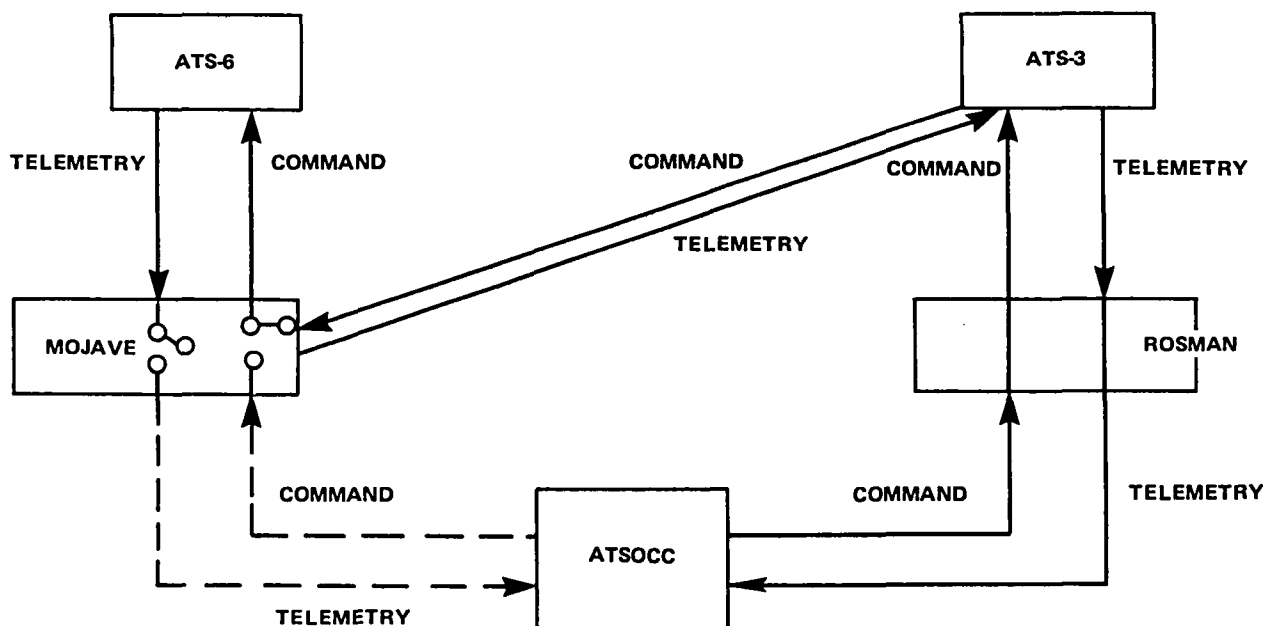


Figure 9-4. Remote Command Test Configuration

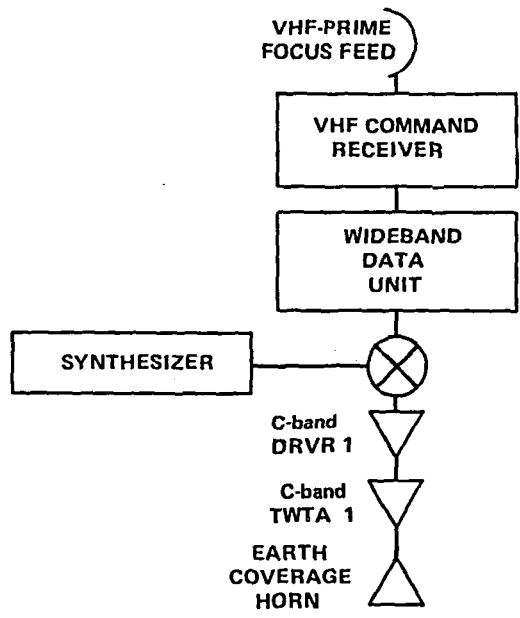


Figure 9-5. Special Data Link Configuration

CHAPTER 10

TELEMETRY AND COMMAND GROUND SUPPORT

INTRODUCTION

As a geosynchronous spacecraft, ATS-6 was in view of a dedicated ground station: Rosman Ground Station for the western hemisphere subsatellite locations, or the Hybrid Ground Station at Madrid, Spain, for the eastern hemisphere operations. No onboard command memory or telemetry tape recorders were used. Operations were planned to be controlled from the ATS Operations Control Center (ATSOCC) based on real-time command verification by telemetry. Processing the telemetry and generating the commands required the full-time use of one of three PDP-11/20 computers. This computer and its associated peripherals comprised the primary system.

The primary operating system was loaded on a PDP-11/20 with a 30 K, 16-bit/word core supplemented by two 256 K disc storage devices, a line printer, digital and analog tape recorders, a Dec-writer,* and cathode-ray-tube (CRT) displays and keyboards. The second PDP-11/20, or the backup system, was also loaded with the ATS-6 operating system and could be brought rapidly on-line if there was a failure in the primary system. When operating some experiments, the backup system was required to generate real-time displays and/or drive a line printer. The third PDP-11/20, or the off-line machine, was used for developing software and processing recorded data. Any one of the three PDP-11 computers could be prime, backup, or off-line. Operators in ATSOCC determined the function of the computers by switching input and outputs.

The Rosman Ground Station also had a PDP-11 system devoted to full-time ATS-6 support. Because of hardware and software limitations, this system had less capability than ATSOCC, but it was more than adequate to process and display telemetry data and generate commands to safely maintain the spacecraft if ATSOCC lost control.

An additional system (including associated rf transmitting and receiving equipment) was installed in trailers. This equipment was validated during the early postlaunch period while located at the Mojave Ground Station in California and then relocated to Madrid as the primary station for operations during the second year when ATS-6 was above 35° East longitude.

SOFTWARE CAPABILITIES

ATS-6 produced a tremendous volume of telemetry data and selected experimental data in real time. The computer software was developed with suitable peripheral equipment to display the real-time status of spacecraft subsystems and experiments in order to make rapid evaluations of abnormal or undesirable situations and to take timely corrective action. The following paragraphs describe the more important software capabilities.

*Trade name for the console typewriter

Three of the seven CRT's had a graphic display capability. The desired display could be either frozen into the data base or created as needed. Up to four sets of parameters could be plotted at the same time in either X-Y or polar coordinates.

Raw telemetry data were converted into calibrated engineering units for further processing and direct display. Most analog parameters were checked for upper or lower limit violations. If a parameter exceeded its limits, it was displayed on one of the five assigned lines of all CRT's. Critical out-of-limit parameters also sounded an audible alarm to alert the operations team.

The computer compared the present commanded spacecraft configuration to the actual configuration that was derived from telemetry during each telemetry frame. Any violations were displayed the same way as analog limit violations. Critical configuration errors sounded an alarm.

The attitude of the three-axis orientated ATS-6 was computed in real time using telemetry data from selected onboard sensors and ephemeris data stored on the PDP-11 disc. The attitude information was displayed, so that the operations team could verify correct pointing and the experimenters could have accurate attitude information to evaluate their experiment.

Seven CRT assemblies presented real-time data to the operations controllers. Each CRT was capable of displaying 4,240 characters or approximately 70 telemetry points divided into two half pages. Any half page contained in the data base could be assigned to any CRT. In addition, wild card half pages could be created by keyboard or card reader input. Five CRT's and their associated keyboard controls were located at the consoles of the subsystem controllers. One of the remaining assemblies generated the data that were normally displayed on the TV projector screen. This display included pertinent telemetry and computer-generated parameters grouped by subsystem and allowed the controllers to monitor the overall spacecraft status on one display. The other remaining assembly was located in the equipment room and, together with two control room CRT's, generated special graphic displays for conducting certain experiments and spacecraft maneuvers. These graphic displays allowed a subsystem engineer to visually check his subsystems configuration and performance.

Four stripchart recorders were located in the control room. Each contained eight analog pens. Two also included eight bilevel (event) pens. During normal operations, two recorders were devoted to the attitude control subsystem (ACS), one to the spacecraft propulsion subsystem (SPS), and one to the power subsystem. Pen channel assignments were changed by console keyboard intervention.

There were a total of seven console positions for ATS-6 in ATSOCC: project operations controller (POC), ground controller, systems engineer, experiment engineer, power/thermal, communications/telemetry and command, and ACS/SPS. During normal operations, only four consoles, the POC, ground controller, ACS/SPS, and systems engineer were manned on a 24-hour per day, 7 days a week basis. The systems engineer was primarily responsible for the communications and experiment operations and configuration, but also monitored the power and thermal subsystems. Each console position was equipped with a voice communication system consisting of two handsets, a pushbutton circuit selection (e.g., CCL, SCAMA, FTS), and commercial telephone lines.

In addition to the CRT displays previously discussed, there were five other CRT monitors installed in the consoles. Each monitor had a video pushbutton arrangement that allowed any one of the seven active CRT pages to be selected and displayed. The TV wall projector display was also pushbutton selected from the command controller's console. There were also remote video monitors: two in the systems engineer's office, one in the data reduction and analysis office, and one in the project office. All of these monitors could display any of the seven available pages. The flexibility provided by the CRT's and the monitors made it possible for each console position to examine his subsystem in detail or concurrently with any other subsystem.

The CRT console keyboards served as the primary man/machine interface. Each of the three PDP-11/20 computers had a Decwriter terminal. The five CRT keyboards had access to the computer to perform all of the programmed functions, including commanding the spacecraft. In practice, however, only the ground controller, under the supervision of the POC, commanded the spacecraft.

There were three standard methods of commanding. Individual commands were typed by the ground controller, displayed on the CRT by its English language descriptor, verified by the POC, and then executed by keyboard input. Group commands contained in the data base were executed in a similar manner. The desired group number was called up by the keyboard, and the first command in the group was displayed and verified. The commands in that group were then executed sequentially. Finally, commands could be issued through the automated sequential processor (ASP) tape. The ASP tape was a digital tape containing computer instructions, English language statements for CRT display of ASP operations being performed, and a series of commands to configure the spacecraft for experiments and operations. The ASP was accessible through the ground controller keyboard. The ASP was updated as needed to reflect changes, additions, and/or deletions of experiment and spacecraft configuration requirements. The ASP provided flexibility to real-time operations, because of its capability to be modified, in real time, from the keyboard. ASP also provided operations personnel with the capability of having a number of contingency plans immediately available for use.

During the assembly and test of the spacecraft, two PDP-11 computer systems (with a limited number of CRT terminals) were installed in the assembly bay at the spacecraft contractor (Fairchild Industries). The telemetry and command subsystem was hardwired to the computers and most of the spacecraft test sequences (described in Volume I) were commanded and verified using the operating software designed for the control center (ATSOCC).

Two other PDP-11 systems were installed in ATSOCC during the tests, and data lines between GSFC and Fairchild Industries were used to verify these computer/software systems.

The two Fairchild computer systems were shipped to the launch site with the spacecraft where commanding and telemetry were conducted over cables at the rf frequencies. One of these computers became the third ATSOCC system after launch.

The ATS-6 Dynamic Simulator (ATSSIM) was a fully dynamic simulator developed by GSFC as a tool for personnel training and ground system checkout. ATSSIM was developed using a 3-axis

dynamic simulation developed by the ATS-6 attitude control system (ACS) subcontractor (Honeywell). GSFC added models to the ACS system of all other relevant subsystems and dynamics to make ATSSIM a fully interactive simulator that would, in most cases, fully represent the spacecraft and its environment.

Once the simulator was developed, it was necessary to make certain that it was fully representative of the spacecraft to complete the checkout and training. The following items were to be accomplished:

- Train personnel to familiarize them with the spacecraft's dynamic responses and discrete responses to excitation (commands, disturbances, etc.).
- Train personnel to familiarize them with the nominal mission plan.
- Verify the flight worthiness of the mission plan with respect to spacecraft response and human factors.
- Train personnel in contingency operations. This includes preplanned (canned) and real-time contingencies.
- Verify effectivity of preplanned contingencies, especially with respect to human factors.
- Establish effective communication between all ATSOCC, IPD, and ground station personnel.
- Establish a time-oriented discipline, so that a lackadaisical attitude would not prevail.
- Train personnel in specialized techniques (e.g., gyro drift calibration, DOC input data block load, etc.).
- Establish the flight worthiness of ATSOCC hardware and software.
- Verify that specialized displays (e.g., CRT half pages, stripcharts, etc.) are adequate for failure detection and solution and are usable in human terms.

Once the total simulator was validated, the ATSOCC hardware and software were validated. Included in this validation was hands-on training of the operation personnel who would be controlling the spacecraft after launch.

After ATSOCC was validated, a program for training was executed. This program was divided into segments based on the launch schedule.

The types of simulations that were conducted included:

- Executing the operations plan for training and for verifying the validity of the plan.

- Switching between ACS modes (prime, alternates, and non-tested modes) using different ACS hardware.
- Executing a “wheel” acquisition sequence and a checkout of all contingency techniques.
- Training in canned and adlib contingency operations by faulting of the simulation.

The first portion of the simulation exercises consisted of a 2-week period where operations personnel were familiarized with ATSOCC hardware and software. During this time, a formalization of ATSOCC procedures for operations personnel was developed. This included all verbal communication between operations personnel and the necessary documentation and procedures that were required during all operations. The next week was devoted to operations with both ATSOCC, the necessary group stations, and IPD to establish a working relationship between personnel and to check the interfaces. During this period, the ground stations were asked to configure to do certain experiments and to play their role in certain key mission plan exercises.

The next 2-week period consisted of switching between predefined modes of operation in a definite order. This was done to demonstrate to operations personnel what the system would do dynamically and statically during the changing of modes and to check out command sequences for their validity. Nontested or unreliable modes were simulated, so that operations personnel would be familiar with the response of these modes. Also during this period, the use of normal ground-control commanding to operate the spacecraft was exercised.

The next 2-week period was devoted to operating the mission plan. The simulation of the plan was divided into segments that applied to the key aspects of the plan and eliminated large blocks of unused time. This familiarized operations personnel with the plan and the contingencies to the plan, and checked its validity. During this period, SAPPAC operation and operations of the yaw gyro were simulated. Training of personnel in both these areas was very important.

The next 2 weeks were devoted to the normal mission plan to train operations personnel in performing the normal operations plan. This included all predefined segments of the simulations.

The final 3 weeks were devoted to full simulations of the operations plan using predefined key segments. Faults were introduced into the simulation to train operations personnel to make real-time decisions and to solve problems from an operational standpoint. The in-depth team participated in isolating and solving the problems, where possible.

Except for the first 2 weeks of the simulations, where two teams were used, a four-team concept was implemented for all simulations. During the final 2 weeks of simulations a 16-hour schedule was followed.

The use of the simulator helped achieve a well run launch period, initial spacecraft checkout, and normal operations. This training period helped to make all elements of the operations run smoothly with no operational problems due to ATSOCC, remote ground stations, or personnel being unprepared to handle all situations.

HARDWARE AND SOFTWARE

The use of hardware and software underwent an evolutionary process within the control center as operational philosophies dictated a shift toward greater versatility in securing data for spacecraft subsystem evaluation. The ATS Operations Control Center (ATSOCC), which was designed in the early 1970's, did not employ fixed displays in its initial design but used a rear projection system display positioned at the front of the mission operations room to present a summary of the spacecraft subsystem configurations. The subsystem consoles in ATSOCC were assigned cathode-ray tube (CRT) displays with pushbutton controls for reassignment of pages at the individual stations. Additionally, there was a menu of 100 selectable pages of information that could be called up by keyboard command. The majority of these pages were contained in the ATS system data base, but a number of pages (designated "wild-card" pages) were reserved to be built in real time by operations and experiment personnel. This method ensured the availability of significant operations data without constantly reediting the data base system. The capability of making real-time changes to the on-line ground flight system added to the ease of operations and made the need for a complete system update less frequent. Modifications of the ground flight system were accomplished after a periodic review of the real-time changes was made. If any other changes or updates were requested, modifications were made to provide smoother operations.

INTEGRATION AND TEST SUPPORT TO OPERATIONS

The Fairchild integration and test data base was transferred to ATSOCC with changes made to adapt its use in operations. Certain parameters had to be changed, a number of CRT pages were modified, and additional ones added to suit operational needs. By doing this, a large part of the system did not have to be recreated, and a saving of both cost and time was realized.

PERSONNEL

ATS-6, as with any new satellite, had a large number of operational console positions manned. As time went on and the learning curve progressed, console duties were reviewed and in some instances merged, thus reducing the number of operational personnel in the control room.

OPERATIONS PLANS AND PROCEDURES

The ATS-6 Flight Operations Plan was prepared by Fairchild Industries for submittal to Goddard Space Flight Center (GSFC). The purpose of the document was to establish an overall ATS-6 mission operations plan and provide detailed information for operating the spacecraft in orbit. This document was used by operations personnel in generating detailed procedures for establishing the various operational modes for each subsystem and a detailed sequence of events for initial spacecraft operations and in-orbit spacecraft evaluation.

The subsystem modes were designed so that mission planning personnel could readily generate flight procedures. Prior to the implementation of the flight procedure, a review was performed by the Flight Operation Working Group composed of representatives of the various companies involved with ATS. The procedure was then checked out operationally using the ATS simulator. Another review was performed by the Flight Operation Working Group and the procedure was released for use.

Spacecraft contingency plans were provided by GSFC (through a contractor) that contained logic diagrams, alternate modes, and other information helpful in determining a course of action in the event of a spacecraft anomaly or an unexpected occurrence during the flight. The implementation procedure for contingency plans followed that used for the operations plan. Later in the mission the contingency plans were derived by the off-line engineers in conjunction with the real-time operations personnel. The review procedure prior to implementation remained the same.

REAL-TIME RECOVERIES

The techniques for real-time recoveries for all foreseeable failures were planned before launch. This was possible because the ATS-6 design contained sufficient modes, redundant attitude and rate sensors, and onboard units to permit a wide range of recovery options regardless of a wide variety of operational or hardware anomalies. For example, whenever the spacecraft was in satellite-track-monopulse mode, recovery from a loss of the monopulse signal could be effected by switching to Earth sensor control or to interferometer control without much, if any, satellite pointing transients. In addition, the yaw-inertial-reference-unit-control mode and the digital-sun-sensor-yaw-backup modes were alternate methods of controlling yaw if the Polaris star tracker failed.

Because of the wide variety of alternate control modes, operations personnel had to be aware of the procedures for changing control modes rapidly. Many of these procedures were incorporated into the automated sequential processor (ASP) tape for quick reference and ease of commanding. Correct sequences of commands for switching spacecraft units or modes could then be planned in advance and incorporated in the ASP tape with remarks and comments on limitations, restrictions, etc., for quick reference by on-shift operations personnel.

The ASP tape was an invaluable tool for operations. Any sequence of commands could be included for ease of commanding. The commands for all possible communications configurations for experiments and normal day-to-day operations, and the command sequences for contingencies were included. A similar method of commanding may be useful in the operation of future spacecraft.

CHECKOUT OF REMOTE SITES

The remote sites used for ATS operations included the Rosman Ground Station, the Mojave Ground Station, and the Hybrid Terminal at Madrid. These remote sites had the capability to run the majority of satellite operations independent of ATSOCC.

Since this capability existed, operations personnel felt that the site should be checked out and the personnel trained in particular operations that were critical to the overall ATS-6 mission. This backup to ATSOCC was particularly necessary during communications outages, emergencies at GSFC, and problems with the real-time computers. The following paragraphs describe the extent of operations at the various remote ATS ground stations.

Rosman Ground Station

During the first year of operation, the Rosman Ground Station was the prime ground station for operations. The equipment at Rosman included PDP-11 computers with most operational software available for use.

The first step in the validation of the Rosman site was a thorough checkout of the software. This included checkout using the telemetry and command simulator located at Rosman and the ATS simulator (ATSSIM) located at GSFC. In general, there were few problems. Once the software was validated, classroom sessions were held with Rosman shift personnel to discuss the operation of the computer system and a brief overview of the spacecraft subsystem operations. After these sessions, hands-on operations with the computer were accomplished using ATSSIM as the training tool. This hands-on operation experience included working with ATSOCC, where the assumption was that a problem existed that precluded normal operations at ATSOCC.

After the hands-on portion of the training, classroom sessions were held again where the emphasis was on the key operations that could be run with the stations. When the classroom sessions were completed, hands-on training was held under simulated emergency situations with the ATSSIM as the primary training tool.

This type of remote ground station training with Rosman was very beneficial to the project from two standpoints. First, it gave the ground station personnel a valuable understanding of the spacecraft operations and a working knowledge of the ground system. This became invaluable during emergency operations when Rosman handled all of them flawlessly. Second, it established communications between Rosman and ATSOCC that made the normal operations between the two much more efficient.

Mojave Ground Station

During the initial mission, the Mojave Ground Station acted primarily as the backup to Rosman. As in the case of Rosman, software checkout was accomplished and classroom sessions were held covering ATS operations and subsystem familiarity. Hands-on training was accomplished using ATSSIM with coordination from ATSOCC. The purposes of these exercises was to familiarize personnel with the operational ground system and to set up a communications protocol with ATSOCC.

Hybrid Terminal, Madrid, Spain

The Hybrid Terminal at Madrid was the primary remote site during the move to India, for the Apollo-Soyuz Test Program (ASTP) and for SITE Indian operations. As with the other ground stations, a full checkout of the hardware and software was accomplished. Since there was not a large staff of software personnel at the station, many of the problems were solved by discussion with ATSOCC software personnel and the solutions voiced or sent tape-to-tape to Hybrid Terminal.

Once the system was validated, classroom sessions were held again to familiarize the personnel with the ground system and the spacecraft. Hands-on training was again accomplished, stressing activities that the Hybrid Terminal would perform in emergency situations and to set up communications protocol with ATSOCC.

The next step in the training was extensive classroom and hands-on experience in the ASTP procedures. This included extensive simulations using ATSSIM and overall coordination with ATSOCC for the ASTP period.

As with Rosman and Mojave, situations occurred during normal and special operations when dependency on the Hybrid Terminal was essential. The Hybrid Terminal was able to handle all situations with no major support problems.

SUMMARY AND CONCLUSIONS

Training at the different remote sites was an important factor in the overall success of ATS-6. Having a well trained team and a validated and dependable ground system at the remote sites gave the project an immense amount of flexibility in handling all normal and contingency operations with a minimum of interruption in service to the experimenters.

Control Center Operations

Spacecraft operations were performed at ATSOCC by contractor personnel from OAO Corporation, Westinghouse Electric Corporation, and RCA Service Company on a 24-hour per day, 7 days a week basis. OAO Corporation had seven engineers assigned to ATS. Four of these engineers were the project operations controllers (POC's), who worked on rotating 12-hour shifts. The two remaining console engineering positions, ACS analyst and systems analyst, were filled by RCA personnel composed of four 2-man teams working 8-hour rotating shifts. RCA also had a systems engineering supervisor and two staff engineering positions that were manned on a normal 40-hour work week.

Operations and Maintenance

Operations and Maintenance (O&M) was initially performed by 31 RCA personnel, including a manager and a secretary. O&M shifts consisted of four 6-person teams working the same schedule as the RCA console analysts. Each team consisted of a shift supervisor, an ATS-6 command controller, an ATS-1, ATS-3, and ATS-5 spacecraft controller, a data operations controller, a computer technician, and a teletype operator. The positions of the ATS-6 command controller and the ATS-1, ATS-3, and ATS-5 spacecraft controller were soon combined. As personnel were trained to operate both positions, the teams were reduced by one person. Data operations controller and computer technician positions were also combined in a similar manner. The rest of O&M personnel worked normal day shift hours. These positions included the maintenance engineer, the PCM technician, the ATS-1, ATS-3, and ATS-5 system analyst, the data control supervisor, and a data clerk.

Experimenter Role in ATSOCC

ATS-6 was a complex, multipurpose spacecraft whose principal objectives were to demonstrate a large, unfurlable antenna structure and precise pointing and attitude control in synchronous orbit. The spacecraft carried 27 experiments involving communications, science, and technology. Because ATS-6 was a real-time spacecraft, the experiments, primarily the communications experiments, operated in real time as well. To coordinate planning, scheduling, and operation of these many experiments, Westinghouse Electric Corporation had a staff of seven engineers assigned to the project to support the experimenters/users who were scattered throughout the world. These engineers were responsible for coordinating the spacecraft configuration, spacecraft pointing, and Rosman support requirements with the users, and for providing a timeline of operations procedures. They were present at ATSOCC to communicate with the remote users on an individual basis during the performance of the operation for which they were responsible.

Scheduling

Operations personnel at ATSOCC coordinated all experimenter requirements and scheduled the spacecraft operations and the activities of the participating ground stations. This function was performed by a mission planner and two schedulers employed by RCA. This group, along with the Westinghouse experiment coordinators, planned and scheduled ATS-1, ATS-3, ATS-5, and ATS-6 operations on a weekly basis. All participating parties received a copy of the weekly schedule in the form of a teletype message. The weekly schedule was supplemented, usually 2 days in advance, by a daily schedule. The daily schedule was also relayed to all participants by teletype message. Once it had been transmitted, any changes in the daily schedule were immediately relayed by teletype.

Anomaly Investigation

Operations personnel conducted or participated in anomaly investigations, analysis, development of operational "workaround" procedures, and assisted in the planning and development of spacecraft operational contingency plans in cooperation with NASA personnel, other contractors, and experimenters.

These activities generally included the following sequence of activities for each anomaly or investigation:

- a. Observation of anomalous spacecraft conditions and/or changes in spacecraft trend behavior in real time by operations personnel.
- b. Real-time implementation of contingency plans and/or switching to redundant units and/or alternate units and procedures.
- c. Reports from operations personnel to the mission operations manager, operations analysts, the NASA and contractor subsystem experts and consultants.

- d. Collection of data in real time and offline. Offline data collection included 16-column printouts of selected spacecraft parameters from a history tape playback, hardcopies of CRT pages displayed from the history tape and/or stripchart printouts in addition to real-time data collection.
- e. Analysis of the anomaly or trend change in conjunction with the NASA personnel and other contractors.
- f. Development of workaround procedures if required.
- g. Testing of workaround procedures.
- h. Implementation of workaround procedures and/or special real-time monitoring procedures.

Anomaly workaround in many cases involved development of new onboard software for the digital operational controller. Several examples of these changes are found in Volume II of this report.

CHAPTER 11

CONCLUSIONS AND RECOMMENDATIONS

DESIGN CONSIDERATIONS

From the perspective of 5 years of successful operation, the ATS-6 telemetry and command subsystem and component designs proved highly satisfactory. All performance requirements were met with ample margins. All units operated without failure, except for the DACU-1 and DACU-2 anomalies, neither of which involved total component failure. Designed to meet a 2-year mission lifetime, it would seem ATS-6 experience indicated the hardware and signal path redundancy (employed to assure life objectives) were unnecessary. Yet, the data acquisition and command unit (DACU) exception proved the rule. Rf and command equipment redundancy in particular became an operations asset, allowing change of uplink frequency and decoder address without setup commands when interference to terrestrial services occurred at the primary frequency, as did the C-band downlink connection for the special data link operations. The necessity for active redundancy in the vhf command equipment (antennas and receivers) was not verified beyond the fact that the commanding function remained 100 percent reliable throughout the mission. In the same vein, dedicated regulators for each command receiver and prime power connections from either essential loads bus or either battery bus to all command equipment served to enhance the reliability. As a more obvious example, signal path redundancy designed into the data switching unit permitted reception of spacecraft telemetry over active redundant downlinks using frequency division multiplex on one vhf frequency via the prime-focus feed and direct modulation on the alternate frequency via an omnidirectional antenna. This flexibility was especially useful when both DACU's were operating. Design innovation in the array command distribution to reduce harness complexity and weight while assuring high interface reliability and noise immunity doubtless contributed to command reliability as well.

In general, the design approaches followed in component and system designs proved highly satisfactory.

Several design oversights did occur during telemetry and command subsystem development that were identified and corrected during the spacecraft test program. The most notable was unexpected electromagnetic interference that desensitized the command receivers because of intermodulation of a telemetry transmitter with a Radio Beacon Experiment carrier. Early in the program, the compatibility of proposed frequency assignments was analyzed by a subcontractor who concluded that telemetry and command subsystem interference potentials were negligible. When significant interference was observed, a second analysis was performed that accurately predicted the observed results. It was found that the earlier analysis had not uncovered this electromagnetic interference potential, because it assumed fifth order intermodulation products to be insignificant. This experience proved the importance of thorough review of limits and conditions used in analytical procedures. The design modifications necessary to alleviate this problem turned out to be straight-forward

(cable shielding). However, if frequency changes had been required, the resulting impact on hardware, program cost, and schedules would have been severe.

A design oversight occurred in not specifying telemetry transmitter modulation sensitivity to power-line conducted noise. A grounded power-return configuration had previously been used in space, whereas ATS-6 used an isolated power return to be grounded to the structure only in the communications module. Since all transmitter component level tests were performed with a grounded return, power-line susceptibility was not suspected until actually observed at the spacecraft level. A short ground strap between the power connector and structure solved the problem. However, if serious ground-loop problems had occurred, program impact would have been significant.

It is concluded and recommended that the level of functional and signal path redundancy used in the ATS-6 telemetry and command subsystem be used in future communications spacecraft having comparable operations and mission requirements. Since technological advancements in active circuit integration, devices, materials, and processing make future use of those used on ATS-6 unlikely, recommendations in these areas are largely unnecessary. Nonetheless, the importance of comprehensive and vigorous quality assurance, reliability, and test programs remain essential ingredients of mission success. Thorough, in-depth review of specifications and analytical procedures is mandatory. Close technical collaboration between NASA and industry avoided many technical, cost, and schedule problems during the ATS-6 program and should continue in future programs.

PERFORMANCE CONSIDERATIONS

As mentioned, the telemetry and command subsystem performance was excellent. Stability of major operating parameters maintained system operation within specification limits throughout the mission. Operating margins were sufficient to allow reasonable latitude in supporting ground station performance. These attributes were recognized as a direct result of thorough systems engineering accomplished prior to the Phase D hardware program in conjunction with definitive procurement and test specifications generated to control hardware performance and test requirements. The success of this approach to the ATS-6 protoflight program is evident and recommended.

OPERATIONS CONSIDERATIONS

Mission operations clearly benefited from the reliability and flexibility engineered into the telemetry and command subsystem. This result is mainly attributable to early and continuous infusion of operational considerations throughout the Phase D program. Support personnel and the equipment and software packages proven during the spacecraft level tests proved a genuine operations asset from launch through all mission phases. This approach to providing a seasoned man-machine team ready for launch and mission operations is highly recommended.

GENERAL CONSIDERATIONS

Close collaboration between NASA, Fairchild, and its subcontractors was largely to be credited with the successful development and flight performance of the ATS-6. Risks associated with a protoflight program were circumvented by a program management and technical team that cultivated and

exploited a free flow of information to maintain high visibility of program activities on a day-to-day basis. Early emphasis on the generation of detailed subsystem, interface, and test specifications resulted in establishment of comprehensive and well-defined requirements before major subcontract awards. Use of proven components helped reduce cost and risk. Insistence on design verification tests early in Phase D helped to resolve open technical matters and strengthen confidence in flight hardware fabrication and test schedules. Calculated risks in component development, such as the command decoder distributor command driver hybrid IC from Collins, were backed up by alternate, qualified sources. Vigorous reliability, parts, and materials programs contributed significantly throughout to the correction of related problems and the ultimately high reliability achieved by ATS-6.

Thorough testing at component level and computer-aided spacecraft level tests revealed piece-part, component, and system faults, some of which might have been missed if less detailed procedures had been followed.

It is recommended that the foregoing ATS-6 program attributes be followed in future programs.

Part D
Data Relay Experiments

CHAPTER 12

TRACKING AND DATA RELAY EXPERIMENT

EXPERIMENT OBJECTIVES

Scientific

The scientific objectives of the Tracking and Data Relay Experiment (T&DRE) were to:

- Improve mathematical models used in orbit determination programs
- Evaluate the effects of the Earth's gravitational anomalies
- Evaluate the effects of multipath on the relay communication link and on precise orbit computation
- Determine the effects of the Earth's atmosphere on satellite tracking and data relay.

Technological

The technological objectives of the Tracking and Data Relay Experiment were to investigate and demonstrate the technical and operational feasibility of the following:

- Multiple-arc and long-arc range and range-rate tracking of Earth-orbiting satellites from a ground station by way of an Earth-synchronous satellite
- Commanding of Earth-orbiting satellites from a ground station by way of an Earth-synchronous satellite
- Relaying of scientific and housekeeping data from Earth-orbiting satellites to a ground station by way of an Earth-synchronous satellite
- Evaluate the communication return link from an Earth-orbiting satellite to a ground station by way of an Earth-synchronous satellite using a variable rate digital test code.

EXPERIMENT DESCRIPTION

Tracking Experiment

There were three modes by which ATS-6 could track a near-Earth satellite. The prime technique was the program track mode that had been incorporated as an essential program in the onboard

digital operational controller (DOC). This mode required onboard knowledge of the tracked satellite's orbit ephemeris that had been coded and transmitted to ATS-6 for insertion into the onboard computer (DOC). ATS-6 would then compute the required offset angles in real time to control the pointing of the appropriate S-band beam towards the near-Earth satellite while using onboard attitude sensors as a reference.

The second tracking technique was monopulse control. ATS-6 would use its attitude control system to actively null on the S-band signal from the tracked satellite by comparing the signal from the S-band monopulse on-axis sum feed with the S-band difference feeds. ATS-6 used its offset N1-S1 and E1-W1 S-band feeds to provide the difference signals for the monopulse roll and pitch error signals respectively. The signals were then compared with the on-axis S-band beam to provide a monopulse nulling signal that was used by the attitude control subsystem to maintain the pointing of ATS-6.

The electroscan (beam-switching) technique was the third tracking mode possible. To facilitate this operation, use was made of an array of S-band receive feeds (see communication subsystem chapters of this volume) aboard ATS-6, selectable upon command. By switching feeds, this system relaxed the ATS-6 pointing requirements while tracking the near-Earth satellite through a series of short arcs.

Nimbus-6

Several types of real-time data were transmitted through the ATS-6 relay link to evaluate the performance of satellite-to-satellite data relay. These types of data were VIP, LRIR, and THIR as defined in the following paragraphs.

- The versatile information processor (VIP) sampled the output of approximately 1000 sensors on board Nimbus-6. The data were digitized, time-multiplexed, and formatted into a 4-kilobits per second (kbps), 10-bit per word serial bit stream.
- The limb radiance inversion radiometer (LRIR) was devised to determine the vertical distribution of atmospheric temperature, ozone, and water vapor on a global scale by using a multispectral scanning radiometer. The radiometer scanned through the atmosphere along a line tangent to the Earth's disc from the spacecraft. The radiometer was a four-channel instrument operating in three major spectral intervals: one channel for ozone emission; two channels for the carbon-dioxide band; and one channel for the rotational water-vapor band. The data were digitized, time-multiplexed, and formatted into a 4-kbps, 10-bit per word serial bit stream.
- The temperature humidity infrared radiometer (THIR) provided day and night mapping of the Earth and its atmosphere in two regions: one channel with a range of 10.5 to 12.5 micrometer (μm) (11.5 nominal); and one channel with a range of 6.5 to 7.0 μm (6.7 nominal). The THIR scanning radiometer provided cloud-top or surface temperatures by the 11.5- μm channel while the 6.7- μm channel provided data about the water vapor content of the upper troposphere and stratosphere. The data frequency modulated a 36.8-kilohertz (kHz) to 50.5-kHz subcarrier at a maximum rate of 360 hertz (Hz).

Nimbus-6 was commanded either directly or indirectly (real-time or stored programmer commands) through ATS-6 to select the VIP or LRIR data for transmission back through ATS-6 to a space tracking and data acquisition network ground station.

The VIP and LRIR data were phase-modulated directly onto the transmitted data array relay carrier to ATS-6 and the THIR data was frequency-modulated on to a subcarrier which then phase-modulated the carrier. As part of the data analysis activity, the data tapes were then compared with data received from a playback Nimbus-6 high data rate storage system that had been transmitted to a ground station either in real-time or by a Nimbus-6 recorder data playback.

GEOS-3

The Geodetic Earth-Orbiting Satellite-3 (GEOS-3) telemetry data were transmitted at 1.562 kbps to an ATS ground station through ATS-6 in either of two modes. The GEOS-3 transmitted telemetry data by itself or simultaneously with range-rate data.

For simultaneous transmission of range-rate and telemetry data, an unmodulated C-band carrier was transmitted from the ATS ground station to ATS-6 where the signal was coherently translated to S-band and then transmitted to GEOS-3. GEOS-3 coherently translated this signal to 2247 megahertz (MHz) and modulated it with the telemetry data. This signal was then transmitted at S-band back to ATS-6 where coherent-frequency translation to C-band occurred prior to its transmission to a ground station for processing.

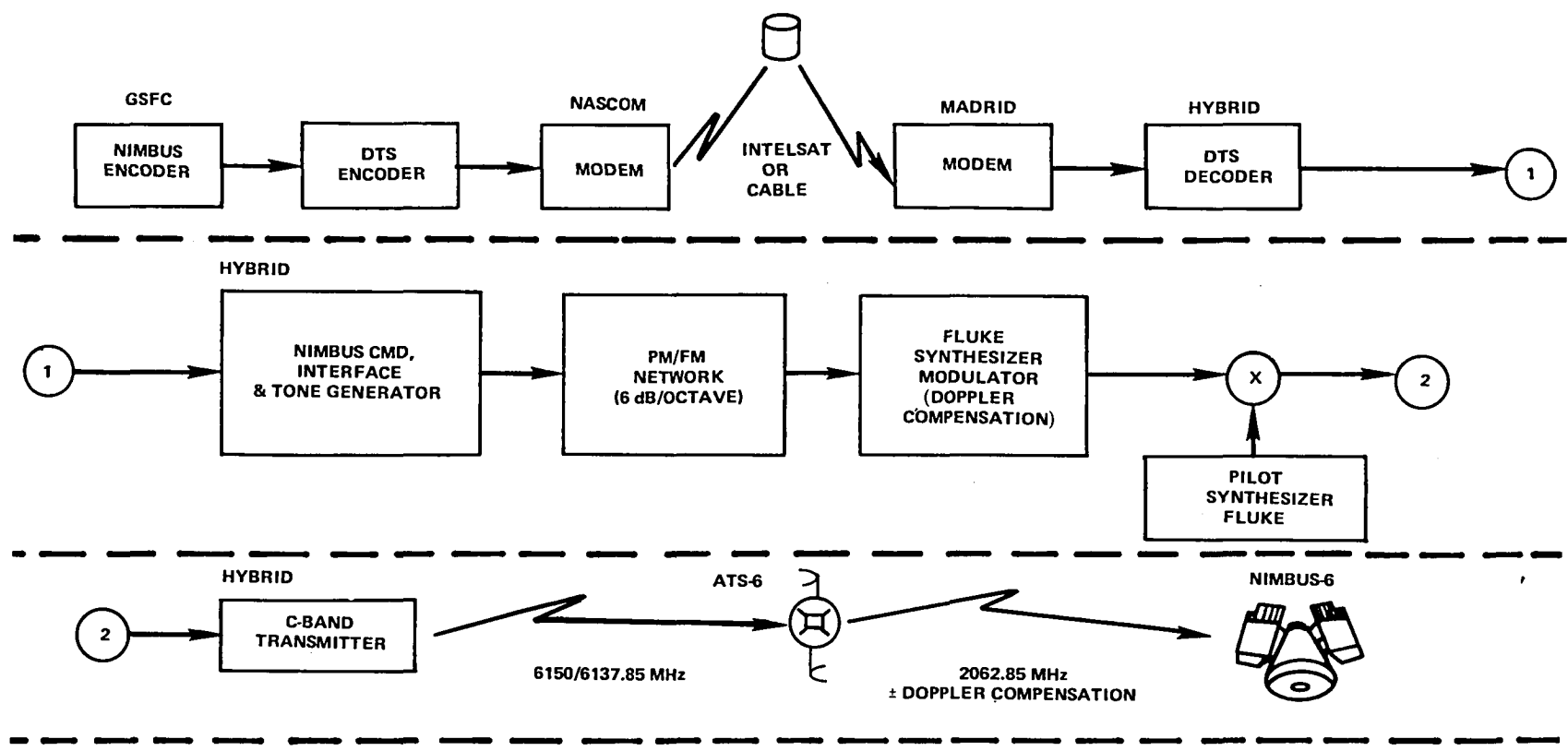
In the telemetry only mode, 1.562-kbps GEOS-3 data were relayed through ATS-6 to an ATS ground station. This mode was simplex where the GEOS-3 S-band carrier was generated by a local GEOS-3 onboard oscillator, then modulated by the telemetry data and relayed to ATS-6.

Data Relay/Command Relay

Nimbus-6/ATS-6 Command Relay

One of the objectives of the Tracking and Data Relay Experiment was to demonstrate the technology of real-time commanding of a near-Earth satellite. For example, commanding Nimbus-6 through a geosynchronous satellite using a National Aeronautics and Space Administration (NASA) command facility. This was accomplished by relaying commands through ATS-6 from the Hybrid Terminal at Madrid, Spain. The Nimbus-6 transponder had been designed to receive command signals at 2062.85 MHz from ATS-6, downconverted to 2.4 MHz and amplitude limited to provide a constant amplitude signal to be FM demodulated for use by the Nimbus digital electronics subsystem. This subsystem demodulated and decoded forward link commands for real-time execution.

The command signal structure consisted of two subcarriers on the ATS-6 2062.8-MHz carrier: 7.68 kHz representing a digital zero (0) and 11.52 kHz representing a digital one (1) (Figure 12-1). The Nimbus T&DRE command encoder, located at Goddard Space Flight Center (GSFC) Nimbus Control Center, was similar to other NASA/GSFC FSK/AM/FM command systems except for



COMMAND CHARACTERISTICS – NIMBUS T&DRE COMMAND

MODULATION: PCM/FSK/AM/FM

BIT RATE : 128 bps

TONES : ONE, 11520 Hz; ZERO, 7680 Hz

MODULATION INDEX : SET TO PRODUCE 25-kHz DEVIATION WITH 8350-Hz TONE

COMMAND LENGTH : DISCRETE COMMANDS, 18 BITS (18 FUNCTIONS) PROGRAM MEMORY LOAD, ≈2000 BITS

NOTE: PROGRAM MEMORY LOAD WAS NOT CAPABLE OF LOADING BY ATS-6 (IT COULD ONLY BE LOADED BY DIRECT GROUND TRANSMISSION.)

Figure 12-1. Nimbus-6 T&DRE Command System Block Diagram

unique tones used for the ATS-Nimbus interface. The unique tones were used to avoid accidental commanding of those Nimbus-6 spacecraft functions not related to the T&DRE experiment package. The encoder was limited to 16 discrete functions plus antenna position commands. The encoder was capable of generating either an FSK/AM analog output to be transmitted to a commanding ground station or a digital output to interface with the GSFC data transmission system (DTS). Since the DTS furnished an asynchronous buffer to interface with the normal NASA Communications Network (NASCOM) commercial modems, this mode was used exclusively in the operations with the Madrid station, since the wideband analog lines needed for regular tone transmissions were available only between GSFC and the Rosman Ground Station.

The commands were transmitted to the Madrid station (Figure 12-1) by the normal NASCOM data circuits at a bit rate of 2000 bits per second (bps). A special interface unit decoded the binary output from the DTS and reconstructed the FSK/AM tone digital bit stream. This bit stream was passed through a 5-decibel (dB) per octave de-emphasis network and PM modulated on to a 70-MHz carrier. This resulted in a narrow-band FM signal with the deviation set at 25 kHz for an input tone of 8350 kHz. The frequency of the modulating synthesizer (Fluke 5105) was manually varied ± 60 kHz about 70 MHz to compensate for the predicted one-way Doppler to Nimbus. This signal was then mixed with the reference pilot for ATS-6 coherent operation and upconverted to the C-band uplink frequency. This composite signal contained a pilot at 6150 MHz that was attenuated to be 10 dB below the information signal and the 6137.85-MHz information signal that contained the command modulation as an FSK/AM/FM signal.

Simulated Digital Data

The digital evaluation mode (DEM) experiment was devised to permit an evaluation of satellite-to-satellite data relay performance at different bit rates and rf power levels. The objective of the DEM experiment was to record sufficient data to permit a determination of the mean bit-error rate as a function of bit-energy-density-to-noise ratio and compare these experimental results with the theoretical performance. Bit-error pattern anomalies and burst-error characterization were also to be ascertained.

The digital evaluation module, which was flown on board Nimbus-6, provided a source of data in the form of a pseudo-random digital code of 2047 bits whose rate was selectable by command to be 50, 100, 200, or 400 kbps. The shift register-generated PN code was applied as phase modulation to the Nimbus-6 rf carrier with a peak-carrier phase deviation of approximately 1.3 radians. The modulated carrier was generated and transmitted from Nimbus-6 at S-band to ATS-6 where the frequency was translated to C-band and then retransmitted to the Hybrid Terminal at Madrid. In addition to the ability to change bit rates by command, the Nimbus-6 T&DRE transmitter power output was also selectable at nominal levels of 2, 4, and 8 watts. This capability permitted an evaluation of the effects of effective isotropic radiated power (e.i.r.p.) variations at constant bit rate and vice versa.

Upon reception at the Hybrid Terminal, the DEM signal was coherently demodulated using the Applications Technology Satellite-Ranging carrier synchronous tracking demodulator. The demodulated signal from the receiver produced an output that was an unlocked split-phase baseband

digital bit stream plus noise. The baseband bit stream was then evaluated using a correlation detector specifically designed for this experiment. The DEM code-correlator-error detector provided an in- or out-of-lock indication, and an indication of the bit-error rate per specified time interval. The DEM code-correlator-error detector also provided reconditioned data from a coincidence gate. The raw data, the reconditioned data, and the bit-error rate were recorded on magnetic tape for later processing and analysis.

The bit-error rate output from the DEM code correlator was also monitored by the ground station PDP-11 computer and relayed via a data modem to the ATS Operations Control Center (ATSOCC) where a special software program gave a real-time cathode-ray tube presentation of the bit-error rate and a computer printout for later analysis. The experiment configuration for relaying DEM data from Nimbus-6 via ATS-6 to Madrid is depicted in Figure 12-2.

Tracking and Orbit Determinations

The tracking and orbit determination phase of the T&DRE was to demonstrate the feasibility of using a geostationary satellite to track a near-Earth satellite and accomplish the subsequent orbit determination without the aid of other ground tracking stations. To determine the feasibility, two forms of tracking data were obtained: satellite range data by measuring signal propagation time and range-rate data by measuring carrier Doppler frequency. An orbit computation computer program used iterative techniques to arrive at an orbit that mathematically best fitted the measured tracking data (the program minimized the residual errors between the measured data and the orbit solution). However, the accuracy of such an orbit prediction was based on determination of the initial spacecraft vector and would degrade with time according to the accuracy to which physical parameters are modeled. Included in the orbit determination model were such items as the Earth's gravitational field, atmospheric drag and refraction, solar pressure, solar and lunar gravity effects, and determination of the tracking station location. Of these parameters, the most critical for a medium altitude spacecraft was the gravity field model.

In principle, the satellite ranging system used ranging tones sequentially phase modulated on to the carrier to provide range ambiguity resolution. The lower frequency tones sequentially used during acquisition were at 20 kHz, 4 kHz, 800 Hz, 160 Hz, 32 Hz, and 8 Hz. After resolution of the range ambiguity, a 100-kHz tone was transmitted to provide sufficient range measurement accuracy.

For the case of satellite-to-satellite tracking experiments, such as a ground station to ATS-6 to a near-Earth satellite, four different propagation links were involved:

Forward Link

- Ground station to ATS-6 (6 GHz)
- ATS-6 to the near-Earth satellite (2 GHz)

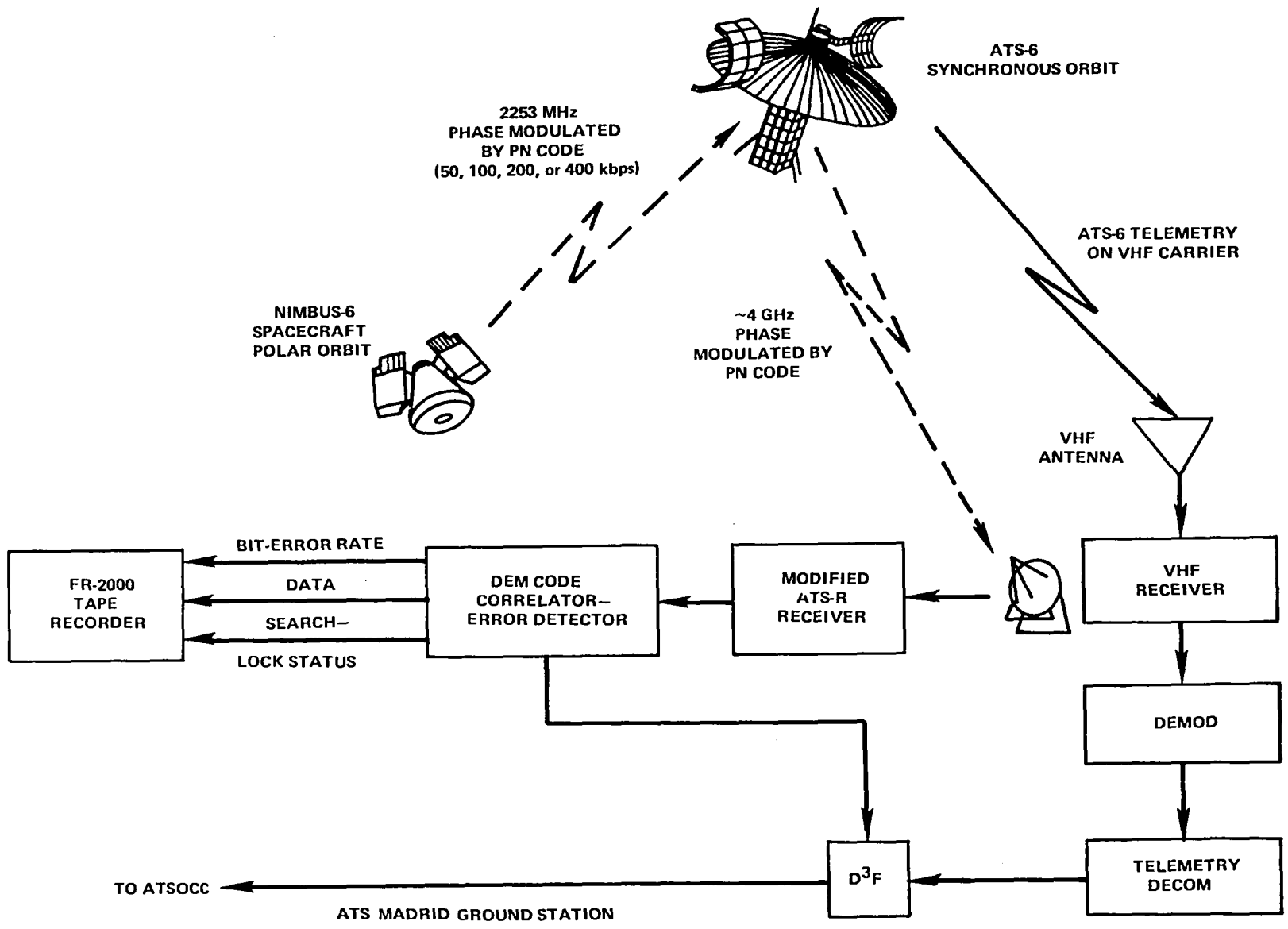
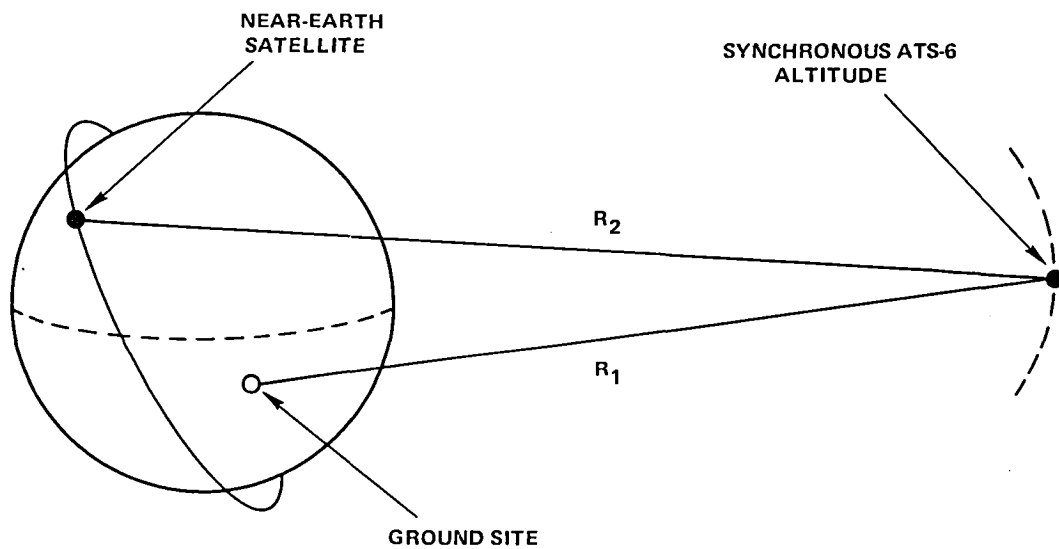


Figure 12-2. Relaying DEM Data from Nimbus-6 to ATS/Madrid Configuration

Return Link

- Near-Earth satellite to ATS-6 (2 GHz)
- ATS-6 to the ground station (4 GHz)

Range-rate information was obtained by the measurement of carrier Doppler frequency. Each cycle of Doppler corresponded to a half wavelength change in total path length relative to a given tracking station at the operating frequency. For the satellite-to-satellite tracking conducted for T&DRE, a nominal carrier frequency of 2 gigahertz (GHz) was used so that each cycle of two-way Doppler corresponded to 7.5 centimeters (cm) of path length change. The Doppler shift on the 4- and 6-GHz links involved was negligible, because the range from the Earth station to ATS-6 was essentially fixed (Figure 12-3).



MEASUREMENT TYPE	RESOLUTION	APPLICABLE FREQUENCY
RANGE ($R_1 + R_2$)	2 meters	100 kHz
DOPPLER ($\dot{R}_1 + \dot{R}_2$)	0.05 cm/sec	2000 MHz

Figure 12-3. Basic Tracking Geometry

Multipath

The general configuration used for the measurement of satellite-to-satellite multipath signals is shown in Figure 12-4. The near-Earth satellite transmitted an unmodulated S-band carrier and ATS-6 received both the direct and reflected signals. This composite signal was translated to C-band and relayed by ATS-6 to the Hybrid Terminal at Madrid, Spain. The ground received signal spectrum was downconverted to the 70-MHz i.f. required by the multipath translator. The local oscillator in the multipath translator was manually adjusted, during a satellite pass, to compensate for Doppler effects and to keep the multipath spectrum of the translator output within a bandwidth of 0 to 15 kHz. The composite multipath spectrum was recorded on an instrumentation recorder for off-line data processing.

It can be seen from the geometry of Figure 12-4 that the total signal received by ATS-6 was a combination of the direct-path signal and the summation of the Earth reflected signals received over all path lengths $S_1 + S_2$. This experiment was primarily concerned with the measurement of the specularly-reflected signal; i.e., when angles ϕ_1 and ϕ_2 were equal. Considering only the specular component of the Earth scattered energy, the direct-path signal and specular-multipath signal received at the ATS-6 satellite is given by:

$$e_{\text{dir}}(t) = \frac{A \exp [(W_c + W_{d1}) t] \lambda f(\theta_d)}{4\pi R} \quad (12-1)$$

$$e_{\text{spec}}(t) = \frac{A \exp [(W_c + W_{d2}) t] \lambda f(\theta_s) R_s e^d}{4\pi (S_1 + S_2)}$$

where

- A = transmitted carrier amplitude
- W_c = carrier frequency
- W_{d1} = direct path Doppler
- W_{d2} = indirect path Doppler
- λ = wavelength
- $f(\theta_d)$ = total antenna voltage-gain pattern over direct path
- $f(\theta_s)$ = total antenna voltage-gain pattern over multipath
- R_s = $P_s DR_o$ = specular-reflection coefficient
- R_o = Fresnel-reflection coefficient for plane smooth Earth
- D = divergence-coefficient for spherical Earth

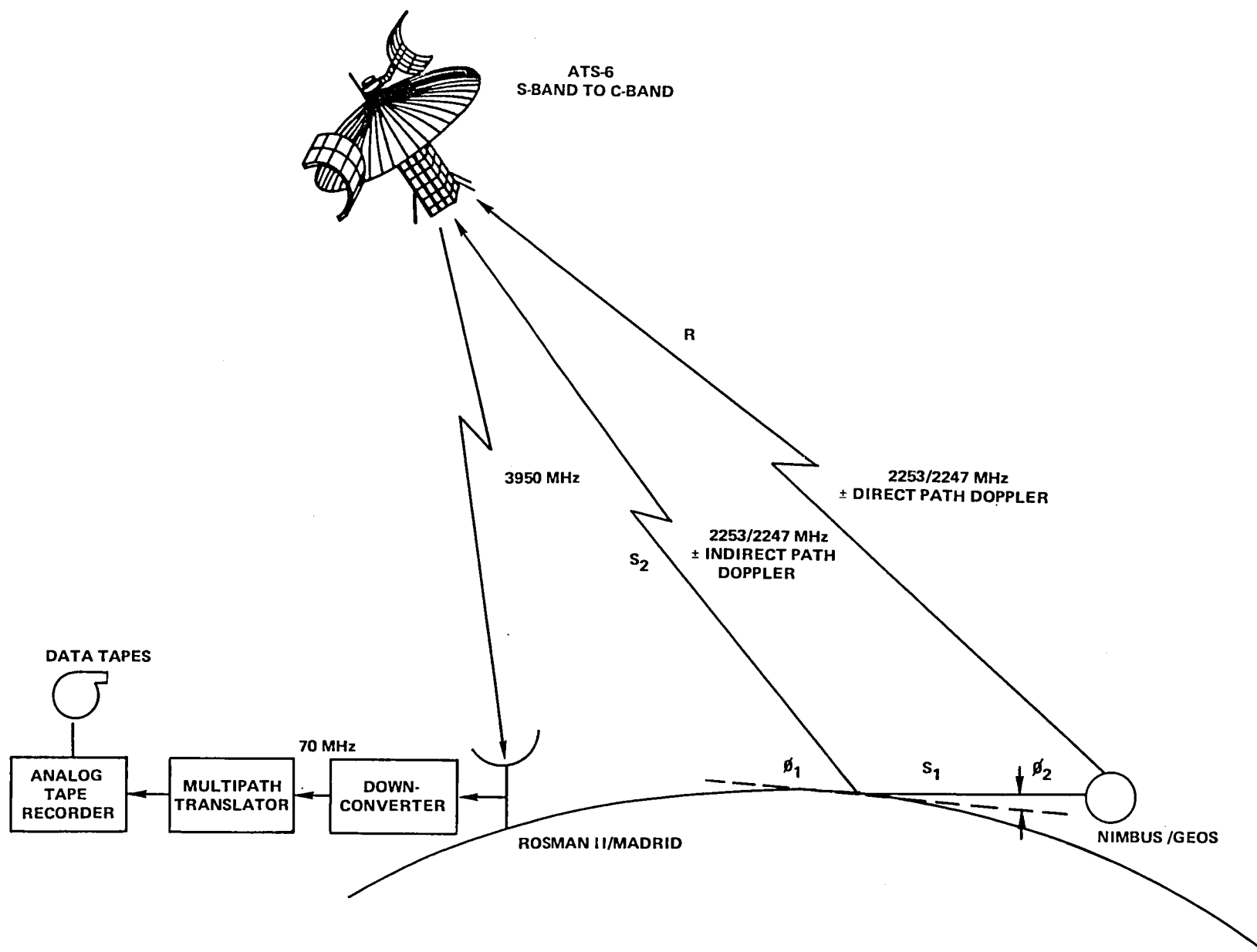


Figure 12-4. General S-Band Satellite-to-Satellite Multipath Experiment

- P_s = scattering coefficient
- R = range from geosynchronous to low-Earth satellite

By the nature of this experiment, the frequency of the received direct-path signal differed from the frequency of the received reflected signal because of the different Doppler shifts over the two paths. It was anticipated that a maximum Doppler difference of 12 kHz could result with the satellites and frequencies used in this experiment. The difference in Doppler frequency provided the means for separating the two components of the signal. The power spectral density of the composite signal was processed on a real-time spectrum analyzer to separate the two components.

The general test procedure was to operate ATS-6 in the satellite tracking mode, dynamically tracking the low-Earth satellite after acquiring its transmitted signal as the satellite crossed over the horizon of the Earth (zero degree grazing angle) and tracking it until the grazing angle was approximately 15 degrees. Then to achieve a different aspect, tracking the test satellite from a point 15 degrees prior to loss of visibility and maintaining the tracking until the satellite disappeared over the Earth's horizon. This was performed to determine the presence of multipath signals at the ends of a satellite-to-satellite pass. Other tests were performed where the spectral point was tracked by ATS-6 in the fixed pointing, electro-scan mode. This was achieved by predicting the locus of spectral points for a given pass of the low-Earth orbit satellite and pointing ATS-6 so that the electro-scan beams could be switched to follow the spectral point in real time (Figure 12-18).

SYSTEM CONFIGURATION

Ground Station Equipment

The Hybrid Terminal located at Madrid, Spain, provided the necessary tracking and data handling facilities for T&DRE while ATS-6 was positioned above 35° East longitude. Also available were the necessary range and range-rate equipment, rf transmitters, receivers, and a 6-meter parabolic antenna to operate with the ATS-6 satellite.

For ranging operations, a 70-MHz signal was generated within the range and range-rate equipment then modulated with the 100-kHz, 20-kHz, 4-kHz, 800-Hz, 160-Hz, 32-Hz, and 8-Hz range tones to facilitate range measurements. For coherent operations, a reference-pilot signal was mixed in the pilot combiner with the 70-MHz signals having the proper offset frequency. This composite signal was then upconverted to C-band where it was amplified and transmitted at 1 kilowatt (kW) with the pilot normally 10 dB below the remaining composite signal level (the uplinked pilot provided the reference signal for coherent-phase-locked operation of ATS-6). All C-band signals, when received from ATS-6, were amplified and downconverted to 70 MHz for the range and range-rate equipment. The station standard was used as a reference to generate coherent frequencies in the range and range-rate equipment to attain the precision required in the ranging operation (Figure 12-5).

Range and range-rate measurements were normally taken using one of two possible modes. In one mode, sometimes referred to as the phase-lock loop mode, range-rate measurements were made by a

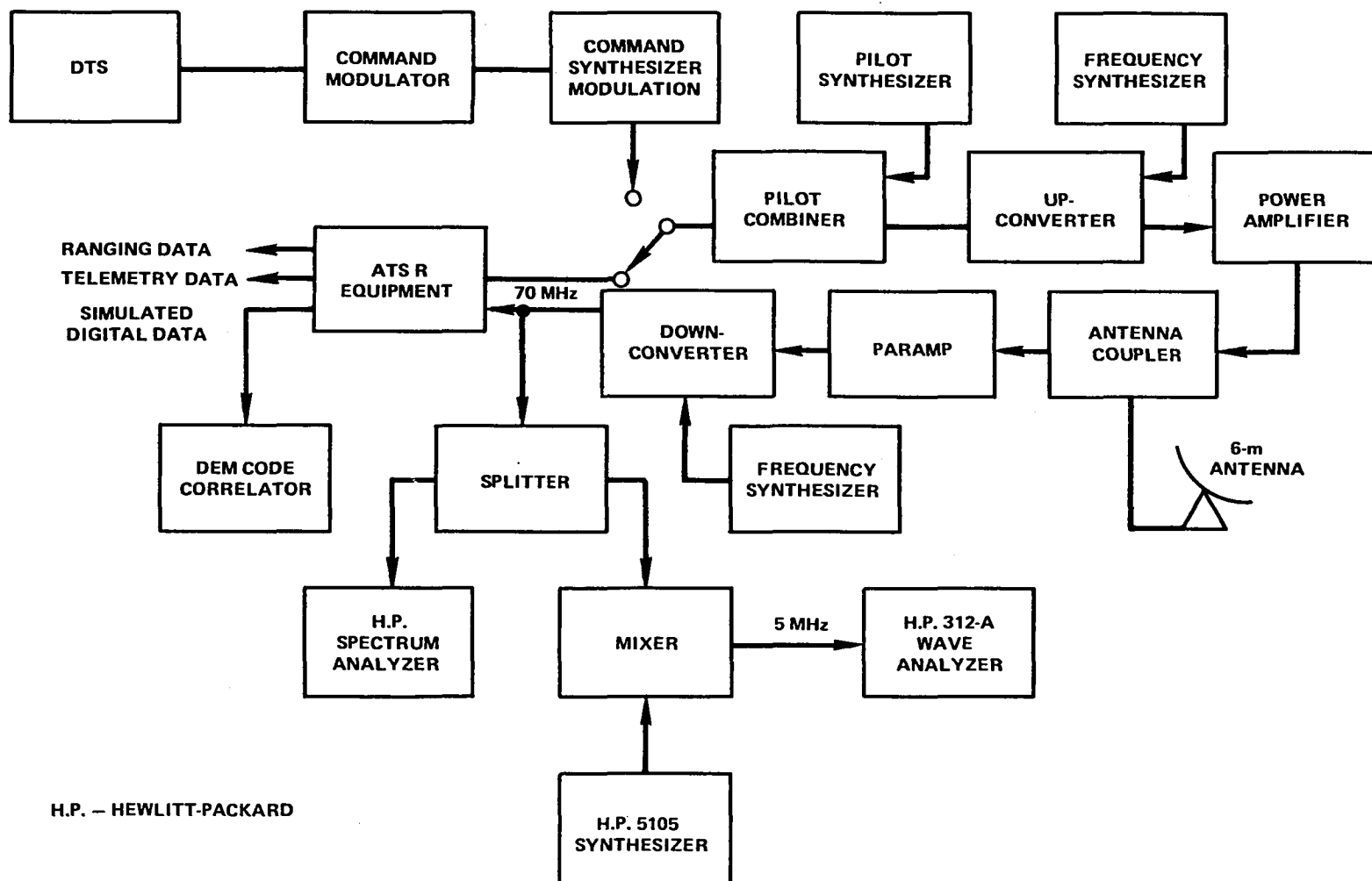


Figure 12-5. Ground Station Equipment Block Diagram

determination of the Doppler shift between the transmitted and received carriers. Range measurements were made by obtaining the time delay between the transmitted and received 100-kHz tone as directly modulated on the return carrier. This ranging mode was used with the phase-locked transponder on GEOS-3.

In the second ranging mode, a subcarrier frequency was available on the return link that contained the forward carrier Doppler. The range tones were received on the subcarrier and were demodulated by a subcarrier receiver. The change in the subcarrier frequency was measured to yield the forward-link Doppler shift. The change in the return-link received carrier frequency was measured to yield the return-link Doppler shift. By combining the two measurements, the total forward-link Doppler shift was obtained free of any variation in the local oscillator frequency of the tracked satellite. This second ranging mode was used with noncoherent, crystal-controlled translation type transponder on Nimbus-6.

Operations Control Centers

Nimbus Technical Control Center—The Nimbus Technical Control Center (NTCC) was responsible for monitoring and controlling the functions of the Nimbus-6 spacecraft. All of the following phases of Nimbus operations were the responsibility of the NTCC: spacecraft and direct-reception ground equipment status; preparation of spacecraft command sequences; evaluation of spacecraft performance; and the providing of spacecraft data summaries. Spacecraft commands were provided to NTCC by the Meteorological Data Handling System (MDHS) and the spacecraft response was monitored at that location during operations. NTCC also had the responsibility of providing (1) a command list of antenna programmer commands for satellite-to-satellite operations with the required start time, (2) the antenna programmer actual start time, (3) a command-station printout of commands versus time, (4) and a comparison of commanded-antenna-pointing angles with the telemetry-pointing angles for the stored-antenna-angle program. During a T&DRE operation, NTCC monitored the MDHS operations network for use of the system. NTCC personnel also monitored spacecraft telemetry data on brush recorders and computer printouts for command verification and status determination.

ATS Operations Control Center—The controlling and monitoring of the functions of ATS-6 were performed at the Applications Technology Satellite Operations Control Center (ATSOCC). An ATS experiment engineer controlled the T&DRE operational tests from ATSOCC. ATSOCC provided a maneuver prediction display that contained a plot of actual ATS-6 ground pointing versus a predicted trace of a tracked satellite as viewed from ATS-6 against the Earth's disc. This display of the maneuver prediction was used to verify that ATS-6 was pointing at the satellite being tracked during operations and aided the experiment engineer in monitoring the operations in real time. Typical examples of the maneuver prediction display are shown in Figures 12-12 and 12-14. The display also provided various alternative computations: ATS-6 computed pitch and roll angles with the predicted ATSOCC/tracked satellite ephemeris data file; the ATS-6 attitude sensor telemetry; and the ATS-6 digital operational controller output with error angles. The error angles were computed by comparing the roll and pitch angles received from the ATS-6 attitude sensors with the predicted pointing based on ephemeris data.

Prior to a given satellite pass, ATSOCC prepared an ATS-6 acquisition table that contained the predicted subsatellite position data for the tracked satellite based on its ephemeris data and roll/pitch angles required for ATS-6 to track the near-Earth satellite. This document was used by the ATS experiment engineer and the ATS attitude control engineer in formulating plans for a given satellite pass. Data pertinent to each completed T&DRE pass were provided by ATSOCC in the form of a pass history printout that contained: Greenwich mean time (G.m.t.); predicted tracked satellite subsatellite position data as computed from the ATSOCC near-Earth satellite ephemeris data file; ATS-6 receiver i.f. automatic gain control (AGC) readouts from the ATS-6 telemetry; and the ATS-6 pitch and roll angles as shown on the maneuver prediction display along with the error angles.

Multisatellite Operations Control Center—The Multisatellite Operations Control Center (MSOCC) served as the Project Operations Control Center for the GEOS-3 mission. All GEOS-3 spacecraft operations and control were served by MSOCC as the central facility. Coordination and monitoring of spacecraft operations support to interface the GEOS-3 mission personnel with other GSFC facilities was also provided by MSOCC. MSOCC had the responsibility for spacecraft evaluation and analysis, command and control, and mission planning for GEOS-3.

Spacecraft Parameters

ATS-6 Parameters

A block diagram of the ATS-6 communications transponder configuration as applicable to the Tracking and Data Relay Experiment is shown in Figure 12-6. For coherent operations, the uplink C-band carrier and pilot were received via the Earth-coverage horn, amplified and downconverted to a 150-MHz i.f. The synthesizer was then locked to the downconverted pilot to achieve phase coherence for all upconverter and downconverter frequencies. The information carrier was then upconverted for transmission on one of the selectable S-band feeds through the 9.14-meter parabolic antenna to the tracked satellite. All received signals from the tracked satellite were received via the same S-band feed, translated to C-band, and transmitted to the ground station via the C-band Earth-coverage horn.

Table 12-1 lists various system characteristics pertinent to satellite-to-satellite operations supported by ATS-6. Of special note, the ATS-6 system had the flexibility to handle variations of 30 dB in e.i.r.p. and 12 dB/K in G/T of the tracked satellite. Additional communication subsystem information can be found in the Communication Subsystem chapters.

Nimbus-6 Parameters

The Nimbus-6 satellite orbited the Earth in a near-polar orbit with a mean altitude of 1110 km at an inclination angle of 100 degrees with a period of approximately 107 minutes. The Nimbus-6 equipment associated with T&DRE consisted of a transponder in which all upconversion and downconversion frequencies were derived using a single-crystal oscillator. The received carrier was downconverted to 2.4 MHz, which was retransmitted to ATS-6 as a subcarrier modulating the return carrier during ranging measurements. The 2.4-MHz subcarrier was varied by the forward-carrier

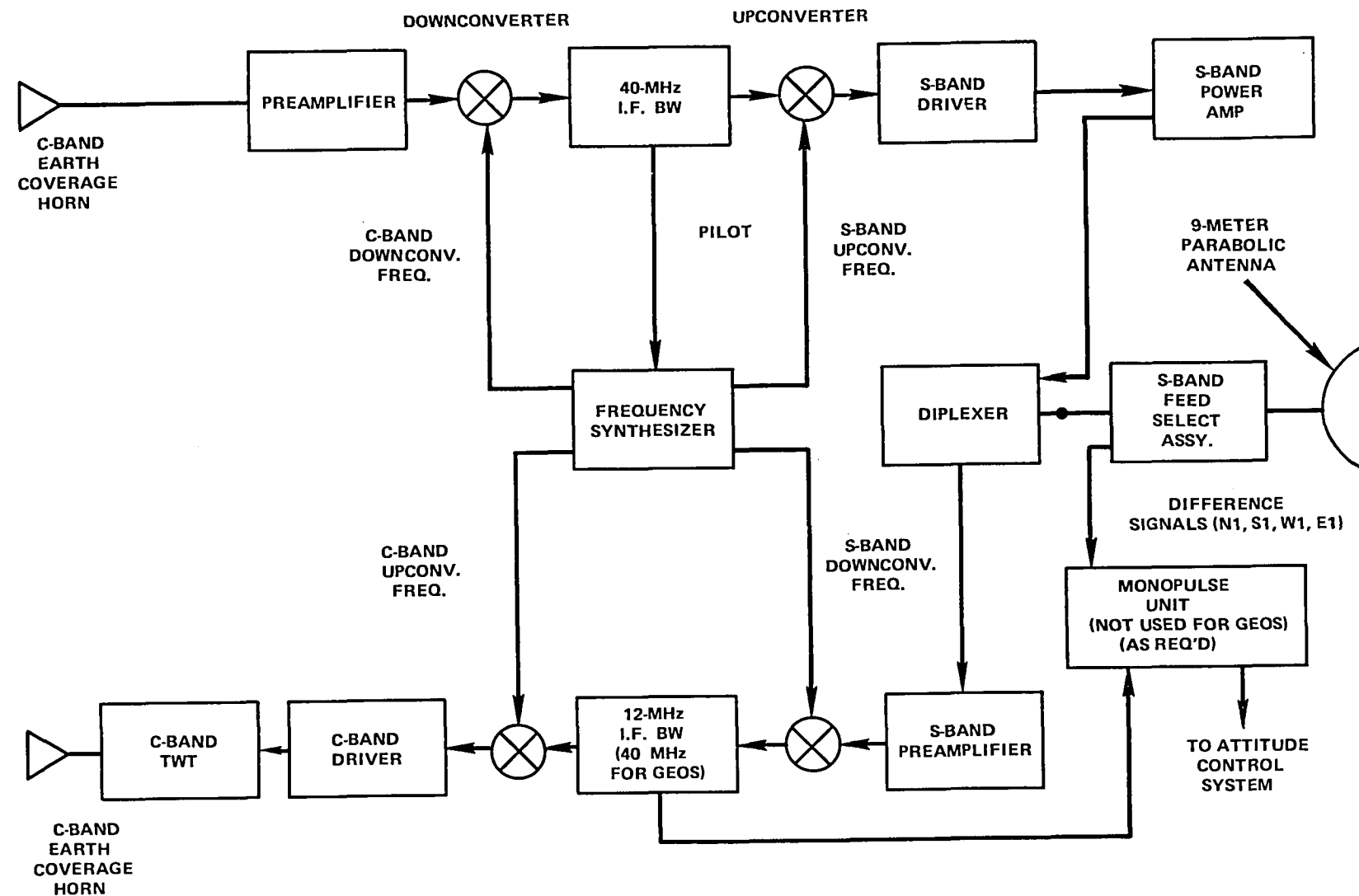


Figure 12-6. ATS-6 Block Diagram of Configuration for T&DRE

Table 12-1
Tracked Satellite Characteristics

	ATS-6	GEOS	Nimbus	
				<u>Units</u>
<u>Orbit</u>				
Inclination	0.4	115	100	deg
Semimajor axis (SMA)	42,166	7,213	7,483	km
Altitude	19,327	454	600	nmi
<u>Transponder</u>				
E.i.r.p. (S-band)	51	40.9	50.1	dBm (max)
G/T	9.4	-27.4	-15.5	dB/K (peak)
Type	Coherent	Coherent	GARR (Xtal)	

Doppler. Ranging tones received on the forward carrier were retransmitted on the 2.4-MHz sub-carrier. Nominal transmitter power levels of 2, 4, and 8 watts were available and could be selected on command.

The spacecraft had an S-band quadhelix antenna with a peak gain of 15 dB. The antenna used a gimbaled X-Y mount where each gimbal could be rotated through an angle of ± 108.8 degrees in steps of 3.4 degrees. The antenna pointing was controlled by real-time commands or a stored program. Nimbus-6 command data (128 bits per second) were received as FSK-AM/FM modulation on the received carrier and detected by a discriminator/decoder at the 2.4-MHz i.f. of the receiver. Discrete mode changing commands, such as data-rate changes and antenna-programmer commands, were achievable through the satellite-to-satellite relay link and by stored program. Nimbus-6 data transmissions were either satellite telemetry data or a DEM signal. The DEM signal was a 2047-bit pseudorandom PN digital code whose rate could be modified on command (i.e., 50, 100, 200, or 400 kbps).

GEOS-3 Parameters

The GEOS-3 satellite orbited the Earth at a mean altitude of 843 km with an inclination angle of 115 degrees at a period of approximately 102 minutes. The GEOS-3 orbit parameters had been selected to minimize resonance of the subsatellite trace with a particular feature on the Earth and to provide a uniform grid of traces on the Earth.

The applicable T&DRE equipment aboard GEOS-3 consisted of a single channel coherent transponder and a four-element space-looking antenna. Within the transponder, there was a voltage

controlled oscillator that had the capacity to phase-lock to a downconverted S-band received signal. All signals for downconversion and upconversion were referenced to the voltage controlled oscillator, so that coherence was maintained between the S-band transmitted and received signal. The nominal transmitter power output was 5 watts. The GEOS-3 antenna associated with T&DRE had selectable elements with a minimum gain of 1.5 dB to ATS-6 over the region of mutual visibility. The transponder was normally operated in the phase-locked mode with a coherent return carrier transmitter unmodulated, or with range tones and/or telemetry data modulating the carrier. Data could also be transmitted in a noncoherent mode by commanding the oscillator to the free-running unlocked mode. Operating modes were command selectable either by real-time commanding from an Earth station or by stored program. GEOS-3 could not be commanded via the satellite-to-satellite link. In the range mode of operation, range tones were detected in the receiver and retransmitted on the return carrier.

EXPERIMENT RESULTS

Data Reduction

Range and Range Rate

The Nimbus-6 range measurement was performed by comparing the time interval between transmitted and received tone zero crossing. The range-rate measurement was performed by counting a fixed number of Doppler cycles and recording the time required to receive the fixed number of cycles. The range and range-rate measures were thus recorded in terms of elapsed time. The tone-ranging measurement resolution was partially dependent upon the accuracy of preflight calibration of both ATS-6 and the near-Earth satellite transponder group delays. The preflight calibration data were recorded for different frequencies and operating temperatures to permit a more definitive range measurement. The results indicated that the total systematic delay error in the ranging measurement could be held to within several meters of the equivalent one-way range.

The Doppler output frequencies were a function of the range rate from ATS-6 to the ground station, the range rate from ATS-6 to the near-Earth satellite, and the choice of uplink frequency. The range and Doppler measurements were also seen to be affected by the Earth's troposphere and ionosphere. At 2 GHz, it was noted that measurement biases resulted that were meters in range and tens of centimeters per second in range rate. Attempts at modeling out atmospheric refraction effects were successful and resulted in using a seventh-degree polynomial for range measurements and a sixth-degree polynomial for range-rate measurements. An iterative solution was used for orbit determination via a navigation analysis computer program that took into account the lengths of the four radio propagation paths.

Earth gravitational anomalies were observed in the satellite-to-satellite Doppler data when tracking near-Earth spacecraft. The Earth's gravitational field in localized areas could be determined by detecting small changes in velocity of the low-orbiting spacecraft; i.e., velocity changes of 1 to 10 millimeters per second that could be translated as direct measurements of local gravity variations. The Earth's gravitational field could be represented as a finite spherical harmonic series expansion

in which the coefficients are determined from a combination of satellite ground tracking data and surface gravimetric data. Such a representation of the global geopotential would not adequately represent local variations in the gravity field because the local variations are very small in wavelength and would require a spherical harmonic series expansion to an order and degree of 100 to 200, which is impractical.

Digital Evaluation Module

Analytical—The communications link power budget for the Nimbus-6/ATS-6/Hybrid link is shown in Table 12-2. The operational power budget was computed to show the range of signal levels that would be expected during a Nimbus-6 operation pass. The table depicts the signal conditions at minimum, nominal, and maximum range. When the Nimbus-6 spacecraft reached the point in its orbit corresponding to the maximum range of ATS-6 (ATS-6 pointing vector grazes the Earth), it was found that the Nimbus-6 antenna had rotated into its gimbals limits of 108.8 degrees. This meant that the rf power radiated from Nimbus-6 to ATS-6 was effectively reduced because the antenna look-angle was not along the antenna boresight. A 3-dB allowance was made in the e.i.r.p. of Nimbus-6 (Table 12-2 worst case column). The root-sum-squared value of the tolerances was computed and used as a plus and minus tolerance about the nominal input signal-to-noise ratio into the delay-lock-loop code correlation synchronizer. The practical limit curve (Figure 12-7) in the Applied Physics Laboratory (APL) manual for the DEM code correlator was used as the nominal curve of bit-error rate versus bit-energy to noise-power-density ratio. The root-sum-squared value of the tolerances in the power budget computation was plotted about the nominal bit-error rate curve to give a range into which experimental values were expected. The received C/N_0 measurement was made using a spectrum analyzer and a frequency selective voltmeter (wave analyzer). The uncertainties in the parameters that may have affected the communications link power budget resulted in a limit of ± 1.3 dB about the nominal bit-error rate curve.

The spectrum analyzer measurements of carrier-to-noise ratio were converted to obtain bit-energy density-to-noise power in a 1-Hz bandwidth. These spectrum analyzer carrier-to-noise ratio measurements were made using a 10-kHz bandwidth and the conversion factor of 38 dB applied to the conversion to a 1-Hz bandwidth and to account for noise foldover. A comparative measurement was also made using a wave analyzer in a 3100-Hz bandwidth. The conversion factor used for the wave analyzer was 34.6 dB. For each of the carrier-to-noise measurements made, a large number of samples of bit-error rate were recorded and the sampling rate chosen was much faster than the rate of change of the carrier-to-noise. Statistical computations were then made of the samples of bit-error rate to find the mean, standard deviation, and 95 percent confidence interval. The real-time DEM data was then in a form to be plotted as bit-error rate versus energy per bit-to-noise density (E_b/N_0) and a comparison made with the practical operating limit.

Digital Computer Use—Reconditioned DEM data from the delay-lock-loop code correlation synchronizer was recorded on analog tape using an FR-2000 tape recorder. The Information Processing Division at GSFC processed the analog tapes in two steps. The first step was to digitize the data using the A-3 analog/digital line under control of a Varian-620/L computer that produced a 9-track tape and a brief quality control listing. The second step was to use the CDC-3200 computer that read the 9-track tape from the first step.

Table 12-2
Nimbus-6 to ATS-6 to Hybrid Return Link Power Budget

Parameters	Units	Best	Nominal	Worst	Tolerance	Remarks
Nimbus xmitter power	dBm		36.5		±0.2	Nimbus-6 Nominal 8 watts
Antenna cable loss	dB		1.8		±0.2	
Antenna gain	dB		15.4		±0.2	
Nimbus-6 e.i.r.p.	dBm	50.1	50.1	47.1		
Free space loss	dB	-190.3*	-191.0**	-192.7***	±0.2	Typical
ATS-6 G/T	dB/K	9.4	9.0	6.3	±0.6	Measured in flight
Receiver C/N (12 MHz bw)	dB	-3.0	-4.1	-11.5		
ATS-6 e.i.r.p. (signal and noise includes off-beam allowance)	dBw	51.9	47.2	41.9	±0.3	
Noise power sharing	dB	-5.0	-5.6	-12.6	±0.2	Function of input signal to noise and spacecraft limiter suppression
Free space loss (38,800 km 3953 MHz)	dB	-196.1	-196.1	-196.2	±0.2	
Hybrid G/T	dB/K	23.0	23.0	20.0	±1.0	
Hybrid C/N _o	dB-Hz	72.4	67.1	51.7	±1.3	†RSS of tolerances

*34,700 km

**37,600 km

***45,550 km

†Root-sum-square

Errors were analyzed in each bit position with each 2047-bit frame of data by comparison with the known bit pattern. A printed output summary from this program summarized the DEM data according to bit rate and Nimbus-6 transmitter power level. A bit-error distribution by bit position for each data file summary was generated and printed as a part of the output of the CDC-3200 program.

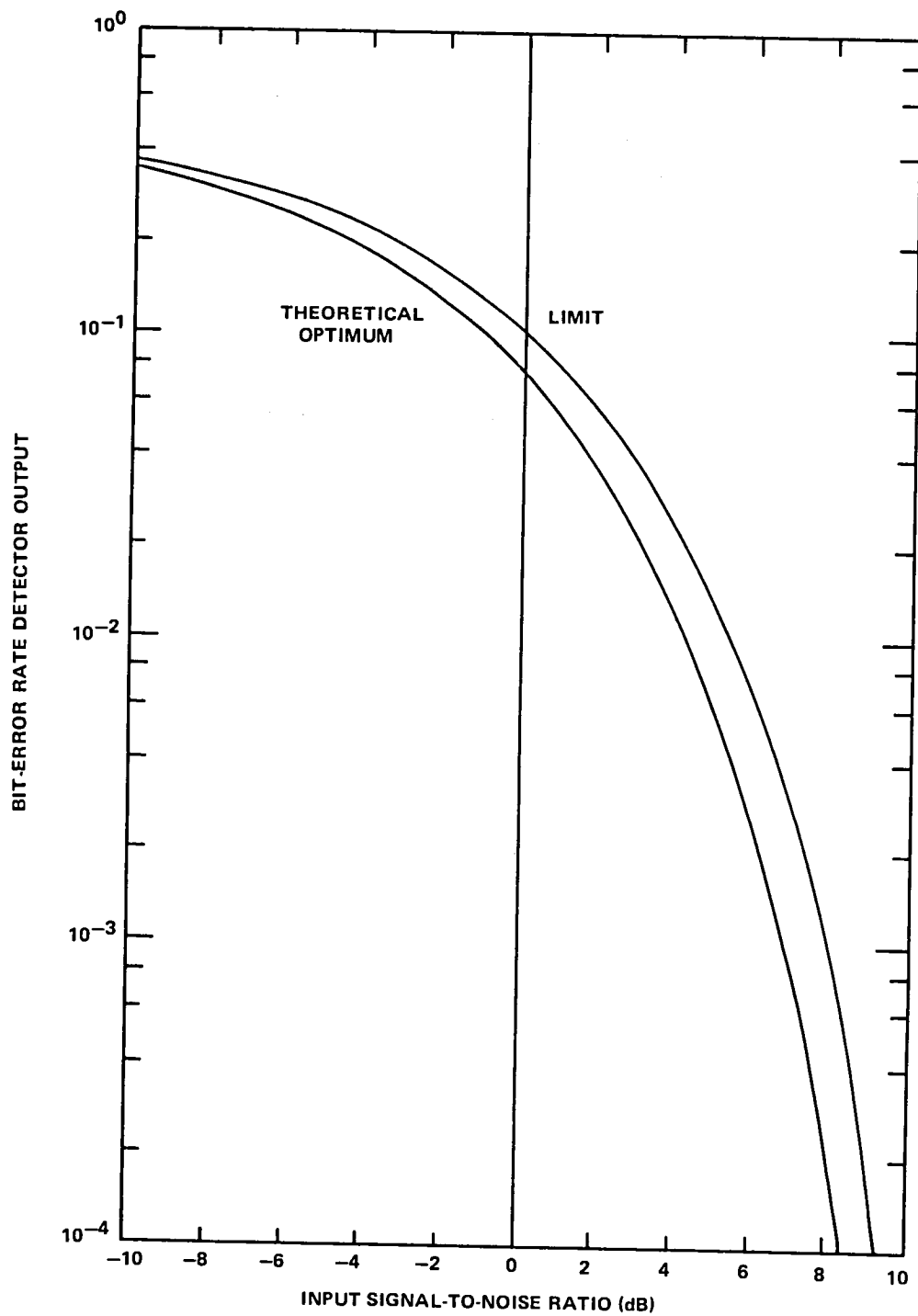


Figure 12-7. Bit-Error Rate Detector Output of Synchronizer

Experimental Results

Range and Range Rate

- **Range and Range-Rate T&DRE Data Evaluation:** Range and range-rate data quality (i.e., system resolution) was consistent with predicted performance. The quality of T&DRE tracking data was verified using a polynomial fit over an 8-minute time span. A seventh-degree polynomial was used for range measurements and a sixth-degree for range-rate measurements. Equivalent one-way range "noise" was typically less than 3 meters and one-way range rate "noise" was on the order of 0.05 cm/sec. A summary of typical tracking data is given in Table 12-3.
- **T&DRE Nimbus-6 Orbit Evaluation:** Early T&DRE data (Nimbus-6 launch through October 1975) was used to verify Nimbus-6 hardware performance such as: Nimbus-6 T&DRE antenna programmer, antenna pointing mechanism, transponder signal-to-noise spectral density, transmitted power levels, and so on. The first Nimbus-6 satellite-to-satellite orbit was computed using T&DRE range and range-rate data recorded on October 17, 1975. The ATS-6 orbit was independently determined using the trilateration technique developed as

Table 12-3
Nimbus-6 T&DRE Tracking Data Quality

Start Time (1976) Mo/Day	HH/MM (G.m.t.)	Range Noise Meters	Range-Rate Noise cm/sec
02/07	16:29	2.9	0.044
02/07	17:55	2.3	0.038
02/07	19:58	1.8	0.055
02/07	23:18	2.1	0.041
02/08	00:42	2.7	0.059
02/08	07:23	2.7	0.045
02/08	09:01	2.8	0.052
02/08	19:32	2.9	0.066
02/08	20:41	2.4	0.046
02/08	22:47	1.3	0.054
02/09	01:00	2.0	0.039
02/14	17:00	1.2	0.076
02/14	18:11	1.9	0.044
02/14	20:14	1.9	0.037
02/14	23:32	2.0	0.049

part of the T&DRE. All Nimbus-6 T&DRE data were recorded at the Madrid Spacecraft Tracking and Data Network (STDN) station, since ATS-6 was positioned at 35°E longitude from the Nimbus-6 launch through August 1, 1976. In the first orbital computation, two relatively short consecutive orbital arcs were used—namely 7 minutes and 15 minutes. Once a Nimbus-6 orbit was computed, one indication of valid results was the difference between observed and calculated parameters over the data span. Such differences are referred to as “orbit residuals.” When the data were compared with the calculated orbit over one or more revolutions, the results were indicative of uncertainty in modeled parameters, such as imperfect gravitational field harmonics and so on. It was clear that to improve such modeling through orbit solutions, the basic orbit determination uncertainty introduced by tracking system errors must be less than the perturbation being resolved.

For the October 17, 1975 T&DRE Nimbus-6 orbit computation, the rms value of the residuals were 7 meters in range and 10 cm/sec in range rate. Subsequently, tracking data from three consecutive weekends were collected at the Madrid site and used for Nimbus-6 T&DRE orbital analysis. This T&DRE tracking test was conducted from January 31 through February 15, 1976. A total of 35 passes range and range-rate tracking were collected with an average span of 55 minutes. The data rate was one sample per 100 seconds.

Using two separate consecutive 6-pass arcs for a given weekend, separate Nimbus-6 range and range rate determined T&DRE orbits were computed. It was found that there was orbit computation agreement at a given epoch within 80 meters in position and 10 cm/sec in velocity. This result was consistent with conventional ground tracking and demonstrated the feasibility of the Tracking and Data Relay Systems concept.

- T&DRE GOES-3 Orbit Evaluation: Preliminary indications were that the accuracy of the a priori positions used for the geostationary satellite (ATS-6 in this case) was a very critical factor in achieving orbit solution convergence. The most effective procedure for two-way satellite-to-satellite orbit determination appeared to be as follows:
 - Acquire satellite-to-satellite range and range-rate data over several successive low satellite passes.
 - Obtain a reasonably accurate (i.e., position within several hundred meters) geostationary orbit by means of, for example, trilateration tracking.
 - Obtain an approximate near-Earth satellite a priori vector based on operational predictions.
 - Solve for both geostationary and near-Earth satellites simultaneously.

In this manner, a 34-hour arc, starting May 2, 1975 at 2300 hours universal time (UT) and ending May 4, 1975 at 0900 hours UT, consisted of ten passes of range and range-rate satellite-to-satellite tracking data. The data were processed to estimate the GEOS-3 orbit, the ATS-6 orbit, range data bias, and solar radiation coefficients for each satellite. The GEM-1 geopotential field was selected for this particular solution, since this field had been most widely distributed to the user community. The a posteriori residuals of the orbital

solution were 1.3 mm/sec rms for range-rate sum residuals and 16 meters for range-sum residuals (Figure 12-8 and Table 12-4). A solution where the ATS-6 state vector was totally constrained yielded larger residuals than the solution above, and an unconstrained solution failed to converge. Overlap tests indicated that satellite-to-satellite tracking could produce orbits comparable to that derived from ground based tracking. For example, the 34-hour arc just described was used to produce two GEOS-3 orbits that were then overlapped. One orbit was computed from the first 24-hour span and the second based on the last 24-hour span. Comparison of the two GEOS-3 orbit vectors thus generated resulted in a maximum position difference of 30 meters.

Digital Evaluation Module

Data Records—Between October 30, 1975 and June 15, 1976, approximately 40 passes of T&DRE DEM data were processed and evaluated. (A “pass” was defined as that portion of a Nimbus-6 orbit that was in view of the ATS-6 satellite.) Typically, the duration of an average data gathering pass was 50 minutes, which was a function of satellite geometry and satellite activation. Approximately

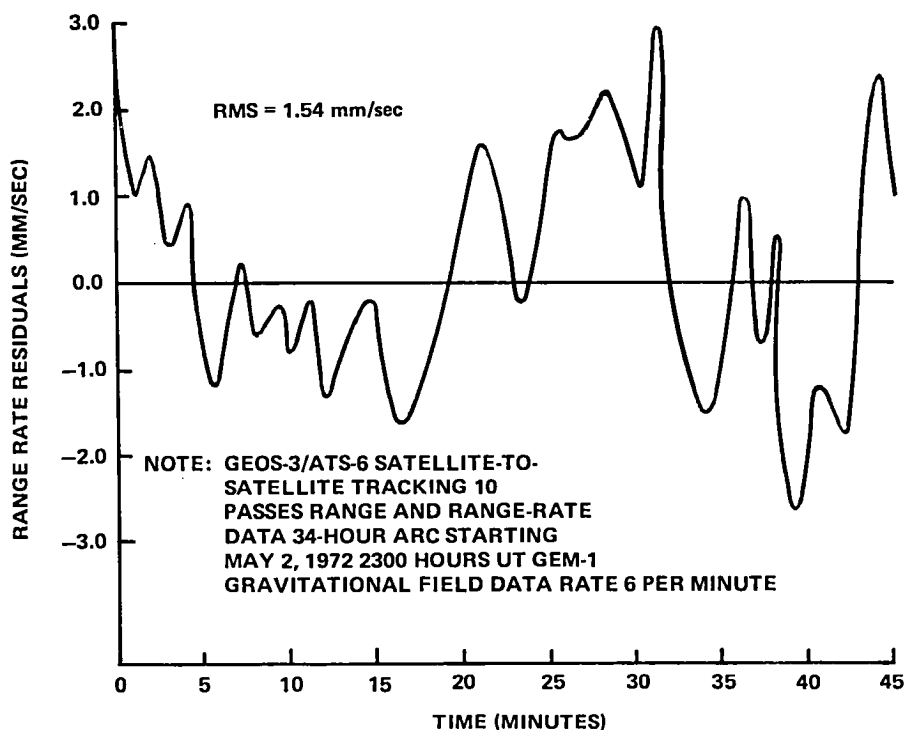


Figure 12-8. Typical GEOS-3 per Pass Orbit Residuals

Table 12-4
GEOS-3 Residual Summary

RMS Observed Minus Calculated		
Pass Number	Range-Rate (mm/Sec)	Range (meters)
1	1.4	—
2	1.3	—
3	*	13.7
4	1.8	—
5	1.5	16.5
6	*	16.5
7	1.1	—
8	0.4	—
9	*	16.8
10	1.3	19.0

Note: Thirty-four-hour arc starting at 2300 hours UT
May 2, 1975 ATS-6/GEOS-3 satellite-to-satellite
tracking.

*Doppler invalid

—No ranging performed

one-third of the aforementioned 40 passes were time-shared with other aspects of the T&DRE experiment during which data were taken.

DEM Data Evaluation—The data that were taken during DEM operations were found to be consistent with the predicted performance. The measured DEM data were compared with the predicted performance after a determination was made of the communications link power budget as listed in Table 12-2. A root-sum-squared value of the return link parameters was calculated and used to establish the prediction uncertainty range.

Figures 12-9 through 12-11 depict typical bit-error rate versus bit-energy to noise-power-density ratio curves of the four bit rates of 50, 100, 200, and 400 kbps during three nominal passes of Nimbus-6. The three Nimbus-6 power levels of 4.5, 2.5, and 1.5 watts were also used during the passes to vary the bit-energy to noise-power-density ratio. The area between the dashed curves on these figures represents the range of uncertainty in the predicted performance. The data points show the mean value of the bit-error rate for each sample group along with the 95 percent confidence interval of the bit-error rate for a given sample group that was plotted as a vertical bar.

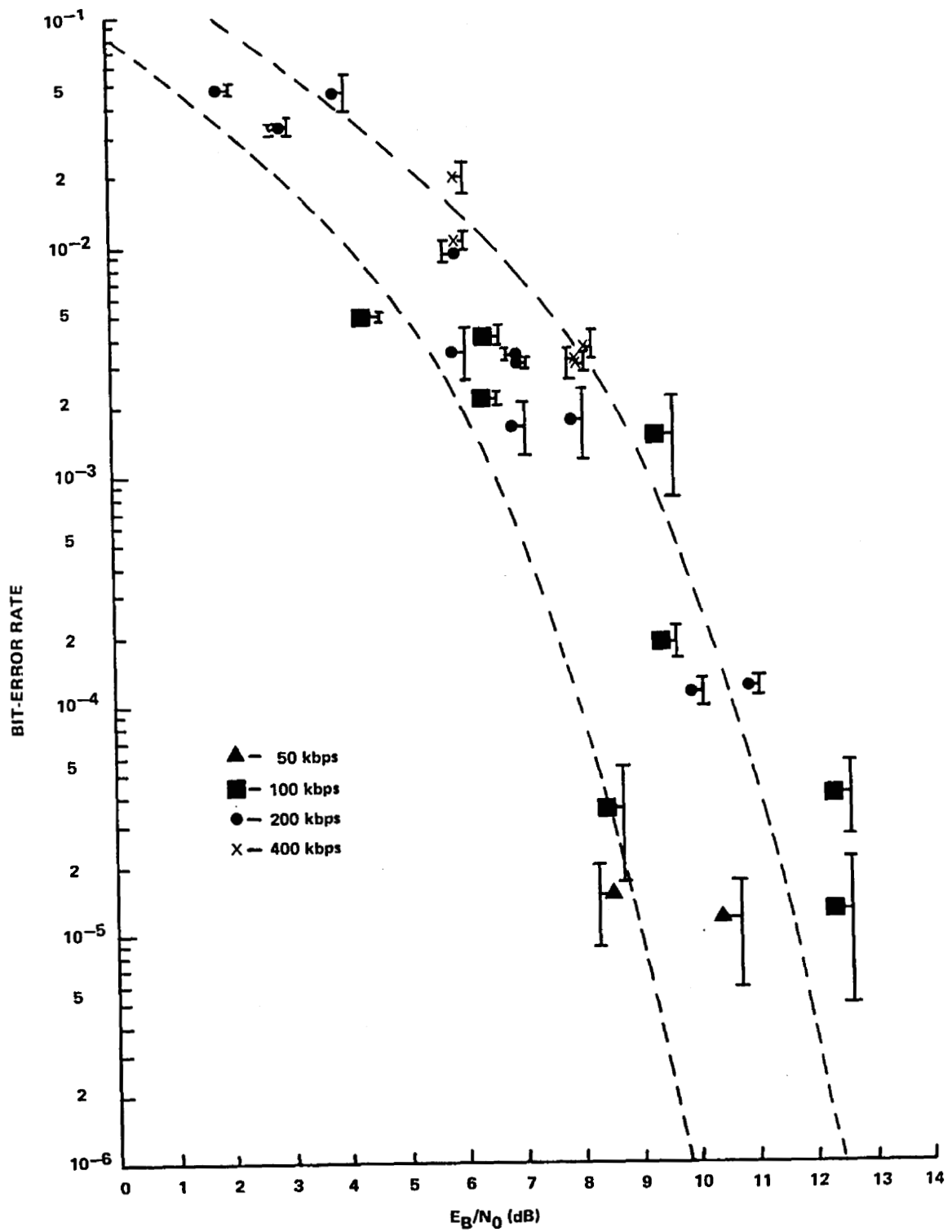


Figure 12-9. Bit-Error Rate vs. Bit-Energy to Noise-Power-Density Ratio for Revolution 4576

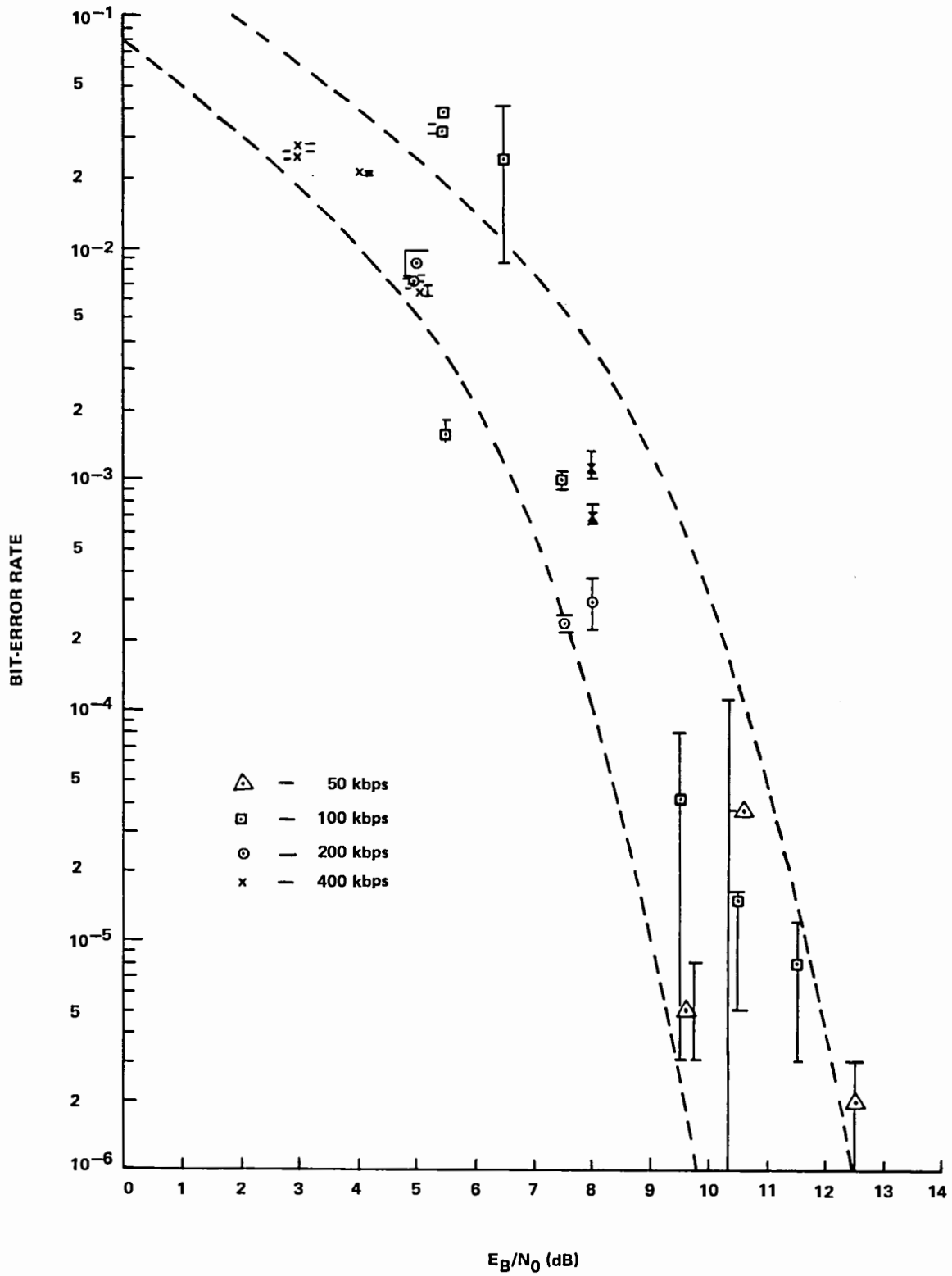


Figure 12-10. Bit-Error Rate vs. Bit-Energy to Noise-Power-Density Ratio for Revolution 4764

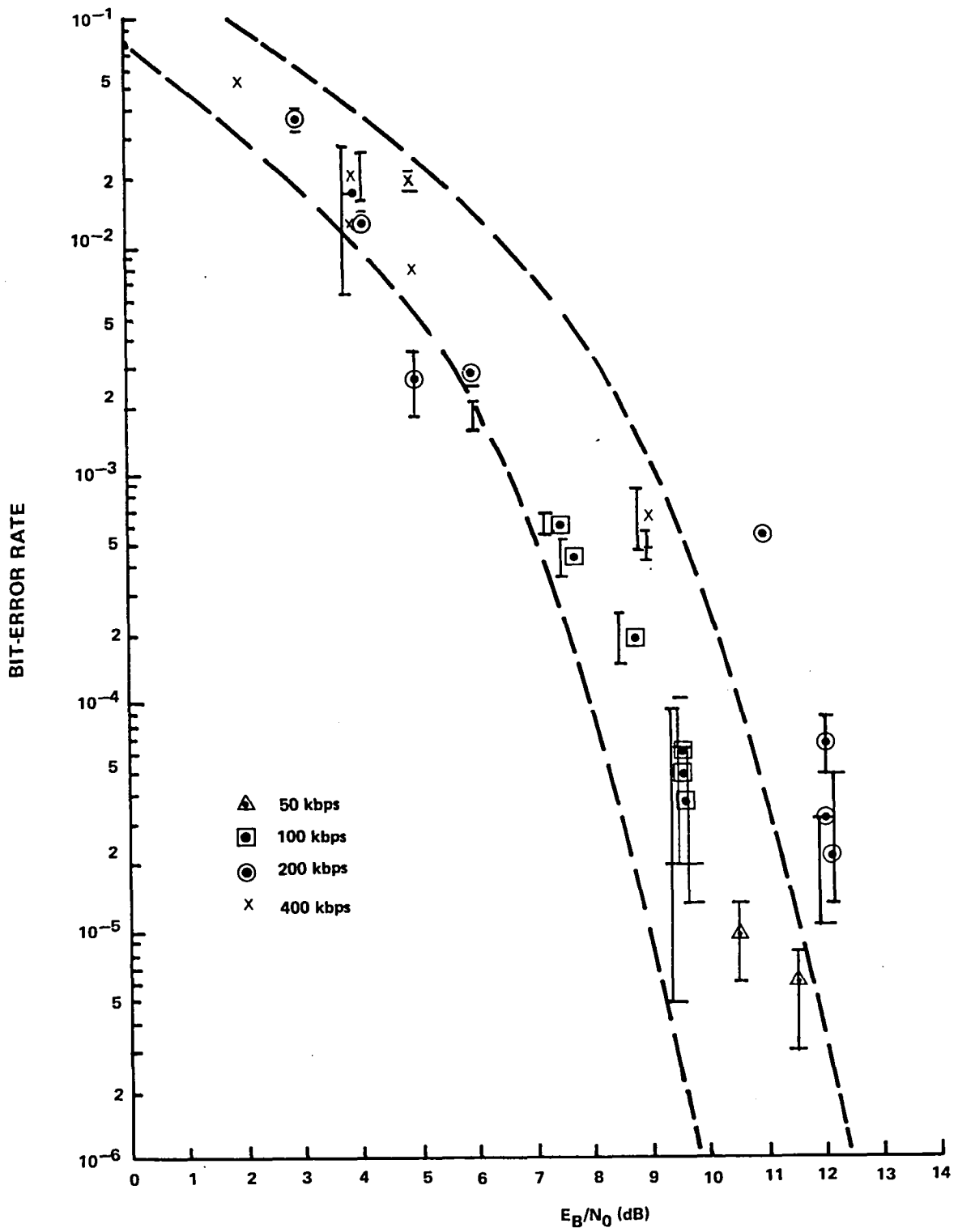


Figure 12-11. Bit-Error Rate vs. Bit-Energy to Noise-Power-Density Ratio for Revolution 4765

The carrier-to-noise ratio was measured at the Madrid Terminal and was reported in conjunction with the bit-error rate output of the delay-lock-loop code correlation synchronizer. The reported carrier-to-noise ratios were measured in the experimental bit-rate bandwidth that was then converted to unity bandwidth and allowance made for carrier drop to arrive at the E_B/N_0 scale along the abscissa.

Figures 12-12 through 12-14 show typical Nimbus-6 orbits as tracked by ATS-6 along with the measured and predicted carrier-to-noise ratios for these orbits. These data were found to agree within 2.3 dB.

IPD Processed DEM Data—Approximately 75 percent of the DEM recorded data processed by the Information Processing Division was manually checked to ascertain burst errors in the PN code bit pattern. The computer program used to process the DEM data after the raw data had been digitized, was initialized to print data records of 160 frames each for each bit rate processed. Each file was also analyzed to determine the bit error distribution. The number of bit errors in each of the 2047 data bit positions (128 words of 16 bits each) was totaled for each file; only good frames were included in the count. The results of the processed DEM data showed a uniform error distribution in the PN bit stream.

Multipath Results

The unique geometry requirements that permitted this experiment to be performed were satisfied by either the GEOS-3 or Nimbus-6 satellites operating with ATS-6 in a satellite-to-satellite configuration. In addition to the scheduled times specifically designated for multipath tests that were performed with an unmodulated carrier, data were also taken during other T&DRE activities. It was seen during these joint ventures that multipath data analysis was most difficult because the carrier was modulated with ranging data, telemetry, etc. In some instances, the modulation completely obscured the specular multipath component. Table 12-5 presents a summary of the total data collected, satellite identification, and the presence or absence of a modulated carrier.

Table 12-6 summarizes the data taken as a function of the grazing angle at the specular point for each of the satellite configurations used in the experiment. Specular multipath signals were measured for a total of 25.08 minutes. The grazing angles for the observed multipath signals ranged from 0.3 degree to 11.9 degrees. Initially, the experiment was configured to operate in the normal satellite track mode with both ATS-6 and the user satellite antennas oriented to provide the maximum gain along the direct path between the two satellites. For this mode, the ability to detect signals reflected from the Earth was limited to grazing angles of approximately 5 degrees for GEOS-3, 10 degrees for Apollo, and 7 degrees for Nimbus-6. These limitations were based on the available transmitted power and the antenna pattern for each satellite.

In December 1975, the experiment was reconfigured to permit the ATS-6 antenna to track the specular point while the user satellite antenna was pointed in the direction of ATS-6. Beam switching techniques were used to select the ATS-6 antenna beam that optimized gain in the specular direction. The increased gain in the direction of the specular point extended the range of measurement

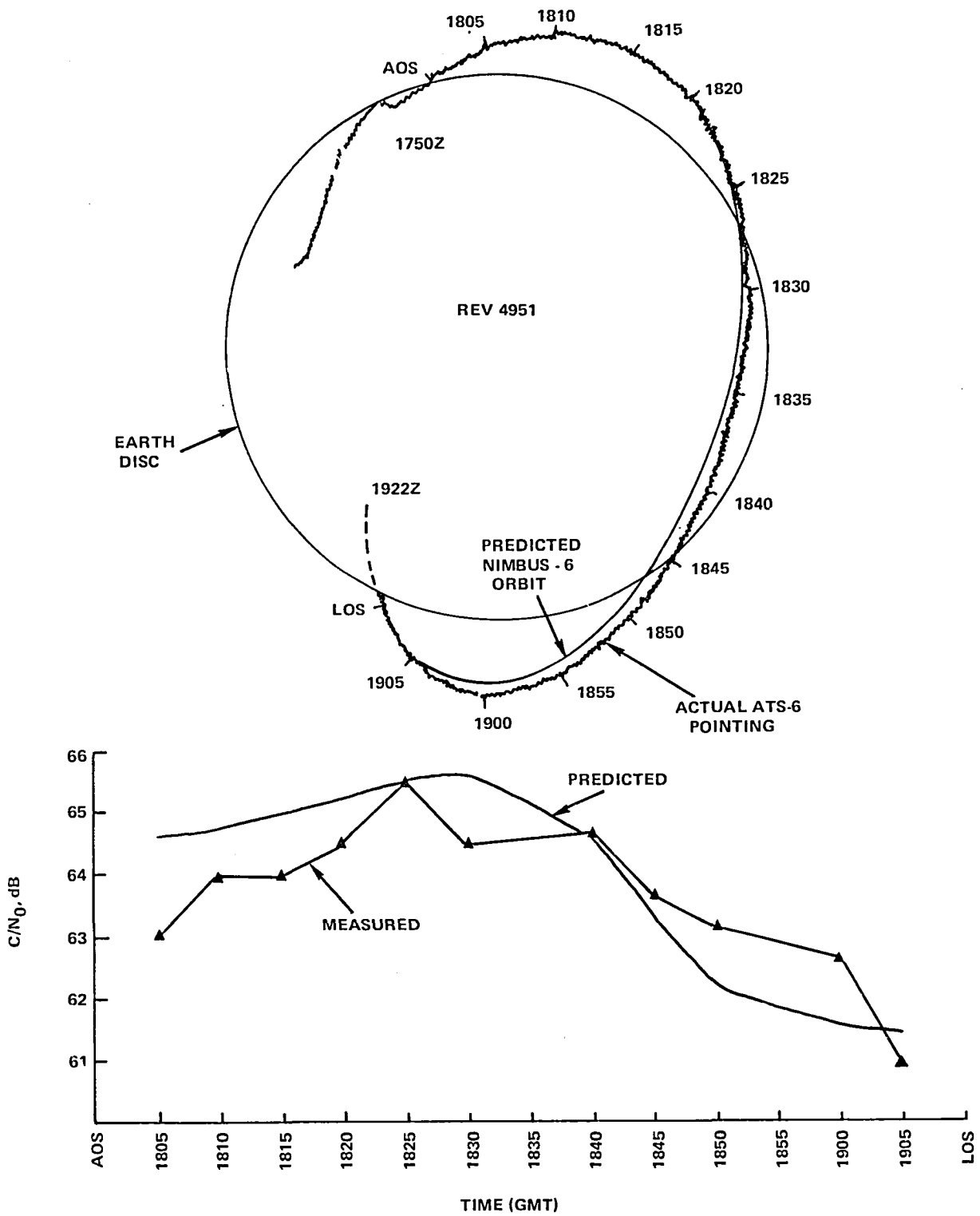


Figure 12-12. Predicted and Measured Carrier-to-Noise Power Density Ratios as a Function of Time for Nimbus-6 Revolution 4951

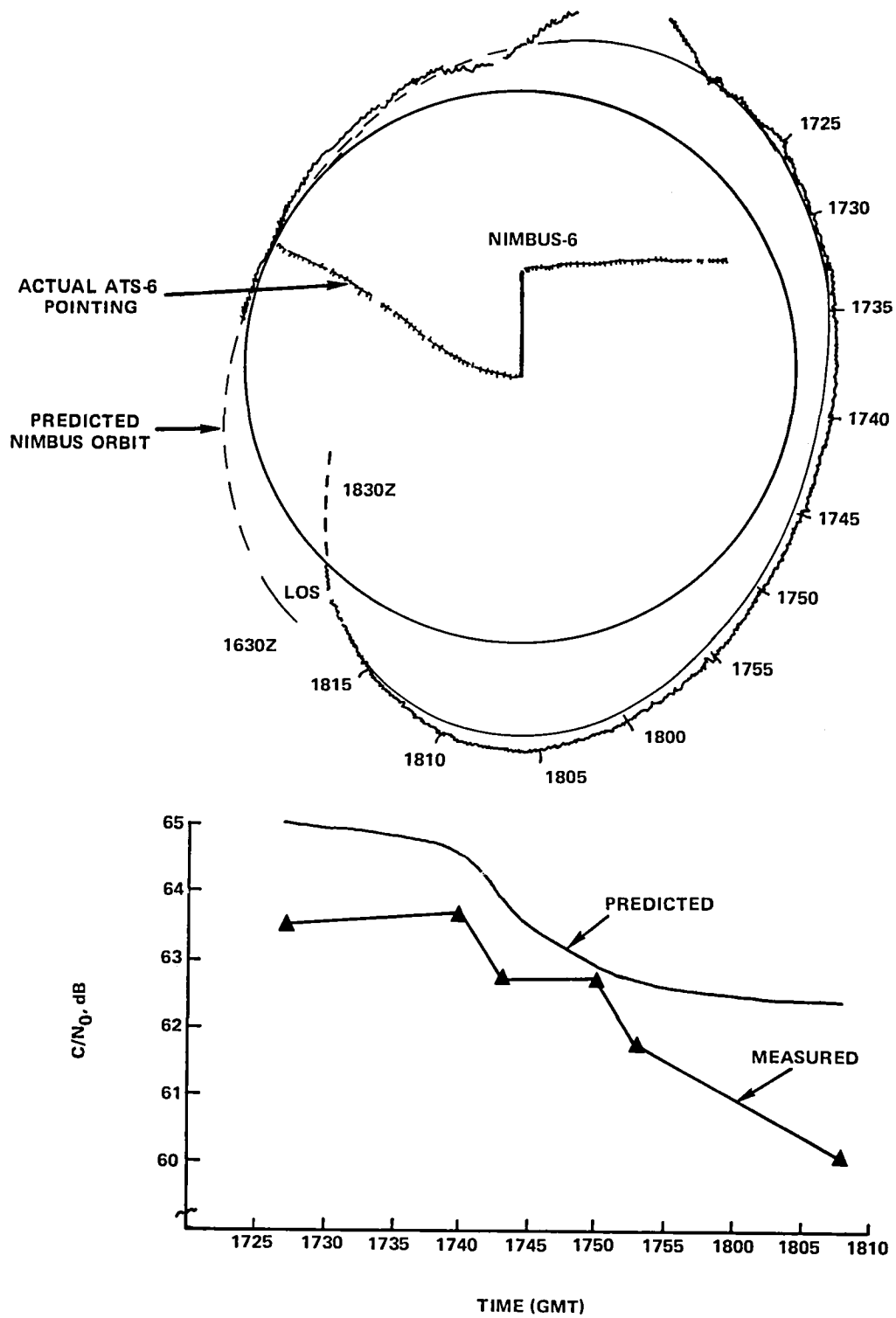


Figure 12-13. Predicted and Measured Carrier-to-Noise Power Density Ratios as a Function of Time for Nimbus-6 Revolution 4763

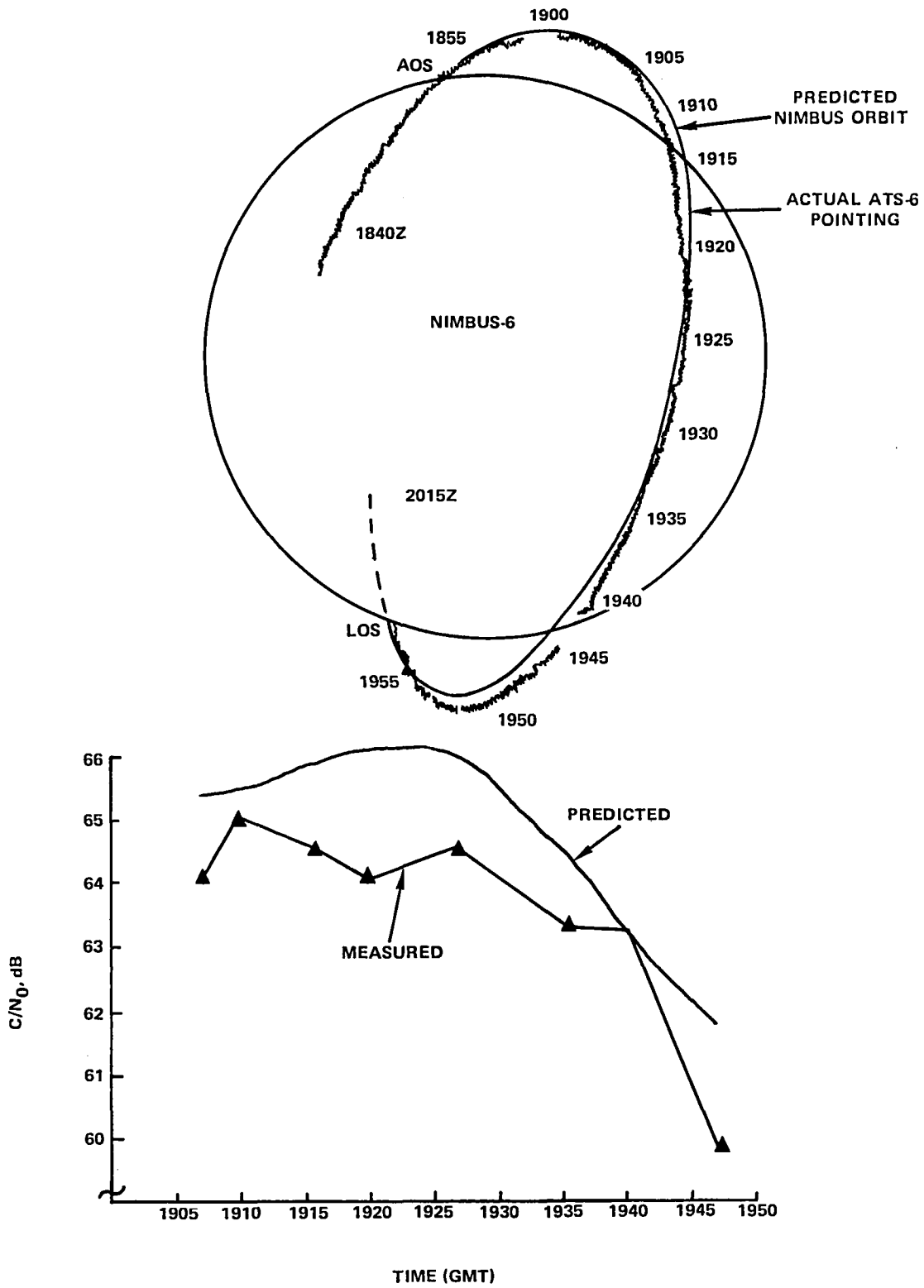


Figure 12-14. Predicted and Measured Carrier-to-Noise Power Density Ratios as a Function of Time for Nimbus-6 Revolution 4764

Table 12-5
Minutes of Multipath Data Recorded

	GEOS-3	Nimbus-6	Apollo	Total
Modulated				
Carrier	384.9	178.6	0	563.5
Unmodulated				
Carrier	129.4	380.43	2006.9	2516.7
Total Data	514.3	559.03	2006.9	3080.2

and increased the frequency of multipath detection as shown in Table 12-6. A Nimbus-6 orbit and corresponding specular point trace for Nimbus-6 revolution 2795 is shown in Figure 12-15.

For each satellite pass, during which significant multipath effects occurred, the data were analyzed to determine the normalized carrier-to-multipath ratios, grazing angle, and reflecting surface characteristics. The normalized carrier-to-multipath ratio showed a variation of 0.5 to 24 dB over the total set of measurements. All multipath incidents occurred at grazing angles ranging from 1.0 to 11.9 degrees except one at 0.3 degree. The majority of the multipath occurrences were noted where the ground surface was frozen Arctic seas or an Arctic land mass with packed snow or ice. Several multipath occurrences were also measured over sea water and normal land surfaces. The percentage of time during which the carrier-to-multipath ratio was in a given range while the specular point was being tracked by ATS-6 is summarized as follows:

<u>C/MP, dB</u>	<u>Percent of Time Measured</u>
2.5 to 5	3.53
5 to 10	9.47
10 to 15	11.3
15 to 20	14.9
20 to 25	4.5
>25 (no multipath observed)	56.3

Figure 12-16 shows an example of the multipath signals measured when the specular point was tracked during Nimbus-6 revolution 2795. The corresponding specular point ground track was plotted on a North Polar region map for the same Nimbus revolution. It is shown in Figure 12-17. A typical power spectral density plot from the X-Y plotter, incorporated in the ubiquitous spectrum analyzer, is shown in Figure 12-18. The direct and indirect signals are displayed with a frequency separation equal to the Doppler difference.

Table 12-6
Minutes of Multipath Data Analyzed Relative to Grazing Angle (ϕ)

GEOS	$\phi \leq 2.5^\circ$	$2.5^\circ < \phi \leq 5.0^\circ$	$5.0^\circ < \phi \leq 10.0^\circ$	$\phi > 10.0^\circ$
Data Analyzed	21.03	27.76	42.64	422.87
Multipath Observed	0.6	0	*	*
Multipath Occurrence	2.85%	0.0%	*	*
Nimbus	$\phi \leq 2.5^\circ$	$2.5^\circ < \phi \leq 5.0^\circ$	$5.0^\circ < \phi \leq 10.0^\circ$	$\phi > 10.0^\circ$
Data Analyzed	28.25	45.35	96.33	280.41
Multipath Observed	1.30	0.50	0	*
Multipath Occurrence	4.60%	1.10%	0.0%	*
Apollo	$\phi \leq 2.5^\circ$	$2.5^\circ < \phi \leq 5.0^\circ$	$5.0^\circ < \phi \leq 10.0^\circ$	$\phi > 10.0^\circ$
Data Analyzed	60.52	86.92	207.64	1651.82
Multipath Observed	0.6	0	0.2	*
Multipath Occurrence	0.99%	0.0%	0.10%	*
Nimbus**	$\phi \leq 2.5^\circ$	$2.5^\circ < \phi \leq 5.0^\circ$	$5.0^\circ < \phi \leq 10.0^\circ$	$\phi > 10.0^\circ$
Data Analyzed	21.49	19.35	31.37	36.48
Multipath Observed	2.6	7.28	9.19	2.75
Multipath Occurrence	12.38%	37.62%	29.29%	7.54%

*Measurement range exceeded

**Specular point tracking with ATS-6

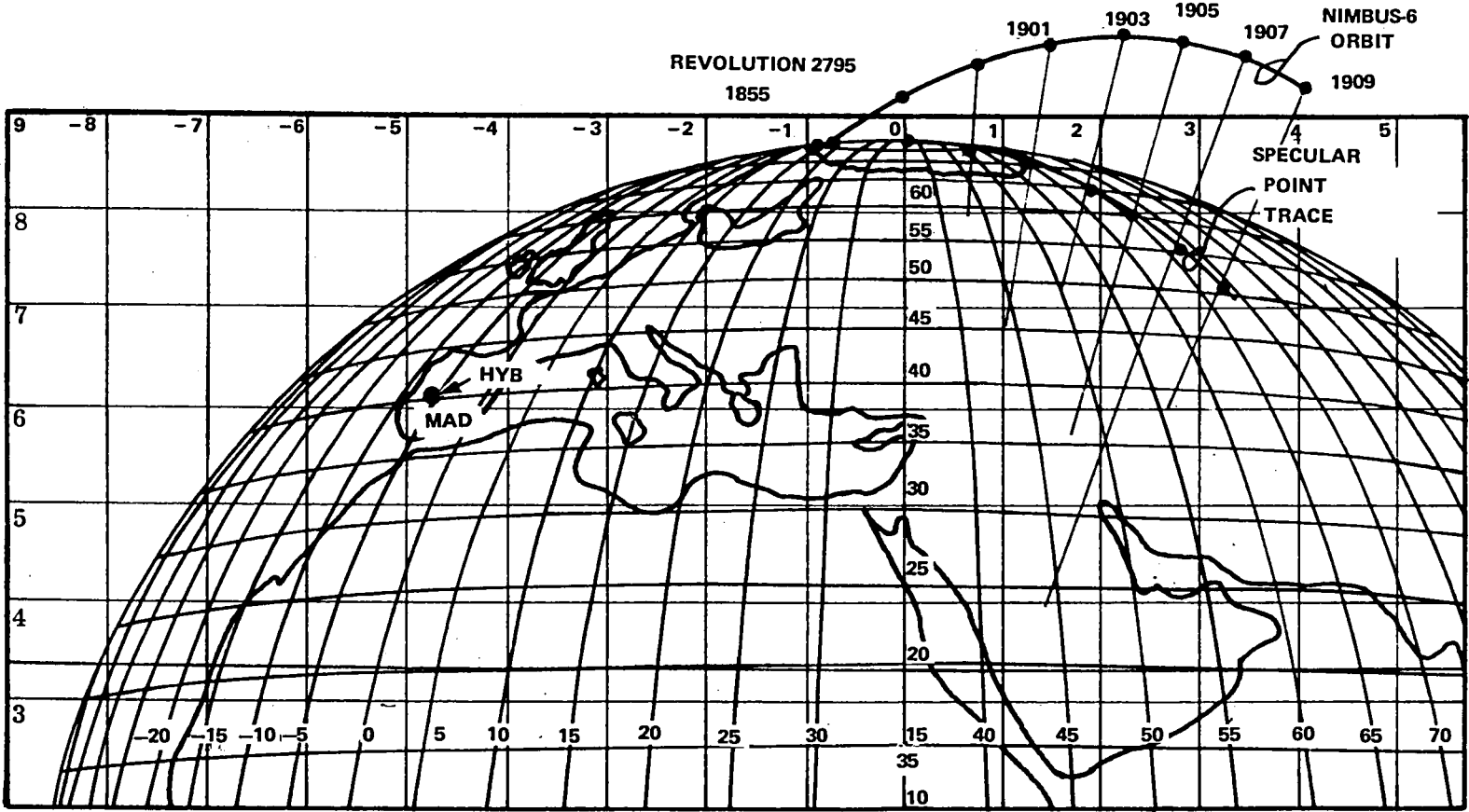


Figure 12-15. Nimbus-6 Orbit and Corresponding Specular Point Trace for Nimbus-6 Revolution 2795

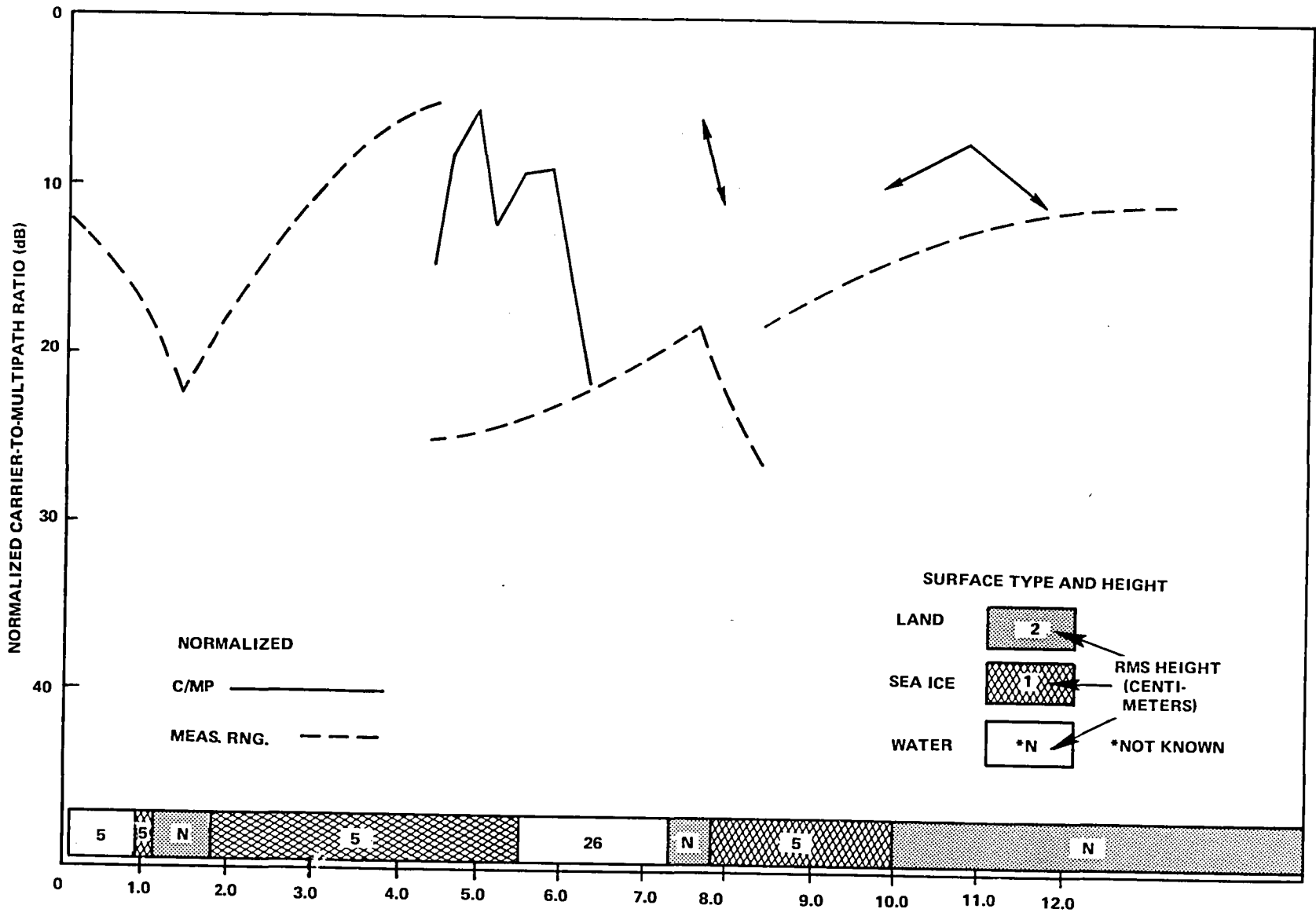


Figure 12-16. Normalized Carrier-to-Specular Multipath Ratio Measured During Nimbus-6 Revolution 2795

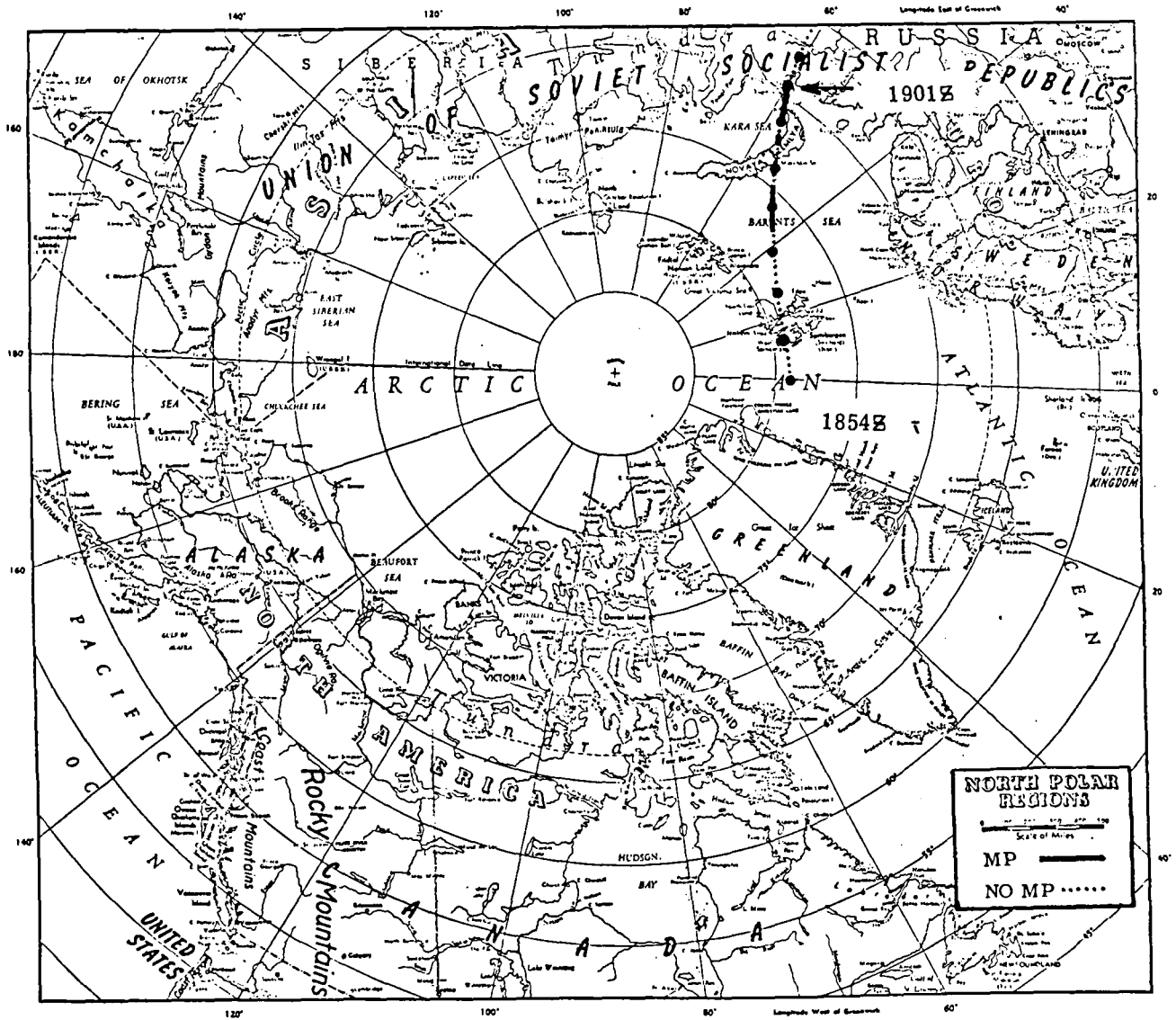


Figure 12-17. Specular Point Ground Track for Nimbus-6 Revolution 2795

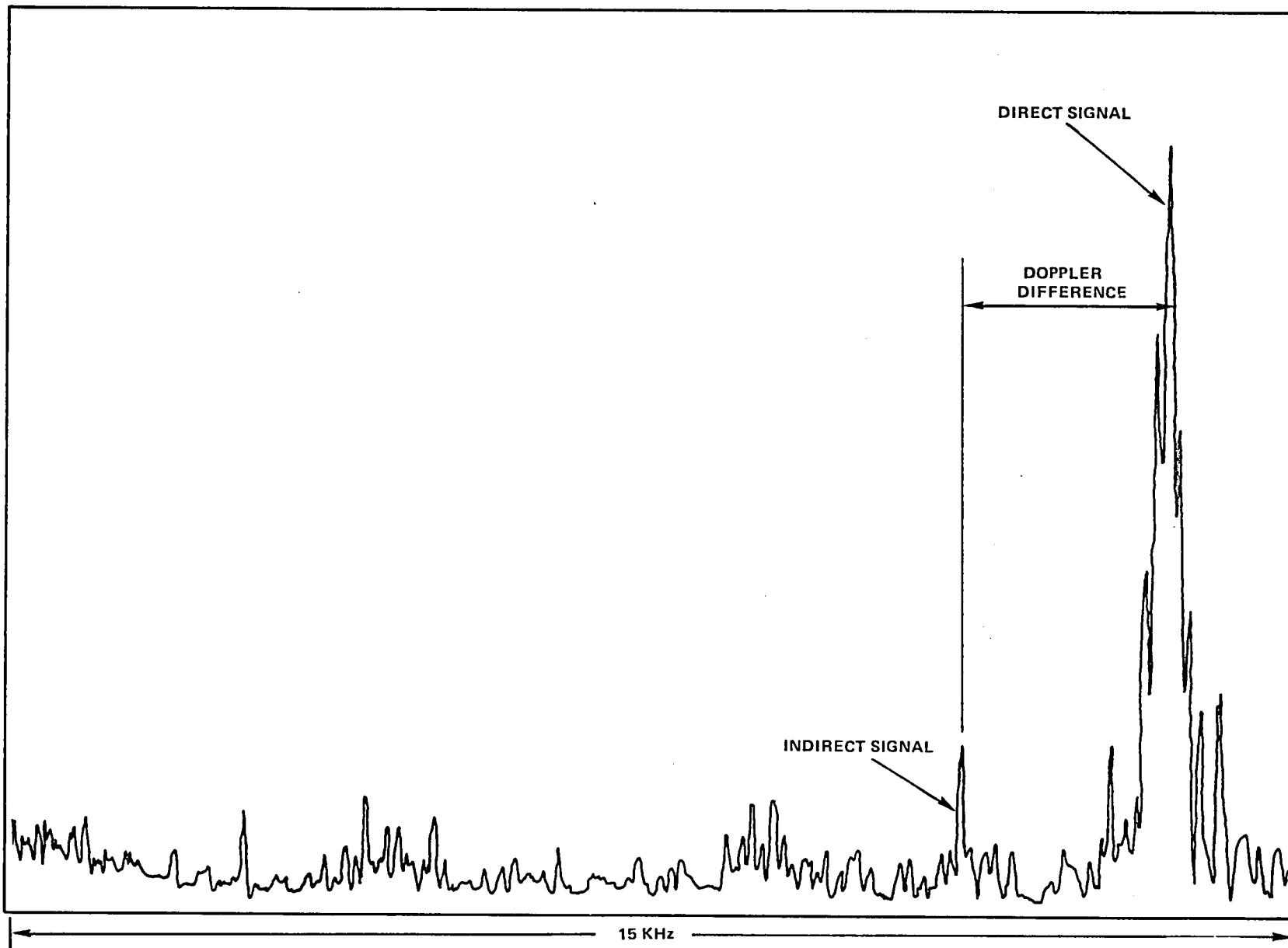


Figure 12-18. Typical Power Spectral Density Plot

Spacecraft Telemetry

Versatile Information Processor—The versatile information processor data, as relayed by ATS-6 during this experiment, were found to be operationally identical to the data received at a STDN station during a scheduled pass.

Limb Radiance Inversion Radiometer—A special limb radiance inversion radiometer (LRIR) data analysis computer program was used to accomplish a comparison of the real-time satellite relay and the recorded LRIR data. This comparison indicated that these data were almost identical, which validates that acceptable LRIR data could be obtained using a satellite relay.

Temperature Humidity Infrared Radiometer—A comparison of the temperature humidity infrared radiometer (THIR) data from the high data rate storage system (HDRSS) and T&DRE is shown in Figure 12-19. The T&DRE THIR data were found to be less noisy than the HDRSS data because of limitations of the Nimbus-6 onboard recorders used to record the “reference” HDRSS data.

Data Relay/Command Relay Results

The relay of commands to Nimbus-6 via ATS-6 was considered successful. Problems were encountered on several occasions but, in most cases, these were attributed to ground equipment problems.

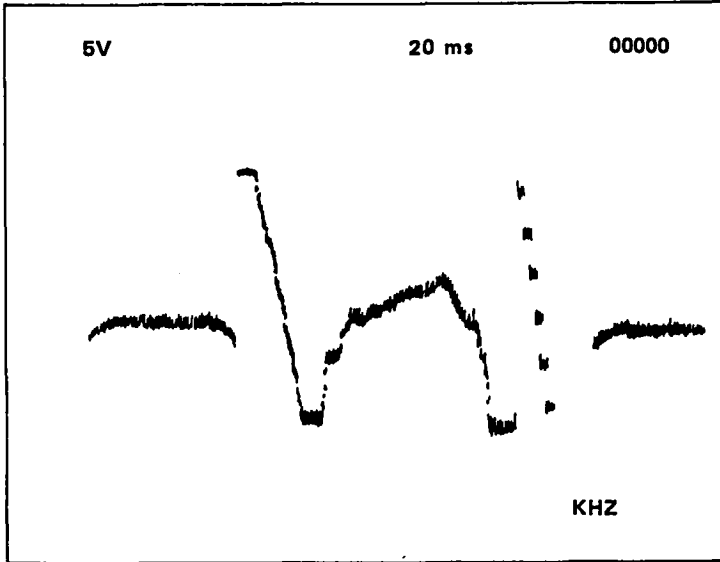
Tracking

The ATS-6 onboard program track mode was usually used to control its pointing during the tracking of Nimbus-6 and GEOS-3, and the pointing was generally maintained within 0.05 to 0.1 degree. The monopulse tracking technique was employed during data acquisition from Nimbus-6 and was found to give enhanced experiment performance. In general, the tracking accuracy with monopulse was maintained to within 0.1 degree or better, which resulted in a 2- to 3-dB improvement in signal level compared to the results obtained using the program track technique. Monopulse tracking eliminated those errors that were introduced by the use of old ephemeris data that were inputs for the program track operations.

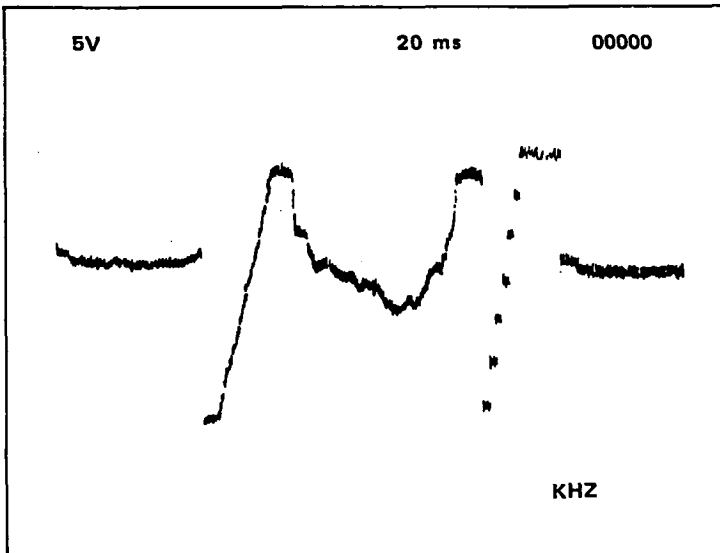
Monopulse tracking was accomplished by ATS-6 on the Nimbus-6 carrier at 2253 MHz (down-converted to 153 MHz). Use of this frequency allowed ATS-6 to be configured with the 12-MHz filter in the i.f. amplifier (150 to 162 MHz). The monopulse driver module in the ATS-6 i.f. amplifier mixed the 153-MHz monopulse signal with a 150-MHz local oscillator signal to obtain a 3-MHz difference signals for processing by the monopulse receiver in the narrowband mode.

When operating with the GEOS-3 satellite, it was necessary to use the 40-MHz filter in the ATS-6 i.f. amplifier (130 to 170 MHz) to receive the GEOS carrier of 2247 MHz (downconverted to 147 MHz). This caused a decrease in S-band link performance and decreased the signal-to-noise ratio (S/N) in the monopulse receiver by 3 dB because of the noise foldover in the driver module. Because of these effects, the GEOS-3 satellite was not tracked using the monopulse technique, since the S-band signal received at ATS-6 was found to be below monopulse threshold.

NIMBUS TELEMETRY DATA
THIR (TEMPERATURE, HUMIDITY, INFRARED RADIOMETER)
6.7N DATA DAY 324 (20 NOV 75) 2047Z



PLAYBACK FROM
NIMBUS ON-BOARD
RECORDER



DIRECT
VIA ATS-6

NOTE: DATA INVERSION OCCURRED DURING THE NIMBUS-6 DATA PLAYBACK.

Figure 12-19. A Comparison of Recorded and Relayed THIR Data

Figure 12-20 is a sample of the ATSOCC tracking display used for T&DRE to demonstrate a comparison of program and monopulse tracking. The display shows the Earth's limb, the predicted Nimbus-6 orbital plan, and the actual ATS-6 on-axis beam location during a pass of Nimbus-6. The variations between program track and monopulse track are noted.

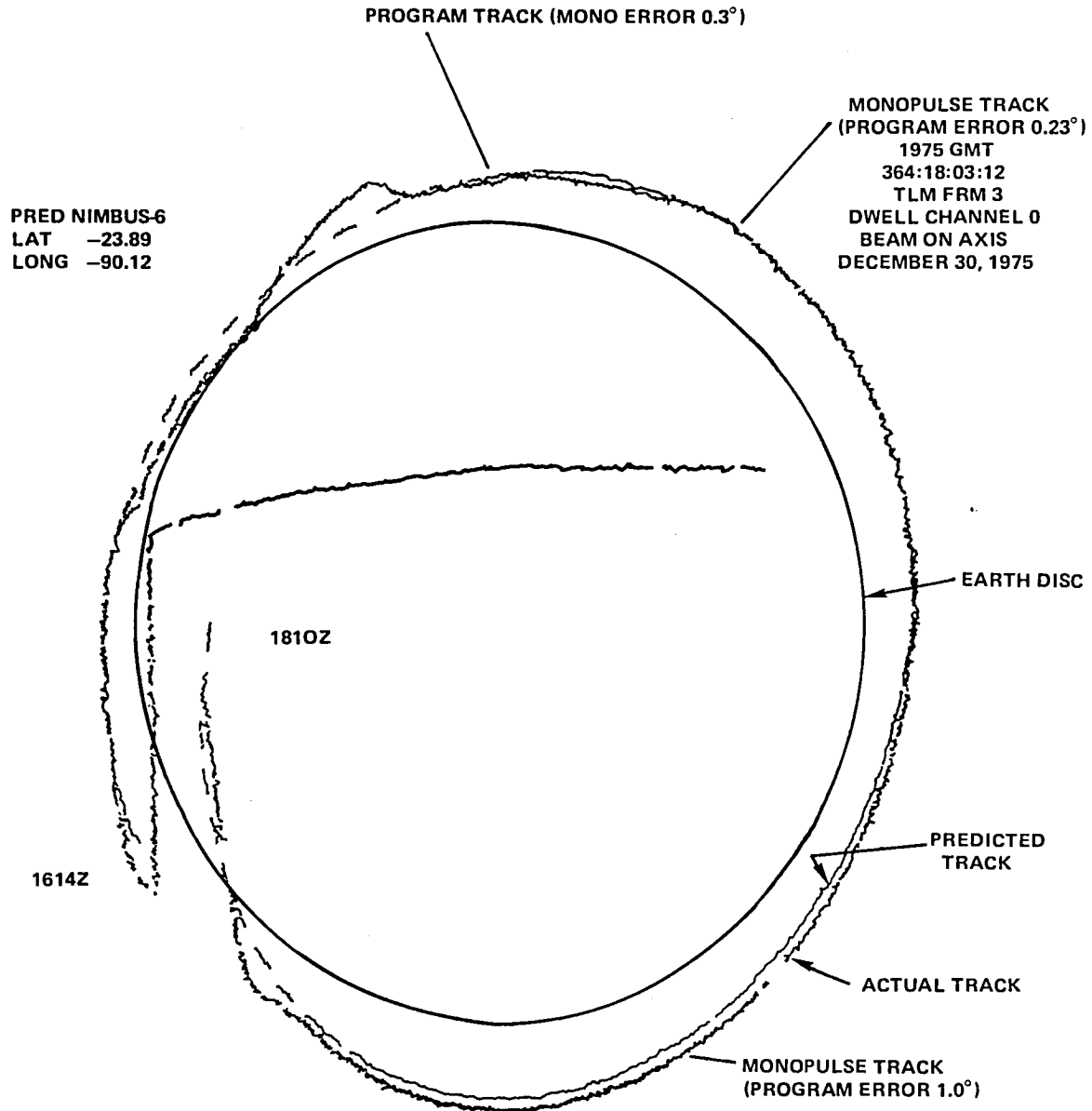
The electroscan technique of tracking was used to collect versatile information processor data from Nimbus-6. The electroscan technique was not useful for DEM data transmissions since it created large variations in the carrier-to-noise ratio. Range-rate data was successfully obtained from GEOS-3 using this technique, which permitted ATS-6 to receive a usable downlink signal in marginal satellite-to-satellite tracking configurations.

SUMMARY AND CONCLUSIONS

The Tracking and Data Relay Experiment was a cooperative effort to evaluate the performance of ATS-6. ATS-6 relayed commands, data, and tracking information between a ground station and a near-Earth satellite (i.e., Nimbus-6 or GEOS-3). One of the major objectives of the experiment was to demonstrate the ability to perform long arc tracking of a near-Earth spacecraft along with the capability of relaying the data created by the increased orbital coverage.

The ability to command low altitude spacecraft and thus control onboard equipment was demonstrated by relaying commands through a geosynchronous satellite. The effectiveness of a geosynchronous satellite acting as a relay of transmissions to and from a near-Earth satellite as opposed to direct transmissions to an Earth station was demonstrated. The predictability of a satellite-to-satellite tracking system measurement resolution was also demonstrated. Resolution of two meters in range and 0.05 cm/sec in velocity was realized with the system. The tracking techniques used with GEOS-3 demonstrated that short-arc orbit solutions can be used with Earth gravity anomaly detection.

The accuracy of satellite-to-satellite orbit determination depended on the refresh rate of the ephemeris data of the geostationary satellite. It was found that trilateration techniques should be employed to reduce synchronous satellite position errors on a periodic basis in support of satellite-to-satellite tracking.



	<u>PITCH</u>	<u>ROLL</u>	<u>ERR</u>	<u>PITCH</u>	<u>ROLL</u>	<u>IN-TK</u>	<u>X-TK</u>	<u>IF#</u>	<u>AGC</u>
PRED	-6.946	-3.699	O-P	-0.0074	1.899	1.884	0.2383	1	-102.6
OBSVD	-6.953	-1.800	MONO	0.0051	0.0081	0.0074	0.0061	2	- 83.39
DOC	0	0	DOC	0	-7.250	-7.189	0.9382	3	- 88

Figure 12-20. ATSOCC Tracking Display Showing Variations Between Monopulse and Program Track

CHAPTER 13

APOLLO-SOYUZ TEST PROGRAM

INTRODUCTION

The ATS-6 planned mission envelope included 18 experiments, one of which was the Apollo-Soyuz television coverage experiment (ASTP-TV) and another the Satellite Instructional Television Experiment (SITE) to mass broadcast educational television programs over the subcontinent of India. These two experiments required ATS-6 to be repositioned above 35° East longitude. This repositioning was completed on June 20, 1975.

The manned U.S. Apollo spacecraft was the 18th in the NASA manned space flight program. Apollo, with T. P. Stafford, V. Brand, and D. K. Slayton aboard, was launched on July 15, 1975, from Kennedy Space Center and injected in a circular orbit with an apogee of 2300 kilometers, a perigee of 219 kilometers and an inclination of 51.8°. Total mission flight time was 217 hours and 28 minutes with splashdown and recovery in the Pacific Ocean occurring on July 24, 1975.

The U.S.S.R. Soyuz spacecraft was launched earlier with approximately the same orbital parameters; and the joint Apollo-Soyuz docking occurred on the 17th of July when mutual experiments between the crews were conducted.

The mission of the Apollo (U.S.)-Soyuz (U.S.S.R.) Test Program (ASTP) was markedly enhanced by the employment of ATS-6 since it provided approximately 55 minutes of communications coverage for every spacecraft revolution of the Earth (90 minutes), versus the 5 to 7 minutes obtainable without the use of ATS-6. (See Figure 13-1.)

Within this employment concept, the primary objective was to originate high quality television signals aboard the Apollo and Soyuz spacecraft and to forward these signals via ATS-6 with minimum distortion to the Johnson Space Center (JSC) at Houston, Texas, for processing and distribution to the U.S.S.R. and the U.S. media. The subsidiary objectives were to:

- Accomplish the primary objectives using the technical facilities and services currently available to NASA in general and JSC in particular, without compromising the other mission requirements.
- Eliminate or minimize television media production constraints.
- Maximize live television coverage time by use of a synchronous relay satellite.

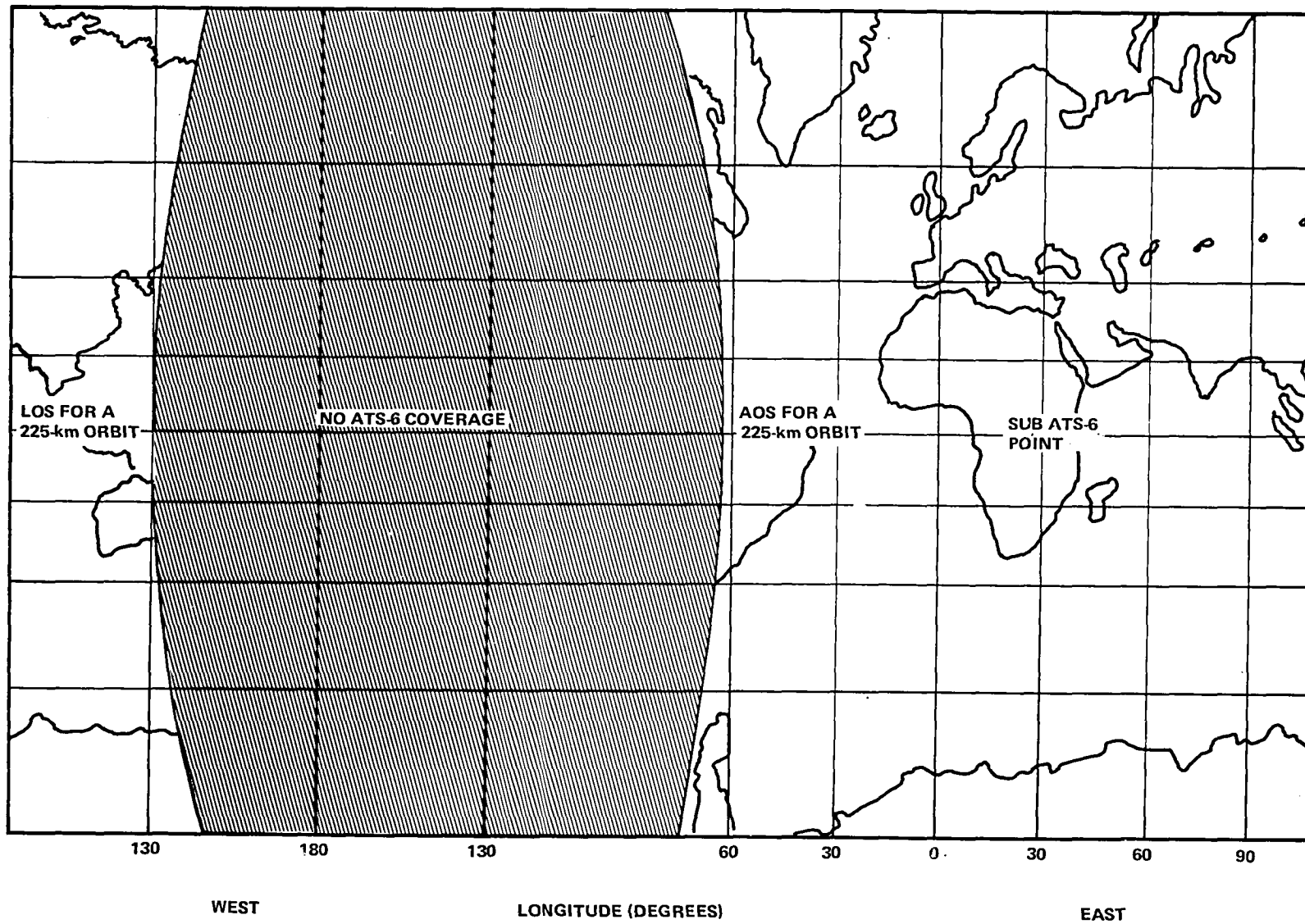


Figure 13-1. ATS-6 Coverage of ASTP

These objectives were to be augmented by:

- Highest quality video coverage of significant activities at JSC and the Kennedy Space Center (KSC).
- Good quality, compatible video from the U.S.S.R.
- Real-time video coverage of spacecraft recovery operations.
- Direct relay, recording, and other television support capabilities at STDN sites.

The CSM 111 acquired ATS-6 through the S-band high gain antenna (HGA), and ATS-6 relayed CSM information to and from the ground by C-band frequencies. All CSM uplink or downlink data requiring relay through ATS-6 was routed by the Madrid (Mad) tracking station. Most of the downlink through ATS-6 was either CSM frequency-modulated (fm) data recorder/reproducer (DRR) dump, or real-time, or video tape recorder CSM fm television. Periods of CSM real-time data on the phase-modulated (PM) downlinks were acquired through the CSM S-band omnidirectional antenna during normal contact with STDN. See Figure 13-2, Relay Services.

Mission Signal Sources for ASTP

The number of input television sources for ASTP were significantly increased over previous Apollo missions to include:

- Soyuz onboard cameras
- Mission Control Center (Moscow) cameras
- Soyuz launch area cameras
- Soyuz recovery area cameras
- Apollo command module and docking module cameras
- Mission Control Center (JSC-Houston) cameras
- Kennedy Space Center launch area cameras
- Apollo recovery area cameras
- Press conference television (JSC-Houston).

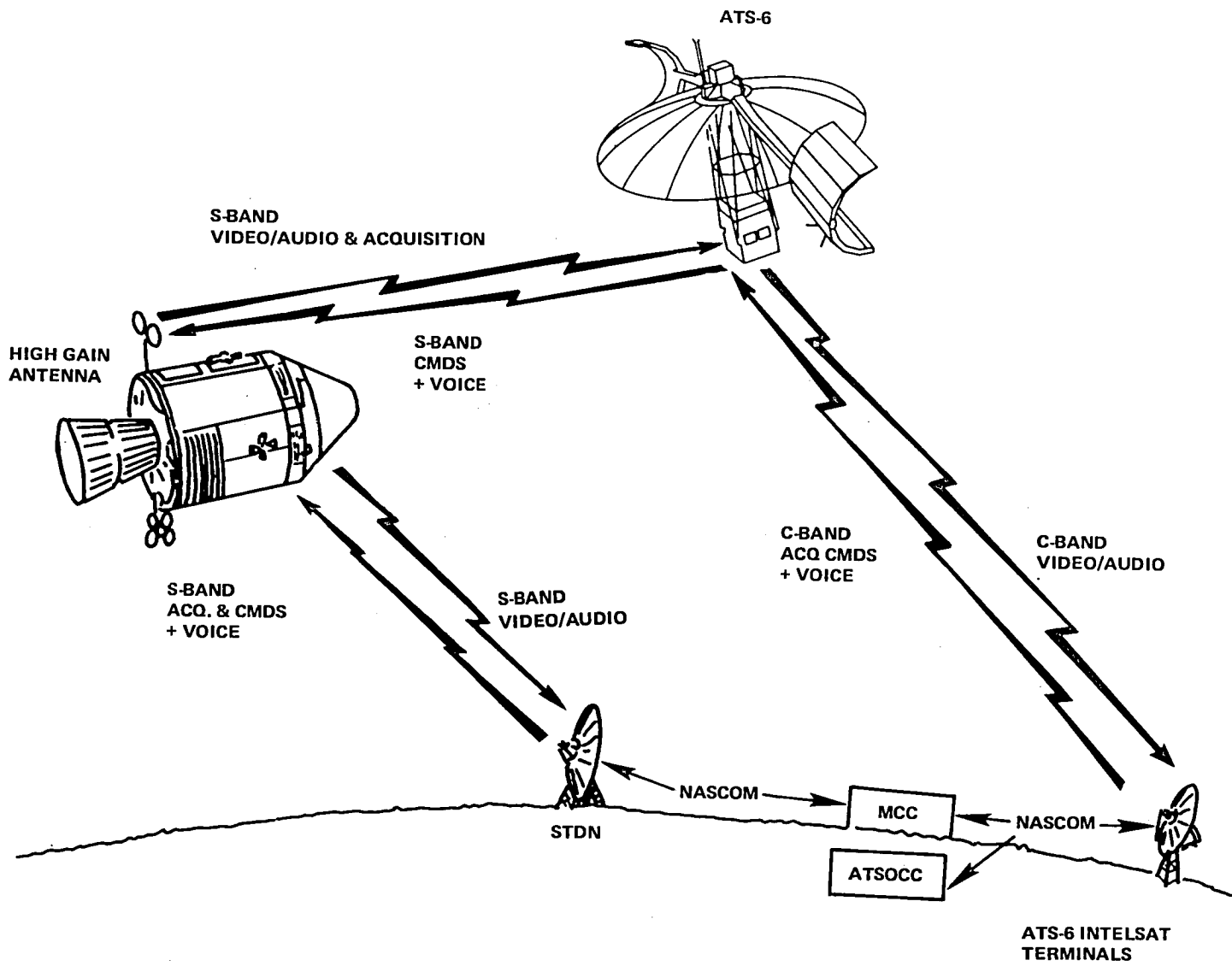


Figure 13-2. Relay Services (Apollo)

These signals were generated in a variety of scanning standards and formats that required conversion for compatibility with indigenous television systems. Scanning standards were the option of the originating country and conversion was the responsibility of the ultimate users.

Additional signal sources were developed as a result of standards conversion, color conversion, and video recording, as follows:

- Field sequential 625/50 to SECAM*
- SECAM to NTSC**
- Field sequential 525/60 to NTSC
- NTSC to SECAM
- Apollo onboard videotape playback
- NASA Buitrago videotape playback
- JSC-Building 8 videotape playback
- JSC-Building 30 videotape playback

For immediate evaluation of all video sources and transmission systems, a family of selected video test signals were interleaved at predetermined terminals. These test signals, in the full-field format, were used also during circuit alignment procedures.

ASTP Television Configuration

The ASTP television configuration was structured to accommodate the SECAM signals from the U.S.S.R., the field sequential signals from the Apollo spacecraft and the NTSC signals from KSC, JSC, and Apollo recovery. These three basic signal categories were treated as independent entities at JSC until transcoding and signal processing had transformed all signals into the NTSC format. In this domain, signals were correlated to be time-base and chrominance-phase coherent with a reference signal that was stabilized by the JSC Rubidium Standards.

U.S.S.R. Configuration

During the Apollo-Soyuz mission, the U.S.S.R. used four principal locations for the origination of video signals:

- Mission Control Center (Kalinin)
- On board Soyuz

*SECAM—Sequential Couleurs a Memoire (III) color (U.S.S.R.)

**NTSC—National Television System Committee color (U.S.)

- Soyuz Launch Complex (Bayknur)
- Soyuz recovery area (Kazakhstan)

These signals were sequentially switched in Moscow, identified as Mission Control Center (MCC-M), relative to the programmed scenario and activity, and were released to the United States in the SECAM format. The SECAM television signal used a raster-scan rate and chrominance transmission mode that was incompatible with the U.S. standards; therefore, these signals had to be transcoded and converted in Europe before transmission to the Mission Control Center at Johnson Space Center, Houston, Texas, identified as MCC-H.

Figure 13-3 shows the U.S.S.R. configuration in simplified form.

Moscow Region Television—The Moscow Region was the gateway terminal for all video released to the United States and served as a major processing, distribution, switching, and origination point for ASTP television. Processing was performed by the Office of Telecommunications, which included frequency correction and color conversion of the Soyuz field-sequential video. This office also provided all the microwave, coaxial, and satellite transmission and interconnections.

The Soyuz field-sequential video from the tracking sites, and the SECAM video from the Soyuz launch and recovery areas entered the Office of Telecommunications building and were selectively switched into a video frequency corrector. This video frequency corrector was fashioned from a pair of video recorders, with the input machine functioning as a recorder and the second performing immediate playback. The playback machine was driven from synchronizing pulses supplied by a sync-pulse generator in the Moscow Television Center, which was also synchronized with the camera signals from the Mission Control Center; therefore, the three signal categories had time-base correlation. The timing error between Moscow-generated video signals and signals relayed from the remote sites was absorbed in the tape-slack between the two videotape machines.

Frequency-corrected signals were fed directly to the Moscow Television Center, if they arrived in the SECAM format, or were processed in the color converter if they arrived in the field sequential format; then the color-converted signals were dispatched to the Moscow Television Center for selection.

Video from the Mission Control Center (Kalinin) was transmitted to the Moscow Television Center for selection and retransmission to the United States. The Moscow Television Center served as the master switching point for selection of video dispatched to Houston, which included the MCC-M cameras, Soyuz color-converted signals, Soyuz launch and recovery activities, and videotape playback. The Moscow Television Center was the insertion point for all full frame and vertical interval test signals.

The Mission Control Center at Kalinin was equipped with five SECAM cameras to cover the flight activities in the control room and the U.S. specialists in the support area. These cameras were selectable at the MCC and dispatched to the Moscow Television Center. Unilateral transmission of each camera video to the Moscow Television Center was based on the availability of interconnecting circuits.

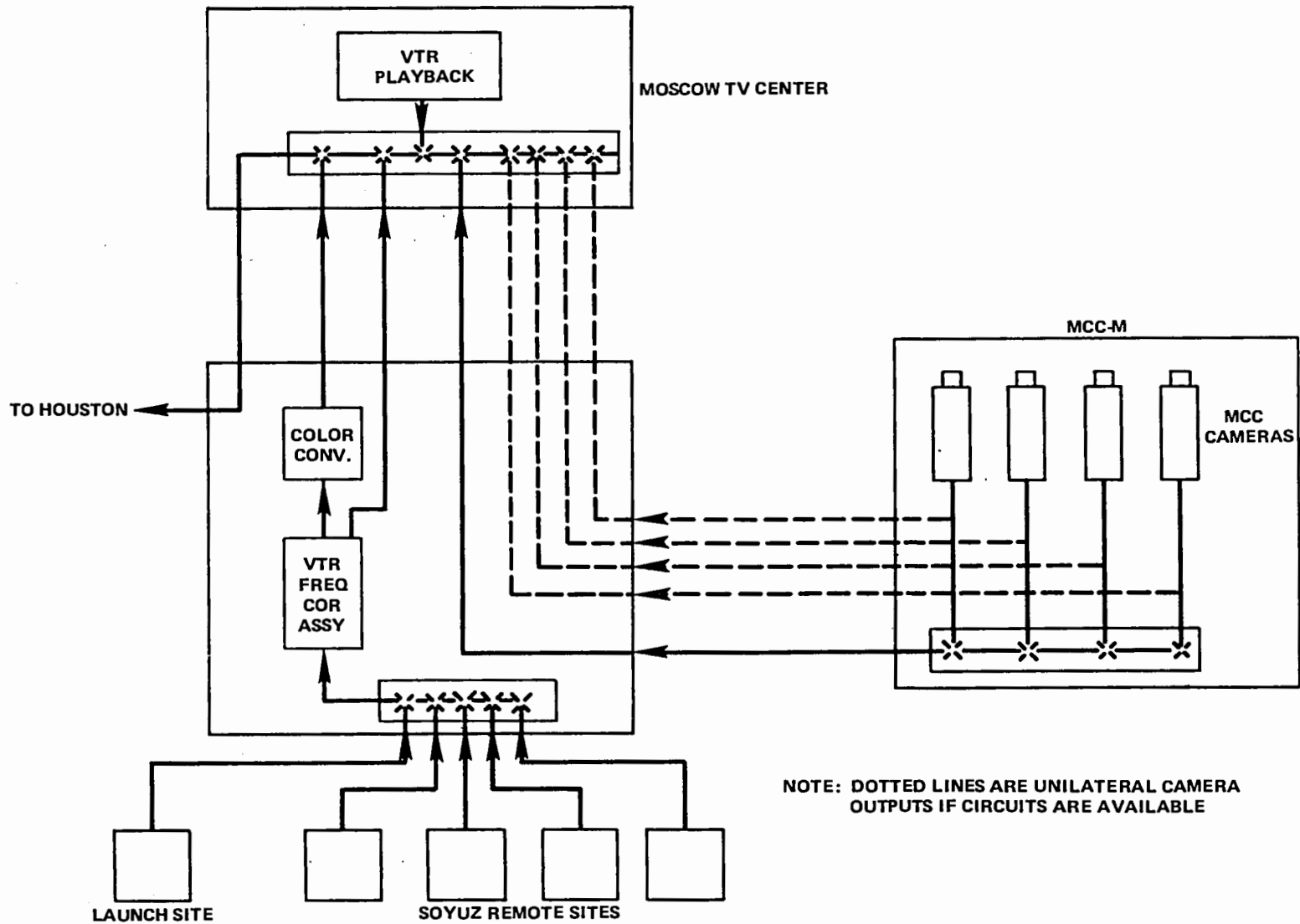


Figure 13-3. U.S.S.R. Television Configuration

Soyuz Onboard Camera Video—Four television cameras, two black and white, and two field-sequential color, were carried on board the Soyuz to cover the cosmonaut activities in the orbital module and the descent vehicle, with an externally mounted black and white camera to cover Apollo-Soyuz docking. Camera selection was made through an onboard switcher and transmitted to U.S.S.R. Ground Tracking Stations on the vhf downlink.

For the Apollo-Soyuz mission, the U.S.S.R. used nine tracking stations, four of which were capable of handling real-time television. These tracking stations with television facilities were:

- Petropavlovsk-Kamchatski (PPK)
- Ussuruisk (USK)
- Evpatoria (EVT)
- Dzhusaly (DJS)

The video, as received at these tracking stations, was relayed to the Office of Telecommunications in Moscow by terrestrial microwave and domestic satellite for frequency correction and color conversion to the SECAM format.

Tracking stations PPK and USK, EVT and DJS, in pairs, provided overlapping or tangent coverage on the majority of the orbits. On orbits where the groundtracks provided coverage from both of the contiguous tracking stations, no coverage was available from the other television-equipped contiguous pair of tracking stations. Some orbits had groundtrack to one station in each contiguous pair, and in some orbits only one tracking station was visible for television. During the mission, Soyuz video for uninterrupted periods ranged from 4 to 12 minutes.

Soyuz Launch—The Soyuz launch from Baykonur, near Tyuratam, was covered by four SECAM cameras, augmented by instrumentation cameras producing black and white video. These signals were transmitted to the Office of Telecommunications in Moscow by terrestrial microwave for frequency correction and dispatched to the Moscow Television Center.

Soyuz Recovery—The coverage of the Soyuz recovery near Kazakhstan was supplied by two SECAM cameras, positioned in separate helicopters. Each helicopter was equipped with a microwave relay with a nominal range of 100 kilometers for transmission of the camera video to a portable Earth station. Camera selection was accomplished by switching between the received microwave signals at the Earth station prior to transmission to the Office of Telecommunications in Moscow by a Molniya satellite circuit. The video was frequency corrected and dispatched to the Moscow Television Center.

Video Conversion and Transmission from Moscow to the U.S.—The video signals released in Moscow were transmitted in the SECAM format over a U.S.S.R. terrestrial microwave circuit through Riga, Tallin, to Helsinki. This segment of the microwave link was protected by automatic "fail-over" to a standby circuit, and was under the jurisdiction of the U.S.S.R. Posts and Telecommunications.

From Helsinki, the video was routed over terrestrial microwave through Stockholm, Copenhagen, to Hamburg.

This route-section was under the jurisdiction of the individual countries that it traversed, and was coordinated by the European Broadcast Union (EBU). This segment was not provided with automatic "fail-over" to alternate circuits, since all European circuits were under constant monitoring and reroute dispatch from the EBU Technical Control Centre in Brussels.

At Hamburg, the SECAM signal was optionally passed through a NASA-supplied time base corrector (TBC) before transcoding to the PAL* format. This TBC was required to reduce the time base instability of the incoming SECAM signal to within acceptable limits to permit transcoding. The time-base stabilized SECAM signal was fed simultaneously to the prime SECAM/PAL transcoder in Hamburg and to the back-up transcoder in Frankfurt. The Hamburg PAL signal was also fed to Frankfurt for protective switching and routing to Raisting, Germany.

At Raisting, the incoming PAL signal, with a raster-scan ratio of 625/50, was converted to the 525/60 National Television System Committee standard and uplinked to the Atlantic Ocean Major Path Intelsat Satellite, with downlinking to Andover, Maine, U.S.

The U.S. segment was by terrestrial microwave from Andover, Maine, to Johnson Space Center with intermediate Television Operational Control Centers (TVO) at Boston, New York, Chicago, Dallas, and Houston. A special bridging connection was applied at New York to supply U.S.S.R. video to the Goddard Space Flight Center and controlled release to the U.S. Congress in Washington. Circuit restoral and reroute procedures were implemented by the Bell System through their normal reporting routines.

U.S. Configuration

During the Apollo-Soyuz mission, the U.S. used five principal locations for the origination of video signals:

- Mission Control Center (JSC-Houston)
- On board Apollo
- Apollo Launch Complex (KSC-Cape Canaveral)
- Press conferences (JSC-Houston)
- Apollo recovery area (Pacific Ocean)

The video signals from these origination points were transmitted to JSC at Houston for processing and synchronization, then released to the U.S. and European networks as unilaterals and also in a fully integrated program format.

*PAL – Phase Alternation Line color (Europe)

In addition, a systematic selection of these signals, relative to the approved U.S.-U.S.S.R. television scenario, was dispatched to Moscow for release within the Soviet Union and to the Intervision Network. These transmissions originated in Houston in the NTSC format and were converted to the European PAL standards at Raisting and transcoded to SECAM at Prague.

Figure 13-4 shows the video configuration in simplified form.

The Apollo video configuration included the onboard cameras, ATS-6, and Madrid/Buitrago Complex. This group contained the major facilities for generation and transmission of the field sequential color television signals.

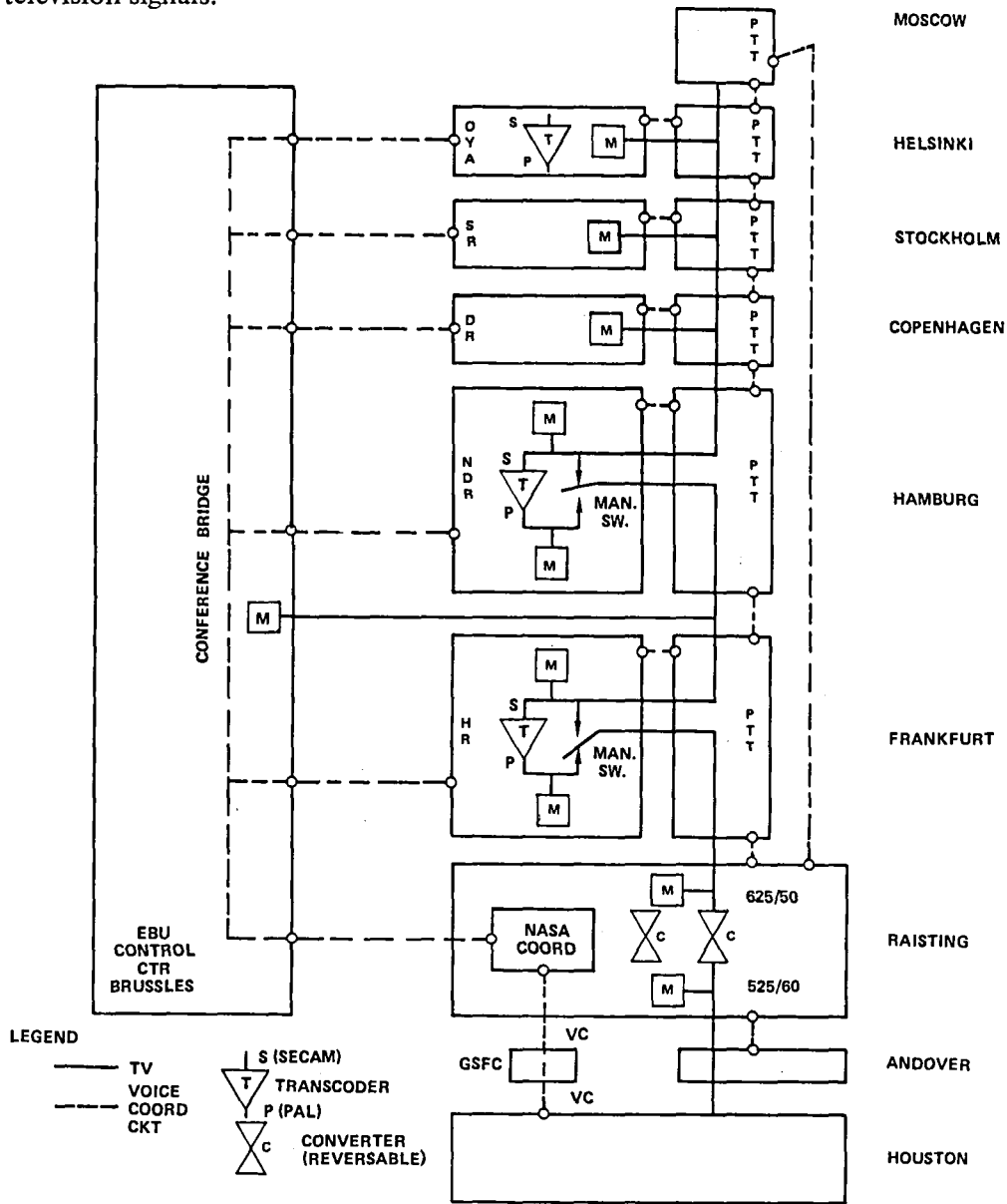


Figure 13-4. ASTP Video Moscow to Houston

Apollo Onboard Camera Video—Four field sequential color cameras were carried on board to cover the activities of the astronauts and cosmonauts in the Apollo command-service module (CSM) and docking module, with provisions for extending the coverage within the Soyuz orbital module. Eight mounting brackets were available for attaching a camera for improved viewing of activities on board.

All cameras were maintained in color-field and line-rate synchronization and selection was made remotely from Mission Control at Houston, with manual override capabilities for the crew.

The onboard video could be transmitted in real time to ground terminals either through ATS-6 or direct to STDN sites and simultaneously recorded by the onboard videotape recorder. Also, real-time video could be relayed by ATS-6 and videotape playback transmitted over the direct link to the STDN sites, with capability to reverse these input signals.

In addition to the field-sequential color video, vertical interval test signals (VITS), camera and color field identification pulses, camera temperature pulses, television audio, and central timing equipment pulse trains were systematically interleaved to provide a coordinated signal with all relevant auxiliaries.

Apollo/ATS-6 Relay—The Apollo/ATS-6 relay was a transmission system inaugurated for the Apollo-Soyuz Test Project that greatly expanded the continuous communications and television coverage periods between the spacecraft and Mission Control. In this new configuration, the main S-band signal from the Apollo CSM was directed toward ATS-6. The transponder within ATS-6 changed this signal to a C-band frequency and directed it to the NASA-leased Intelsat Earth Terminal at Buitrago, Spain. At this terminal, the communications and television information was demodulated in a specially-installed NASA terminal, and rerouted to Mission Control in Houston by the Atlantic Ocean Intelsat satellite and NASA Communications Network (NASCOM) circuits.

ATS-6 was launched May 30, 1974, into a geosynchronous orbit at an altitude of 35,869.7 km (22,288.4 statute miles) and originally positioned over the equator at 94° West longitude. Prior to the ASTP mission, ATS-6 was repositioned to 35° East longitude.

Apollo was launched into an orbit, inclined 51.8° to the Equator, at an altitude of 225 km (139 statute miles), with a revolution period of 88 minutes, 50.2 seconds. From this low-altitude orbit, Apollo was visible to ATS-6 for an average of 57.75 percent of each revolution, producing continuous communication and television contact for an average of 51.31 minutes. During each revolution, as Apollo approached the nonocculted position with ATS-6, the high gain S-band antenna was prepositioned to the predicted pointing angles for acquisition of the ATS-6 signals. Concurrently, the ATS-6 9.14-meter S-band antenna was slewed to predicted pointing angles at the horizon of the Earth. The Apollo high gain antenna array was configured with four wideangle S-band horn antennas centered within the cluster of four narrow-beam S-band parabolic-reflector antennas. When the S-band 2077.4-MHz signal from ATS-6 was acquired by Apollo through the wideangle horn antennas, the antenna system was transferred to the narrow-beam parabolic antennas. The reacquisition process in the narrow beam state included the automatic tracking mode that supplied continuous pointing-angle correction signals to maintain optimum contact between Apollo and ATS-6 as their relative positions changed during the orbital pass.

Simultaneously, the S-band 2256-MHz Apollo transmitted signal, as received by ATS-6, provided antenna pointing information for the 9.14-meter diameter reflector for contact with Apollo. This S-band 2256-MHz signal, frequency modulated for television and phase-modulated for high bit rate data, was changed to a C-band 3756-MHz signal and radiated to the ground receiving terminals at Buitrago and Madrid, Spain.

These ground terminals transmitted communications and command data to ATS-6 on a C-band 5952.4-MHz carrier, that was changed by the transponder to S-band at 2077.4 MHz for retransmission to the Apollo command-service module.

ATS-6 operational parameters were controlled by a NASA hybrid terminal, installed at the NASA STDN site at Madrid, while ATS-6 was stationed at 35° East longitude.

Madrid—During the Apollo-Soyuz mission, four terminal facilities in the Madrid area actively supplied support: Madrid STDN site, the hybrid terminal (collocated at Madrid STDN), Intelsat Ground Terminal (Buitrago), and the NASCOM Switching Center (Robledo).

- Madrid STDN. The Madrid STDN site functioned as one of the prime realtime video direct link stations during the ASTP mission. This role included processing and remoting to Johnson Space Center (JSC) any television received during an orbital pass or recording for later transmission. In principle, this was a backup mode to the television transmission relayed through ATS-6 and downlinked to the NASA terminal at Buitrago.

Video from the Madrid STDN site was relayed to NASA Buitrago by redundant terrestrial microwave circuits. The microwave segment from Madrid STDN to Prado Del Rey was a temporary installation for the mission period. The segment from Prado Del Rey to Buitrago occupied two channels in the permanent microwave facilities, with one channel serving as NASA prime and the second channel shared with the Spanish “Companie Telefonica Nacional de Espana” (CTNE) as a standby circuit. These microwave channels terminated in the NASA terminal installed at the Intelsat Ground Terminal at Buitrago. Selection of video received from Madrid STDN and video received at NASA Buitrago, for retransmission to JSC, was controlled at the NASA Buitrago terminal. The Madrid STDN site was equipped to receive only the S-band direct link.

- Madrid Hybrid Terminal. The Madrid Hybrid Terminal was a special transportable system temporarily installed at the Madrid STDN site and had a multipurpose assignment. The prime requirement was to provide operational control for ATS-6 after ATS-6 was repositioned to 35° East longitude to support the Indian Government television experiments and the direct relay of the Apollo signals during the ASTP mission. At this orbital position, ATS-6 was not visible to the regular STDN sites of Rosman and Mojave.

The Madrid Hybrid Terminal had receiving capabilities for the ATS-6 downlink C-band signals containing the relayed video from Apollo. Although the 6.4-meter diameter parabolic antenna did not possess the desired G/T, mission observations concluded that signals would be usable should failures be encountered at NASA, Buitrago. This video from

the hybrid terminal was delivered to the Madrid STDN site by an intrasite coaxial cable and was transmitted to NASA Buitrago by the Madrid STDN-NASA Buitrago microwave link for backup selection. The 6.4-meter diameter parabolic antenna presented a limitation only to the downlinked video signal-to-noise ratio, possessing adequate gain for the transmission and reception for ATS-6 command and control signals.

- NASA Terminal at Buitrago. A special NASA terminal was installed at the CTNE Intelsat Ground facility at Buitrago, Spain. During the mission, a 30-meter parabolic antenna and associated signal down-conversion equipment were leased from CTNE. The downlinked C-band signal from ATS-6 was converted to a 70-MHz intermediate frequency signal and the Apollo video was demodulated in the special NASA terminal.

The NASA terminal was configured as a dual system, offering full redundancy. This arrangement permitted processing of the Apollo video relayed through ATS-6 and downlinked to Buitrago through one channel, and backup video from the Madrid Hybrid Terminal Madrid STDN site through the other channel. Either channel could be selectively switched to feed the CTNE Intelsat ground facility for transmission to JSC-Houston. The dual channel capability permitted separate forms of processing independently in each channel.

Interleaved in the Apollo video were the pulse amplitude modulated (PAM) signals that represented the television audio. The audio was extracted from these pulses at the ground terminals processing the downlinked Apollo video. For Apollo signals relayed through ATS-6 and downlinked to Buitrago, the audio was recovered in the NASA Buitrago terminal and fed by program sound channels in the Intelsat facility to JSC. The Apollo signals processed by the Madrid Hybrid Terminal and Madrid STDN site extracted the accompanying audio at the respective terminals and transmitted the audio over the sound channel of the Madrid STDN-NASA Buitrago microwave circuits.

The NASA Terminal at Buitrago served as the major reception point for the Apollo downlinked video relayed through ATS-6, and served also as the backup transmission point to the Madrid Hybrid Terminal for uplinking ATS-6 command and control data, and communications signals for relay through ATS-6 to the Apollo command-service module.

- Robledo. Robledo was part of the Madrid Complex and served as a major NASCOM switching center. During the mission, voice-frequency communications and data transmission circuits were provided through this switching center. Robledo had administrative jurisdiction over the terrestrial video microwave circuits provided between Madrid STDN and NASA Buitrago.

Prelaunch and Launch Television Coverage—Prelaunch and launch television coverage was provided by the Kennedy Space Center cameras at Pad B and the reception and retransmission of onboard television signals by the Merritt Island Launch Annex.

Johnson Space Center, Houston—Johnson Space Center was the primary point for television signal processing, switching, and distribution and served as the ASTP Mission Control Center. These activities were performed in several separate buildings that were interconnected by a configuration of equalized, balanced coaxial cables carefully engineered to maintain television phase coherence between the chromance subcarriers. This cable network was provided by Southwestern Bell Telephone Company.

The Mission Operations Control Room (MOCR) was the final video and audio selection point for release to the media networks and separate transmission to Moscow. These selections were guided by coordinated scenario, prior knowledge of planned onboard activities and the quality of received TV signals. The NASA Public Affairs Office, which was responsible for the released video and audio, accomplished this activity through a monitoring system and three separate switching matrices in the MOCR feeding to the television networks, the writing press room, and to the U.S.S.R. staff support room.

The following functional description of the Johnson Space Center ASTP-TV configuration relates to the video routing and signal processing for the Apollo television signals, as received through ATS-6 and the STDN stations. Additionally, the Soyuz and other U.S.S.R. television signals, after standards conversion in Europe, were processed and distributed. The Johnson Space Center ASTP-TV configuration provided for processing of the Apollo signals over two independent routes, and included a provision for contingency backup processing of the U.S.S.R. incoming signals. Additionally, signals originating at Kennedy Space Center and at Johnson Space Center (JSC) press conferences were similarly processed to be coherent with basic JSC signals, permitting smooth transitions between selections of the various signals for television network and pool release.

- Basic Concept of Video Processing

The Apollo signals, derived from ATS-6 at Buitrago and STDN stations, were received in parallel in Buildings 8 and 30. Each building independently selected the optimum (or available) signal for processing that included: color field compensation, frequency correction, and color conversion.

Building 8 introduced additional processing in the form of image enhancement and noise reduction when signal-to-noise ratios were not too low and when excessive motion did not occur within the image.

The independently processed signals from Buildings 8 and 30 were routed to an engineering evaluation switcher, located in Building 30, for comparison, judgment, and selection as the Apollo video for any given interval. This parallel processing gave the optimum Apollo video for the varying transmission conditions during each orbit, and also provided online redundancy against malfunctions within any processing unit. The capability to subjectively compare the “basically” processed video from Building 30 with the “extensively” processed video from Building 8 provided the better signal at all times.

The Soyuz video and other U.S.S.R. signals were received in Houston in the NTSC format and were branched to Buildings 8 and 30, with Building 8 performing the primary signal processing and Building 30 terminating the signal for contingency use.

All signals originating externally to Buildings 8 or 30 were asynchronous, but were retimed through the two digital field resynchronizers in Building 8 and a digital frame resynchronizer in Building 30. These signal outputs were pretimed to be coherent at the Public Affairs Office preview switcher in Building 30.

For periods when additional signals were available for selection, these signals were routed through Building 30, and included:

- Kennedy Space Center prelaunch video
- Public Affairs Office press conference from Building 2
- Video tape recorder playback from Building 8
- Video tape recorder playback from Building 30
- U.S.S.R. video

The selected video was routed through the Building 30 digital frame resynchronizer in lieu of a selected Apollo signal for coherence at the engineering evaluation switcher.

Additional video sources within Building 30 were the front and rear Mission Operational Control Room (MOCR) cameras and the color camera in the U.S.S.R. staff support room.

Two independent video switchers were included in Building 30 for use by the U.S. Public Affairs Office and one by the U.S.S.R. Public Affairs Office respectively. Each position contained a preview and program selector, with identical input video sources that included:

- Apollo (delegated output)
- U.S.S.R. (delegated output)
- MOCR camera (front)
- MOCR camera (rear)
- U.S.S.R. staff support room camera
- Kennedy Space Center (auxiliary)
- Video tape recorder playback—Building 8
- Video tape recorder playback—Building 30
- Scan converter 1
- Scan converter 2
- Scan converter 3
- Public Affairs Office return (auxiliary)

The output of the U.S.S.R. Public Affairs Office switcher was processed and fed directly to the Soviet Union. The output of one U.S. Public Affairs Office (PAO) switcher was routed through Building 8 to Building 2 as PAO-1 out, for the switchable release to the television networks and press

pool. Additionally, the U.S.S.R. (delegated video) and three color cameras were also fed to Building 2 unilaterally for coherent use by the television networks.

The Johnson Space Center system distribution is shown in Figure 13-5.

TECHNICAL AND OPERATIONAL EVALUATIONS

This section pertains to the technical and operational evaluations of the television systems during the period of the mission. The primary system detailed in this section were:

- Moscow to Houston video
- Moscow to Houston audio
- Apollo field sequential video relayed through ATS-6
- Buitrago to Houston video
- Johnson Space Center audio selection and transmission
- Johnson Space Center video system timing
- Johnson Space Center processing and distribution

The evaluations were based on performance characteristics obtained during the mission, the pre-mission tests, and expected values derived from published specifications. The recommendations were alternatives that could be implemented to circumvent the degraded segments in the system and the inclusion of more sophisticated video processing facilities.

Moscow to Houston Video Transmission

This circuit had the potential for being more susceptible to transmission degradations because of the enroute signal processing requirements.

The Moscow signals from the Mission Control Center were originated in the SECAM format and appeared to be of excellent luminance and chrominance quality. Cameras had good match, and interior lighting gave good luminance distribution.

Video from the Baykonur Cosmodrome was also originated in the SECAM format, with good camera match. Color saturation appeared to be low, but this loss of chrominance probably occurred in the Baykonur-Moscow transmission link that introduced high levels of noise and was susceptible to frequent video interruptions. The monochrome tracking camera, following the launch trajectory of the Soyuz, had excessive level causing blooming and video breakup.

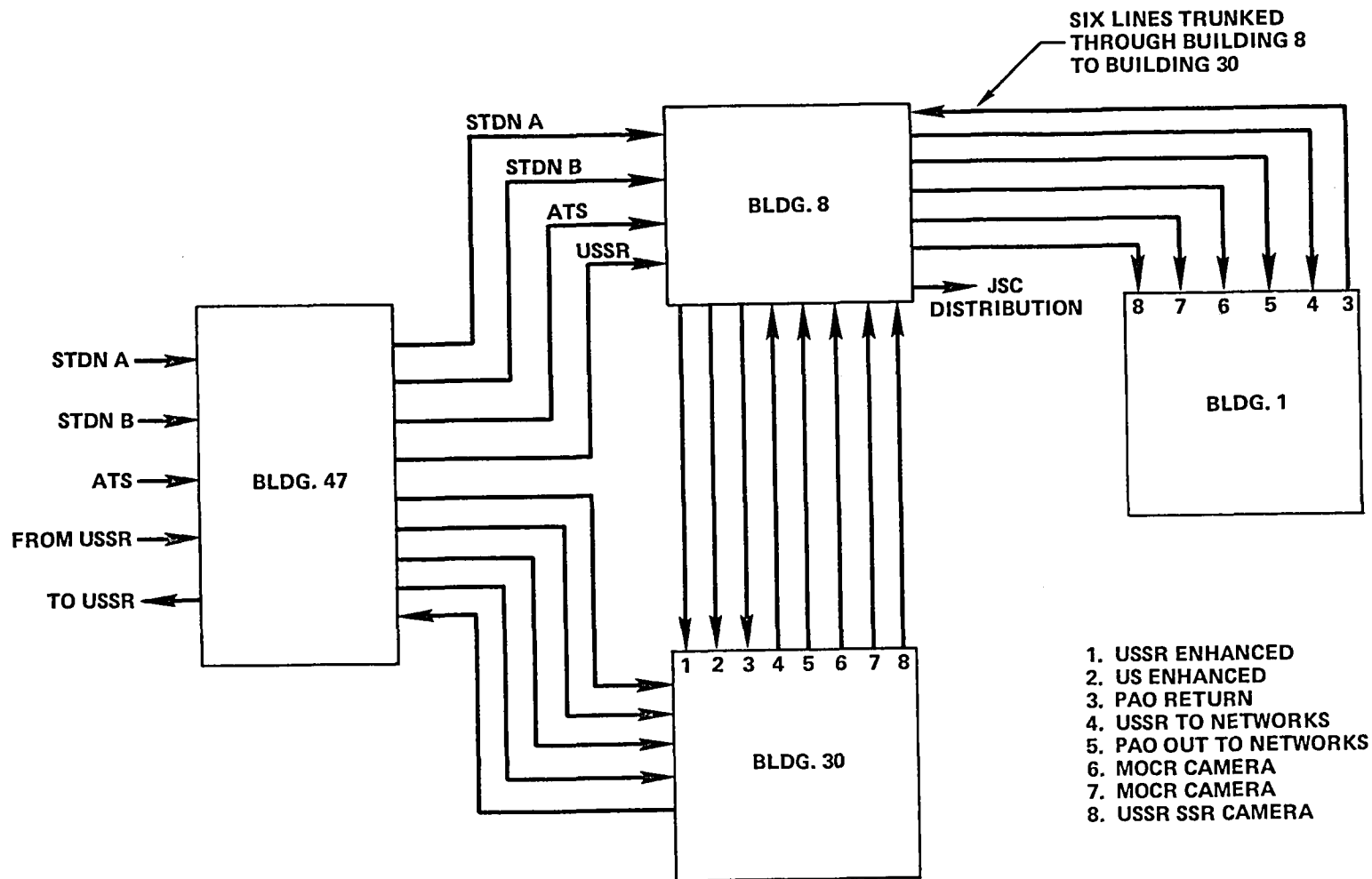


Figure 13-5. JSC System Distribution

The onboard Soyuz video was not available until the second day of the mission because of malfunctions in the onboard camera/switching system. This outage cancelled the Soyuz onboard scenes during launch and prevented the use of the two onboard monochrome cameras, one of which was positioned to cover the external operations during the Apollo-Soyuz docking maneuvers. During the Soyuz revolutions, field sequential color signals were downlinked to four U.S.S.R. tracking stations. Coverage through these ground terminals varied from 3 to 11 minutes, with the video transmitted to Moscow by microwave links and Molniya satellites. Color conversion to SECAM was performed in Moscow. The onboard scenes were generally good, but color saturation was low. Picture detail was reduced by the low signal-to-noise ratio and poor transient response that produced excessive smearing.

Video signals from the Baykonur Cosmodrome and Soyuz were not fully synchronized with the video signals originating at the Mission Control Center; therefore, every switching transition produced an unstable interval for approximately four video fields. The proposed videotape frequency corrector was not evident during these switching intervals.

The NASA-installed time base corrector at Hamburg functioned as expected, since no time-base instability was detected during the requested videotape playback periods from Moscow. Instabilities had been encountered during premission tests and simulations. The time base corrector was probably instrumental in reducing the switching transients to horizontal displacements rather than full picture roll.

The transmission characteristics of the European terrestrial microwave appeared excellent and performance was within the expected limits. Detected degradation occurred in the Moscow-Helsinki segment, produced by variances in the video level at the Moscow input terminal. Transmission outages on this segment were related to heavy storm activity along the route, and service was restored by alternate routing.

The SECAM-to-PAL transcoder located at Hamburg, and the alternate transcoder located at Frankfurt, performed as expected with no serious degradation to the video. These transcoders were fed by the NASA time base corrector that maintained the SECAM signal within the window of the horizontal Sync-PAL subcarrier ratio, eliminating the spurious color bars when this input ratio was exceeded.

Standards conversion from European PAL to U.S. NTSC was performed at the Raisting Earth Terminal. The conversion process exhibited the expected results, with the major degradation occurring in the inherent loss of vertical resolution due to line interpolation. The vertical interval reference signal and the vertical interval test signals that were inserted at Raisting, provided reference data for isolating video degradations incoming to Raisting and those degradations that occurred between Raisting and Houston.

The NTSC signals, derived from standards conversion from European PAL were transmitted to the U.S. ground terminal at Andover, Maine. Raisting did not have monitoring capability for evaluating

the downlink from the Intelsat, so this examination was performed at CTNE Buitrago. Display of the Raisting-inserted vertical interval test signals confirmed that no detectable degradations were occurring in the Intelsat segment.

Transmission from Andover to Houston was by Bell System terrestrial microwave. This circuit suffered the most severe degradations of any of the signals supplied to Johnson Space Center. The major impairment was complete video breakup and continuous video pull up. The vertical sync interval was severely disturbed and unstable. Poor transient response, producing excessive smear and streaking reduced the resolution of the video detail. Abnormal differential gain adversely affected the color saturation.

The measured values, tabulated below, were typical for all the transmission from the U.S.S.R.:

- Random video breakup (sync tip to peak white)
- Vertical sync instability
- Differential gain: 25 percent to 30 percent
- Poor transient response; 20 IRE residual above pedestal following white-to-black transitions, producing objectionable smearing
- Horizontal (line rate) tilt: 20 percent
- Frequency response: -4.5 dB midfrequency saddle, -3.2 dB droop at 3.58 MHz
- Insertion gain: varied from -1.7 dB to -2.2 dB
- Ringing on 2T pulse: first lobe 20 percent, second lobe 10 percent (sometimes reversed)
- Video signal-to-noise ratio: 33 dB to 34 dB
- Chrominance/luminance delay: 150 nsec
- Chrominance/luminance gain: -2 dB
- Resolution: 200 to 240 lines

The expected values for this circuit configuration, based on published line-up test procedures, were typically:

- Differential gain: 15 percent
- Ringing on 2T pulse: 1st lobe 10 percent, 2nd lobe 5 percent

- Video signal-to-noise ratio: 50 dB or better
- Chrominance/luminance delay: 100 nsec
- Chrominance/luminance gain: +1 dB to -2 dB
- Line rate tilt: 2 percent
- Field rate tilt: 4 percent
- Insertion gain: 1 dB
- Resolution: 325 lines

Comparison between the expected values and the averaged receive values clearly identified a severe differential. Coordinated monitoring isolated the majority of the impairments to the U.S. terrestrial microwave segment, with minimum degradation occurring in the satellite segment. Based on these results, it is obvious that if the U.S. terrestrial microwave segment had been replaced with a satellite segment, the terminal results would have been radically improved. To have used this superior routing, the standards-converted NTSC signals would have been uplinked at Raisting and downlinked to the Canadian Earth terminal at Newfoundland, and directly uplinked to the Anik satellite with domestic downlink to Dallas. The terrestrial microwave circuit from Dallas to Houston performed well during the mission.

The optimum alternate route would have provided uplinking to Intelsat at Helsinki in the SECAM format, downlinking to Newfoundland and direct uplinking to Anik. The Anik downlink would be received in a terminal within the Johnson Space Center complex, with digital standards conversion with SECAM to NTSC. This route was not an active candidate since a receiving terminal with the required G/T did not exist at Johnson Space Center and timely delivery of a digital standards converter could not be assured for the scheduled mission period.

Moscow to Houston Television Audio

The television-associated audio was a selectable, that was switched in Moscow to provide the basic sound that corresponded to the video being released to the U.S. The content was primarily descriptive commentary by the U.S.S.R. Public Information Officer and Soyuz air/ground communications. This circuit was basically a "voice-grade" channel that was separately routed from the video path from Moscow through Warsaw, to East Berlin, Frankfurt into Raisting. At Raisting, the audio was uplinked through "program-grade" channels as a companion to the video, and was delivered from Andover to Houston as schedule A service.

This circuit experienced several outages during the mission, but more frequently failed to establish Moscow to Houston continuity at the time the video service was received. Circuit identification, using a "chirp tone" rather than a continuous 800-Hz tone, was useful in establishing circuit continuity in a more timely manner during the latter part of the mission.

During intervals when audio was not received, the U.S. Public Affairs Officer substituted Soyuz air/ground audio.

Measurements of the audio from Moscow were typically:

Insertion gain	-2.5 dB
Signal-to-noise ratio	37 dB
Total harmonic distortion	2.8 percent

Compensation for some of the transmission impairments could have been implemented if the service had been terminated in the video processing area, and if standard bandpass filters and graphic equalizers were available.

Apollo Field Sequential Video Relayed Through ATS-6

The selected Apollo field sequential color video was modulated in the command-service module (CSM) unified S-band system and directionally transmitted through the steerable high gain antenna towards ATS-6. The S-band signal was changed to C-band by the transponder and retransmitted through the ATS-6 Earth-coverage antenna to the 30-meter diameter receiving antenna at Buitrago, Spain. The C-band signal was downconverted to the conventional 70-MHz intermediate frequency, then demodulated to video baseband in the NASA terminal temporarily installed at Buitrago.

Two-way signal acquisition between the Apollo CSM and ATS-6 occurred precisely on predicted schedules during each scheduled revolution and lock was continuously maintained, except during one Apollo CSM maneuver that was expected. This discontinuity lasted less than 2 minutes.

The only signal degradations occurred during revolutions 27 through 31 and 42 through 45 when the steerable antenna on ATS-6 was near nadir for continuity with the Apollo CSM; it was then boresight-aligned to a U.S.S.R. Soyuz tracking radar. The simultaneous reception of the Apollo CSM S-band signal and the U.S.S.R. radar produced an interference pattern of visible white tears of approximately 5-nsec duration in the displaced video. The U.S.S.R. tracking radar was silenced during the remaining revolutions when Apollo and Soyuz were in a docked configuration, which eliminated this source of interference.

The demodulated field sequential color video at Buitrago had a signal-to-noise ratio of 45 dB with no detectable degradations. The performance of the Apollo/ATS-6 relay was flawless, with limitations confined to the constricted bandwidth of the Apollo CSM S-band system. Overall performance was approximately 7 dB better than predicted.

The ATS-6 C-band signal received by the Hybrid Terminal at Madrid had a reduced signal-to-noise ratio, because of the 6.4-meter diameter receiving antenna, but video was stable and usable as a contingency backup to the NASA Buitrago signal if it had been required.

Buitrago to Houston Video Transmission

This circuit was not considered to be particularly susceptible to transmission degradations, since it was configured from a single Intelsat satellite segment and one U.S. terrestrial microwave segment from Andover, Maine or Etam, West Virginia to Houston. The video was already in the 525/60 line-field ratio and did not contain the phase sensitive chrominance subcarriers.

Transmissions from NASA Buitrago consisted of the demodulated video from the active Apollo onboard cameras and onboard videotape playback, and groundbased test signals and color bar patterns in the field sequential color format. These signals were accompanied by vertical interval test signals, injected at the output of the NASA Buitrago terminal, that represented the input to CTNE Intelsat. The "back downlink" was monitored at Buitrago to confirm satellite transmission and status of the vertical interval test signals that were used in the objective analysis, since they remained independent of the incoming Apollo signals.

The major degradations resulted from poor frequency and transient response that produced tilt, undershoot, and excessive smearing, which could not be fully compensated by NASA post-processing. Additionally, a reduced signal-to-noise ratio, excessive differential gain, and intermittent tears from malfunctioning clamping amplifiers persisted during all scheduled transmissions.

The examination of the satellite back downlink at Buitrago confirmed normal transmission through the satellite, and tests showed that transmissions by Southwest Bell Telephone from Houston to Johnson Space Center were excellent. Both concluded that these impairments were occurring in the long lines segment. As in the premission tests, efforts to eliminate these impairments through coordination with AT&T/Bell long-lines personnel were unsuccessful.

Tabulation of typical measurements made at Johnson Space Center were as follows:

- Frequency response: high frequency roll-off 3.2 dB
- Horizontal tilt (line): 10 percent
- Transient response: poor, 20 IRE residual on pedestal after white-to-black transitions, producing smear
- Ringing on 2T pulse: 1st lobe 10 percent, 2nd lobe 10 percent
- Chrominance/luminance gain: -2.8 dB
- Chrominance/luminance delay: 120 nsec
- Differential gain: 25 percent
- Video signal-to-noise ratio: 34 dB to 35.5 dB
- Insertion gain: -0.64 dB.

Expected values were:

- Frequency response: +0.7 dB to -1.0 dB
- Horizontal tilt: ± 1 percent
- 2T transient response: 1st lobe 6 percent, 2nd lobe 3 percent
- Chrominance/luminance gain: +0.75 dB to -1.01 dB
- Chrominance/luminance delay: 80 nsec
- Signal-to-noise ratio: 53 dB
- Insertion gain: 0.5 dB
- Resolution: 325 lines.

Since all the detectable impairments occurred in the U.S. terrestrial microwave, the alternative would be to replace the microwave segment with a satellite segment as suggested for the transmission from Moscow.

Johnson Space Center Audio Processing and Transmission

During the initial part of the mission, a point of confusion existed between the audio auxiliary switchers associated with Public Affairs Office (PAO) 1 and PAO 2 releases. Selections made on PAO 1 auxiliary switcher were being transferred to the PAO 2 output line and conversely, selections made on PAO 2 switcher were being transferred to the PAO 1 output line.

Immediate investigation disclosed that the PAO 1 audio-follow-video bus had been incorrectly connected to the audio-follow-video input to the PAO 2 auxiliary switcher that fed PAO 2 distribution as designated. Concurrently, the PAO 2 audio-follow-video bus had been incorrectly wired to the audio-follow-video input of the PAO 1 auxiliary switcher that fed PAO 1 distribution as designated. This ambiguity was resolved by reversing the panel designations for the two auxiliary switchers. It would have been more desirable to have corrected the wire-straps, which would have retained the console-panel symmetry to reduce operator constraint.

The U.S.S.R. PAO switcher and auxiliary switcher were not affected by this wiring error and operated as designed.

The basic audio concept for the ASTP mission provided for audio routing to parallel the associated video processing routes. For flexibility, these prime routes were switchable to permit substitution of composite signals and contingency audio. The ultimate result would produce a continuous timely description of the events.

One composite source was available for use with video supplied from the U.S.S.R. The normal audio was Public Information Office narrative descriptions and Soyuz air/ground interchange in the Russian language. During these transmissions, the Russian language was translated to English as "Soyuz Comm English." This translation was added to the original Russian transmission in an "override" mix and was a selectable input on each PAO auxiliary switcher.

A second composite audio source was the "real-time" mixture of the Capsule Communicator (Cap Com) and the astronauts. Basically, this required the combining of the transmit side and receive side of the air/ground circuit. In the past missions, this mixing was done at the STDN stations and was in composite format when received at Johnson Space Center, Houston. In ASTP, the Cap Com had to be mixed at Johnson Space Center to maintain lip synchronization, since real-time video of the Capsule Communicator was frequently scheduled. This circuit performed as designed.

The major degradation in the television audio was the low signal-to-noise ratio. The high noise level (-36 dB below program level) resulted from the noise plateau in the frame room. Since all circuits were treated as communication circuits, each was limited by this noise threshold.

The condition could have been improved if the television audio circuits could have been terminated in the video area, with audio processing equipment made available, such as level-restoring amplifiers, variable equalizers, and bandpass filters. The processed audio could then be distributed directly and linearly to the media users with improved signal-to-noise ratios and clarity.

Johnson Space Center System Timing

The Johnson Space Center system timing concept provided for all incoming asynchronous signals to be retimed to have time-base and chrominance-phase coherence at the inputs to the U.S. Public Affairs Office and U.S.S.R. Public Affairs Office switchers and at the media interfaces in Buildings 2 and 30.

Initial coherence was established through digital resynchronizers in the processing centers in Buildings 8 and 30. After color-conversion and signal processing in these two locations, the signals were correlated by synchronization pulses and stabilized by rubidium standards that were referenced to the designated rubidium standard in Building 30. The closed-loop reference signals cancelled the propagation delay between buildings. After initial coherence was established, transmission coherence was maintained by calibrated cable routes.

The system performed as designed and implemented throughout the mission period.

Johnson Space Center Processing and Distribution

The video processing at the Johnson Space Center proceeded according to the planned format, using the redundant processing capabilities of Buildings 8 and 30. The major deviation was the necessity to introduce signal conditioning video equalizers for incoming signals from Moscow and Buitrago in

an effort to compensate for the video degradations imparted by the Bell System transmissions from Andover to Houston. The introduction of this equipment necessitated processing of the U.S.S.R. signals predominantly in Building 30 and the Apollo signals by Building 8.

These serious degradations required that both buildings maintain processing equipment at optimum efficiency and exercise constant manual attention. The digital frame resynchronizer was particularly sensitive to the changes in the drastically-deformed color-burst on the incoming U.S.S.R. signals.

There were no equipment malfunctions in the principal processing chains in either building, and the optimum signals were continuously available for selection and distribution by the public affairs officers.

Appendixes

APPENDIX A
SAMPLE LINK CALCULATION

Link calculations were accomplished for each of the different spacecraft/Earth station/band combinations used for the various experiments performed using ATS-6. Included in Table A-1 is a sample link calculation worksheet completed for one such experiment (C-band drift phase tests, April 1975). The predicted and measured parameters for the Rosman and Hybrid stations are presented. (The Hybrid station was located near Madrid, Spain.)

Table A-1
C-Band Drift Phase Test Link Calculation

Uplink Power Budget and Ground Station E.I.R.P. Measurement					
		<u>Rosman</u>		<u>Hybrid (Madrid)</u>	
		<u>Predicted</u>	<u>Measured</u>	<u>Predicted</u>	<u>Measured¹</u>
Frequency	(MHz)		6150		6150
Transmitter Power	(dBm)	45	45	60	60
Transmitter Antenna Gain ²	(dB)	59.7	59.7	46.9	(45.1) ³
E.I.R.P.	(dBm)	104.7	104.7	106.9	105.1
Free Space Loss	(dB)	199.9	199.9	199.9	199.9
P _{rs}	(dBm)	-95.2	-95.2	-93.0	-94.8
Spacecraft Antenna Gain ⁴	(dB)	17.9	(13.2) ⁵	17.9	13.2
Spacecraft AGC	(dBm)	-77.3	-82.0	-75.1	-81.6
Downlink Power Budget and Ground Station G/T Measurement					
Frequency	(MHz)		3950		3950
Transmitter Power	(dBm)	38.6	37.2	38.6	37.2
Transmitter Antenna Gain ⁶	(dB)	16.3	16.8	16.3	16.8
E.I.R.P. ⁷	(dBm)	54.9	54.0	54.9	54.0
Free Space Loss	(dB)	195.8	195.8	195.8	195.8
P _{rg}	(dBm)	-140.9	-141.8	-140.9	-141.8
R _x Antenna Gain ⁸	(dB)	58.3	58.3	44.8	43.4
Total Receive Power	(dBm)	-82.6	-83.5	-96.1	-98.4
Ground Station G/T	dB/K	39.6	39.0	24.8	23.0
Ground Station C/N	(dB)	23.7	23.2	10.9	8.2
Ground Station C/N ₀	(dB/Hz)	96.3	95.8	82.5	79.8

¹Hybrid measured e.i.r.p. is relative to Rosman measured values.

²Rosman Ground Station net antenna gain per Nicholson TWX GSOC 260A 27/1930 June 1974 Hybrid predicted antenna gain per NASA X-460-74-340 ATS Exp C/O Report.

³Calculated Hybrid transmitter antenna gain (45.1 dB, e.i.r.p. 105.1 dBm @ 1 kW transmitter power).

⁴Rosman predicted spacecraft antenna gain per NASA X-460-74-340. Nominal peak values were used, adjusted for 3° off boresight (-0.5 dB from peak).

⁵Calculated spacecraft antenna gain based on measured Rosman e.i.r.p. (This value was used for hybrid antenna gain and e.i.r.p. calculation.)

⁶C-band measured Earth coverage horn antenna gain based on measured Rosman carrier-to-noise and noise power.

⁷C-band e.i.r.p. per NASA X-460-74-340 pp. 9-22 including -0.8 dB for 3° pitch offset.

⁸Rosman receiver antenna gain per Nicholson memo, Hybrid predicted antenna gain per X-460-74-340.

APPENDIX B

IN-ORBIT MEASUREMENT OF G/T OF A HARD-LIMITING TRANSPONDER WITH AUTOMATIC GAIN CONTROL

The technique of measuring G/T is one of measuring the system noise temperature. This is readily accomplished for a linear amplifier using well established techniques developed for measuring amplifier noise figure; i.e., measure amplifier output power with no input, then measure change in output with a known input. The problem becomes more complex if the amplifier has automatic gain control (AGC) and assumptions must be made as follows:

1. The total output power is constant for all input levels.
2. The IM products due to front end noise are negligible.

Using the above assumptions, the spacecraft noise power input, P_n , referred to the preamplifier input is as follows:

$$P_n = KTB \quad (1)$$

where:

- K = Boltzman's constant
= $1.38 (10)^{-23} \text{ w}^\circ/\text{Hz}$ (-198.6 dBm $^\circ$ /Hz)
- T = Spacecraft system noise temperature (Kelvin)
- B = Spacecraft bandwidth = 40 MHz (76 dB-Hz)

The spacecraft output power, P_{out} , is proportional to the signal power input, P_s , multiplied by the antenna gain, G, plus the noise power input P_n ;

$$P_{out} = P_{s \text{ out}} + P_{n \text{ out}} \approx P_s G + P_n \quad (2)$$

where:

$$P_s = \text{Ground station e.i.r.p. (dBm)} - \text{path loss (dB)}$$

For large $P_s G$ (on the order of -70 dBm), P_n becomes negligible and the total output power may be considered to be due to the signal input $P_s G$. The signal power output $P_{s \text{ out}}$, may be observed and measured on a spectrum analyzer or a narrowband tuned voltmeter. As P_s is decreased, a decrease in $P_{s \text{ out}}$ will occur, and $P_{n \text{ out}}$ must then increase to maintain a constant P_{out} .

From Equation (2)

$$\text{at high power: } P'_{out} = P'_{s out} = C'P'_sG \quad (2A)$$

$$\text{and at low power: } P_{out} = P_{s out} + P_{n out} = C(P_sG + P_n) \quad (2B)$$

where C is a constant of proportionality and (') is used to indicate the high power conditions.

From the above, since $P_{out} = P'_{out}$, we have:

$$P'_{s out} = P_{s out} + P_{n out} \quad (2C)$$

$$C'P'_sG = C(P_sG + P_n) \quad (2D)$$

from which:

$$P'_sG = \frac{C}{C'}(P_sG + P_n) \quad (2D)$$

From equation (2C):

$$P_{n out} = P'_{s out} - P_{s out} \quad (2E)$$

Also, from (2B) and (2A):

$$P_{n out} = CP_n \text{ and } P'_{s out} = C'P'_sG$$

that substituted into (2D) gives:

$$P'_sG = \frac{P_{n out}}{P_n} \frac{P'_sG}{P'_{s out}} (P_sG + P_n)$$

Substituting for $P_{n out}$ from (2E) gives:

$$P'_sG = \frac{P'_{s out} - P_{s out}}{P_n} \frac{P'_sG}{P'_{s out}} (P_sG + P_n)$$

dividing through by P'_sG gives:

$$1 = \left(\frac{P'_{s out} - P_{s out}}{P'_{s out}} \right) \left(\frac{P_sG + P_n}{P_n} \right)$$

or

$$1 = (1 - P_{sr}) \left(\frac{P_s G + P_n}{P_n} \right) \quad (2F)$$

where

$$\frac{P_{sr}}{P_{s \text{ out}}} = \frac{P'_{s \text{ out}}}{P_{s \text{ out}}}$$

Expanding (2F) yields:

$$P_n = P_n - P_{sr} P_s G + P_s G - P_{sr} P_n$$

From which

$$P_{sr} P_n = (1 - P_{sr}) (P_s G)$$

or

$$P_n = \frac{1 - P_{sr}}{P_{sr}} P_s G \quad (3)$$

For the special case where $P_{sr} = 0.5$ (3 dB-drop), $P_{n \text{ out}}$ is equal to $P_{s \text{ out}}$, and P_n is equal to $P_s G$ as follows.

Equation (3) evaluated for $P_{sr} = 0.5$ becomes:

$$P_n = \frac{1 - 0.5}{0.5} P_s G = P_s G$$

or

$$\frac{P_n}{P_{sr}} = -3 \text{ dB} = P_s G \quad (4)$$

Substituting for P_n in Equation (1) gives:

$$P_s G = KTB \text{ or } \frac{G}{T} = \frac{KB}{P_s}$$

Assuming 40-MHz spacecraft BW:

$$G/T \text{ (dB)} = -198.6 + 76 - P_s = -122.6 - P_s \tag{5}$$

where:

$$P_s = \text{Ground station e.i.r.p. (dBm)} - \text{path loss (dB)}$$

The more general case of Equation (5) becomes:

$$G/T \text{ (dB)} = -122.6 \text{ dB} - 10 \log \left(\frac{1 - P_{sr}}{P_{sr}} \right) - P_s \text{ (dB)} \tag{6}$$

Calculation of Equation (6) is simplified by use of the nomogram shown in Figure B-1 that solves for the correction factor, C.F.:

$$\text{C.F.} = 10 \log \left(\frac{1 - P_{sr}}{P_{sr}} \right) \tag{7}$$

EXAMPLE

For synchronous altitude (spacecraft subsatellite point at 94°W longitude), Rosman L-band transmitter:

$$P_s = P_{gnd} \text{ (dBm)} + G_{gnd} \text{ (dB)} - L \text{ (dB)} \tag{8}$$

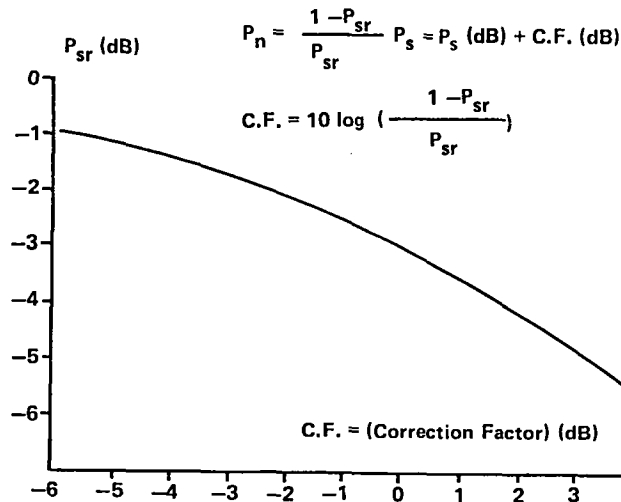


Figure B-1. G/T Nomogram Correction Factor

where:

$$P_{\text{gnd}} = \text{Rosman } T_x \text{ power (dBm)}$$

$$G_{\text{gnd}} = \text{Rosman antenna gain} = 33.4 \text{ dB}$$

$$L = \text{Path loss at 1650 MHz} = 188.2 \text{ dB}$$

Thus:

$$P_s = P_{\text{gnd}} \text{ (dBm)} - 154.8 \text{ dB}$$

Substituting (7) and (8) into (6) gives the expression for ATS-6 G/T as a function of Rosman transmitter power:

$$G/T \text{ (dB)} = -122.6 - \text{C.F.} - P_{\text{gnd}} \text{ (dBm)} + 154.8$$

$$G/T \text{ (dB)} = 32.2 - \text{C.F.} - P_{\text{gnd}} \text{ (dBm)}$$

Similarly, for the Madrid Hybrid Ground Station (spacecraft at 35°E longitude) we have:

HYB L-band Tx

$$G/T \text{ (dB)} = 32.6 - \text{C.F.} - P_{\text{gnd}} \text{ (dBm)}$$

HYB S-band Tx

$$G/T \text{ (dB)} = 36.5 - \text{C.F.} - P_{\text{gnd}} \text{ (dBm)}$$

APPENDIX C

I.F. AUTOMATIC GAIN CONTROL CALIBRATION

BACKGROUND

ATS-6 received signal strength, P_{rs} , was indicated by onboard detectors that sensed the i.f. automatic gain control (AGC) signal. Each of the spacecraft i.f. strips contained two AGC detectors: one used in the FT mode and one used in the PLACE mode, so there were a total of six AGC detectors.

Each AGC detector was calibrated before spacecraft launch. This appendix shows the recalibration of the AGC detectors relative to Rosman's calibrated e.i.r.p.

SPACECRAFT CONFIGURATION

The spacecraft configuration for in-flight AGC calibration was identical to the prelaunch configuration:

- FT mode: C-band preamplifier No. 1 to C-2 downconverter to the selected i.f. (wide BW)
- PLACE mode: C-band preamplifier No. 1 to C-2 downconverter to the selected i.f. (Narrow band). PLACE bandwidth wide (5 MHz).

Note: Other spacecraft configurations, i.e., L-band downconverter, were accommodated by adding correction factors to the basic calibration curve.

TEST DESCRIPTION

The Rosman C-band transmitter provided calibrated rf outputs at 6152 MHz to the 25.9-meter antenna, which was kept peaked on ATS-6 by monitoring the downlink received signal strength. The 25.9-m antenna feed polarization was peaked for maximum spacecraft received signal. This coincided with maximum ground station received signal. The spacecraft received signal, P_{rs} , was then calibrated as follows:

		<u>Comments</u>
Ros transmitter pwr (dBm)	P_t	
Ros net antenna gain (dB)	53.5	Per Keating 8/76
Free space loss (dB)	-200.2	(39800 km)
S/C rec antenna gain (dB)	17.4	Earth coverage horn peak gain
S/C antenna off beam loss (dB)	-0.2	(-1° pitch offset)
$P_{rs} = P_t -$		124.5 dBm

All six AGC detectors were calibrated with Rosman transmitting over a 40-dB range of transmitter power (from approximately 20 to 63 dBm). The spacecraft AGC telemetry was recorded in decimal counts, for each Rosman transmitter power level. The calculated P_{rs} and recorded telemetry (AGC decimal counts) were then plotted to form a calibration curve. To extend the calibration range, the spacecraft was configured with the prime-focus feed to increase the spacecraft receive antenna gain. The spacecraft pointing was stabilized by using S-band monopulse (Rosman transmitted a 2250-MHz S-band signal), and Rosman repeated the C-band transmission.

Figure C-1 shows the result of the foregoing for i.f.-3, PLACE mode. The abscissa shows the calculated P_{rs} using the spacecraft Earth coverage horn. The curve is extended by using the prime-focus feed data. As shown in Figure C-1, the Earth coverage horn and prime-focus feed data overlap over approximately a 20-dB range. Similar curves were developed for the remaining five spacecraft configurations.

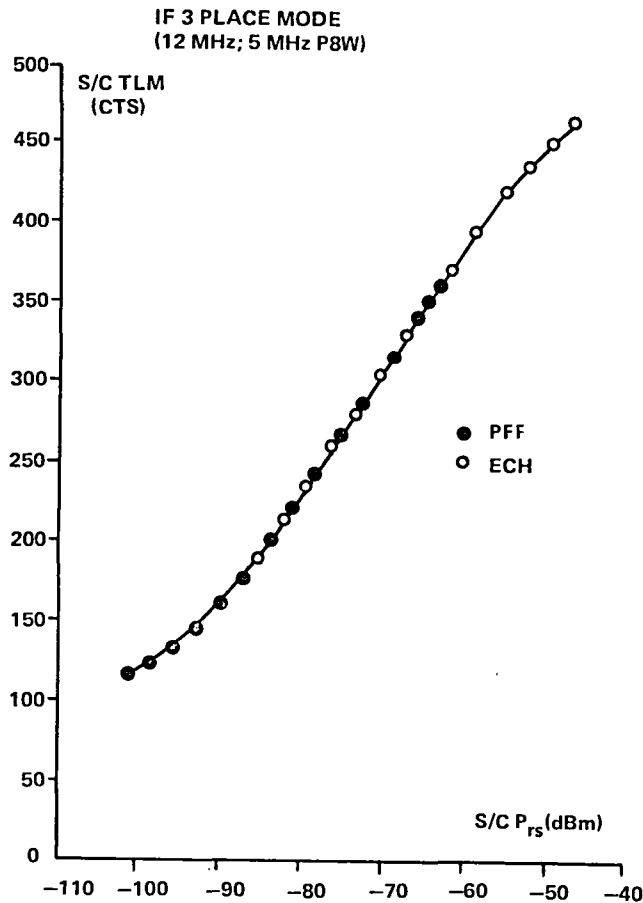


Figure C-1. I.F.-3 PLACE Mode (AGC)

TEST RESULTS (CALIBRATION CURVES)

Each of the AGC detector response curves was approximated by another curve consisting of seven line segments (fitted to within ± 2.5 decimal counts of the response curve). The six curves are shown in Figure C-2. (Note that the abscissa has been adjusted to show all of the curves on one sheet.)

RECOMMENDATIONS

It was recommended that the ATS-6 AGC calibration values presented be incorporated into the update of the data base.

The initial AGC calibration used seven line segments that divided the AGC range into essentially equal segments. This division was not optimum, since the actual AGC detector response curve is more linear in the central portion of the curve (requiring fewer line segments for a good fit). The proposed calibration curve recognized this fact (Figure C-2).

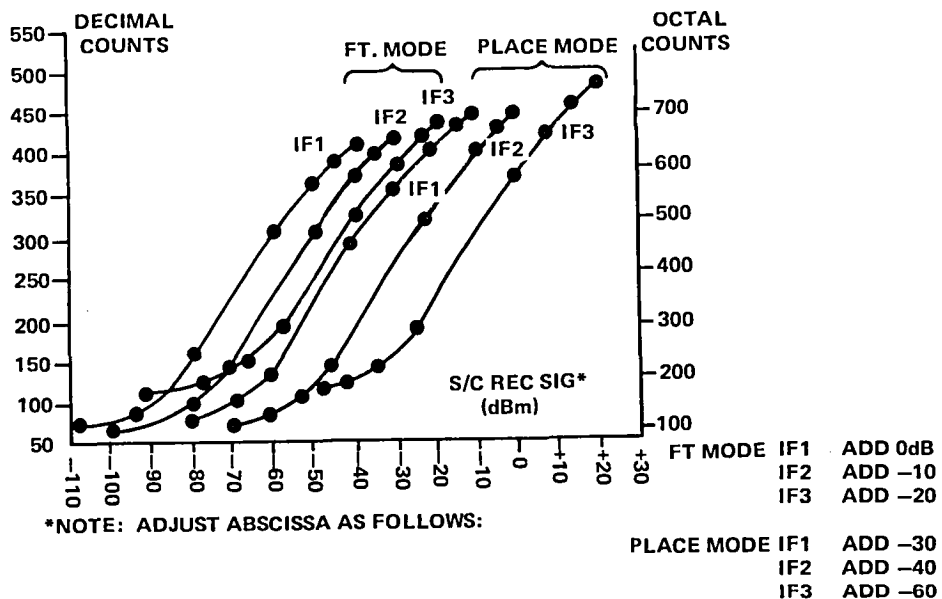


Figure C-2. Composite AGC Detector Response Curve

APPENDIX D
L-BAND TRANSMITTER NOISE

L-BAND TRANSMITTER NOISE CHARACTERIZATION

Spacecraft configuration:

Forward link	CxL, I.F.-2
Return link	LxC, I.F.-1
Bandwidth	40 MHz (both i.f.'s)
Spacecraft synth	noncoherent

When the L-band transmitter was on, but no driving signal present, the L-band transmitter coupled noise into the L-band receiver and effectively desensitized it (the coupled noise was equivalent to a -67 dBm signal at the spacecraft). This effect could be minimized by transmitting a carrier through the L-band transmitter.

The following sequence of tests established that the noise was being coupled into the L-band receiver from the output of the L-band transmitter:

- a. A reference noise spectrum was established (CxL, LxC) in the C-band downlink with the system all on and no L-band uplink.
- b. The forward link beacon was turned on; there was no resultant change in the return spectrum. If the coupling was taking place before the L-band transmitter, the beacon would have caused some suppression of the out-of-band transmitter noise; however, the L-band transmitter was not broad band enough to pass the beacon signal (30 MHz above center frequency), thus the beacon could not suppress the transmitter noise coupling if it occurred at the transmitter output (or further removed from the transmitter). The L-band transmitter was turned off, and a normal noise spectrum was observed on the return link.
- c. The L-band transmitter was turned off and the return link spectrum showed normal noise, proving that the transmitter noise was being coupled into the L-band receiver. A forward link signal (6150) was then radiated from the ground to provide noise suppression resulting in a normal noise spectrum on the return link. (No return link signal was radiated.)

L-BAND TRANSMITTER NOISE QUIETING

Figures D-1 and D-2 show the effects of a tone in the L-band transmitter on L-band received noise.

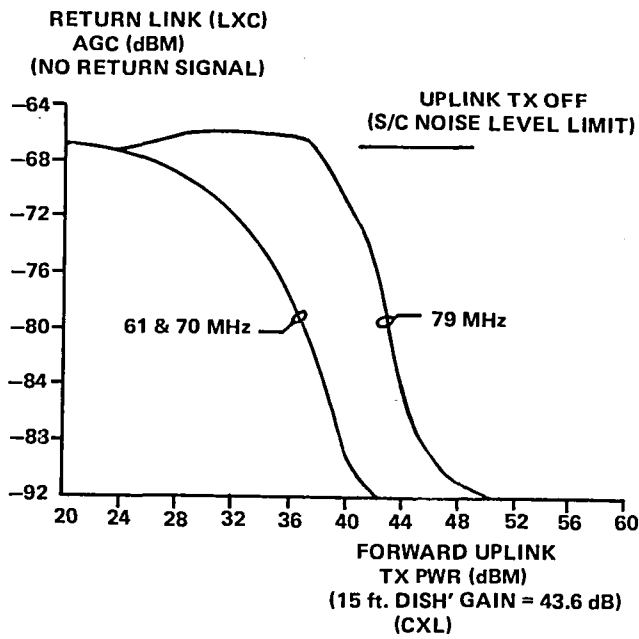


Figure D-1. Spacecraft L-Band Receiver Noise Power (LxC) Versus Spacecraft L-Band Tx (CxL)

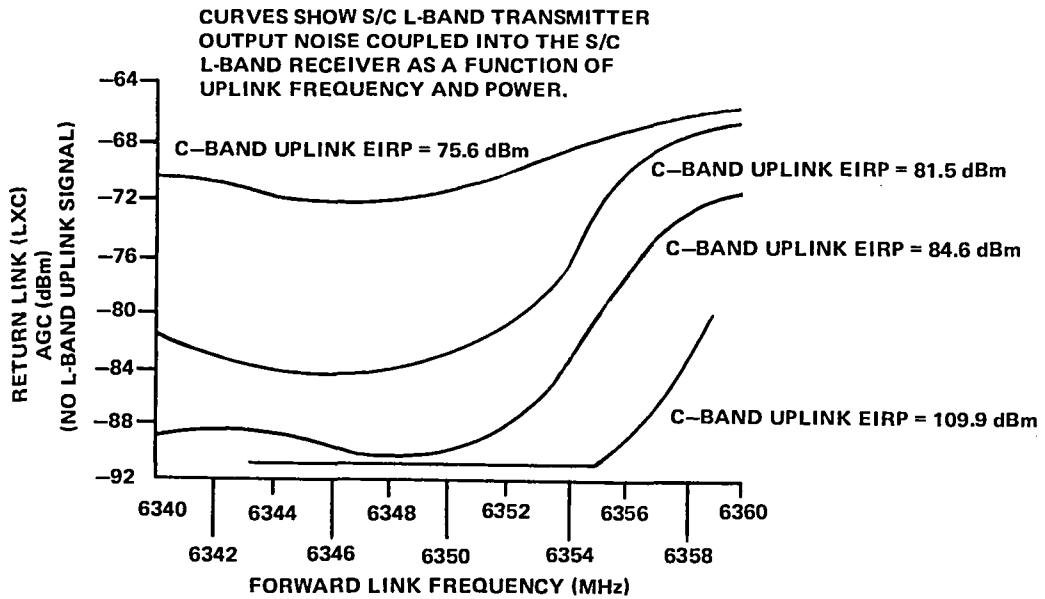


Figure D-2. L-Band Receiver Noise Power Versus Frequency of Noise Suppression Signal

In Figure D-1, the uplink power was varied from 100 mW to 1 kW at center frequency (ground station i.f. of 70 MHz) and ± 9 MHz from center frequency. The Rosman 4.7-meter antenna (gain 43.6 dB) was used. Figure D-1 shows that similar effects were observed with the tone at center frequency (70 MHz) and at -9 MHz (61 MHz); however, when the noise suppressing tone was at +9 MHz (79 MHz), approximately 5 to 10 dB greater signal level was required to achieve the same degree of noise suppression.

Figure D-2 shows the effect of a tone at constant power as the frequency was varied from 10 MHz below center frequency to 10 MHz above center frequency. The bottom curve shows results from a previous test at a constant power of 109.9 dBm e.i.r.p. (This curve is shown for information only—it was obtained using i.f.-2 in the return link, whereas, this test used the finalized PLACE configuration with i.f.-1 in the return link.) The curves in Figure D-2 show that the effective suppression was less at higher i.f. frequencies.

LxL-BAND LINK C/N PERFORMANCE

Figures D-3 and D-4 show the LxL-band link carrier-to-noise ratio (C/N) performance with various levels of noise suppression for the 12- and 40-MHz i.f. bandwidth configurations, respectively. In each case, the Mojave Ground Station provided a relatively large signal at 1651 MHz to suppress the spacecraft L-band transmitter out-of-band noise, while the Rosman Ground Station completed an LxL link at 1655 MHz at various uplink power levels. The C/N of the resulting downlink signal (1555 MHz) was measured.

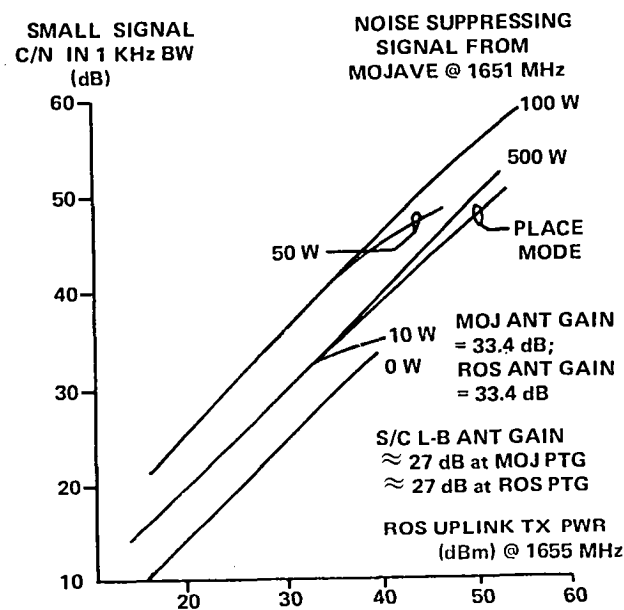


Figure D-3. LxL C/N Performance in 12-MHz I.F. Bandwidth Versus Noise Suppression Carrier Power

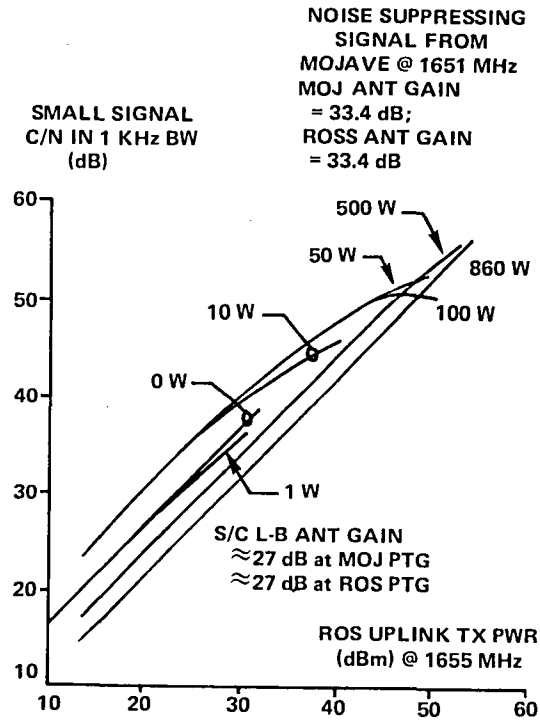


Figure D-4. LxL C/N Performance in 40-MHz I.F. Bandwidth Versus Noise Suppression Carrier Power

Both figures show that for very low uplink signals (Rosman transmitter 20 to 30 dBm) the best link performance was obtained with a noise suppression uplink signal of 10 to 100 watts (40 to 50 dBm). For a relatively higher uplink signal (50 dBm), correspondingly larger noise suppression signals were required. For very large signals, the noise suppression was accomplished by the signal itself, and no additional noise suppression was required. Note also (Figure D-3) that noise suppression could also be achieved by simultaneously driving the L-band transmitter with an unused spacecraft i.f. configured in the PLACE mode (PM).

APPENDIX E
E.I.R.P. AND G/T SUMMARY

Table E-1 presents a summary of the required specifications of the e.i.r.p. and G/T and the actual measured values of each. Sometimes the stated value was derived from other sources. These other sources are flagged with an index number as follows:

1. Extrapolated from hard reflector data
2. Extrapolated from nominal case values
3. Extrapolated from worst case values
4. The end-of-life receive antenna gain measurements at 6150 MHz (reflector) were measured on July 17, 1977. Accurate measurements after that time were complicated by problems with accurate spacecraft pointing.
5. The end-of-life 1650-MHz fan reflector G/T was computed from the measured G/T of the 1650-MHz pencil antenna and the measured difference in gain between the fan and pencil transmit (1550 MHz) beams.
6. The decrease in transmitter power and e.i.r.p. was caused by a partial failure of the 2075-MHz transmitter Number 1. The parameters for transmitter Number 2 are shown in parentheses.

It should be noted that all end-of-life tests were made using the Rosman Ground Station, and that the absolute accuracy of the measurements depended upon the accuracy of the calibration of the appropriate Rosman equipment. A significant value of the end-of-life tests lay in the close comparison between the prime and redundant components on ATS-6.

Finally, the communications performance requirements levied upon ATS-6 at launch were often below the originally specified values.

Table E-1
E.I.R.P. and G/T Summary

	Spec.	Measured		Post-Launch	End-of-Life
		Best	Worst		
<u>6150-MHz ECH</u>					
Receiver NF (dB)	7.3	7.8	8.3		
Antenna Gain, Peak (dB)	14.9	17.4	17.4		16.0
G/T Peak (dB/K)	-17	-15.0	-15.5	-14.0	-16.8 (-13.7)*
HPBW (degrees)		17.9 × 25.8	17.9 × 25.8	19.4 × 27.6	
VSWR	1.3	1.2	1.3		
Axial Ratio (dB)	25	33	29		
Spec. FOV (degrees)	20 × 20	20 × 20	—	20 × 20	
Gain Over FOV (dB)	11.9	13.5 × 15.6	13.5 × 15.6	12.2 × 26.0	
G/T Over Spec. FOV (dB/K)	-20	-18.9 × -16.8	-19.4 × -17.6	-21.6 × -20.0	
<u>3950-MHz ECH</u>					
Transmitter Power (dBW)	8.3	8.3	7.8		8.2
Antenna Gain, Peak (dB)	16.4	18.2	18.2		15.7
E.I.R.P. Peak (dBW)	25.4	26.5	26.0	25.7	23.9
HPBW (degrees)		26.3 × 19.0	26.3 × 19.0	24.2 × 17.4	
VSWR	1.3	1.3	1.4		
Axial Ratio (dB)	25	30	25		
Spec. FOV (degrees)	20 × 13	10 × 13	—	20 × 13	
Gain Over FOV (dB)	13.4	16.2 × 16.6	16.2 × 16.6	16.6 × 14.0	
E.I.R.P. Over Spec. FOV (dBW)	24	24.5 × -24.9	24.0 × 24.4	21.8 × -21.2	
<u>6150-MHz Parabolic Reflector</u>					
Receiver NF (dB)	7.3	7.8	8.3		
Antenna Gain, Peak (dB)	45.6	47.9	46.9	44.4	35.5 ⁽⁴⁾
G/T Peak (dB/K)	13.7	15.5	14.0	16.0	
HPBW (degrees)		0.38 × 0.35	0.40 × 0.33		
VSWR	1.4	<1.4	<1.4		
Axial Ratio (dB)	2.5	27 ⁽¹⁾	25 ⁽¹⁾		
Difference Peaks (dB)	5	2.2 × 6.5 ⁽¹⁾	7.8 ⁽¹⁾		
Spec. FOV (degrees)	0.4	—	—		
Cross-Coupling (dB)	20	15 ⁽¹⁾	13.7 ⁽¹⁾		
Gain Over FOV (dB)	42.6	44.6 × 43.9	43.9 × 42.0		
G/T Over Spec. FOV (dB/K)	10.7	12.2 × -11.5	11.0 × 9.1		

*Preamp No. 2

Table E-1
E.I.R.P. and G/T Summary (continued)

	Spec.	Measured		Post-Launch	End-of-Life
		Best	Worst		
<u>3950-MHz Parabolic Reflector</u>					
Transmitter Power (dBW)	8.3	7.8	7.3		
Antenna Gain, Peak (dB)	43.0	42.2	40.9		
E.I.R.P., Peak (dBW)	53.3	50.0	48.2	48.7	
HPBW (degrees)					
VSWR	1.4	<1.4	1.58		
Axial Ratio (dB)	25.0	33.7 ⁽¹⁾	33.7 ⁽¹⁾		
Spec. FOV (degrees)	0.6				
Gain Over FOV (dB)	40.0	38.7 × 38.2	37.9 × 36.2		
E.I.R.P. Over Spec. FOV (dBW)	50.3	46.5 × 46.0	45.2 × 43.5		
<u>1650-MHz Parabolic Reflector (Fan Beam)</u>					
Receiver NF (dB)	6.2	5.7	6.5		
Antenna Gain, Peak (dB)	No Req't	30.8 ⁽¹⁾	30.8 ⁽¹⁾	28.0	26.1
G/T Peak (dB/K)	-2.0	0.5	-0.3	-0.6	-0.4 ⁽⁵⁾
HPBW (degrees)	—	7.5 × 1	7.5 × 1	7.5 × 1	
VSWR	1.4	<1.4	<1.4		
Axial Ratio (dB)	2.5	2.2 ⁽¹⁾	2.2 ⁽¹⁾		
Spec. FOV (degrees)	7.5 × 1	—	—		
Gain Over FOV (dB)	25.8	27.8 × 24.8 ⁽¹⁾	27.8 × 24.8 ⁽²⁾		
G/T Over Spec. FOV (dB/K)	-5.0	-2.5 × -5.5	-3.3 × -6.3	2.6	
<u>1550-MHz Parabolic Reflector (Fan Beam)</u>					
Transmitter Power (dBW)	15.0	15.4	15.3	16.1	15.6
Antenna Gain, Peak (dB)	No. Req't	31.8 ⁽¹⁾	31.8 ⁽²⁾	28.1	26.4
E.I.R.P., Peak (dBW)	45.0	47.2	47.1	44.2	42.0
HPBW (degrees)	—	7.2 × 1	7.2 × 1	7.2 × 1	
VSWR	1.4	<1.4	<1.4		
Axial Ratio (dB)	2.5	1.85 ⁽¹⁾	1.85 ⁽¹⁾		
Spec. FOV (degrees)	7.5 × 1	—	—		
Gain Over FOV (dB)	27.0	28 × 26.3 ⁽¹⁾	28 × 26.3 ⁽²⁾		
E.I.R.P. Over Spec. FOV (dBW)	42.0	43.4 × 41.7	43.3 × 41.6	42.1	

Table E-1
E.I.R.P. and G/T Summary (continued)

	Spec.	Measured		Post-Launch	End-of Life
		Best	Worst		
<u>1650-MHz Parabolic Reflector</u> (Pencil Beam)					
Receiver NF (dB)	6.2	5.7	6.5		
Antenna Gain, Peak (dB)	36.2	28.4 ⁽³⁾	38.4	35.8	35.5
G/T Peak (dB/K)	5.5	8.1	7.3	7.6	7.5
HPBW (degrees)		1.3 × 1.3 ⁽³⁾	1.3 × 1.3		
VSWR	1.4	<1.4	<1.4		
Axial Ratio (dB)	2.5	1.8 ⁽¹⁾	1.8 ⁽¹⁾		
Spec. FOV (degrees)	1.3				
Gain Over FOV (dB)	33.3	35.4 × 35.4	35.4 × 35.4		
G/T Over Spec. FOV (dB/K)	2.5	5.1 × 5.1	4.3 × 4.3		
<u>1550-MHz Parabolic Antenna</u> (Pencil Beam)					
Transmitter Power (dBW)	1.5	15.4	15.3	15.6	15.7
Antenna Gain, Peak (dB)	36	37.7 ⁽³⁾	37.7	35.6	34.3
E.I.R.P., Peak (dBW)	51	53.1	53.0	51.2	50.0
HPBW (degrees)	—	1.4 × 1.4 ⁽³⁾	1.4 × 1.4	1.3 × 1.3	
VSWR	1.4	<1.4	<1.4		
Axial Ratio (dB)	2.5	2.3 ⁽²⁾	2.3 ⁽¹⁾		
Spec. FOV (degrees)	1.3				
Gain Over FOV (dB)	33	35 × 34.8 ⁽³⁾	35 × 34.8		
E.I.R.P. Over Spec. FOV (dBW)	48	50.4 × 50.2	50.3 × 50.1		
<u>2250-MHz Parabolic Reflector</u> (Scan Beam)					
Receiver NF (dB)	4.8	4.8	5.6	*	
Antenna Gain, Peak (dB)	No Req't	40.7 ⁽¹⁾	40.6 ⁽²⁾	39.9	
G/T Peak (dB/K)		11.3	10.4	10.0	
HPBW (degrees)					
VSWR	1.4	<1.4	<1.4		
Axial Ratio (dB)	2.5	0.8 ⁽¹⁾	3.7 ⁽¹⁾		
Spec. FOV (degrees)	9.8				
Gain Over FOV (dB)	36.4	36.9 × 35.6 ⁽¹⁾	36.8 × 35.5 ⁽²⁾		
G/T Over Spec. FOV (dB/K)	7.0	7.5 × 6.2	6.6 × 5.3		

*N-1 Beam

Table E-1
E.I.R.P. and G/T Summary (continued)

	Spec.	Measured		Post-Launch	End-of Life
		Best	Worst		
<u>2075-MHZ Parabolic Reflector</u> (Scan Beam)					
Transmitter Power (dBW)	12.0	13.0	11.4	11.1	
Antenna Gain, Peak (dB)	38.4	41 ⁽¹⁾	40.9 ⁽²⁾	41.2	
E.I.R.P., Peak (dBW)	51.0	54	52.3	52.3	
HPBW (degrees)					
VSWR	1.4	<1.4	<1.4		
Axial Ratio (dB)	2.5	1.5 ⁽¹⁾	3.6 ⁽¹⁾		
Spec. FOV (degrees)	9.8				
Gain Over FOV (dB)	35.9	36.5 × 35.7 ⁽¹⁾	36.4 × 35.6 ⁽²⁾		
E.I.R.P. Over Spec. FOV (dBW)	49	49.5 × 48.7	47.8 × 47.0		
<u>2250-MHz Parabolic Reflector</u> (On-Axis)					
Receiver NF (dB)	4.8	4.8	5.6		
Antenna Gain, Peak (dB)	38.9	40.0	39.9		40.6
G/T Peak (dB/K)	9.5	10.6	9.7	10.4	8.9 (9.2) [†]
HPBW (degrees)					
VSWR	1.5	<1.5	1.72		
Axial Ratio (dB)	2.5	8.0 ⁽¹⁾	8.0 ⁽¹⁾	7.05	
Difference Ratio (dB)	3	0.6 × 0.0 ⁽¹⁾	0.8 × 0.3 ⁽¹⁾		
Spec. FOV (degrees)	1				
Cross-Coupling (dB)	20	21.2 ⁽¹⁾	20 ⁽¹⁾		
Gain Over FOV (dB)	35.9	36.6 × 36.3	36.5 × 36.2 ⁽²⁾		
G/T Over Spec. FOV (dB/K)		7.2 × 6.9	6.3 × 6.0		
<u>2075-MHz Parabolic Reflector</u> (On-Axis)					
Transmitter Power (dBW)	12.0	13.0	11.4		11.4
Antenna Gain, Peak (dB)	38.4	40.2 ⁽¹⁾	40.1 ⁽²⁾		37.4 [†]
E.I.R.P., Peak (dBW)	51.0	53.2	51.5	52.5	(48.8)
HPBW (degrees)		0.98 × 0.97 ⁽¹⁾	0.98 × 0.97 ⁽¹⁾	0.98 × 0.97	
VSWR	1.4	<1.4	<1.4		
Axial Ratio (dB)	2.5	3.9 ⁽¹⁾	3.9 ⁽¹⁾		
Spec. FOV (degrees)	1				
Gain Over FOV (dB)	35.4	37 × 26.7 ⁽¹⁾	36.9 × 36.6 ⁽²⁾		
E.I.R.P. Over Spec. FOV (dBW)		50 × 49.7	48.3 × 48.0		

*N-1 Beam

†Preamp No. 2

Table E-1
E.I.R.P. and G/T Summary (continued)

	Spec.	Measured		Post-Launch	End-of-Life
		Best	Worst		
<u>2570-MHz Parabolic Reflector</u>					
Transmitter Power (dBW)		11.9	11.1		
Antenna Gain, Peak (dB)	Prop. 41.9	41.3 ⁽³⁾	41.2		
E.I.R.P., Peak (dBW)	53.0	53.2	52.3	52.7	
HPBW (degrees)		0.90 × 0.79 ⁽³⁾	0.90 × 0.79	0.8 × 1.1	
VSWR	1.4	<1.4	<1.4		
Axial Ratio (dB)	Prop. 2.5	0.75 ⁽¹⁾	0.75 ⁽¹⁾	3.1	
Spec. FOV (degrees)	Prop. 0.85				
Gain Over FOV (dB)	38.9	50.5 × 37.8 ⁽³⁾	38.4 × 37.6		
E.I.R.P. Over Spec. FOV (dBW)	50.0	50.5 × 49.7	49.5 × 48.7		
<u>2670-MHz Parabolic Reflector</u>					
Transmitter Power (dBW)		12.0	11.6		
Antenna Gain, Peak (dB)	Prop. 41.4	40.9	40.7		
E.I.R.P., Peak (dBW)	52.3	52.9	52.3		
HPBW (degrees)		0.82 × 0.83	0.80 × 0.80	0.80 × 0.80	
VSWR	1.4	<1.4	<1.4		
Axial Ratio (dB)	Prop. 2.5	2.2 ⁽¹⁾	2.2 ⁽¹⁾	3.9	
Spec. FOV (degrees)	Prop. 0.85				
Gain Over FOV (dB)	Prop. 38.4	37.8 × 27.8	37.4 × 37.4		
E.I.R.P. Over Spec. FOV (dBW)	49.5	49.8 × 49.8	49.0 × 48.9		
<u>860-MHz Parabolic Reflector</u>					
Transmitter Power (dBW)	18.1	19.2	18.7		
Antenna Gain, Peak (dB)	39.2	33.5 ⁽³⁾	33.5 ⁽¹⁾		
E.I.R.P., Peak (dBW)	51.0	52.7	52.2	52.6	
HPBW (degrees)				3.0 × 2.7	
VSWR	1.3	<1.3	<1.3		
Axial Ratio (dB)	2.5	1.4	1.7		
Spec. FOV (degrees)	2.8				
Gain Over FOV (dB)	29.9	30.5 × 30.2 ⁽³⁾	30.5 × 30.2 ⁽¹⁾	30.5 × 30.8	
E.I.R.P. Over Spec. FOV (dBW)	48	49.7 × 49.4	49.2 × 49.8	49.2 × 49.5	

Table E-1
E.I.R.P. and G/T Summary (continued)

	Spec.	Measured		Post-Launch	End-of Life
		Best	Worst		
<u>150-MHz Parabolic Reflector</u>					
Receiver NF (dB)	11.7	10.9	11.8		
Antenna Gain, Peak (dB)	14.3	14.4	14.4	14.4	
G/T Peak (dB/K)	-22	-21.1 ⁽³⁾	-22.0	-22.0	
HPBW (degrees)		15.0 × 14.3 ⁽³⁾	15.0 × 14.3		
VSWR	1.6	3.2	4.3		
Axial Ratio (dB)	3.0				
Difference Peaks (dB)	5	9 × 5 ⁽¹⁾	9 × 5 ⁽¹⁾		
Spec. FOV (degrees)	15				
Cross-Coupling (dB)	17	15.7 ⁽¹⁾	7.5 ⁽¹⁾		
Gain Over FOV (dB)	11.3	11.4 × 10.9 ⁽³⁾	11.4 × 10.9		
G/T Over Spec. FOV (dB/K)	-25	-24.1 × -24.6	-25 × -25.5		
<u>136-MHz Parabolic Reflector</u>					
Transmitter Power (dBW)	0.8	0.5	0.3		
Antenna Gain, Peak (dB)	14	13.8	12.8		
E.I.R.P., Peak (dBW)	14.8	14.3	13.1		
HPBW (degrees)		16 × 16 ⁽¹⁾	16 × 16 ⁽¹⁾	16 × 16	
VSWR	1.4	<1.4	<1.4		
Axial Ratio (dB)	3.0	3.8 ⁽¹⁾	3.8 ⁽¹⁾		
Spec. FOV (degrees)	15				
Gain Over FOV (dB)	11.0	10.9	9.9		
E.I.R.P. Over Spec. FOV (dBW)	11.8	11.4	10.2		

APPENDIX F

9.14-METER ANTENNA PATTERN MEASUREMENTS

INTRODUCTION

ATS-6 employed a 9.14-meter diameter parabolic antenna as a major component of its many configurations of communication links. Figure F-1 provides a description of the ATS-6 antenna and its prime-focus feed (PFF).

Antenna pattern measurements were accomplished by changing the attitude of the spacecraft in predetermined maneuvers that were executed from the ATS Operational Control Center (ATSOCC). The resultant attitudes during the maneuvers were measured, and referred to the line of sight to the Rosman Ground Station, in spacecraft body coordinates. The attitudes were computed and correlated to universal time (UT) at the ATSOCC in 3-second intervals and relayed to Rosman for input to the PDP-11 computer. Relative signal power was determined and correlated to UT for input to the PDP-11 computer. The results provided relative signal level power measurements, corresponding to attitude data suitable for antenna pattern plots. The patterns obtained from this method were those of radio frequency beams transmitted from the spacecraft. A similar method was employed to achieve receive antenna patterns while recording the signal level received by the spacecraft.

MEASUREMENT AND SIGNAL PROCESSING

The antenna patterns were derived by measuring signal power received at the ground station and at the spacecraft. These signals were collected at the ground station by Radio Frequency Interference Measurements Experiment (RFIME) equipment that included a special receiver/analyzer. The method determined the patterns in terms of relative gain, and positioned the patterns in spacecraft body coordinates. The results of the measurement were recorded at the ground station on digital tapes and ATSOCC line printers for computer and manual reduction.

The general procedure for antenna pattern measurement was to control the spacecraft attitude, so that it scanned the antenna pattern being measured (the spacecraft was slewed over the Rosman Ground Station). The actual resultant attitude, defining the line-of-sight to Rosman as the reference point in terms of spacecraft body coordinates, shown in Figures F-2 and F-3, was computed and relayed to Rosman in 3-second intervals for input to the RFIME receiver/analyzer system. Signal level power measurements were made by use of the linear detector in the RFIME receiver/analyzer and were subsequently correlated with the attitude data to define the spacecraft transmit antenna patterns. The spacecraft receive antenna pattern was determined from the measured signal power

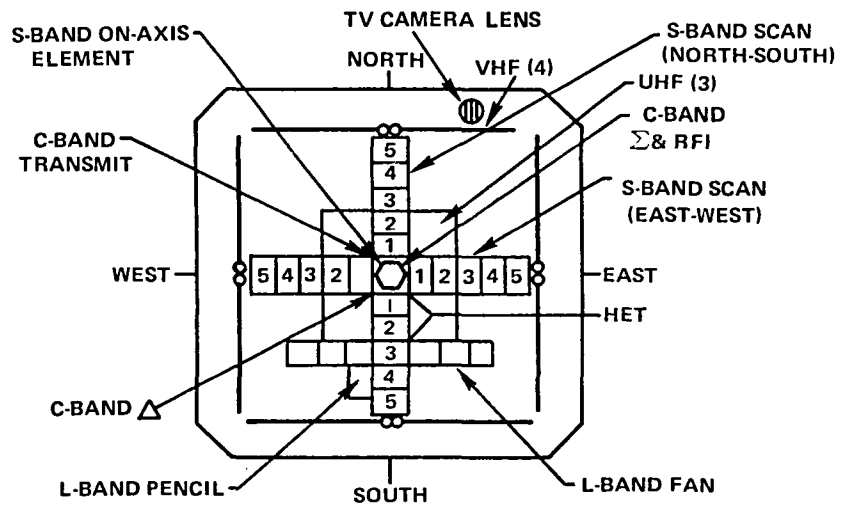
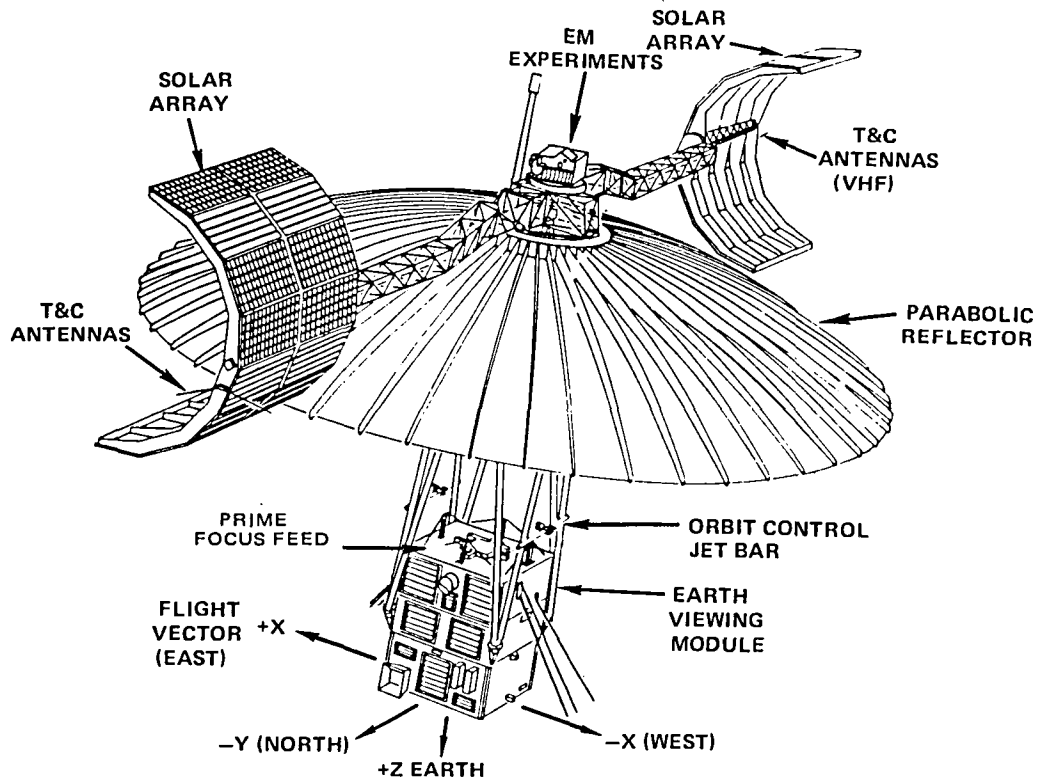


Figure F-1. ATS-6 Configuration In-Orbit and Prime-Focus Feed Diagram

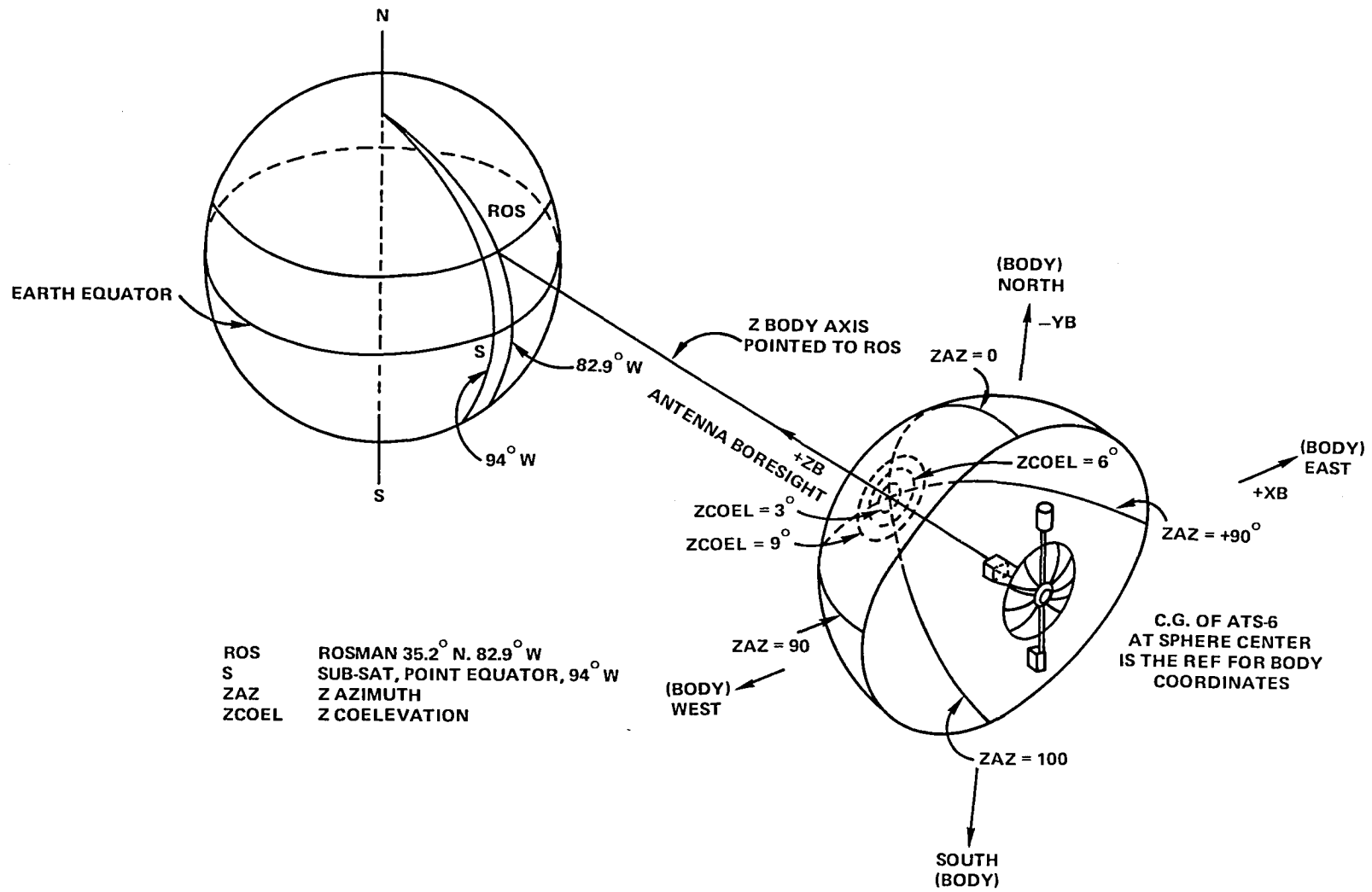


Figure F-2. ATS-6 Body Coordinates

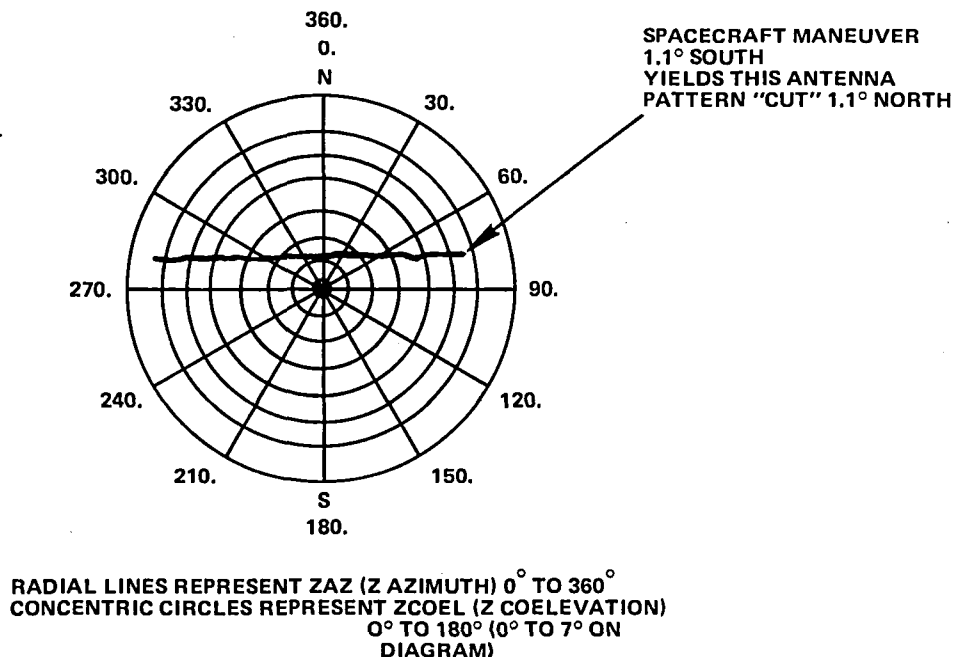


Figure F-3. ATS-6 Body Coordinates for Antenna Patterns

received at the spacecraft and sent to the RFIME equipment by spacecraft telemetry. The measurement results were produced by the RFIME receiver/analyzer in the following forms:

1. Raw Data

Raw data were recorded on magnetic tape in digital form to be used for off-line computer determination and analysis of antenna patterns. This data contained the attitude, time of year, and selected telemetry parameters on a 3-second sample period. The power measurements received at the spacecraft were obtained every 100 milliseconds.

2. Reduced Data

Reduced data were a line printer output of derived antenna pattern data that were used for off-line manual determination and analysis of antenna patterns. The data included relative antenna gain, attitude, time of year, and selected telemetry parameters. All data were on a 3-second sample period.

IN-ORBIT ANTENNA PATTERN MEASUREMENT

In-orbit antenna patterns were made by slewing the spacecraft. The attitude of the spacecraft during the slews, in particular, the directions of the line-of-sight to the Rosman Ground Station, was described in a spacecraft body centered coordinate system. Figure F-2 shows the defining geometry of

the body centered *Zaz*, *Zcoel* (*Z*-azimuth, *Z*-coelevation) coordinate system in which the line-of-sight to the ground station is described during an antenna pattern measurement slew. These plots accompany the antenna patterns and indicate the relative motion between the ground station and ATS-6. The coordinates defined in Figure F-3 are the ATS-6 body coordinates for antenna patterns used in the *Zaz*, *Zcoel* diagrams that accompany the patterns. Figure F-3 depicts an east-west antenna pattern cut 1.1° north of the body *Z*-axis. The spacecraft maneuver to achieve this cut was a west-to-east maneuver 1.1° south of the roll axis.

SPACECRAFT MANEUVERS FOR ANTENNA PATTERN MEASUREMENT

The actual vhf patterns and the required maneuvers to measure them are described to illustrate the general procedures used in measuring the antenna patterns.

VHF Antenna Patterns

The vhf prime-focus feed patterns were measured at 137.11 MHz. The antenna feed element locations are shown in Figure F-1.

Figure F-4 shows ATS-6 maneuvers for the vhf pattern measurement, and depicts the motion of the spacecraft *Z*-axis projected on the surface of the Earth during the maneuvers. Arrows have been manually added to the figure to show the directions of the slewing. Care was taken during the antenna pattern maneuvers to keep the spacecraft pointed to within $\approx 2^\circ$ of the Earth's disc, to allow the Earth sensors to remain locked to the Earth. Figure F-5 illustrates the antenna pattern cuts obtained from the maneuver shown in Figure F-5. Figure F-6 shows a composite pattern of all the cuts shown in Figure F-5 (each cut represents a segment of the composite pattern).

UHF Antenna Patterns

The uhf patterns were measured at 860 MHz. Antenna feed locations on the prime-focus feed are shown in Figure F-1. Preflight, in-orbit, and end-of-life measurements are shown in Figure F-7. The excellent agreement that is evident between the end-of-life measurement and the earlier measurements is proof of the antenna's integrity.

L-Band Pencil Beam Patterns

The L-band pencil beam was offset from the spacecraft *Z*-axis by 1° to the east and 3.9° to the north. (Figure F-1 shows the feed offset to the west which places the beam offset to the east.)

The end-of-life pattern is shown in Figure F-8. It indicated that the main lobe of the L-band pencil beam remained essentially the same compared to the initial in-orbit measurement made approximately 5 years earlier.

L-Band Fan Beam Patterns

The L-band fan beam was offset to cover the North Atlantic area with the fan beam when ATS-6 was located at 94°W longitude. (Transatlantic aircraft communications was tested in this area.)

To compare the in-flight patterns with preflight measurements, cuts were chosen 3.1°N for the E-W slew and 1°E for N-S slew. These patterns were “overlayed” on the preflight pattern and the results are shown in Figures F-9 and F-10. The correlation is quite good for the E-W results except for the “dip.” This may be because the preflight pattern used the hard reflector instead of the flight model. Similarly for the same reason, the results for the N-S patterns show some discrepancy.

A contour pattern of the L-band fan beam showing contours of equal power levels, scaled in pitch and roll, is shown in Figure F-11.

S-Band Antenna Patterns

As shown in Figure F-1, the prime-focus feed contained more S-band antenna elements than any of the other frequency bands. The on-axis S-band feed consisted of the antenna elements (annulus) surrounding the C-band feed. The antenna patterns for the on-axis feed are shown in Figures F-12 and F-13.

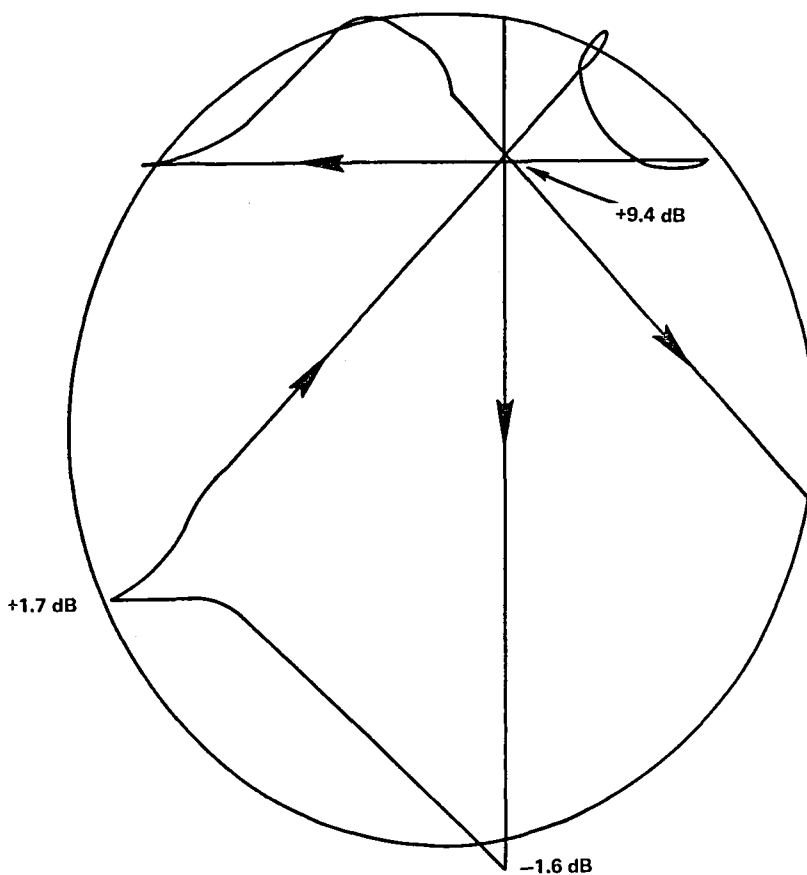
The S-band cross-axis antenna patterns are presented in a composite fashion for the E-W and N-S axes. These antenna patterns show only the main lobes and are compared with the preflight patterns. Good correlation was achieved between the preflight and in-orbit patterns as is shown in Figures F-14 and F-15. Patterns for the individual S-band feeds were measured with extra attention paid to N1 and N2 beams (S1 and S2 feeds) that were used for the Health, Education, Telecommunications (HET) experiment. Figure F-16 shows the antenna pattern for the N1 beam for in-orbit, preflight and end-of-life measurements indicated. It is interesting to note that the in-orbit pattern “skipped” the first nulls on either side of the main beam, while the end-of-life measurements were made at a much slower rate and indicate the existence of the null on the easterly side of the main beam. The antenna pattern for Beam N5 is presented in Figures F-17 and F-18. This beam provided an example of an antenna pattern for a feed element at the extreme end of the S-band array in the prime-focus feed.

C-Band On-Axis Prime-Focus Feed Beam Patterns

Figures F-19 and F-20 show preflight and inflight patterns using the C-band prime-focus feed. The differences may be explained, in part, by the preflight model (hard reflector) being different from the flight model (soft reflector) structure.

CONCLUSION

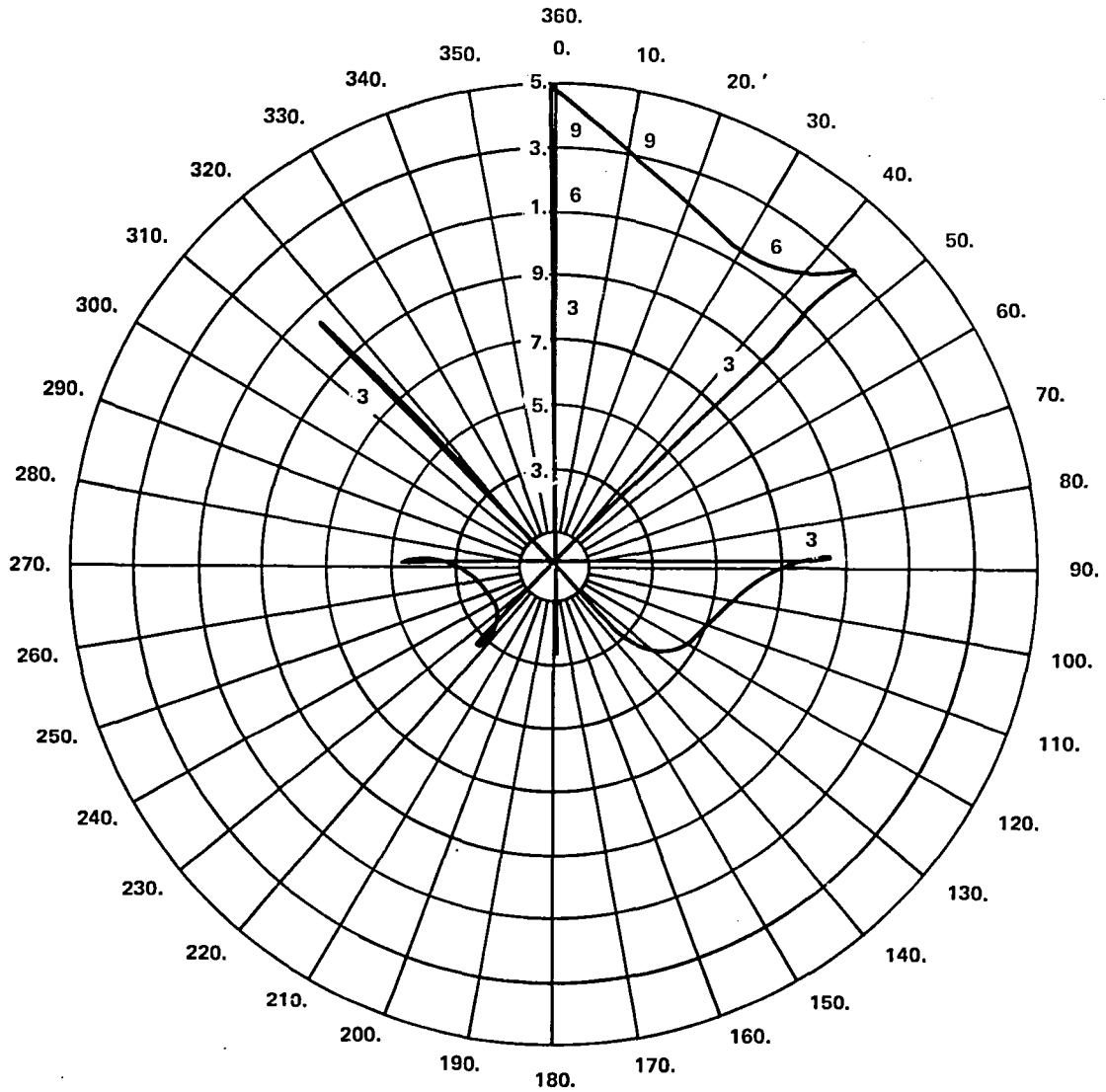
The end-of-life antenna pattern measurements show that the 9.14-meter parabolic dish of ATS-6 kept its integrity throughout its entire life. Additional antenna pattern information is available in NASA Technical Note D-8135, entitled "ATS-6 Spacecraft: In-Flight Antenna Measurement," by L. W. Nicholson et al., January 1976.



REFERENCE NOTATIONS AND VALUES HAVE BEEN MANUALLY ADDED.

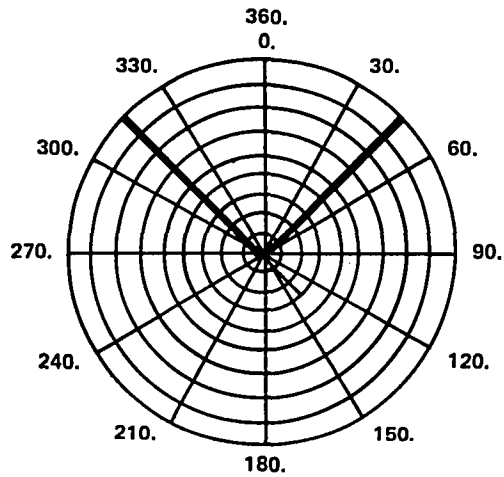
Figure F-4. Earth Disc Display of Spacecraft Maneuvers for VHF Antenna Pattern Measurement

ATS-6 ANTENNA PATTERN GAIN VS. ATTITUDE



ATTITUDE EXPRESSED AS ZAZ AND ZCOEL IN DEGREES

Figure F-5. Antenna Pattern "Cuts" for VHF Measurement



ATS-6 INFLIGHT ANTENNA PATTERN
FEED: VHF BEAM: ON-AXIS
FREQ: 137.11 MHz SCAN: N-S, SE-NW, E-W, SW-NE
DAY: 048 DATE: FEB. 17, 1975

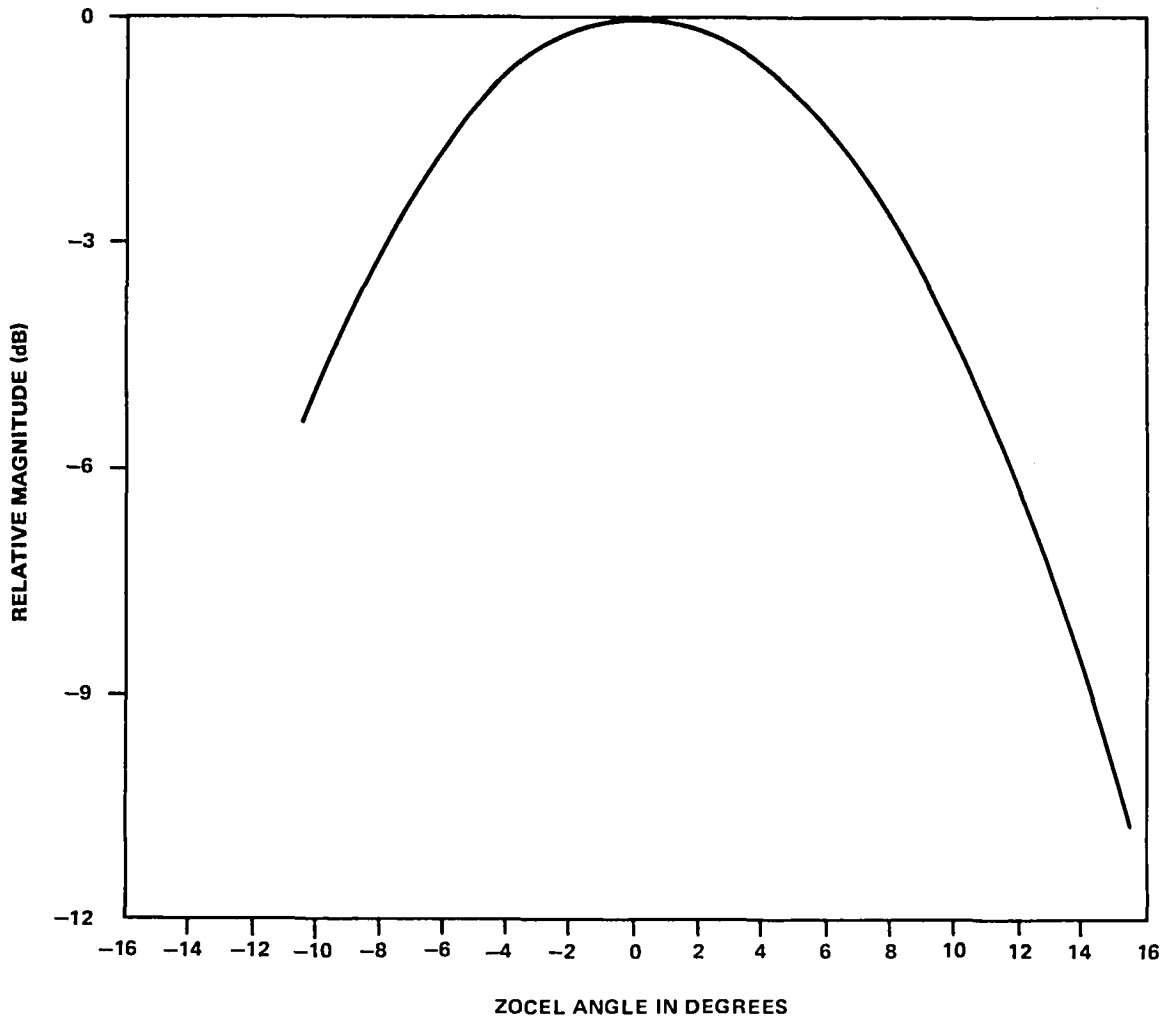
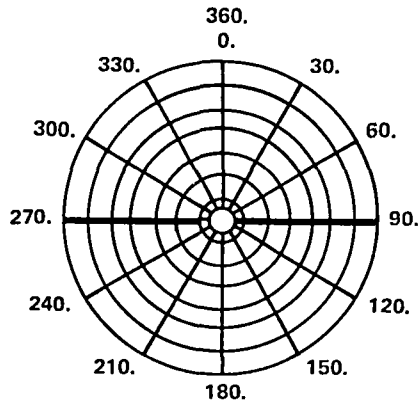


Figure F-6. VHF Antenna Pattern Composite

ATS-6 FINAL ENGINEERING PERFORMANCE REPORT



ATS-6 INFLIGHT ANTENNA PATTERN
 FEED: UHF BEAM: ON-AXIS
 FREQ: 860 MHz SCAN: E-W
 DAY: 166 DATE: JUNE 15, 1974
 DURING TIME: 0755 TO 0825 Z

PREFLIGHT PAT. NO. 27
 SEPT. 25, 1973 HARD REFLECTOR

PREFLIGHT
 IN-ORBIT

END-OF-LIFE TESTS: XXX
 DAY 191 DATE: JULY 10, 1979
 DURING TIME 1707 Z TO 1721 Z

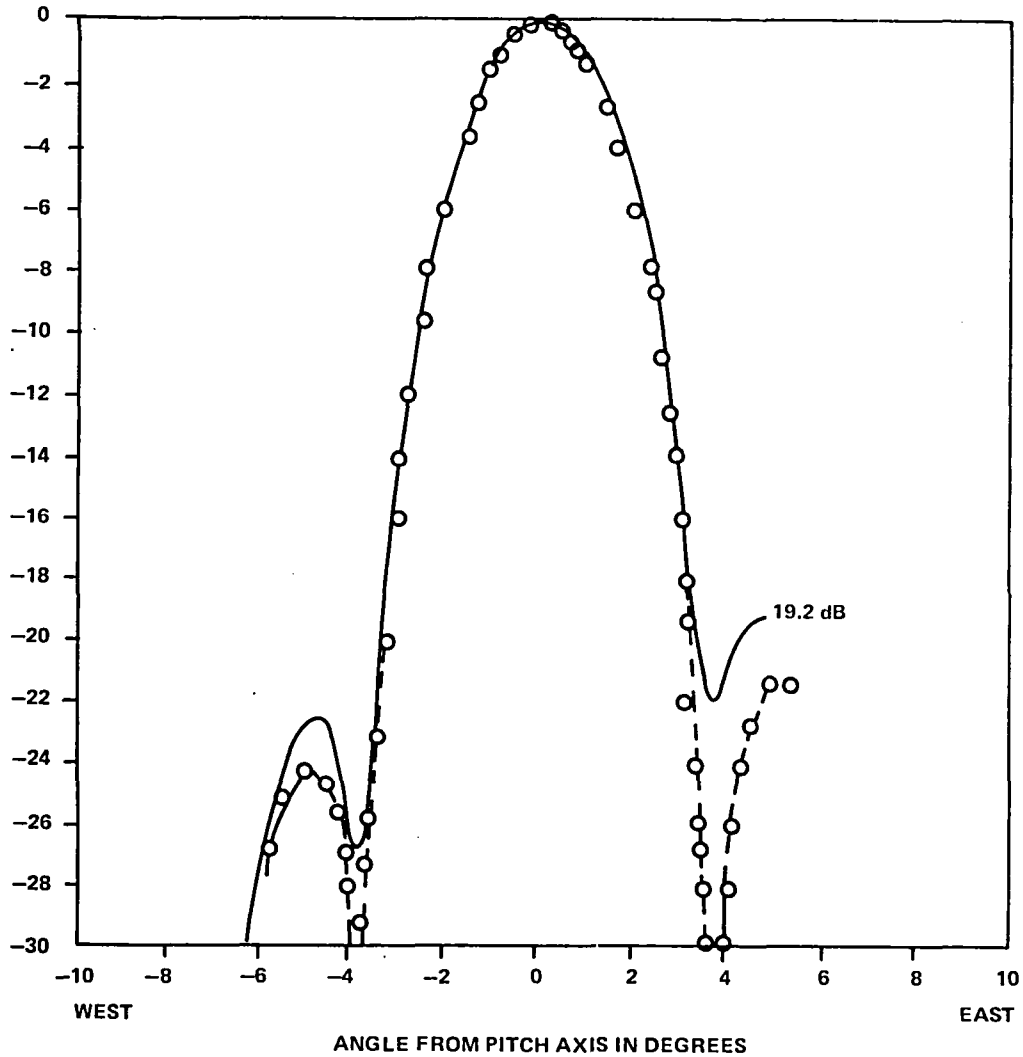


Figure F-7. UHF Antenna Pattern E-W

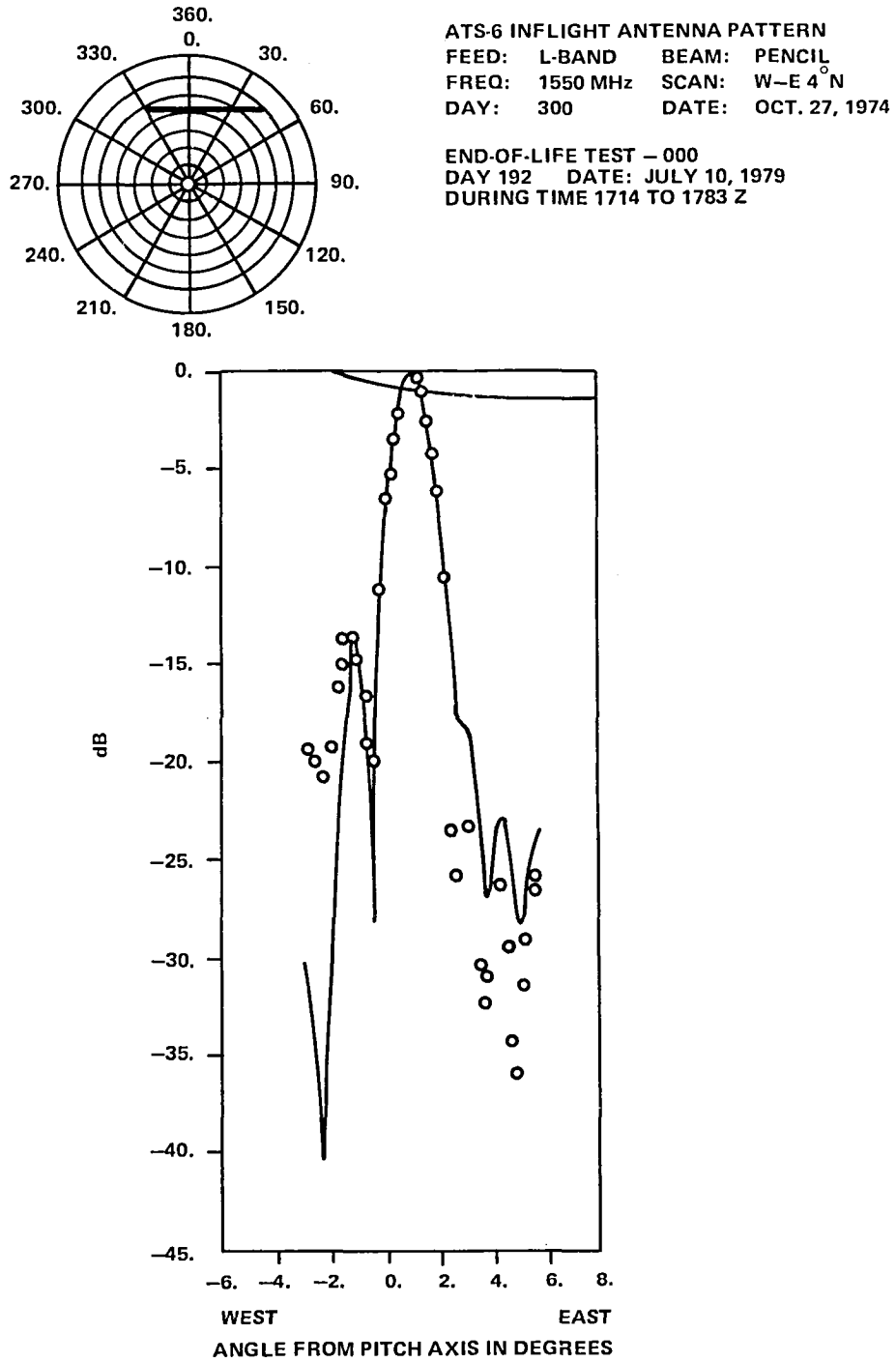
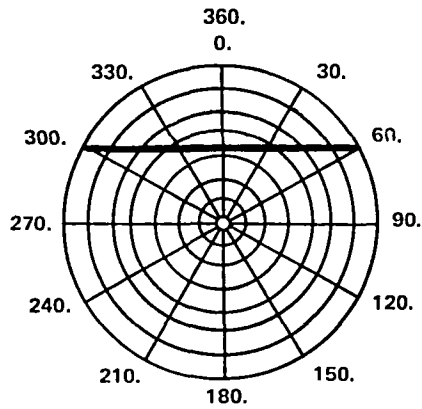


Figure F-8. L-Band Pencil Beam Antenna Pattern



ATS-6 INFLIGHT ANTENNA PATTERN
 FEED: L-BAND BEAM: FAN
 FREQ: 1850 MHz SCAN: E-W 3.1° N
 DAY: 279 DATE: OCT. 6, 1973
 DURING TIME: 2220 Z TO 2213 Z

PREFLIGHT PATTERN NO. 10 SEPT. 28, 1973
 HARD REFLECTOR 1650 MHz RCP

LEGEND: INFLIGHT PATTERN ○-○-○
 PREFLIGHT PATTERN ———

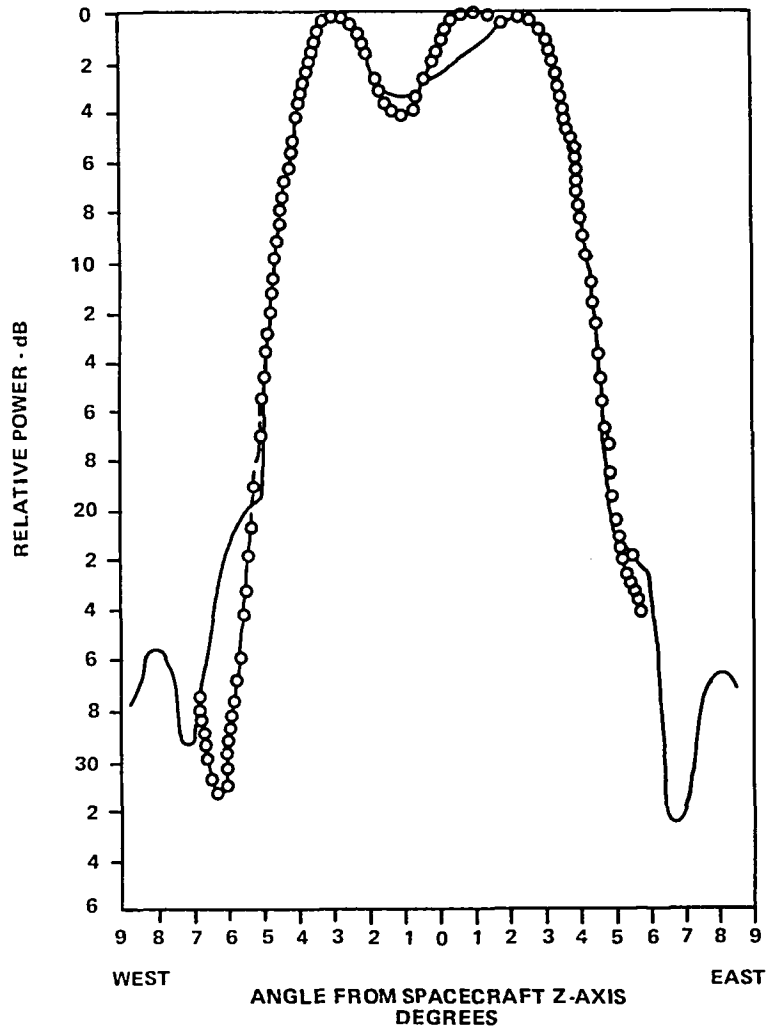
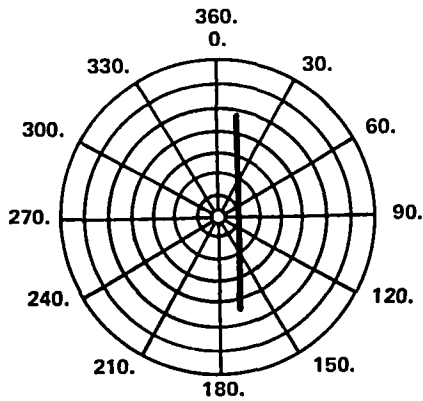


Figure F-9. L-Band Fan Beam Pattern E-W 3.1° N



ATS-6 INFLIGHT ANTENNA PATTERN
 FEED: L-BAND BEAM: FAN
 FREQ: 1650 MHz SCAN: N-S 1° E
 DAY: 279 DATE: OCT. 6, 1974
 DURING TIME: 1540 Z TO 1610 Z

PREFLIGHT PATTERN NO. SEPT. 28, 1973
 1650 MHz RCP, HARD REFLECTOR

LEGEND: INFLIGHT PATTERN ○○○○
 PREFLIGHT PATTERN ———

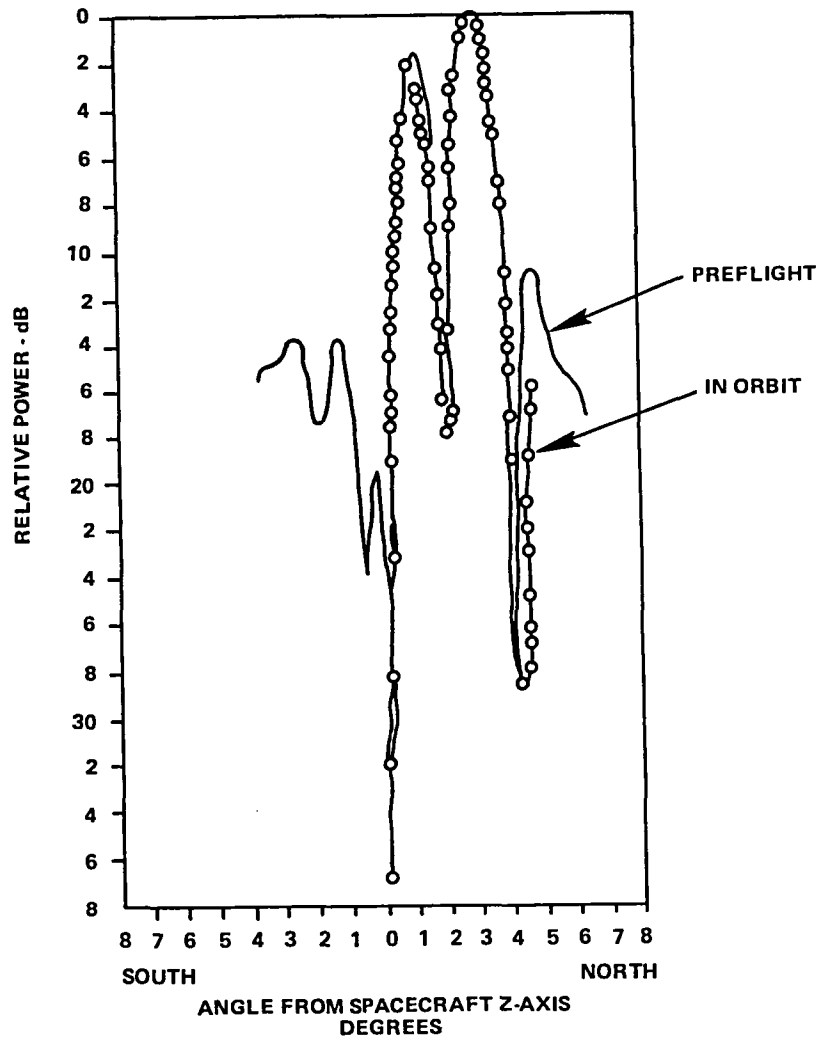


Figure F-10. L-Band Fan Beam Pattern N-S 1° E

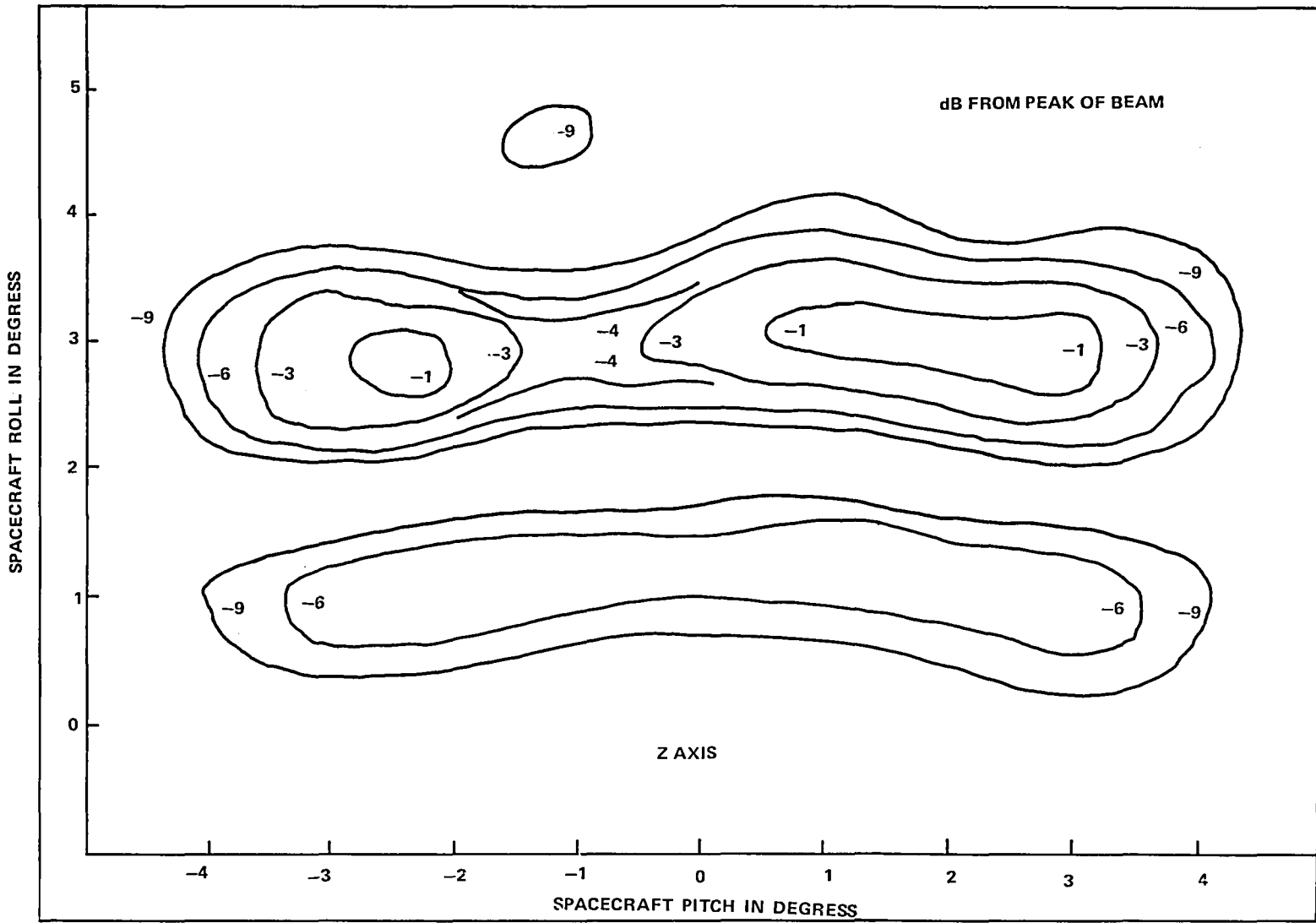
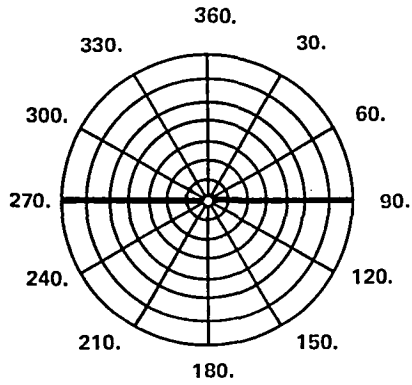


Figure F-11. L-Band Fan Beam Contours of Equal Power Levels



ATS-6 INFLIGHT ANTENNA PATTERN
FEED: ON-AXIS BEAM: ON-AXIS TRANSMIT
FREQ: 2075 MHz SCAN: E-W
DAY: 306 DATE: NOV. 2, 1974
DURING TIME: 1945 Z TO 2000 Z

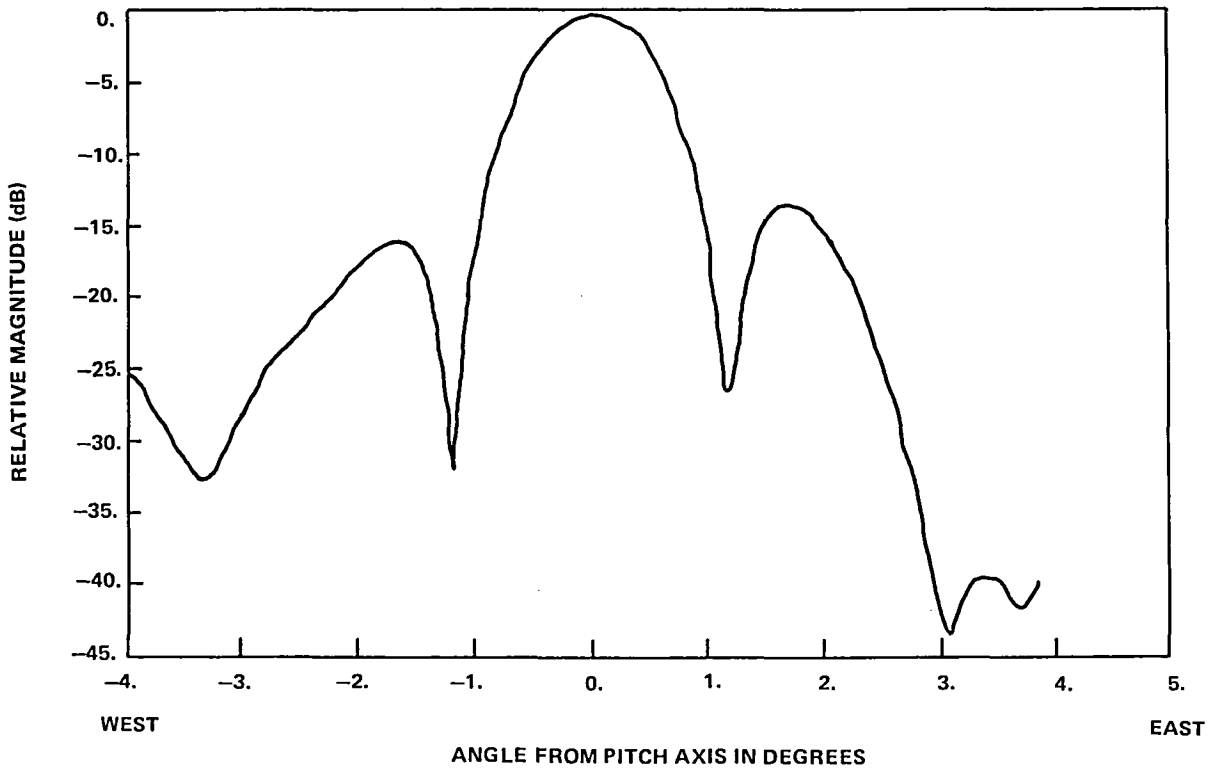


Figure F-12. S-Band On-Axis Beam E-W

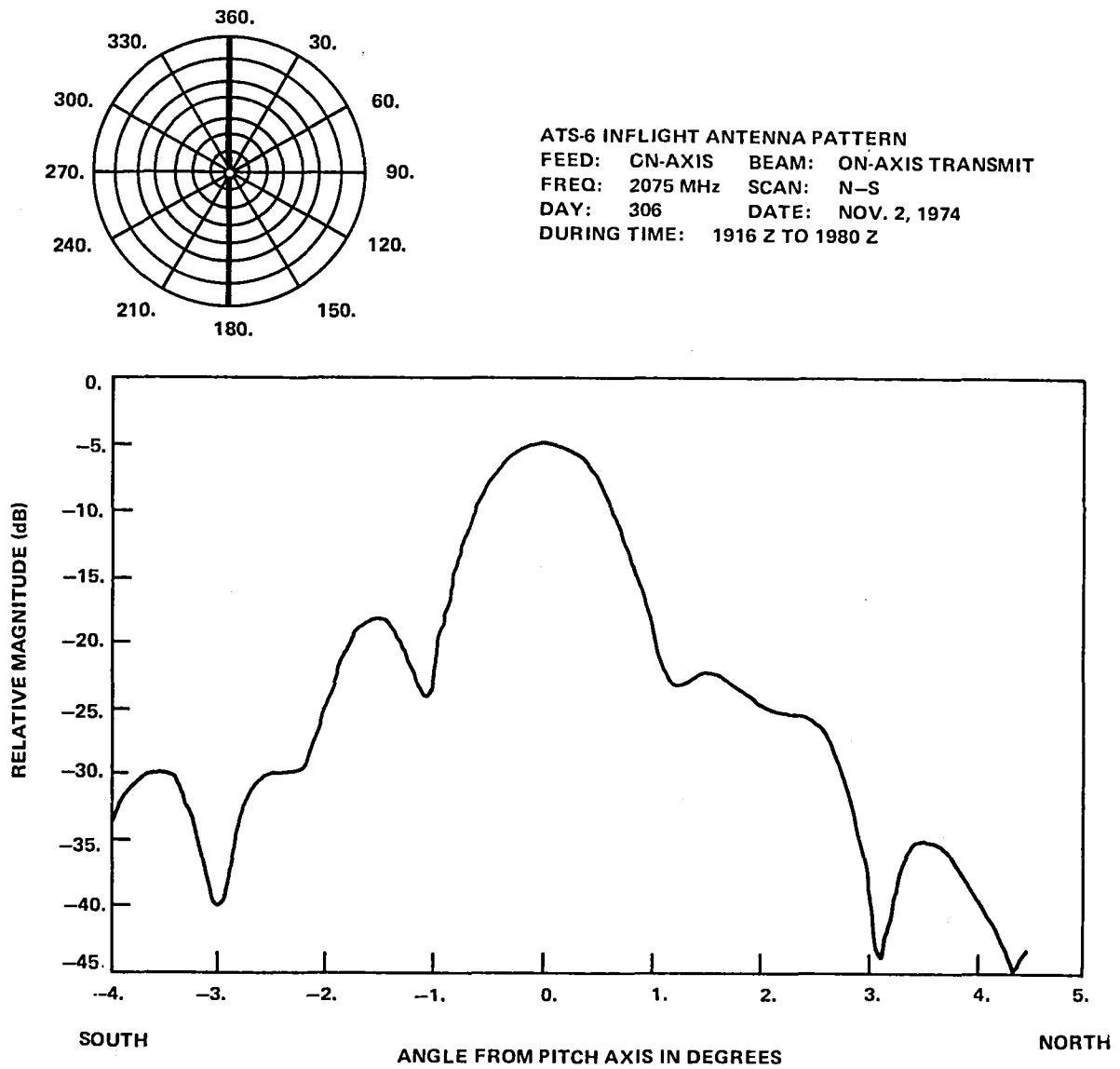
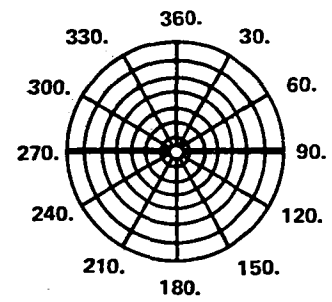
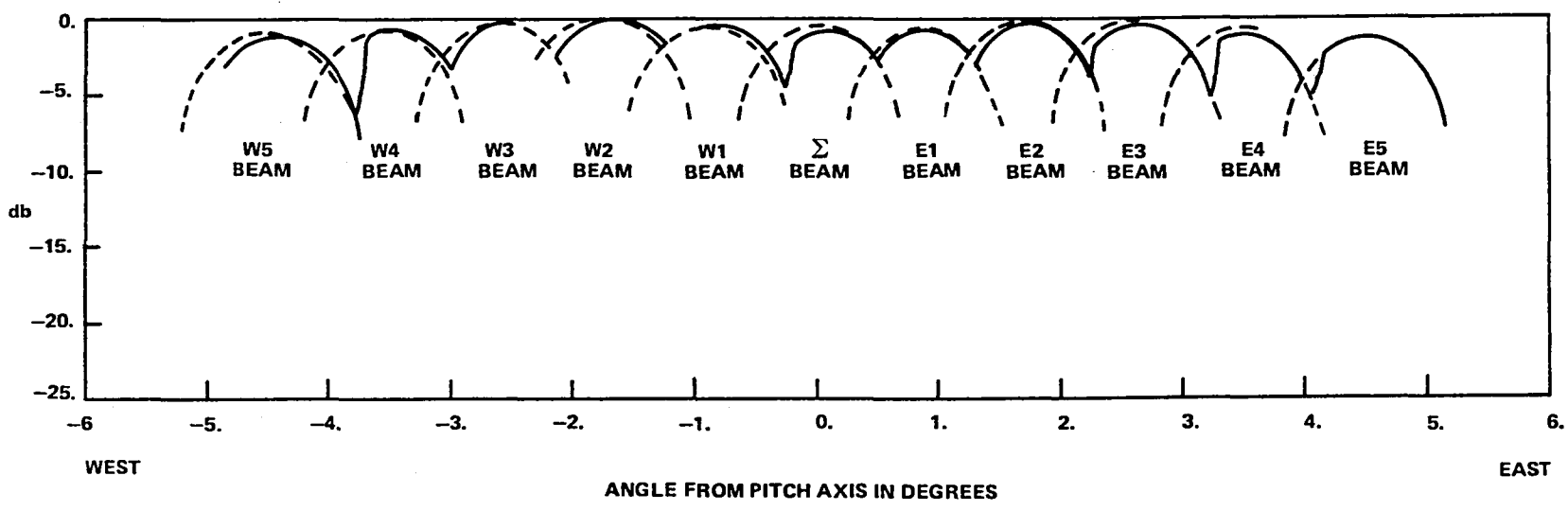


Figure F-13. S-Band On-Axis Beam N-S

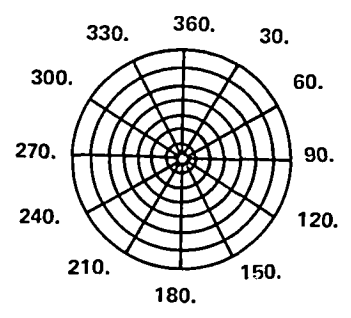


ATS-6 INFLIGHT ANTENNA PATTERN
FEED: E5-W6 BEAM: W5-E6 AS INDICATED
FREQ: 2075 MHz SCAN: W → E
DAY: 308 DATE: NOV. 4, 1974
DURING TIME: 0120 Z TO 0144 Z

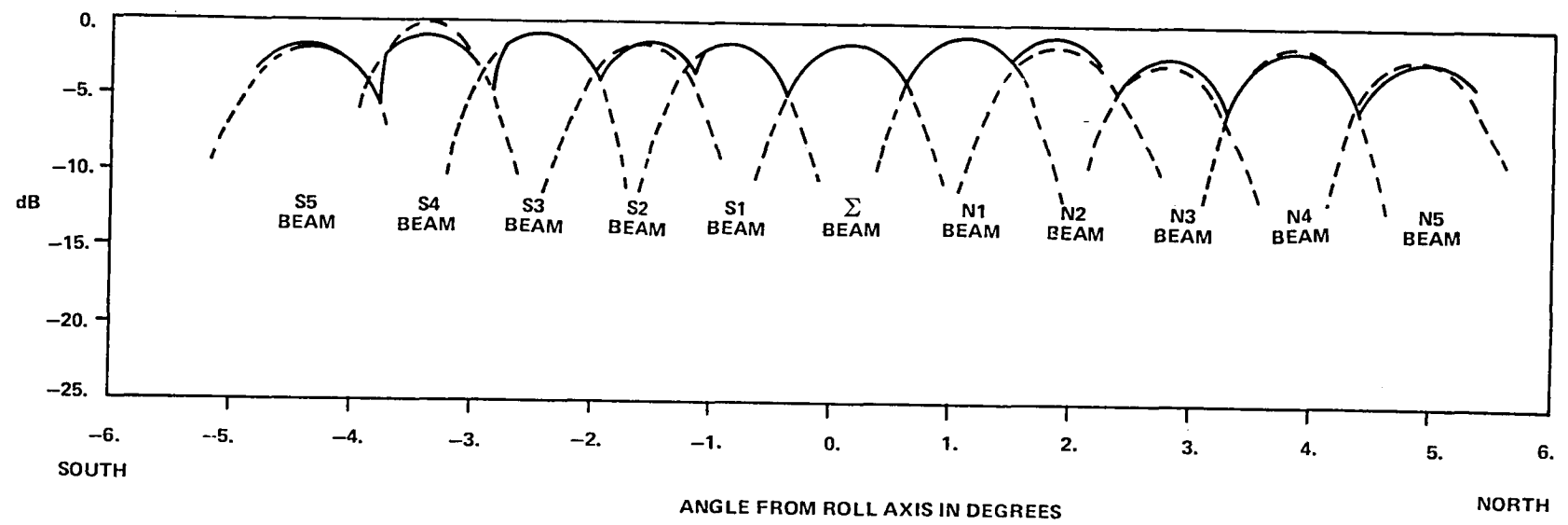


LEGEND: IN-ORBIT ———
PREFLIGHT - - - - -

Figure F-14. S-Band Cross-Axis Patterns E-W

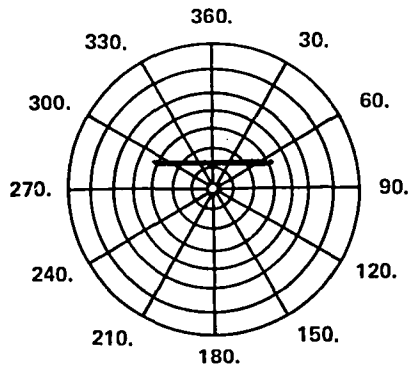


ATS-6 INFLIGHT ANTENNA PATTERN
 FEED: N5-S5 BEAM: S5-N5 AS INDICATED
 FREQ: 2075 MHz SCAN: S N
 DAY: 308 DATE: 11/4/74
 DURING TIME: 0214 TO 0235 Z



LEGEND: IN-ORBIT ———
 PREFLIGHT - - - - -

Figure F-15. S-Band Cross-Axis Patterns N-5



ATS-6 INFLIGHT ANTENNA PATTERN
 FEED: S1 BEAM: N1
 FREQ: 2569.2 MHz SCAN: E-W 1.1°N
 DAY: 306 DATE: NOV. 2, 1974
 DURING TIME: 1006 Z TO 1017 Z

LEGEND: IN-ORBIT ———
 PREFLIGHT - - -
 HARD REFLECTOR OCT. 1, 1973
 2569 MHz
 LCP P06
 END-OF-LIFE ○ ○ ○
 DAY 190 DATE: JULY 8, 1974
 DURING TIME: 1639 Z TO 1651 Z

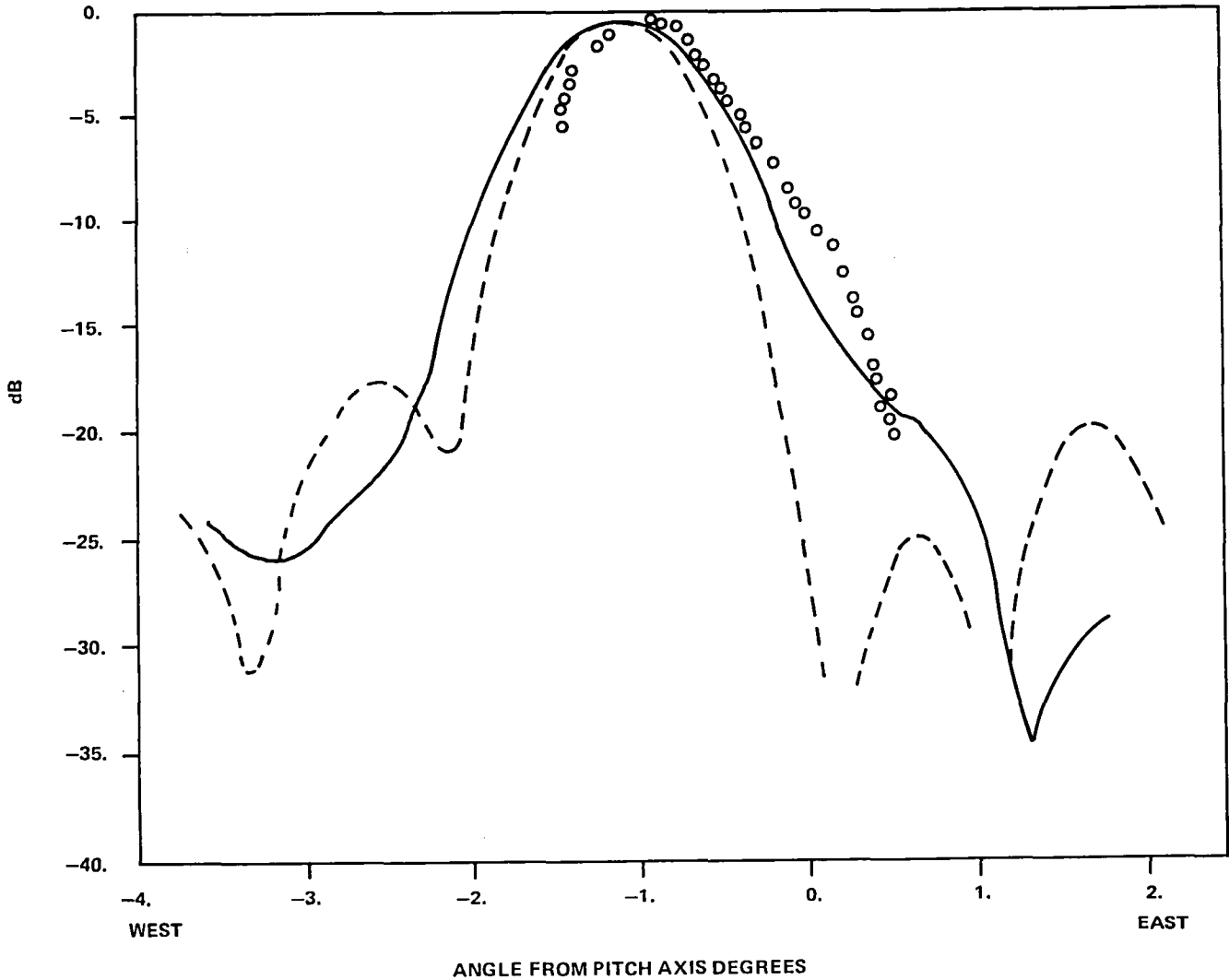
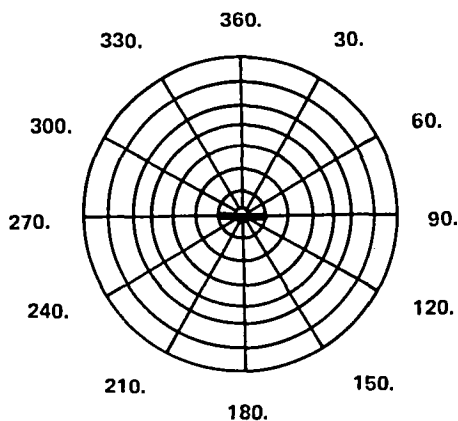


Figure F-16. S-Band HET E-W 1.1°N



ATS-6 INFLIGHT ANTENNA PATTERN
 FEED: CBANDPFF BEAM: RECV. ON-AXIS
 FREQ: 5972 MHz SCAN: E-W
 DAY: 19 DATE: JAN. 19, 1975
 DURING TIME: 01482 TO 0154 Z

PREFLIGHT PATTERN NO. 6
 SEPT. 25, 1973

HARD REFLECTOR 5925 MHz
 LEGEND: PREFLIGHT PATTERN ———
 INFLIGHT PATTERN ○—○—○—○

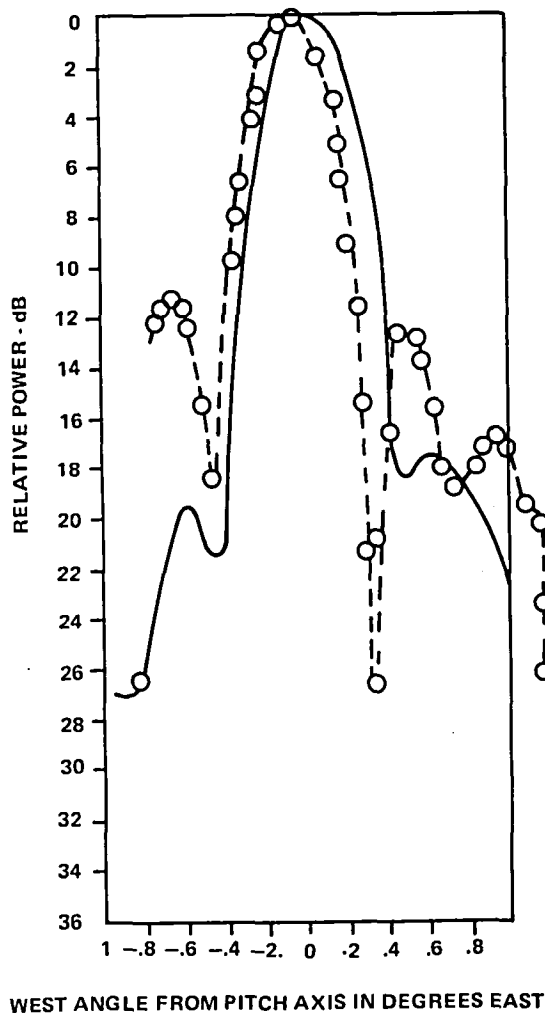
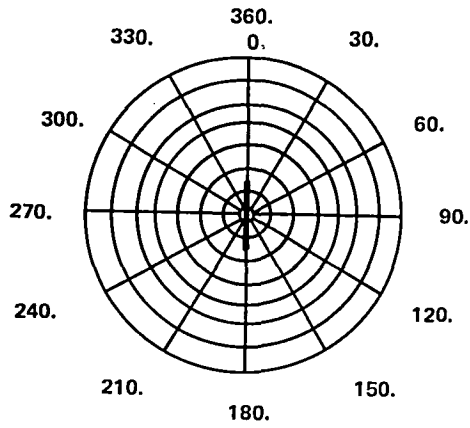


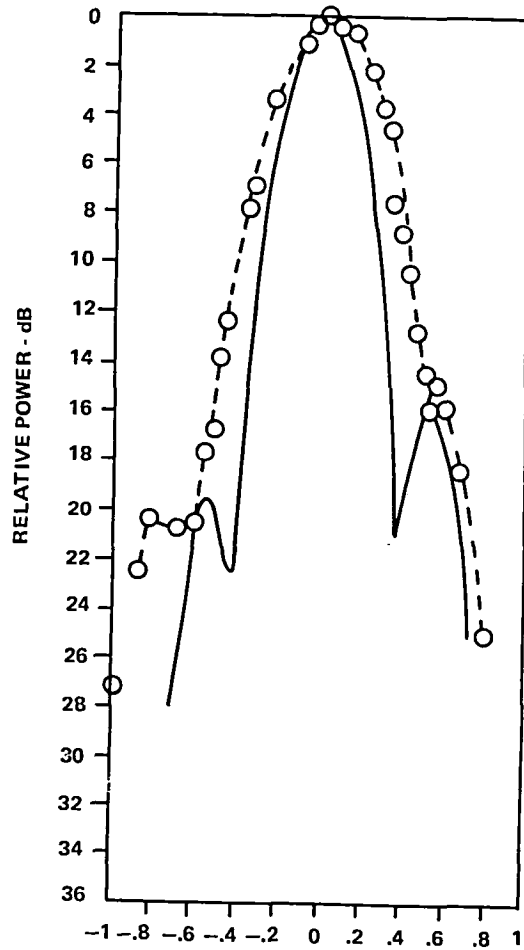
Figure F-19. C-Band Beam E-W

ATS-6 FINAL ENGINEERING PERFORMANCE REPORT



ATS-6 INFLIGHT ANTENNA PATTERN
 FEED: CBANDPFF BEAM: RECV. ON-AXIS
 FREQ: 5972 MHz SCAN: N-S
 DAY: 19 DATE: JAN. 19, 1975
 DURING TIME: 05012 TO 0538 Z

PREFLIGHT PATTERN NO. 19
 SEPT. 25, 1973
 HARD REFLECTOR 5925 MHz
 LEGEND: PREFLIGHT PATTERN ———
 INFLIGHT PATTERN —○—○—○



SOUTH ANGLE FROM ROLL AXIS IN DEGREES NORTH

Figure F-20. C-Band Beam N-S

Appendix G
Acronyms and Abbreviations

APPENDIX G
ACRONYMS AND ABBREVIATIONS

A

A	ampere
Å	Angstrom
ABC	analog backup controller
AC	attitude control
a.c.	alternating current
ACE	actuator control electronics
ACP	acquisition control program
acq.	acquisition
ACS	attitude control subsystem
ACSN	Appalachian Community Service Network
A/D	analog to digital
ADC	analog-to-digital converter
ADPE	automatic data processing equipment
ADS	automatic deployment sequencer
ADSS	auxiliary digital Sun sensor
ADVM	adaptive delta voice modulation
A/E	absorbitivity to emissivity
Aerosat	aeronautical satellite
AES	Ahmedabad Earth Station
AESP	Appalachian Education Satellite Project
af	audio frequency
AFC	automatic frequency control
AFTE	Advanced Thermal Control Flight Experiment
AGC	automatic gain control
AGE	aerospace ground equipment
Ah	ampere-hour
AID	Agency for International Development
AIDSAT	Agency for International Development Television Demonstration
AIR	All India Radio
ALC	automatic level control
ALED	Alaska Education Experiment
am, AM	amplitude-modulation
AMP	amplifier
AOS	acquisition of satellite
APM	antenna pattern measurement

APT	automatic picture transmission
ARC	Appalachian Regional Commission
ASC	Aerospace Corporation
ASP	automated sequential processor
ASSY	assembly
ASTP	Apollo-Soyuz Test Program
ASTP-TV	ASTP television coverage experiment
ATA	automatic threshold adjust
AT&T	American Telephone and Telegraph (Spacecraft)
ATC	air traffic control, active thermal control
ATFE	Advanced Thermal Control Flight Experiment
atm, ATMOS	atmosphere(s)
ATS	Applications Technology Satellite
ATS-6	Applications Technology Satellite-6
ATSOCC	ATS Operations Control Center
ATS-R	ATS ranging
ATSSIM	ATS simulator
Atten	attenuator (attenuation)
Aux	auxiliary

B

B&E	Broadcast and Engineering
BAM	building attenuation measurement
BB	baseband
BER	bit error rate
bps	bits per second
BRC	Balcones Research Center
BSA	bit synchronization acquisition
BTC	binary time code
BTE	bench test equipment
Btu	British thermal unit
BW	bandwidth

C

C	Celsius
Cap Com	Capsule Communicator
CCIR	International Radio Consultative Committee
CDD	command/decoder distributor
CEE	designator for "career education course for elementary-grade teachers"
CES	designator for "career education course for secondary-grade teachers"
CESP	computer executive system program
CFSS	coarse/fine Sun sensors

CIC	command interface control
CIE	cesium ion engine
C/L	capacitance-to-inductance
cm	centimeter
CM	communications module
C/M	carrier-to-multipath
CMD	command
CMOS	complimentary metal oxide semiconductor
C/N ₀	carrier power to spectral noise density ratio
CNR, C/N	carrier-to-noise ratio
cntr	center
Comsat	Communications Satellite Corporation
ConUS, CONUS	Continental United States
CONV	converter
COSMOS	complimentary symmetry metal oxide semiconductor
CPI	cross polarization isolation
CPR	cross polarization ratio
CPU	central processing unit
CRT	cathode-ray tube
CSM	command-service module
CSP	command service program
CSS	coarse Sun sensor
CTNE	Companie Telefonica Nacional de Espana
CW	carrier wave, continuous wave

D

DA	design adequacy
D/A	digital to analog
DACU	data acquisition and control unit
DAF	Data Acquisition Facility
dB	decibel
dBi	decibel isotropic (gain relative to an isotropic antenna)
dB/K	decibel per degree Kelvin
dBm	decibels referred to 1 milliwatt
dBW	decibel (reference level 1 watt)
DC	downconverter
d.c.	direct current
DCP	data collection platforms
DDDF	duplex digital data formatter
DDS	digital Sun sensor
DECPSK	differentially encoded coherent phase shift key (modulated)
DEG, deg	degree

DEM	digital evaluation mode
Depl	deployment
DES	Delhi Earth Station
DESA	double electrostatic analyzer
DIB	data input buffer
div	division
DIX	data interface transmitter
DJS	Dzhusaly (designator)
DLO	dual local oscillator
DM	docking module
DOC	digital operational controller
DOD	depth-of-discharge
DOT	Department of Transportation
DOT/FAA	The Department of Transportation/Federal Aviation Administration
DOT/TSC	The Department of Transportation/Transportation Systems Center
DPRI	diagnostic and prescriptive reading instruction
DR	Copenhagen (designator)
DRR	data recorder/reproducer
DRS	direct reception system
DSS	digital Sun sensor
DSU	data switching unit
DTS	data transmission system
DUT	Denver Uplink Terminal

E

EBU	European Broadcast Union
ECH	Earth-coverage horn
ECI	Earth centered inertial
e.d.t., EDT	eastern daylight time
e.i.r.p.	effective isotropic radiated power
EME	Environmental Measurements Experiments
emi, EMI	electromagnetic interference
EML	equivalent monomolecular layer
enc	encoder
Eng.	engineering
EOL	end-of-life
EPIRB	Emergency Position Indicating Radio Beacon
EPS	electrical power subsystem
ERP	effective radiated power
ES	Earth sensor
ESA	Earth sensor assembly, European Space Agency
ESA/PSA	Earth sensor assembly/Polaris sensor assembly
e.s.t., EST	eastern standard time

ETR	Eastern Test Range
eV	electronvolt
EVM	Earth-viewing module
EVT	Eupatoria (designator)

F

f	frequency
F	Fahrenheit
FAA	Federal Aviation Administration
FCC	Federal Communications Commission
FCHP	feedback-controlled variable conductance heat pipe
FCP	flight computer program
FCT	fixed calibration terminal
f/d	ratio of focal distance to diameter
FDM	frequency diversity modulation; frequency division multiplexer
fm, FM	frequency modulated
FOV	field-of-view
FOWG	Flight Operations Working Group
Freq.	frequency
FRMS	Federation of Rocky Mountain States
fsk	frequency shift keying
FSS	fine Sun sensor
ft	foot, feet
FT	frequency translation
ft-lb	foot-pound
FTO	functional test objective
FTS	Federal Telecommunications System

G

g	grams, gravity
G	gain
GAC	ground attitude control
GEOS-3	Geodetic Earth-Orbiting Satellite-3
GFRP	graphite fiber reinforced plastic
GHz	gigahertz
gm	gram
G.m.t., GMT	Greenwich mean time
GRD	ground
GRP	group
GSFC	Goddard Space Flight Center
G/T	dB/K antenna gain over system noise temperature
GTT	ground transmit terminal
GVHRR	Geosynchronous Very High Resolution Radiometer

H

HAC	Hughes Aircraft Company
HDRSS	high data rate storage system
HET	Health, Education, Telecommunications (experiment)
HEW	Department of Health, Education, and Welfare
hf	high frequency
HGA	high gain antenna
HI	Honeywell International
HPBW	half power bandwidth
HR	hour
HSE	high-speed execute
HTR	heater; high-time resolution
Hz	hertz

I

IBM	International Business Machines
IDT	image dissector tube
IEB	interface electronics box
i.f.	intermediate frequency
IFC	in-flight calibration
IHS	Indian Health Service (Alaska)
IHSDL	interferometer high speed data link
IM	intermodulation
IMF	interplanetary magnetic field
IMP	Interplanetary Monitoring Platform
in.	inch
in.-oz	inch-ounce
Intelsat	International Telecommunications Satellite
INTF	interferometer
I/O	input/output
IPD	Information Processing Division
IR	infrared
IRAC	Interdepartment Radio Advisory Committee
ISRO	Indian Space Research Organization
IT	intensive terminal
ITS	Institute of Telecommunications Sciences
ITU	International Telecommunications Union
I-V	current voltage
IW	inertia wheel
IZMIRAN	Institute of Terrestrial Magnetism, Ionosphere and Radio Wave Propagation

J

JAM	jet-assist mode
Joburg	Johannesburg (designator)
JSC	Johnson Space Center

K

K	Kelvin
kbps	kilobits per second
keV	kiloelectronvolt
kg	kilogram
kHz	kilohertz
km	kilometer
KSC	Kennedy Space Center
kW	kilowatt

L

lb	pound
LC	inductive-capacitance
LD	linear detector
LFT	long form test
LIC	load interface circuit
LLD	lower level discriminator
LO	local oscillator
LOS	line-of-sight
LRIR	limb radiance inversion radiometer
LSB	least significant bit
LT	local time
LV	local vertical
L.V.	latch valve

M

m	meter
m ²	square meter
mA	milliamperes
Mad	Madrid
MAD-HYB	Madrid Hybrid
Mage	U.S./U.S.S.R. Magnetometer Experiment
Marad	Maritime Administration
MASEP	main sequential program
Max.	maximum

MCC-H	Mission Control Center, Houston
MCC-M	Mission Control Center, Moscow
MDAC	McDonnell-Douglas Aircraft Corporation
MDHS	meteorological data handling system
MESC	magneto-electrostatic plasma containment
MeV	megaelectronvolts
MHz	megahertz
μf	microfarad
μm	micrometer (micron)
μs , μsec	microsecond
MILA	Merritt Island Launch Annex
min, MIN	minute
mlb	millipound
MMW	Millimeter Wave Experiment
mN	millinewton
MOCC	Multisatellite Operations Control Center
MOCR	Mission Operations Control Room
MONO	monopulse
MOR	Mission Operations Room
MOS	metal oxide semiconductor
MSB	most significant bit
ms, msec	millisecond
m/s	meters per second
MT	multitone
mV	millivolts
mW	milliwatt
MWE	Millimeter Wave Experiment
MW XMTR	microwave transmitter

N

N	Newton
NAFEC	National Aviation Facilities Experiment Center
NASA	National Aeronautics and Space Administration
Nascom	NASA Communications Network
NBFM	narrowband frequency modulation
NCC	Network Coordination Center
NCE	normal command encoder
NDR	Hamburg (designator)
nm	nanometer
NMRC	National Maritime Research Center
NOAA	National Oceanic and Atmospheric Administration
N/P	negative/positive
NRL	Naval Research Laboratories

ns nanosecond
 NTSC National Television System Committee color (U.S.)

O

O&M operations and maintenance
 OC orbit control
 OCJ orbit control jet
 OCP operational control program
 o.d. outside diameter
 OD Operations and Distribution (Center)
 omni omnidirectional
 OSR optical solar reflectors
 OSU Ohio State University
 OYA Helsinki (designator)

P

PA power amplifier, preamplifier
 PAL phase alternation live color (Europe)
 PAM pulse amplitude modulated
 PAO Public Affairs Office
 PARAMP parametric amplifier
 PB phonetically balanced
 PBS Public Broadcasting Service
 P_c course phase measurement
 pcm, PCM pulse code modulation
 pcm/fsk/am pulse code modulation/frequency shift keying/amplitude modulation
 PCT portable calibration terminal
 PCU power control unit
 PDM pulse duration modulation
 pf picofarad
 PFD power flux density
 PFF prime-focus feed
 PGE PLACE ground equipment
 PIC power interface circuit
 PLACE Position Location and Aircraft Communications Experiment
 PLU Project Look-Up
 PM phase-modulated
 PN pseudo-noise
 POCC Project Operations Control Center
 p-p peak-to-peak
 PPK Petropavlovsk-Kamchatski (designator)
 ppm parts per million

P_R	reference (phase) signal
P_{rgi}	power received at ground into an isotropic antenna
P_{rsi}	power received at spacecraft into an isotropic antenna
PRU	power regulation unit
PSA	Polaris sensor assembly
P_{SE}	probability function
psia	pounds per square inch absolute
PSK	phase shift keyed
Pv	vernier phase measurement
pW	picowatt
PWR	power

Q

QCM	Quartz-crystal microbalance contamination monitor
Q-M	quadrature phase modulation

R

Radsta	U.S. Coast Guard Radio Station
R&RR	range and range rate
RBE	Radio Beacon Experiment
RCA	Radio Corporation of America
RCC	Resource Coordinating Center
RCV	receive
RDA	rotating detector assembly
REC	receive
Ref., REF	reference
Rel	release
RESA	Regional Education Service Agency
rf	radio frequency
RFC	radio-frequency compatibility
rfi	radio frequency interference
RFIME	Radio Frequency Interference Measurement Experiment
RGA	rate-gyro assembly
RME	Rocky Mountain East
RMPBN	Rocky Mountain Public Broadcast Network
rms	root mean square
RMW	Rocky Mountain West
ROT	receive-only terminal
rpm	revolutions per minute
RR	rain rate

S

S/A	solar array
SAPPSAC	Spacecraft Attitude Precision Pointing and Slewing Adaptive Control (Experiment)
SAR	search and rescue
S&R	surveillance and ranging
Satcom	Satellite Communications
SC	sudden commencement
S/C	spacecraft
SCAMA	switching, conferencing, and monitoring arrangement
SCAMP	small command antenna medium power
SE	system effectiveness
sec, s	second
SECAM	Sequential Couleurs a Memoire (III) color (U.S.S.R.)
SEL	Space Environment Laboratory
SENS	sensor
S.G.	signal generator
SITE	Satellite Instructional Television Experiment
SITEC	sudden increase in total electron content
SIU	squib interface unit
S-IVB	Saturn IB second stage
SMSD	spin motor sync detector
SNR, S/N	signal-to-noise ratio
Spec	specification
SPS	spacecraft propulsion subsystem
SPU	signal processing unit
sr	steradian
SR	Stockholm (designator)
SRT	SAPPSAC remote terminal
SSC	sudden storm commencement
SSEA	Sun sensor electronics assembly
SSR	Staff Support Room
STA	station
STADAN	Space Tracking and Data Acquisition Network
STDN	Spaceflight Tracking and Data Network
STRUCT	structural
SWBT	Southwestern Bell Telephone Company
SYN	synthesizer
SYNC	synchronous
SYSSIM	system simulator

T

TACH	tachometer
T&CS	telemetry and command subsystem
T&DRE	Tracking and Data Relay Experiment
TART	transmit and receive terminal
TASO	Television Allocation Study Organization
TBC	time base corrector
TCD	transponder command decoder
TCS	telemetry and command subsystem, thermal control subsystem
TDA	tunnel diode amplifier
TDRE	Tracking and Data Relay Experiment
TEMP	temperature
THIR	temperature-humidity infrared radiometer
TID	traveling ionospheric disturbances
TLM, TM	telemetry
TORQ	torquer
TRUST	Television Relay Using Small Terminals
TSM	thermal structural model
TSP	telemetry service program
TSU	temperature (control) and signal (conditioning) unit
TT/N	test-tone signal-to-noise ratio
TTY	teletype
TV	television
TVOC	Television Operational Control Centers
TWT	traveling wave tube
TWTA	traveling wave tube amplifier

U

UC	upconverter
UCLA	University of California at Los Angeles
UCSD	University of California at San Diego
uhf	ultrahigh frequency
UK	United Kingdom
UKTV	University of Kentucky Television
ulf	ultralow frequency
UNH	University of New Hampshire
U.S.	United States
USA	ubiquitous spectrum analyzer
USAF	United States Air Force
USCG	United States Coast Guard
USK	Ussuriisk (designator)

U.S.S.R. Union of Soviet Socialist Republics
 UT universal time
 UV ultraviolet

V

v velocity
 V volt
 VA Veterans Administration
 VCA voltage controlled amplifier
 VCHP passive "cold-reservoir" variable conductance heat pipe
 VCXO voltage controlled crystal oscillator
 Vdc volts direct current
 V/deg volts per degree
 Vert. vertical
 vhf, VHF very high frequency
 VHRR very high resolution radiometer
 VIP versatile information processor
 VIRS vertical interval reference signal
 VITS vertical interval test signals
 VPI Virginia Polytechnic Institute
 vs. versus
 VSWR voltage standing-wave ratio
 V/T voltage/temperature
 VTR video-tape recorder
 VU MTR VU meter

W

W watt
 WAMI Washington, Alaska, Montana, Idaho (medical education)
 WBDU Wideband Data Unit
 WBVCO wideband voltage-controlled oscillator
 WHL, WH wheel

X

XMIT transmit
 XMTR transmitter
 XTAL crystal
 XTAL DET. crystal detector

Y**YIRU** yaw inertial reference unit**Z****ZAZ** Z-axis azimuth
Zcoel Z-coelevation

BIBLIOGRAPHY

1. Apollo/Soyuz Test Project Directive No. 4, M-D MA-1400.165, Headquarters, NASA.
2. Apollo/Soyuz TV Integration Program Final Report Vols. IOIV, 1974-1976; Westinghouse Electric Corporation, NASA-JSC Contract NAS 9-14030.
3. ASTP-CSM Manual, 1 August 1974, Rockwell International, Inc.
4. ASTP 42000, Mission Requirements, Headquarters, NASA.
5. ASTP 30000, Project Schedule Headquarters, NASA.
6. ASTP 20050, Public Information Plan, Headquarters, NASA.
7. ASTP 50000 Series, Interacting Equipment Documentation, Headquarters, NASA.
8. ASTP-TV-300, Rev. D, 28 August 1974; Westinghouse Electric Corporation, NASA-JSC contract NAS 9-14030.
9. ASTP-TV-301A, ASTP Television Interface Specifications, March 1975, Westinghouse Electric Corporation, NASA-JSC Contract NAS 9-14030.
10. LaVigna, T., "The ATS-6 Power System—An Optimized Design for Maximum Power Source Utilization," presented at Tenth Intersociety Energy Conversion Engineering Conference Proceedings, 759157, August 18-22, 1975, pg. 1048.
11. LaVigna, T., and K. Sizemore, "Design and Analysis of a Highly Efficient Power System for the Small Scientific Satellite (S³)," NASA TMX 70573, November 1969.
12. LaVigna, T., and F. Hornbuckle, "The ATS-6 Power System: Hardware Implementation and Orbital Performance," presented at Intersociety Energy Conversion Conference, 1976.
13. LaVigna, T., and F. Hornbuckle, "The ATS-6 Power System: Hardware Implementation and Orbital Performance," NASA Technical Paper 1023, September 1977.
14. Pardoe, C. T. and P. J. Grunberger, "Delay-Lock-Loop-Code Correlation Synchronizer," The Johns Hopkins University Applied Physics Laboratory, Silver Spring, Maryland, APL/JHU CP 032, April 1975.

15. Schmid, P. E., et al., "ATS-6 Satellite-to-Satellite Tracking and Data Relay Experiments," IEEE Transactions on Aerospace and Electronic Systems, Vol. AES-II, November 1975.
16. Schmid, P. E., et al., "Satellite-to-Satellite System and Orbital Error Estimates," NASA Goddard Space Flight Center, Greenbelt, Maryland, TMX 71093, January 1976.
17. Smith, A., T. LaVigna, and L. Pessin, "Design Impact of a Unique Solar Array Configuration for the ATS-F Electrical Power Subsystem," presented at Eighth IECEC, August 1973.
18. Smith, A., F. Hornbuckle, and F. Betz, "Evaluation of Flight Acceptance Thermal Testing for the ATS-6 Solar Array," presented at the 11th IEEE Photovoltaic Specialist Conference, 1975.
19. STDN No. 601/ASTP, Network Operations Support Plan for the Apollo/Soyuz Test Project, December 1974; NASA Goddard Space Flight Center, Greenbelt, Maryland.

BIBLIOGRAPHIC DATA SHEET

1. Report No. NASA RP-1080	2. Government Accession No.	3. Recipient's Catalog No.	
4. Title and Subtitle ATS-6 Final Engineering Performance Report Volume III - Telecommunications and Power	5. Report Date November 1981		6. Performing Organization Code 415
	8. Performing Organization Report No. 81F0034		
7. Author(s) Robert O. Wales, Editor	10. Work Unit No.		
9. Performing Organization Name and Address Goddard Space Flight Center Greenbelt, Maryland 20771	11. Contract or Grant No. NAS 5-25464		
	13. Type of Report and Period Covered Reference Publication		
12. Sponsoring Agency Name and Address National Aeronautics and Space Administration Washington, D.C. 20546	14. Sponsoring Agency Code		
	15. Supplementary Notes		
16. Abstract			
<p>The Applications Technology Satellite 6, an experimental communications spacecraft, operated for five years in a geosynchronous orbit. The six volumes of this report provide an engineering evaluation of the design, operation, and performance of the system and subsystems of ATS-6 and the effect of their design parameters on the various scientific and technological experiments conducted.</p> <p>This volume (III) describes the design, details and performance of the communications, telemetry and command, and power subsystems.</p>			
17. Key Words (Selected by Author(s)) Spacecraft Communication, Evaluation, Spacecraft Performance, Communications Technology Satellite, Telemetry, Command and Control		18. Distribution Statement Unclassified - Unlimited Subject Category 18	
19. Security Classif. (of this report) Unclassified	20. Security Classif. (of this page) Unclassified	21. No. of Pages 298	22. Price* A13

*For sale by the National Technical Information Service, Springfield, Virginia 22161.

GSFC 25-44 (10/77)

National Aeronautics and
Space Administration

Washington, D.C.
20546

Official Business

Penalty for Private Use, \$300

SPECIAL FOURTH CLASS MAIL
BOOK

Postage and Fees Paid
National Aeronautics and
Space Administration
NASA-451



NASA

POSTMASTER: If Undeliverable (Section 158
Postal Manual) Do Not Return
